2.12.3 DROP ANALYSIS FOR THE TRAVELLER XL SHIPPING PACKAGE

Two finite element models were developed for the Traveller XL package undergoing the prescribed regulatory drop tests. The first model reflected the prototype configuration used for initial exploratory ("scoping") tests conducted in January 2003. The second model reflected the Qualification Test Units tested in September 2003 that included modifications based on the prototype test results. These models were used to develop a crash-worthy design, minimizing structural cost and weight, determining the "worst-case" drop orientations.

The objectives of this effort are:

- To validate the techniques used in these models by documenting the conservative agreement found between predictions and results of the prototype drop tests; and,

- To determine the appropriate number of drop tests and their orientation(s) needed for the qualification drop tests. By regulation, the shipping package must be dropped at orientations that are most damaging to the fuel assembly and to the shipping package.

The finite element models developed for the Traveller were not developed to predict actual stress and strains accurately. With the computational resources available, the models can identify regions of high stress and strain but cannot accurately predict component failure unless predicted values are significantly above or below failure points. Instead, they were developed to understand relative deformations, decelerations and energy absorption between drop orientations. The models have been used to compare predicted stresses and strains for different drop orientations to allow intelligent selection of drop orientations for testing. The Traveller program utilized extensive full-scale tests to prove the acceptability of the Traveller design. These tests results are described in sections 2.12.4 below and the results are compared with the FEA in this section.

2.12.3.1 Analysis Results

The Traveller XL shipping package complies with 10 CFR 71 and TS-R-1 requirements, respectively for all drop orientations. Test orientations which are most challenging are a 9 meter vertical drop with the bottom end of the package hitting first as shown in Figure 2-52A and a 9 meter CG-forward-of-corner drop onto the TN end of package with an 18° forward rotation, Figures 2-44 and Figure 2-45. The former has the greatest potential to damage the fuel assembly and the latter is most damaging to the shipping package itself. Successful drop tests in these two orientations are adequate demonstration that the Traveller XL design meets/exceeds the HAC drop test requirements.

The Traveller XL shipping package will survive the HAC drop tests in any orientation with few or no closure bolt failures. Horizontal side drops onto the hinges or latches, Figures 26A and B, result in the highest hinge/latch bolt loads. The analyses indicate ten ¾-10 stainless steel bolts/side are sufficient to ensure the Outerpack remains closed during such drops. The miminum predicted factor of safety for the Outerpack latch and hinge bolts is 1.12.

Damage to the Traveller XL shipping package from the HAC drop tests is predicted to be minor and primarily involves localized deformations in the region of impact. Both the Outerpack and Clamshell structures remain intact and closed. Fuel assembly damage is confined to the top or bottom region depending on drop orientation. This damage primarily involves localized buckling and deformation of the nozzles.

This page intentionally left blank.

Temperature and foam density have a minor effect on drop performance of the Traveller XL package. For the orientation predicted most damaging to the Outerpack, a package with nominal foam density and dropped at "normal temperature" (75°F) experiences 8.5 and 13.7% higher loads than, respectively, one containing low density foam and dropped at 160°F or one containing high density foam and dropped at -40°F, Figure 2-62. Fuel assemblies in packages containing the highest allowable density foam and dropped at the lowest temperature extreme will experience accelerations that are very similar to those in packages with lowest allowable density foam and dropped at the highest temperature extreme, Figure 2-63. However, the accelerations at these extremes are only 5% greater than for a package dropped at 75°F containing nominal density foam.

A maximim indentation of 67 mm is predicted for the 1 m pin puncture test when the package is impacted from underneath, Figure 2-65A, and dropped horizontally with its CG directly above the pin. The steel outer skin should not be ruptured during this test. Overall, the 1 m pin puncture test is a relatively benign test for the Traveller XL package.

In some drop orientations, the moderator blocks lining the inside walls of the upper and lower Outerpack assemblies prevent the Clamshell from radically changing shape as might otherwise occur.

An accurate and conservative methodology for predicting HAC impact performance of the Traveller XL shipping package was developed. The LS-DYNA finite element code was used to develop drop and pin puncture models of the prototype and qualification units. In comparisons against test, a model of the prototype unit, at worst, correlated to within 27% for displacements. Predicted accelerations matched measured traces well. However, due to a limitation on mesh density, predicted stresses and strains should be interpreted in a comparative manner. This limitation applies to the models of both the prototype and qualification units.

2.12.3.2 Predicted Performance of the Traveller Qualification Test Unit

2.12.3.2.1 Most Damaging Drop Orientations

A primary objective of this study was to determine the worst case drop orientation(s) for the HAC drop tests. This requirement is to drop test the shipping package in orientations that most damage: a) the shipping package, and b) the fuel assembly. It was quickly realized that the most damaging orientation for the shipping package, would not necessarily be the same for the fuel assembly. Based on the robust performance of the Traveller XL drop units during testing, orientations that were most severe to the fuel assembly became more significant.

Determination of the worst case orientation for the shipping package was facilitated by the Traveller XL computer analysis and results of the prototype tests. Many orientations can be eliminated from consideration due to inherent design features of the Traveller. For example, the circumferential stiffeners on the upper Outerpack, and the legs/forklift pocket structure, Figure 2-21, greatly reduce the crushing of the Outerpack since they crush prior to impact of the main body of the Outerpack. Drop orientations where one or the other of these structures directly contacts the drop pad, Outerpack damage is reduced in

comparison to orientations where these features are not impacted. This is because the energy absorbed in crushing these features cannot be absorbed by the Outerpack.

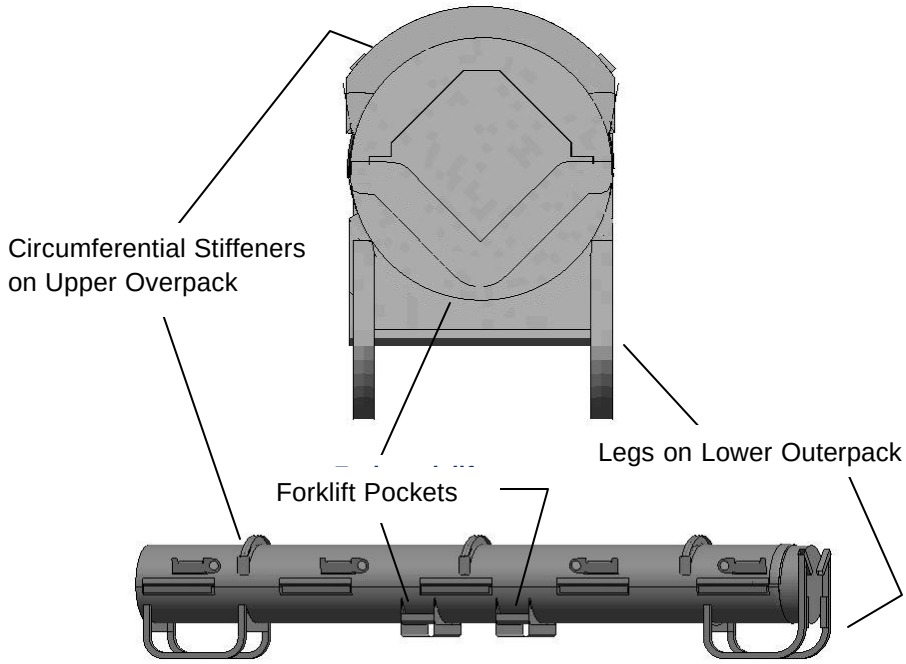

Figure 2-21 Traveller Stiffeners, Legs, and Forklift Pockets

Test results supported this hypothesis. Indeed, in the two available tests of relevance, these features absorbed almost all the energy and very little damage was incurred by the Outerpack. For example, Prototype-1, Test 1.1 was a low angle slap down test resulting in extensive crushing of the upper Outerpack stiffeners, Figure 2-22. Aside from this crushing, very little Outerpack damage was incurred. Prototype-2, Test 3.2 was the second example. In this test, the Outerpack was dropped horizontally onto its legs from 9 m. This resulted in significant crushing of the Outerpack legs and feet, Figure 2-22B, and the forklift supports, not shown. However, the Outerpack was otherwise not significantly damaged.

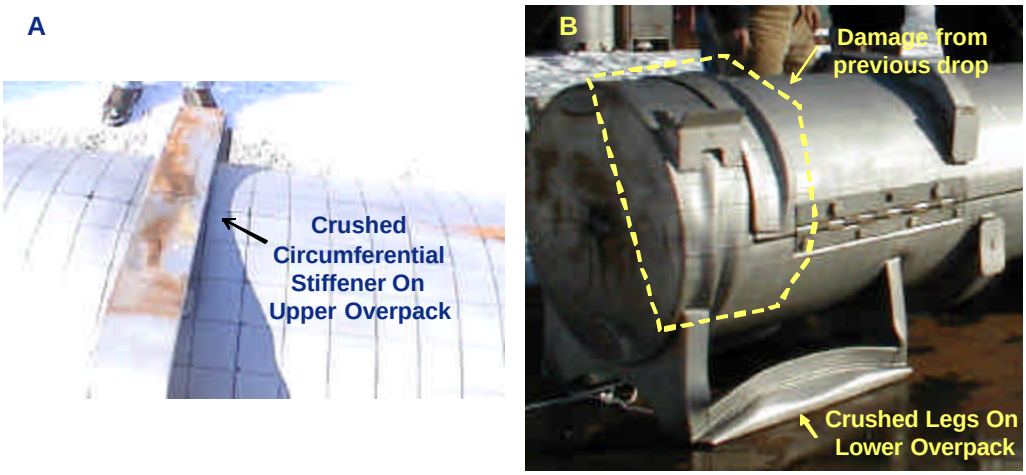

Figure 2-22 Results of Prototype Drop Test

Alternately, neither the stiffeners, nor legs hit first for orientations in which the Outerpack ZX plane defined in is perpendicular to the impact surface, Figure 2-23. Such orientations include side drops or slap downs onto the hinged sides of the Outerpack and vertical drops onto the either end of the package. Thus, our analysis of the most damaging Outerpack orientations focused on these orientations.

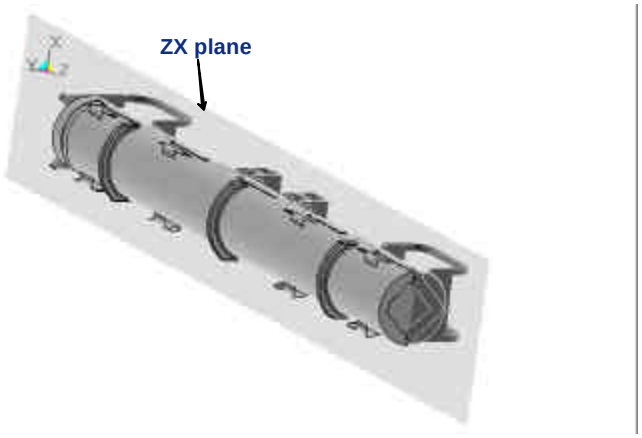

Figure 2-23 Side Drop Orientation

Determining which drop orientations in the ZX plane most damage the shipping package was also facilitated by the Traveller XL design itself. In particular, "slap down" drops, low- to medium-angle impacts where one end of the package hits before the other, as shown in Figure 2-24, divide the impact energy primarily between the top and bottom impact limiters. Generally, this energy is absorbed in a manner that induces relatively little damage for this design. An example of the damage associated with a 15° slap down is shown in Figure 2-25. This figure reflects the damage obtained in Test 1.1 of the Prototype test campaign.

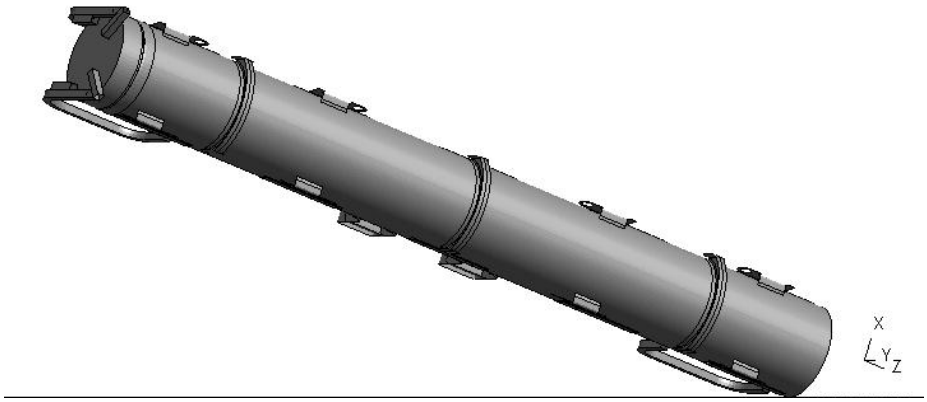

Figure 2-24 Low Angle Drop Orientation

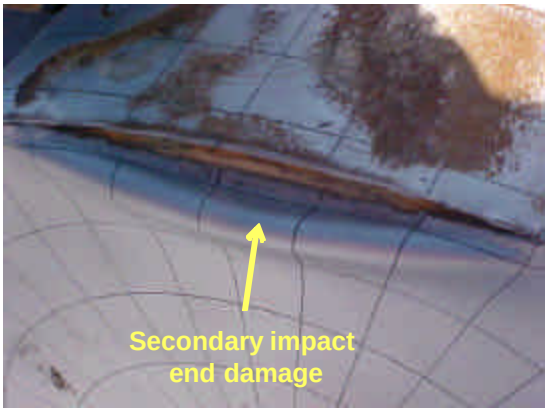

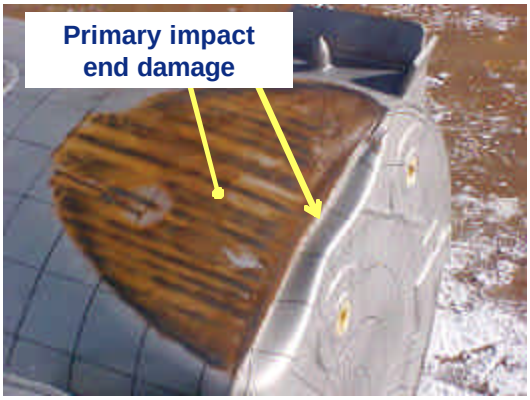

Figure 2-25 Damage from Prototype Low Angle Drop (Test 1.1)

The shipping package may be dropped in some orientations outside the ZX plane and still not be protected by its stiffeners and legs/forklift pocket structure, Figure 2-21. In vertical and nearly vertical orientations, the impact limiter will hit the drop pad first. In these cases, the primary impact energy may be entirely absorbed by the impact limiters and Outerpack walls with little, if any, being channeled into the stiffeners or legs. Indeed, the stiffeners and legs provide no benefit unless the shipping package actually falls over for a secondary impact.

Thus, analysis of orientations most damaging to the Outerpack was focused on horizontal drops onto the Outerpack side (i.e., onto the hinges/latches), vertical drops (onto either end of the package) and nearly vertical drops.

2.12.3.2.2 Horizontal Side Drops

The two possible orientations for a horizontal side drop test involve either a drop onto the opening or latched side of the Outerpack, Figure 2-26A, or a drop onto the permanently (or semi-permanently) hinged side, Figure 2-26B.

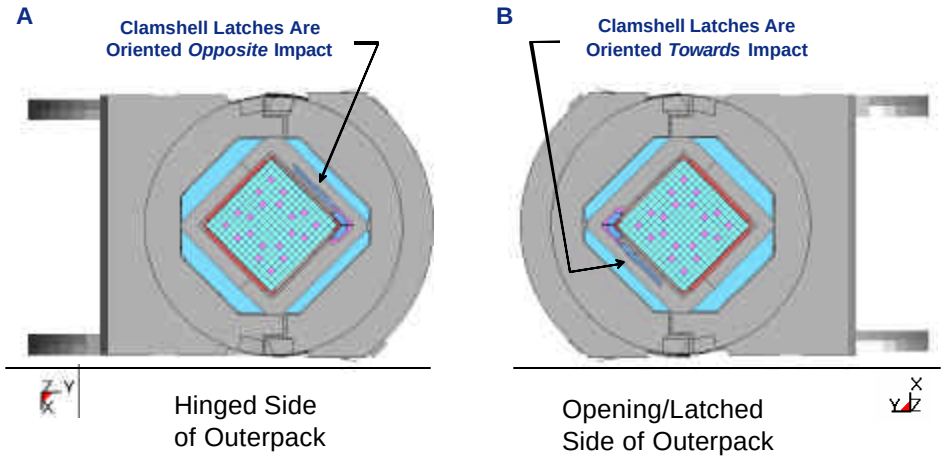

Figure 2-26 Horizontal Drop Orientations

Energy and Work Histories – Global energy and work for the Outerpack horizontal side drops are shown in Figures 2-27 and 2-28. The similarity of these two drops is reflected in these plots. Both plots (as do all the 9.14m (30ft) drops reported herein for the qualification unit) have an initial total energy (TE) of 204 kJ. This value correctly reflects the initial velocity (v) of 13.4 m/s applied to the 2,270 kg (5,005 lb) package mass (m) since our simulation is initiated at the end of Outerpack free fall from 9.14 m (30 ft.); the total energy is comprised only of kinetic energy (KE), and $KE = \frac{1}{2}mv^2$. Total energy remains nearly constant throughout both drop simulations. This reflects the relatively small overall deformations predicted for this drop, i.e., the almost negligible external work done by the package under gravity loading. In both simulations, the event was essentially completed within 10 milliseconds as seen by the flattening of the kinetic energy and internal energies after that time. Moreover, acceptable levels of hourglass, sliding, and stonewall energies were obtained although the sliding energy ultimately reached 10% of the internal energy. This latter issue is not critical since it occurs after the maximum Outerpack/drop pad force has been reached.

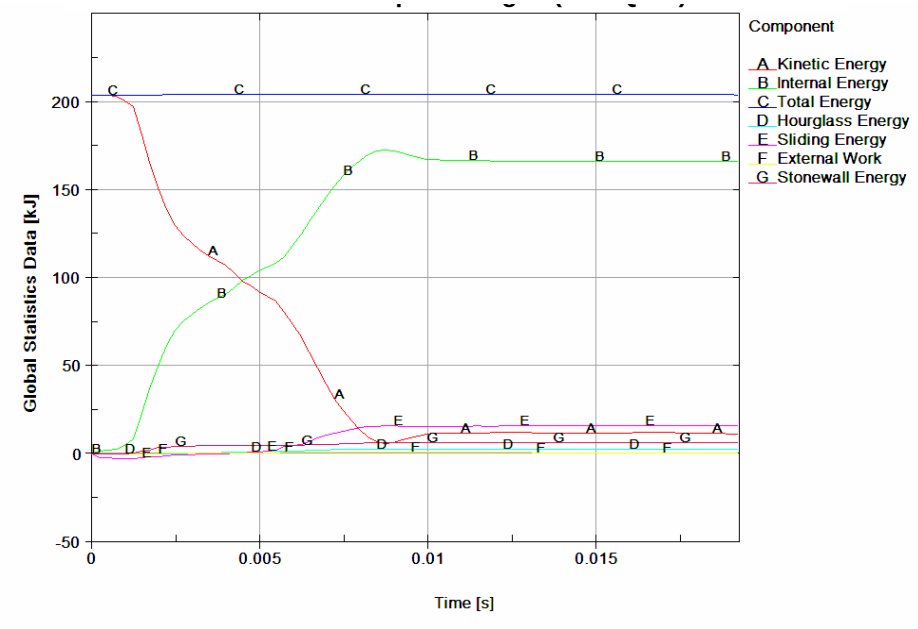

Figure 2-27 Predicte d Energy and Work for 9m Horizontal Drop Onto Outerpack Hinges

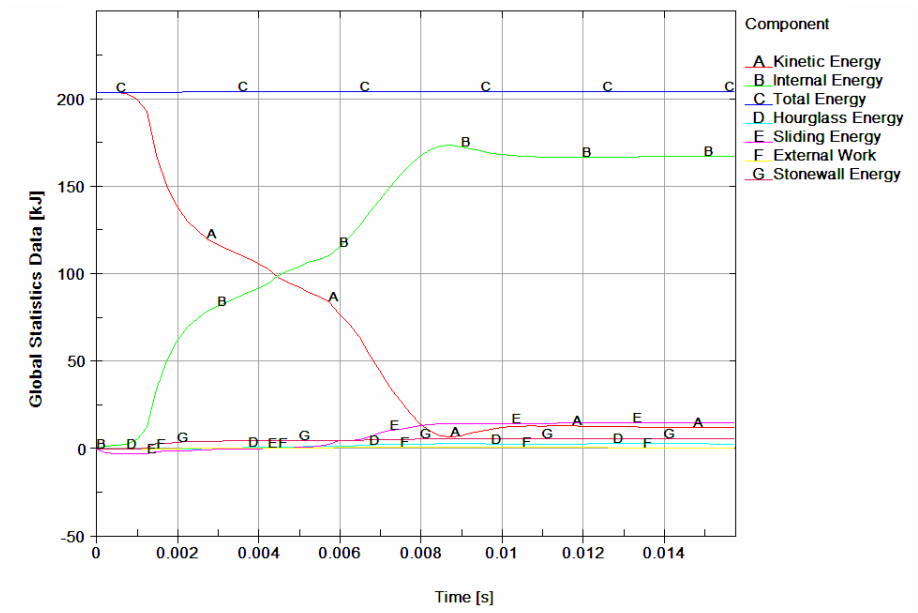

Figure 2-28 Predicted Energy and Work Histories for a 9m Horizontal Drop Onto the Outerpack Hinges

Rigid Wall Forces – Neglecting the very soft shock mounts that tie them together, the Traveller XL shipping package consists of an essentially de-coupled Outerpack and Clamshell/fuel pair. Indeed, the predicted drop scenario consists of the Outerpack crushing onto the pad while the Clamshell/fuel assembly continues falling until it hits the inner surfaces of the Outerpack. Then the Outerpack, Clamshell, and fuel assembly crush further onto the pad. This scenario is reflected in the rigid wall force history shown in Figure 2-29.

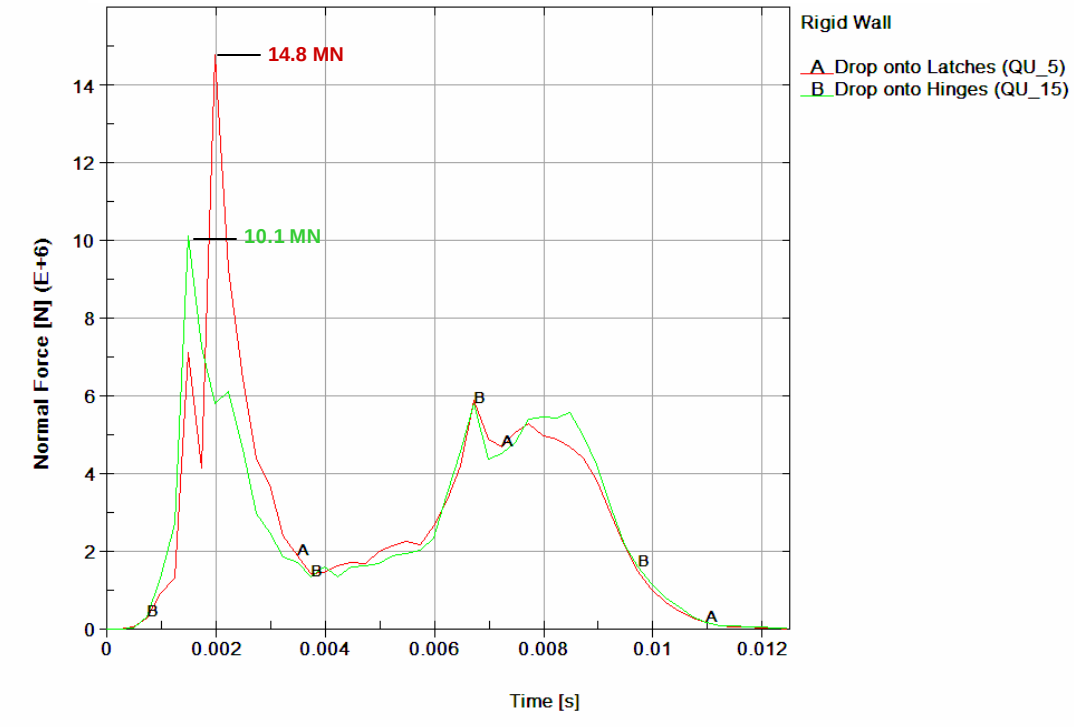

Figure 2-29 Predicted Rigid Wall Force Histories for 9m Horizontal Drops Onto the Outerpack Latches and Hinges

In Figure 2-30A, the initial impact between the Outerpack and pad is seen in the first 4 milliseconds, peaking at approximately 1.5 milliseconds for the drop onto hinge (run QU_15) and 2.0 milliseconds for the drop onto latches (run QU_5). This disparity is attributed to slight errors in the model geometrical definition (rather than to any actual non-symmetry within the design itself). Further, we postulate resolution of this disparity would lower the predicted forces for the drop onto Outerpack latch simulation (run QU_5) and increase those for the simulated drop onto the Outerpack hinges (run QU_15). However, we choose not to resolve this difference but simply used the QU_5 predictions as a bounding and conservative case. At approximately 4.0 milliseconds, the force between the Outerpack and drop pad has decreased and it appears the Outerpack might soon rebound. However, the Clamshell/fuel assembly then contacts the inner surface of the Outerpack and drives it into back into the drop pad, Figure 2-30B.

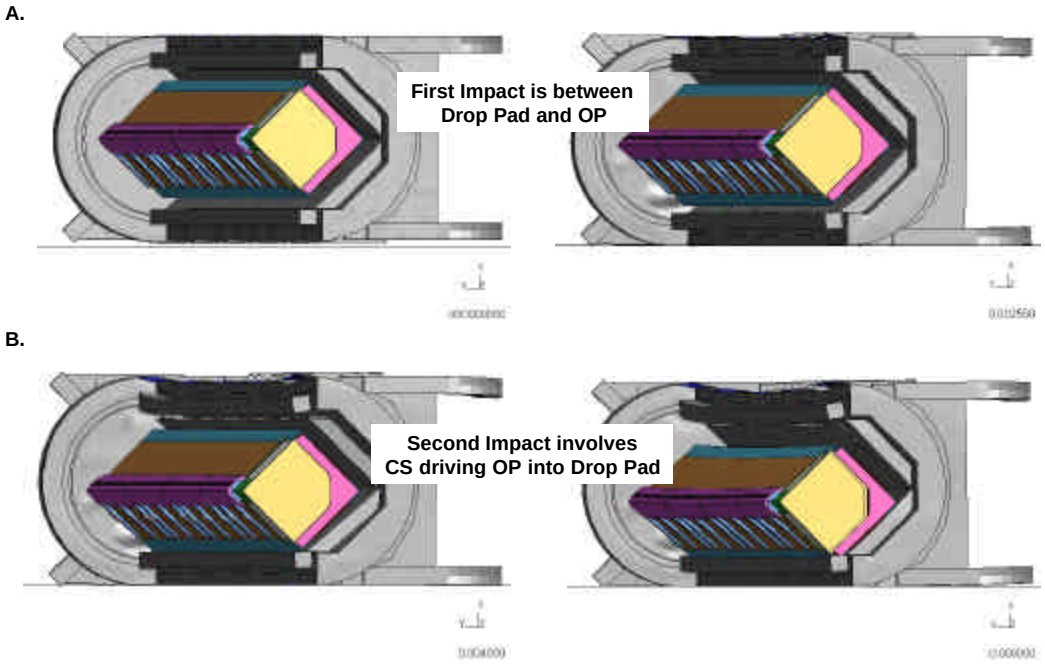

Figure 2-30 De-coupled Impacts for 9 m Horizontal Side Drop

The forces between the Outerpack and drop pad during the first portion of a horizontal side drop are the highest predicted forces for any orientations analyzed. However, these forces are so high because the deformations (i.e., cushioning) are small. Thus, despite the high forces, the package (Outerpack and Clamshell) should be relatively undamaged provided its components remain closed. For the Outerpack, this requires that the majority of the Outerpack latch/hinge bolts do not fail. In the case of the Clamshell, the latch bolts, the top and bottom end plate bolts, and, as will be described, the lipped/groove interfaces between the Clamshell end plates themselves (top end) and between the Clamshell doors and plate (bottom end) must not be comprised. During Prototype testing the robustness of these features was confirmed, as no Outerpack bolts failed, and the Clamshell latches remained closed.

Note that the Clamshell cross-sectional shape is predicted to stay essentially unchanged during the horizontal side drops, Figure 2-30. This is due in large part to the moderator blocks which form a "cradle" for the Clamshell. These moderator blocks prevent the Clamshell from radically changing shape as might otherwise happen since three of the Clamshell edges are either hinged or latched. This is an important structural benefit of the conformal shape of the interior of the Outerpack.

Outerpack Hinge Bolts – The Outerpack hinges are secured to the Outerpack with Type 304 stainless steel bolts, Figure 2-31. The bolts securing the bottom flange of the hinge (or latch) to the lower Outerpack are not removed during normal operation. Thus, the number of bolts used in this area is not critical from a user/operation standpoint. However, the bolts securing the top half of the latch to the upper Outerpack must be removed whenever the package is opened. Thus, the desire is to minimize the number

of these bolts while still insuring the package is not compromised during HAC drop tests. As such, the development of the Traveller XL design started with three 7/8" diameter (2.2 cm) for each hinge segment. A total of five (5) hinge segments per Outerpack side were utilized. The second Prototype unit therefore was tested with only 2 of 3 bolts in each hinge section (10 per side) to verify that design margins were present in the design.

Based on the successful testing of 10 bolts per side, evaluations were initiated to determine if smaller ¾" diameter (1.91 cm) bolts had sufficient strength to sustain impact loads. These were shown to be acceptable. The QTU-1 and QTU-2 units were dropped with ten ¾" (1.91 cm) bolts on each side.

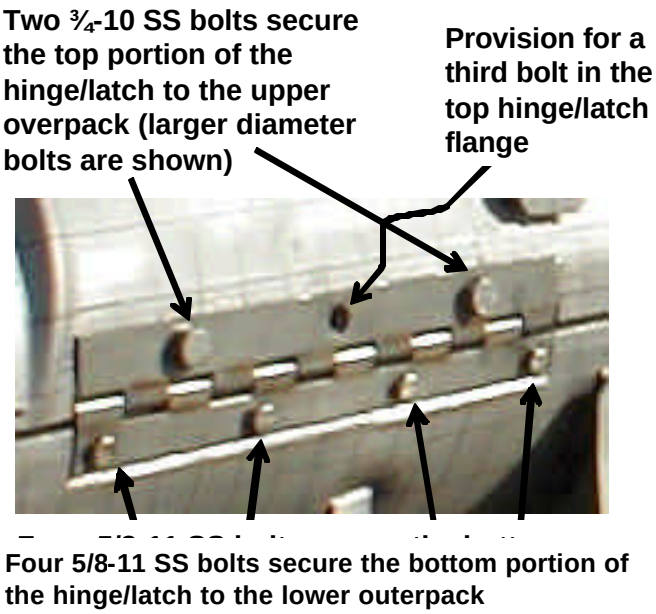

Figure 2-31 Bolts on Prototype Outerpack

Prototype-2, Test 3.3 was a side drop in which two 7/8-9 stainless steel bolts were used to secure the top portion of the hinge to the upper Outerpack and four 5/8-11 stainless steel bolts were used to secure the bottom hinge flange to the lower Outerpack. In this test, no bolts were broken. Our analyses indicate two ¾-10 stainless steel bolts/latch and hinge are sufficient to insure the Outerpack remains closed during the 9m side drop. This is seen by reviewing the predicted safety factors of the top latch bolts when the package is dropped on its latching side, Figure 2-26B. As shown in Table 2-10, the minimum factor-of-safety (FS) for the top Outerpack latch bolts was 2.15 based on the bolt minimum tensile (125 ksi). This minimum was calculated for a latch bolt when the Outerpack was dropped onto its latched side, Figure 2-26B.

Table 2-10 Top Outerpack Latch Bolt Minimum Factors of Safety (FS) for 9m Side Dropped		
ID (Figure 2-32)	FS/Time	
	Dropped On OP Latches (Figure 2-30B)	Dropped On OP Hinges (Figure 2-30A)
B917	2.22/0.0082 s	2.20/0.0077 s
B921	**2.15/0.0065 s**	2.21/0.0065 s
B923	2.16/0.0065 s	2.17/0.0065 s
B927	2.20/0.0062 s	2.18/0.0065 s
B929	2.19/0.0057 s	2.19/0.0062 s
B933	2.19/0.0067 s	2.20/0.0077 s
B935	2.20/0.0067 s	**2.16/0.0065 s**
B939	2.18/0.0065 s	2.18/0.0065 s
B941	2.21/0.0085 s	2.23/0.008 s
B945	2.32/0.0045 s	2.43/0.0045 s

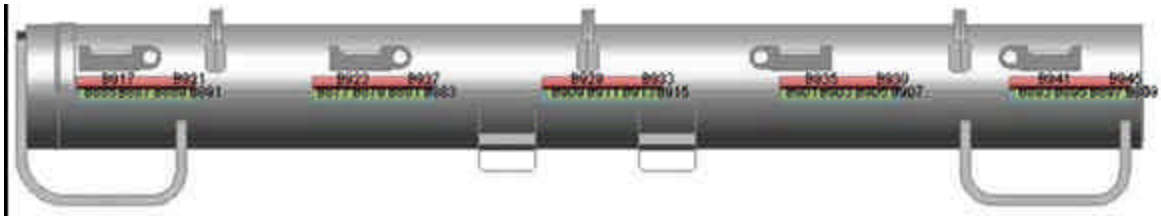

Figure 2-32 Bolt Labels for Right Outerpack

Hinge bolt FS for horizontal 9m side drops on the latched and hinged side of the Outerpack are shown in Table 2-10. If the shipping package were exactly symmetrical, FS for the hinge bolts calculated for a drop on the Outerpack hinges would correspond with those for the latch bolts when the package was dropped onto the latches, etc. However, this was not the case as can be seen by comparing the results shown in Table 2-10 with those in Table 2-11. This small irregularity is primarily attributed to slight errors in the model geometrical definition and to a lesser extent on actual non-symmetry within the design itself. The analysis indicates little likelihood of compromising the Outerpack closure during a 9m side drop.

Table 2-11 Top Outerpack Hinge Bolt Minimum Factors of Safety (FS) for 9m Side Drop		
ID (Figure 2-33)	**FS/Time**	
	Dropped On OP Latches (Figure 2-30B)	**Dropped On OP Hinges (Figure 2-30A)**
B947	**2.34/0.0025 s**	2.20/0.0077 s
B951	3.05/0.0027 s	2.21/0.0065 s
B953	2.58/0.0022 s	2.17/0.0065 s
B957	2.93/0.0022 s	2.18/0.0065 s
B959	2.82/0.0017 s	2.19/0.0062 s
B963	3.19/0.0017 s	2.20/0.0077 s
B965	2.52/0.0022 s	**2.16/0.0065 s**
B969	2.22/0.0117 s	2.18/0.0065 s
B971	2.52/0.0055 s	2.23/0.008 s
B975	2.54/0.0032 s	2.43/0.0045 s

For the CTU and production designs, minor changes to the design were made to improve burn test performance, as well as simplify manufacturing. To ensure a conservative design, two additional bolts were added on each side of the Outerpack full-length hinge sections. Therefore, the CTU and production packages utilize 12 bolts per side per hinge leaf. This change allowed the reduction of the planned high strength (125 ksi ultimate strength) bolt to be replaced with a lower strength bolt, since there are more bolts, and since the 70 ksi bolts were marginal in performance. It should also be noted that the Prototype-2 package was dropped on its side from 9 m and showed no visible signs of strain on any of the bolts. One explanation for this may be that friction is ignored in the calculation of bolt factors of safety.

The increase in number of bolts, 20%, (= 12/10) and the increase in strength of the allowable bolt material, ASTM A193 Class 1 B8, of 7% (= 75 ksi/70ksi – 1) causes the factors of safety of the worst bolt in a side drop to be reduced from 2.15 to 1.12. Since this is the greatest loading for any orientation, all bolts have an adequate safety margin.

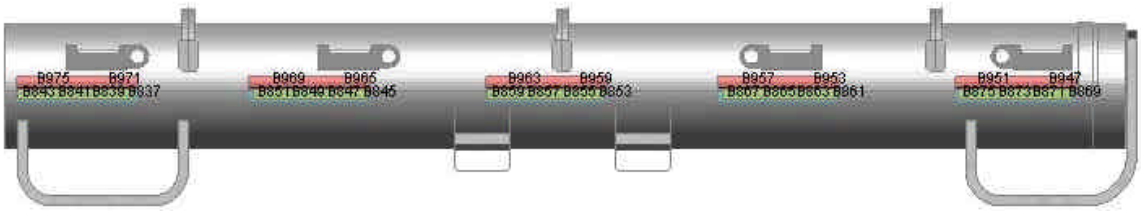

Figure 2-33 Bolt Labels for Left Outerpack

Clamshell Keeper Bolts – The inner Clamshell is restrained during shipment by eleven (11) quarter-turn latches as shown in Figure 2-34. This design was incorporated after Prototype testing, primarily for improved handling characteristics. One half of the latch, the latch handle, is welded to the one Clamshell door hinge. The portion of the latches which is physically turned to allow opening and closing is attached to the opposite door is called the "keeper." Each keeper is attached to the Clamshell door with ½-13 stainless steel bolts.

Factors-of-safety for the Clamshell keeper bolts are shown in Table 2-12. The analyses indicate that these bolts are unlikely to fail during side drops onto either the Outerpack latches or Outerpack hinges. Further, the modeling of the fuel assembly as a rigid structure likely makes little difference to these predictions since the fuel rods would not be expected to buckle in this drop orientation.

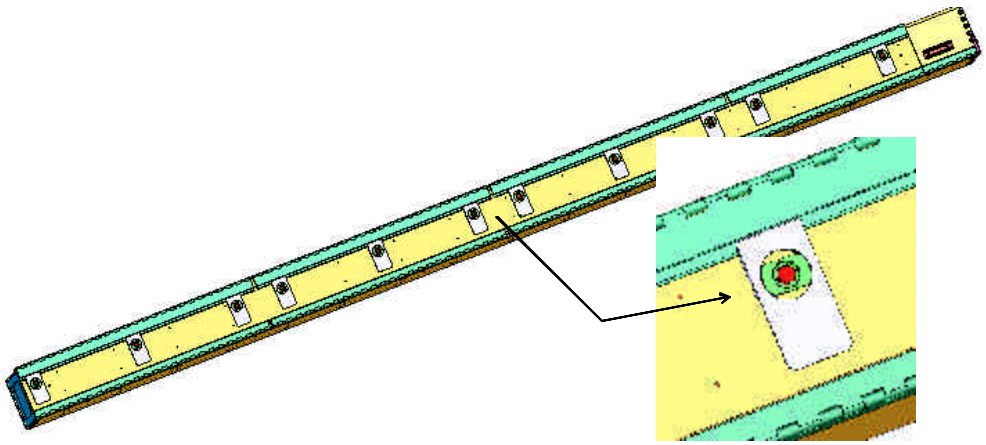

Figure 2-34 Clamshell Closure Latches and Keeper Bolts

Table 2-12 Clamshell Keeper Bolt Minimum Factors of Safety for 9m Side Drop		
ID (Figure 2-35)	**FS/Time**	
	Dropped On OP Latches (Figure 2-30B)	**Dropped On OP Hinges (Figure 2-30A)**
B6271277	2.10/0.0067 s	**1.72/0.006 s**
B6271278	2.15/0.007 s	**1.72/0.0085 s**
B6271279	3.17/0.0062 s	3.36/0.0075 s
B6271280	2.12/0.0072 s	4.40/0.01 s
B6271281	2.90/0.008 s	4.03/0.0092 s
B6271282	2.50/0.0082 s	2.48/0.0067 s
B6271283	3.70/0.0055 s	2.16/0.0067 s
B6271284	2.56/0.007 s	1.84/0.0062 s
B6271285	**1.93/0.0072 s**	2.64/0.008 s
B6271286	2.62/0.0072 s	3.00/0.0082 s
B6271287	1.94/0.0075 s	2.29/0.0082 s

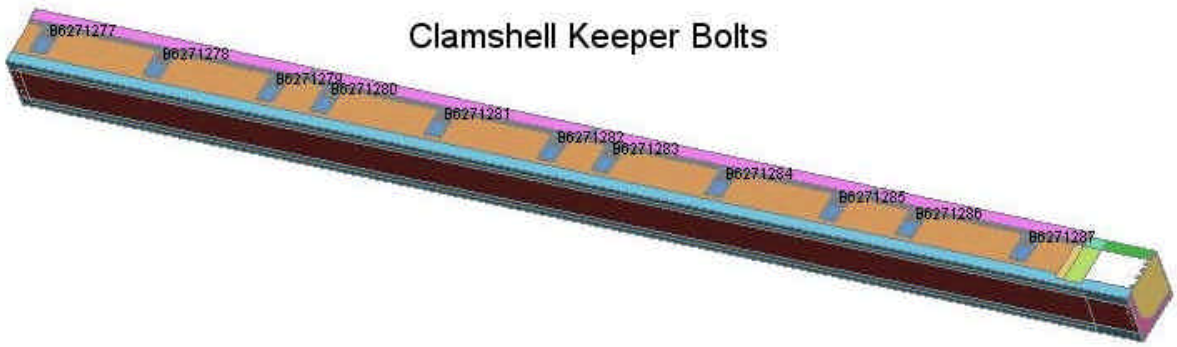

Figure 2-35 Clamshell Keeper Bolt Labels

Clamshell Top and Bottom Plate Bolts – In addition to the Clamshell latch bolts, there are thirty ½-13 stainless steel bolts securing the Clamshell top and bottom end plates. The twenty bolts securing the top end plate are distributed five per side as shown in Figure 2-36A. These bolts are not removed during normal operation and are permanently adhered to the plates. The ten bolts securing the bottom end plate are distributed equally to the two walls of the Clamshell V-shaped bottom extrusion as shown in Figure 2-36B. These bolts are also permanently adhered.

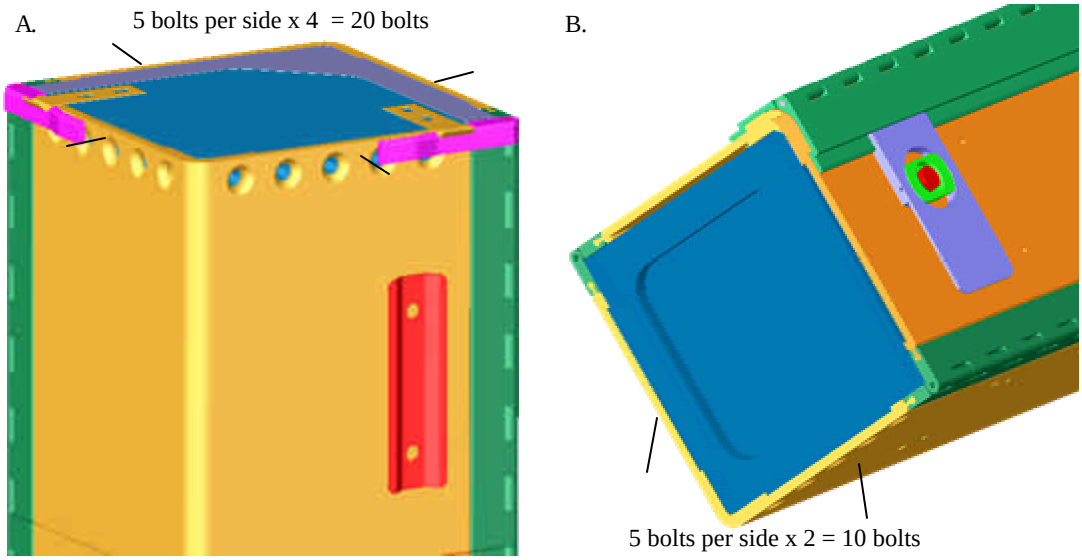

Figure 2-36 Clamshell Top and Bottom End Plates

The analyses indicates that none of the Clamshell bolts at the top and bottom ends will fail during a side drop on either the Outerpack latches or Outerpack hinges. This is evident from the minimum factors of safety shown in Tables 2-14, 2-15 and 2-16. (Our modeling of the fuel assembly as a rigid structure likely makes little difference to these predictions since the fuel rods would not be expected to buckle in this drop orientation.)

Table 2-13 Clamshell Bottom Plate Bolt Minimum Factor of Safety for 9m Side Drops

ID (Figure 2-37)	FS/Time	
	Dropped on OP Latches (Figure 2-30B)	Dropped on OP Hinges (Figure 2-30A)
B6168785	**2.39/0.0047 s**	**2.33/0.0107 s**
B6168786	2.84/0.0070 s	4.29/0.0065 s
B6168787	6.40/0.0092 s	6.96/0.0062 s
B6168788	9.56/0.0092 s	6.26/0.0062 s
B6168789	6.62/0.0190 s	3.96/0.0060 s
B6168794	3.84/0.0062 s	5.43/0.0102 s
B6168793	19.4/0.0050 s	7.61/0.0102 s
B6168792	13.5/0.0087 s	7.88/0.0102 s
B6168791	4.37/0.0065 s	3.57/0.0055 s
B6168790	2.41/0.0060 s	2.48/0.0050 s

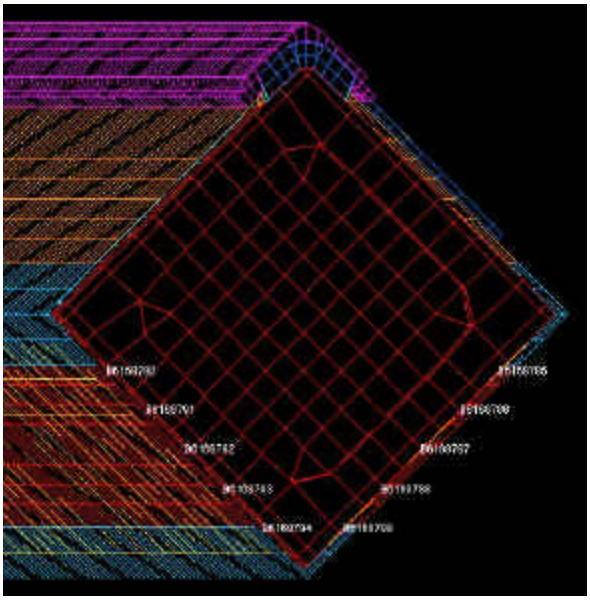

Figure 2-37 Clamshell Bottom Plate Bolt Labels

Table 2-14 Clamshell Grooved Top Plate Bolt Minimum Factors of Safety for 9m Side Drops

ID (Figure 2-38)	FS/Time	
	Dropped on OP Latches (Figure 2-30B)	Dropped on OP Hinges (Figure 2-30A)
B6168781	4.19/0.006 s	5.21/0.0052 s
B6168780	21.1/0.0065 s	12.67/0.0057 s
B6168779	32.1/0.0077 s	21.22/0.0057 s
B6168778	17.5/0.0095 s	33.37/0.007 s
B6168773	2.29/0.0065 s	**2.73/0.005 s**
B6168774	**2.25/0.0062 s**	4.97/0.0087 s
B6168775	3.88/0.0075 s	33.54/0.0092 s
B6168776	24.5/0.0057 s	52.4/0.0077 s
B6168777	13.2/0.0057 s	54.49/0.009 s
B6168769	2.99/0.0052 s	4.77/0.006 s

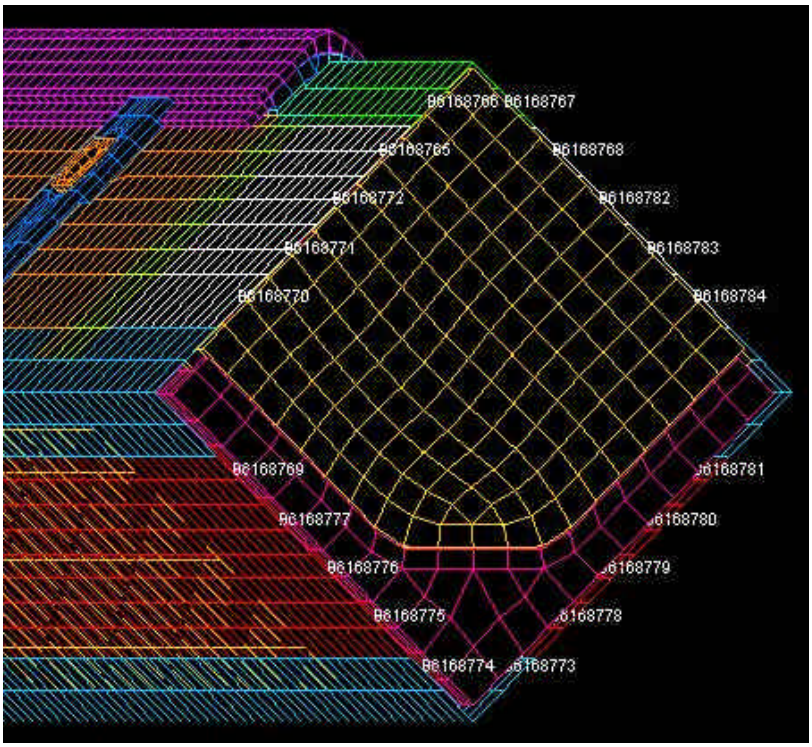

Figure 2-38 Clamshell Top Plate Bolt Labels

Table 2-15 Clamshell Lipped Top Plate Bolt Minimum Factors of Safety for 9m Side Drops

ID (Figure 2-38)	FS/Time	
	Dropped on OP Latches (Figure 2-30B)	Dropped on OP Hinges (Figure 2-30A)
B6168770	2.32/0.005 s	3.38/0.0077 s
B6168771	5.65/0.005 s	10.4/0.006 s
B6168772	5.95/0.005 s	11.6/0.007 s
B6168765	9.29/0.0085 s	18.8/0.0065 s
B6168766	7.27/0.0057 s	7.99/0.007 s
B6168767	6.54/0.007 s	6.58/0.006 s
B6168768	9.68/0.007 s	11.7/0.006 s
B6168762	9.14/0.007 s	9.16/0.006 s
B6168783	6.18/0.0085 s	5.65/0.0122 s
B6168784	4.22/0.008 s	**2.25/0.0047 s**

Clamshell Top End Plate Joint – One goal of the Traveller package design was to minimize the time and effort associated with loading and unloading the fuel. This necessitated the number of bolts that had to be removed during these operations be as kept as low as possible. To accomplish this, the top end of the Clamshell consists of two interlocking plates as shown in Figure 2-39. One of these plates is grooved and is permanently attached to the V-shaped lower portion of the Clamshell, Figure 2-36A. The other has a lip and is permanently attached to an upper housing above the Clamshell doors, Figure 2-39. This groove-and-lip design should indeed facilitate rapid loading and unloading, however, the joint must not separate to any significant extent during the HAC drop tests that the fuel rods might slip out of the Clamshell.

Fortunately, our analysis indicates that the separation during impact is small, Figure 2-40. Furthermore, the separation is transient/temporary as can be seen by the reduction in the separation distance in the later stages of the analysis, Figure 2-40B compared with Figure 2-40A. These predicted results were obtained from the analysis of the Outerpack drop onto its latches. In this case, the Clamshell latches are positioned underneath the fuel, towards the ground, Figure 2-26B. Analysis of the Outerpack drop onto its hinges yielded similar results although the predicted separation of this joint was slightly less.

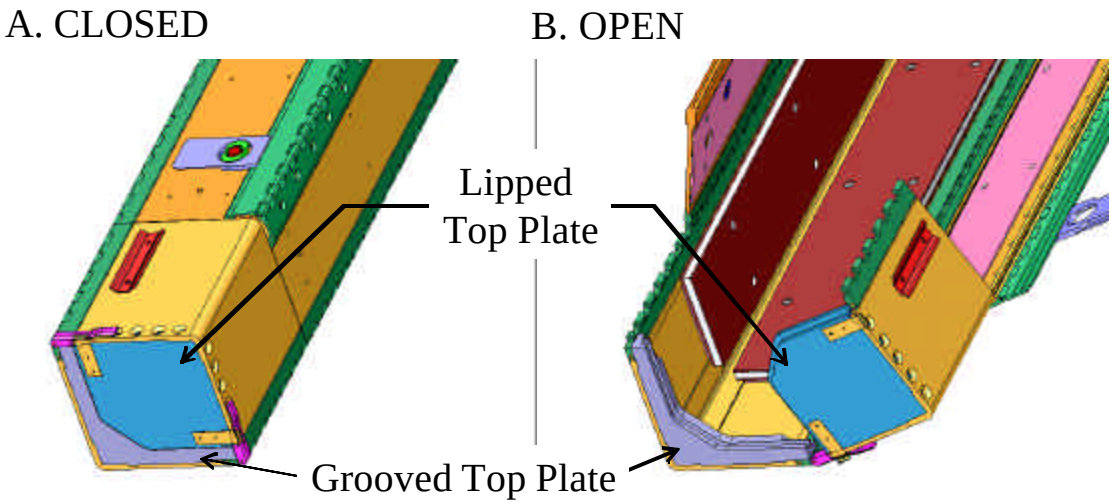

Figure 2-39 Clamshell Doors

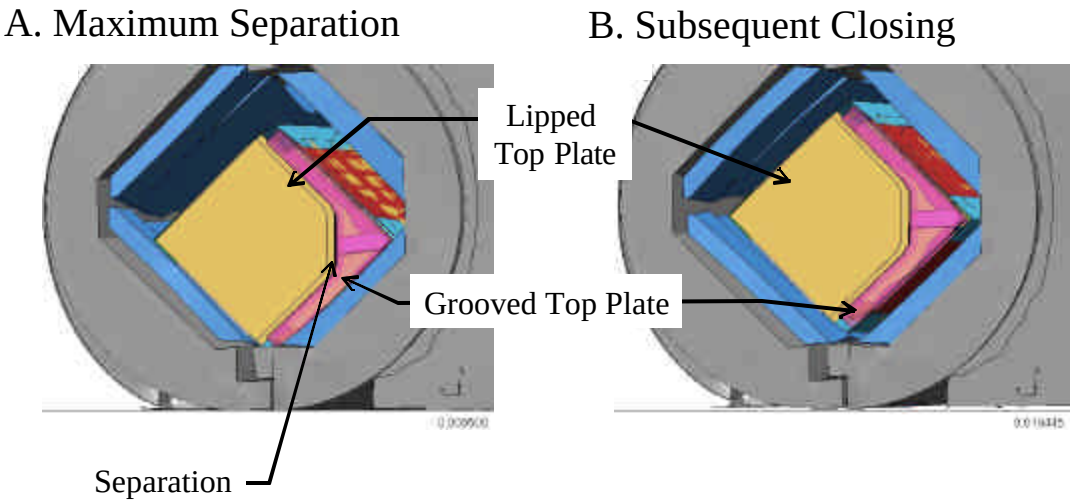

Figure 2-40 Clamshell Response during Side Drop

Clamshell Bottom End Plate/Door Joints – In keeping with the goal of minimizing the time and of loading and unloading the fuel, no bolts must be removed at the bottom end of the Clamshell during these operations. To accomplish this, the bottom Clamshell plate and doors have an interlocking feature consisting of a lip on the bottom end plate and corresponding grooves in both Clamshell doors, Figure 2-41. As described previously for the top end, these joints also do not separate to the extent that a fuel rod could slip through the opening.

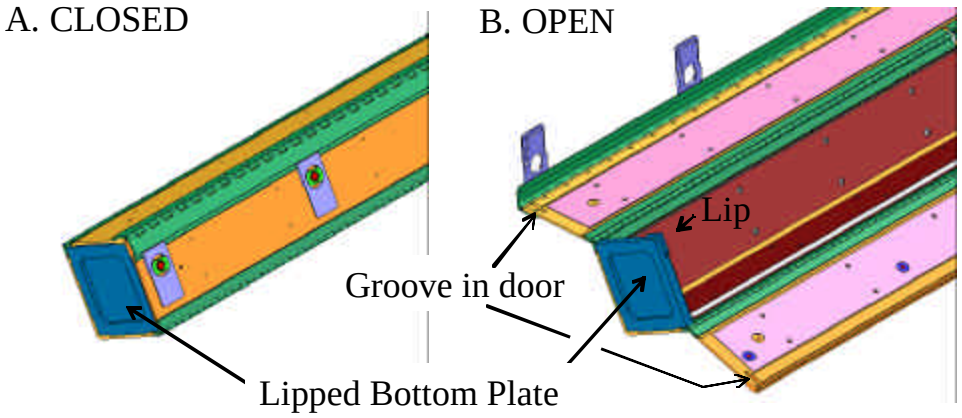

Figure 2-41 Clamshell Doors at Bottom Plate

A small separation of one of these joint during impact is predicted, Figure 2-42. Because the separation is at the upper joint is small, it is not possible that a fuel rod could slip through this joint. Furthermore, the other joint is predicted to remain closed and the bottom end plate should remain intact. These predicted results were obtained from the analysis of the Outerpack drop onto its latches. In this case, the Clamshell latches are positioned underneath the fuel, towards the ground, Figure 2-26B. As with the joint at the top Clamshell plate, the predicted separation of this joint was slightly less for a drop onto the Outerpack hinges.

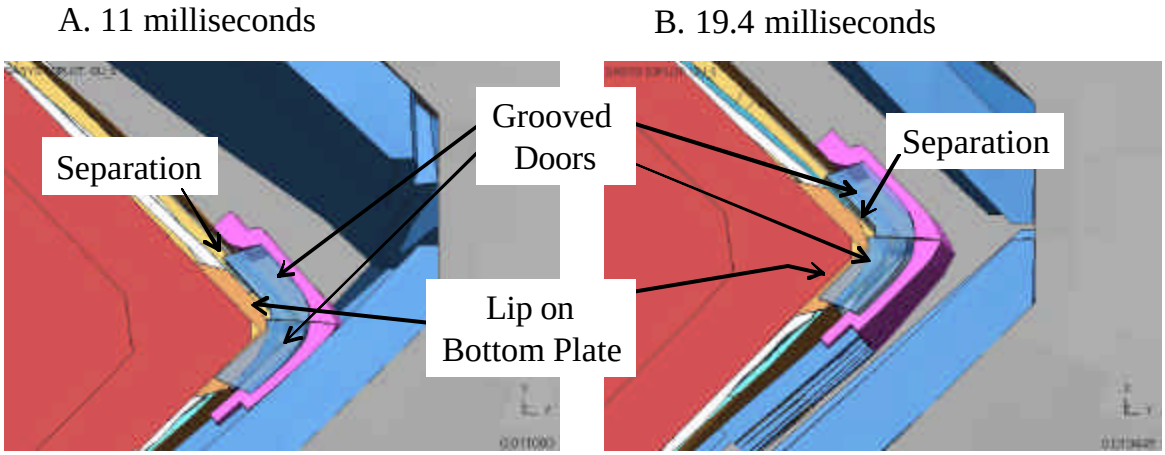

Figure 2-42 Predicted Response of Clamshell Bottom Plate and Doors During 9m Horizontal Drop onto Outerpack Latches

2.12.3.2.3 "CG-over-Corner" and "CG-forward-of-Corner" Drops onto Top Nozzle End of Package

As indicated in Figure 2-43, almost vertical orientations may result in the package center of gravity (CG) being positioned directly above the impacting corner of the package. When this occurs, the drop is designated as a "CG-over-corner" impact. In a CG-over-corner impact, the shipping package will initially continue translating in the direction of impact without rotating. However, deformation of the impacted corner may eventually result in the package tilting and falling over.

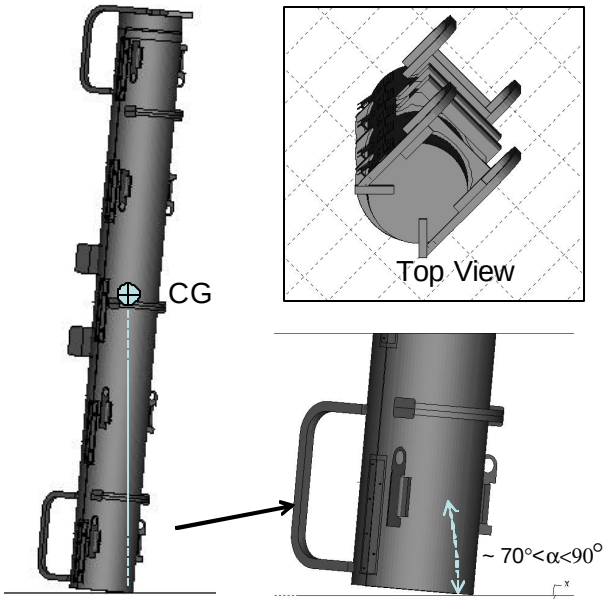

Figure 2-43 Top Nozzle Analysis Drop Orientation

CG-over-corner impacts direct all the drop energy to only a portion of the impact limiter Thus, except for a specific feature of the Traveller XL package, a CG-over-corner impact (either onto the top or bottom end of the package) would probably be the most damaging "nearly vertical" drop. However, as subsequently shown, some drops onto the top nozzle at angles that put the CG forward of the impact corner, i.e., in the "fall" direction of Figure 2-44, are predicted to be more damaging. This is because the resulting deformation involves the Outerpack top corner bending about an (imaginary) axis between the knuckles of the first hinge and latch Figure 2-45.

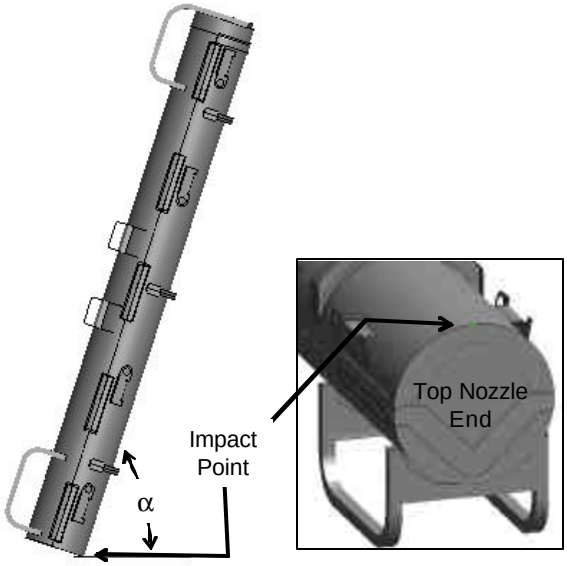

Figure 2-44 Location of Impact

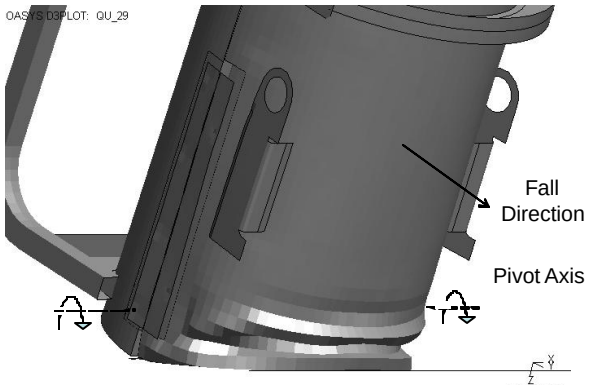

Note: the package is shown falling in a "forward" direction.

Figure 2-45 Damage to Outerpack During Angled Drop onto Top Nozzle End of Package

The most damaging drop orientation for the Outerpack is a top nozzle down, CG-forward-of-corner configuration having an 18° rotation (α=72°), see Figure 2-44. With smaller rotations, the detrimental opening of the Outerpack seam is predicted to be less despite a greater amount of energy being absorbed by the impact limiter. This is because portions of both the upper and lower Outerpack assemblies contact the drop pad and this significantly reduces their relative motion. With larger rotations, Outerpack seam opening is also predicted to be less. This is because the pivot axis moves well in front of the hinge knuckles in Figures 2-45 and 2-46.

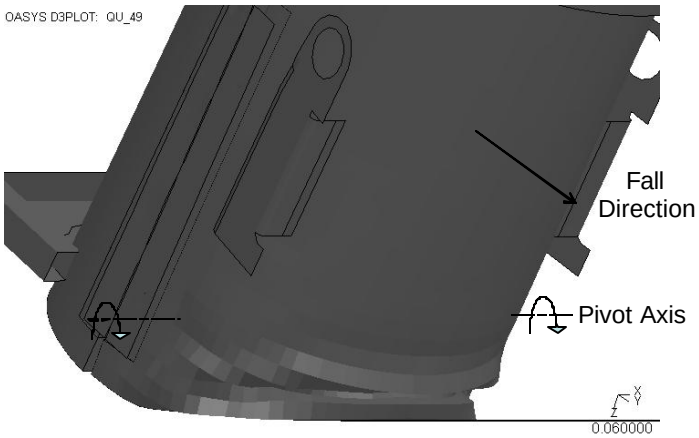

Note: the package is shown falling in a "forward" direction.

Figure 2-46 Predicted Deformation of Outerpack Top Nozzle Impact Limiter

For the subsequent 1 meter pin puncture drop, the premise is that this is the worst possible additional damage for the Outerpack seam to be further opened. Thus, the most damaging pin puncture orientation following a CG-forward-of-corner test is clearly one where the damaged face of the Outerpack is

perpendicular to the pin as depicted in Figure 2-47. The combination of these scenarios; a high angle drop followed by a pin puncture in the location of the initial impact was the basis for the QTU-1 unit testing.

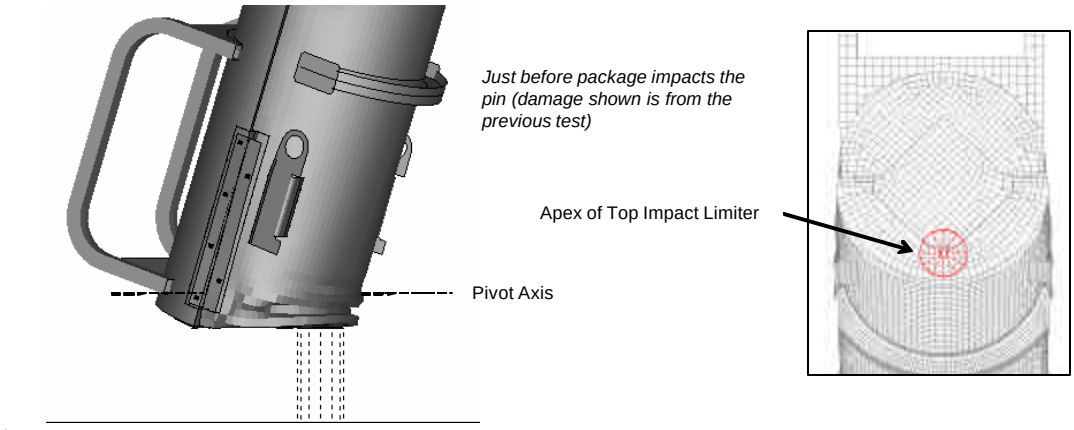

Figure 2-47 Predicted Pin Puncture Orientation after a CG-Forward-of-Corner Test

The FEA of the pin drop incorporated package deformations and stresses calculated to result from the 9m drop. The methodology for including the deformation and stresses involved defining the nodal coordinates in the pin puncture model as the deformed nodal positions of the previous analysis plus a rigid-body-rotation to locate the "model with previous damage" to the proper position/orientation for the pin puncture test. The element stresses were extracted from the first analysis and included as initial stresses in the second analysis.

Finally, from a computation standpoint, it was not practical to compute the secondary impact. This is because the secondary impact is preceded by a lengthy free-fall. Long (multi-day) computations would have been required to run an analysis through the free-fall and secondary impact. Fortunately, secondary impacts for such nearly vertical drops as this are known not to cause much additional damage. This is especially so for the Traveller XL design which will be protected by the circumferential stiffeners on the upper Outerpack. Thus, not having predictions of the secondary impact should be no limitation.

"**Worst Case Drop Angle" Determination** – As previously discussed, our damage criterion for the CG-forward-of-corner drops onto the top nozzle end of the package was the degree of separation between the upper and lower Outerpack assemblies. Three orientations: 11, 18, and 25° were investigated and it was determined that an angle of 18° resulted in the most separation, Figure 2-48.

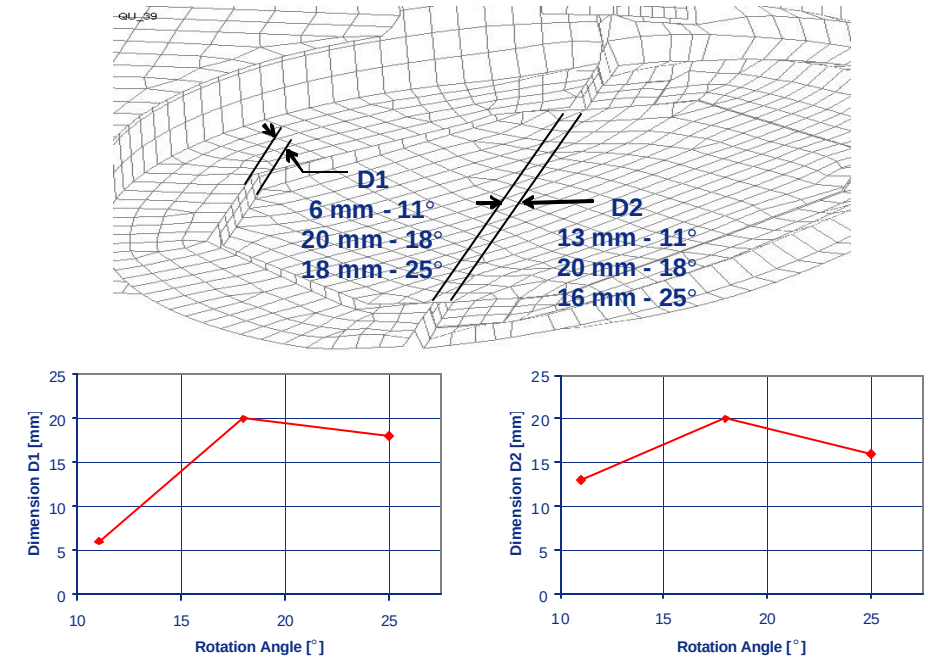

Figure 2-48 Outerpack Top Separation vs. Drop Angle

Energy and Work Histories – Predicted global energy and work histories for the primary impact of three CG-forward-of-corner drops onto the top nozzle end of the package are shown in Figure 2-49. These plots were obtained for forward rotations of 11, 18, and 25°, respectively. As before, the initial total energy (TE) of 204 kJ and increases slightly during the run in concert with the external work due to gravity. In each of these plots, the internal energy (IE) and kinetic energy (KE) traces become flat between 50-60 milliseconds into the impact event. This indicates completion of the primary impact and initiation of rollover. (Rollover and secondary impact were not numerically investigated as previously justified.) Note as drop rotation angle decreases, the internal energy absorbed by the Outerpack is predicted to increase. However, as explained earlier, this should not result in the largest Outerpack seam opening. Finally, hourglass, sliding and stonewall energies are low in each plot. This indicates overall numerically sound analyses. However, late in the analysis, hourglass energy does reach 4.1% of the total energy. While this is a low percentage, the hourglass error is concentrated in the XL pins (PID 10764) and the Clamshell cushioning pads (PIDS 2003 and 2013) in the vicinity of impact. An investigation of this error which involved using fully integrated elements found the energy previously dissipated as hourglass deformation was now (correctly) forced into the bottom impact limiter. This had only a marginal effect on the predicted force in the primary impact of Figure 2-50 and Figure 2-62. However, it did reduce predicted FA accelerations by about 17% (from the 47.3 g's shown in Figure 2-63 to 39.3 g's.). This latter effect was not significant enough to change any conclusions within the report.

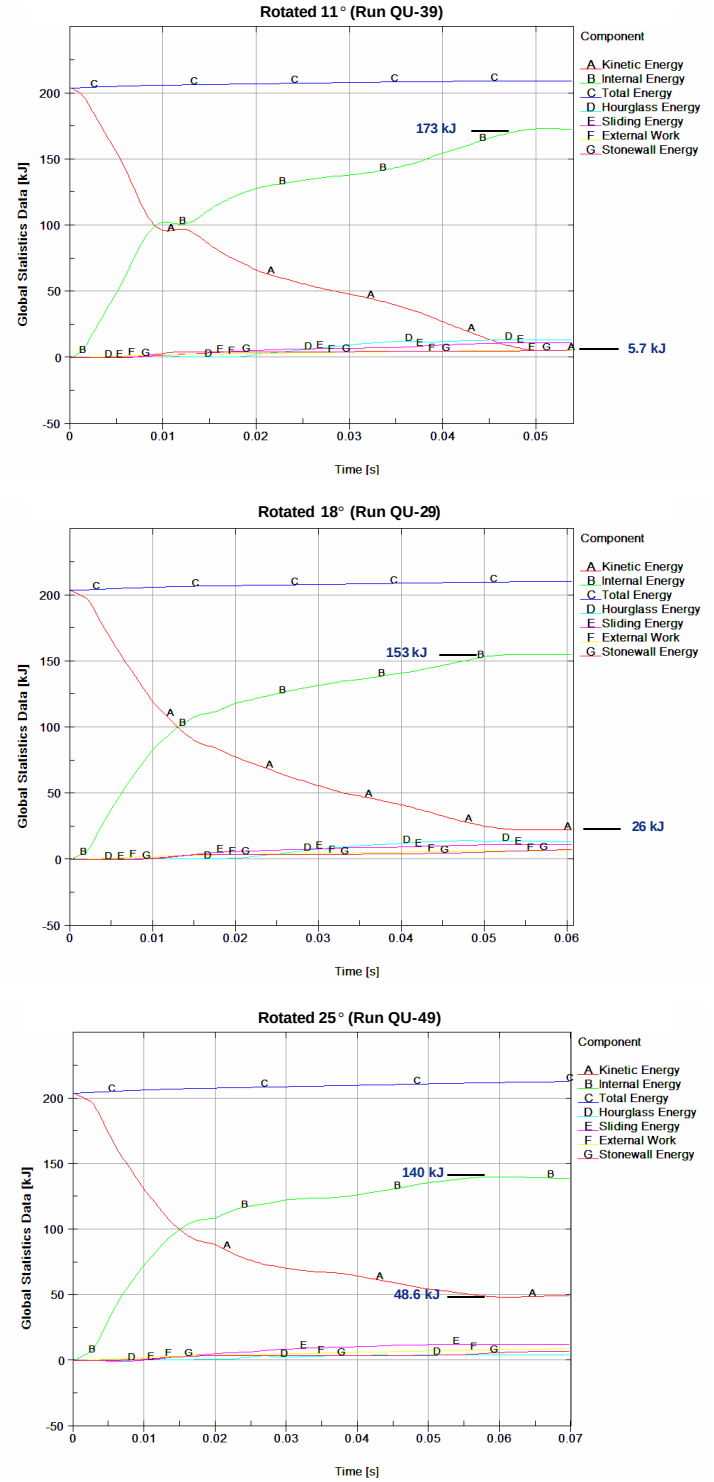

Figure 2-49 Predicted Energy and Work Histories for 9 m CG-over-Corner Drop onto the Top Nozzle End at Various Angles

Rigid Wall Forces – The predicted rigid wall force histories are shown in Figure 2-50 for CG-forward-of-corner drops on to the top end of the package rotated 11, 18, and 25°. These plots show only the primary impact (since the secondary impact due to fall-over was not calculated). The primary impact is divided into two separate events. From impact onset to approximately 25 milliseconds, the Outerpack impacts the drop pad while the Clamshell is still in free-fall. (This is due to the de-coupling between Outerpack and Clamshell previously discussed in section 2.1.1.1.1.) Secondly, the Clamshell hits the inner surfaces of the Outerpack and drives it back into the drop pad from approximately 25 milliseconds into the impact until about 70 milliseconds. Figure 2-50 shows the highest predicted loads for the Outerpack in these three orientations will be encountered at an 11° rotation. This agrees with the previous prediction that as drop rotation angle decreases, the internal energy absorbed by the Outerpack increases.

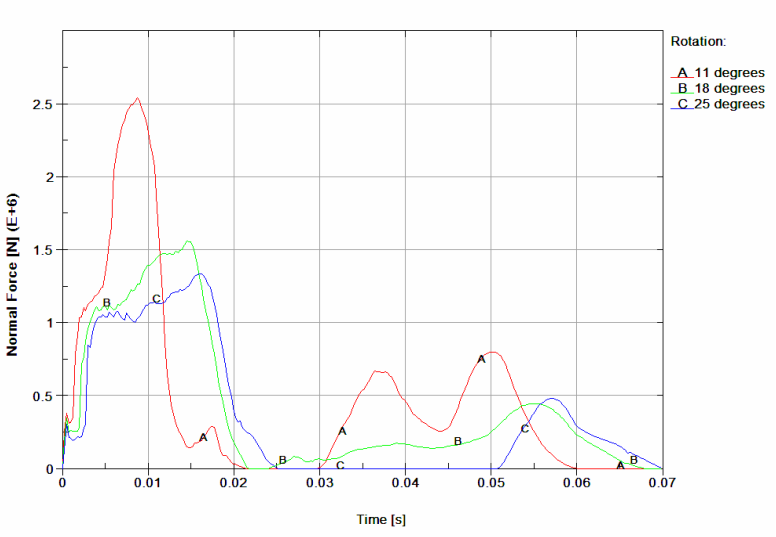

Figure 2-50 Predicted Rigid Wall Forces

As previously stated, the primary concern with CG-forward-of-corner drops onto the top nozzle end of the package is whether or not the thermal integrity needed to protect against the 30 min burn test will be compromised. It was shown that the deformation most likely to induce such damage is greatest when the Traveller XL package is rotated approx. 18° forward from a vertical orientation Figure 2-48. The main concern with the higher loads sustained and additional energy absorbed by the Outerpack at smaller rotation angles is if this jeopardized the Outerpack bolts. This issue is addressed in the following section.

Outerpack Hinge/Latch Bolts – The analysis indicates there is little likelihood of the Outerpack latch and hinge top bolts failing during a 9m CG-forward-of-corner drop onto the top end of the package. This is evident from the relatively high predicted factors of safety for these bolts, Tables 2-16 and 2-17.

Table 2-16 Top Outerpack Latch Bolt Minimum Factors of Safety for 9m CB-Forward of Corner Drops			
ID (Figure 32)	**FS/Time**		
	11° Forward Rotation	**18° Forward Rotation**	**25° Forward Rotation**
B917	3.80/0.0143 s	7.57/0.0102 s	5.08/0.0105 s
B921	3.94/0.014 s	6.89/0.0247 s	6.19/0.0102 s
B923	3.10/0.0225 s	2.63/0.0245 s	3.87/0.0245 s
B927	3.28/0.0227 s	2.70/0.0247 s	4.04/0.0262 s
B929	2.61/0.012 s	2.29/0.0112 s	2.36/0.0147 s
B933	2.45/0.0065 s	2.25/0.0112 s	2.38/0.0147 s
B935	**2.22/0.0117 s**	**2.22/0.0072 s**	**2.22/0.008 s**
B939	**2.22/0.0117 s**	**2.22/0.0072 s**	**2.22/0.0075 s**
B941	2.23/0.0032 s	2.23/0.0052 s	2.23/0.0057 s
B945	**2.22/0.0057 s**	2.23/0.0077 s	2.23/0.0097 s

Table 2-17 Top Outerpack Hinge Bolt Minimum Factors of Safety for 9m CB Forward of Corner Drops			
ID (Figure 33)	**FS/Time**		
	11° Forward Rotation	**18° Forward Rotation**	**25° Forward Rotation**
B947	3.59/0.014 s	6.37/0.0337 s	5.13/0.0105 s
B951	3.73/0.014 s	7.49/0.0232 s	6.17/0.0135 s
B953	2.95/0.0225 s	3.04/0.0245 s	4.19/0.0322 s
B957	3.19/0.0225 s	3.26/0.0245 s	4.30/0.0322 s
B959	2.65/0.0065 s	2.32/0.0115 s	2.34/0.0147 s
B963	2.51/0.0065 s	2.27/0.011 s	2.40/0.0122 s
B965	2.21/0.0062 s	2.21/0.0243 s	2.21/0.0077 s
B969	2.22/0.006 s	2.21/0.0235 s	2.23/0.0072 s
B971	**2.20/0.006 s**	**2.20/0.0095 s**	**2.20/0.0110 s**
B975	2.22/0.0055 s	2.23/0.0072 s	2.23/0.0077 s

It should also be noted that the latch and hinge bolts nearest impact were predicted to have the smallest (although still very adequate) safety factors. This is logical.

Clamshell Keeper Bolts – Our analysis indicates there is little likelihood of the Clamshell keeper bolts failing during a 9m CG-forward-of-corner drop onto the top nozzle end of the package. This is evident from the relatively high predicted factors of safety for these bolts, Table 2-18.

Table 2-18 Clamshell Keeper Bolt Minimum Factors of Safety for 9m CG-Forward-of-Corner Drops

ID (Figure 35)	FS/Time		
	11° Forward Rotation	18° Forward Rotation	25° Forward Rotation
B6271277	5.86/0.0255 s	8.71/0.038 s	10.86/0.0237 s
B6271278	5.75/0.027 s	4.79/0.0285 s	4.43/0.0277 s
B6271279	22.6/0.029 s	8.46/0.0287 s	6.63/0.0237 s
B6271280	17.4/0.0258 s	10.89/0.026 s	3.29/0.0225 s
B6271281	13.38/0.023 s	12.31/0.0522 s	7.96/0.024 s
B6271282	19.48/0.0455 s	8.13/0.0375 s	8.85/0.0282 s
B6271283	16.85/0.0207 s	5.41/0.0332 s	5.78/0.0258 s
B6271284	33.54/0.0285 s	8.89/0.0392 s	7.3/0.0252 s
B6271285	17.56/0.0405 s	11.32/0.0132 s	11.69/0.0197 s
B6271286	14.73/0.016 s	9.67/0.0415 s	8.09/0.024 s

It should be noted that the keeper bolt nearest impact was predicted to have the smallest (although still very adequate) safety factor.

Clamshell Top and Bottom Plate Bolts – The analyses indicate that none of the Clamshell bolts at the top and bottom ends will fail during a 9m CG-forward-of-corner drop onto the top nozzle end of the package. This is evident from the minimum factors of safety shown in Tables 2-19, 2-20 and 2-21. (The modeling of the fuel assembly as a rigid structure likely makes little difference to these predictions since the fuel rods would not be expected to buckle in this drop orientation.)

Table 2-19 Clamshell Bottom Plate bolt Minimum Factors of Safety for 9m CG-Forward-of-Corner Drops			
ID (Figure 37)	**FS/Time**		
	11° Forward Rotation	**18° Forward Rotation**	**25° Forward Rotation**
B6168785	**2.36/0.0495 s**	**2.38/0.0245 s**	2.50/0.0197 s
B6168786	8.27/0.0497 s	5.85/0.0243 s	4.48/0.0235 s
B6168787	100.3/0.0262 s	94.5/0.0225 s	60.8/0.0235 s
B6168788	97.8/0.0262 s	112/0.0515 s	89.5/0.0235 s
B6168789	51.1/0.0227 s	27.0/0.0230 s	43.3/0.0437 s
B6168794	40.2/0.0222 s	31.0/0.0317 s	27.7/0.0317 s
B6168793	99.9/0.0262 s	83.3/0.0305 s	59.3/0.0385 s
B6168792	100.7/0.0618 s	86.7/0.0202 s	44.2/0.0402 s
B6168791	11.2/0.0412 s	6.55/0.0202 s	7.69/0.0200 s
B6168790	2.84/0.0412 s	2.43/0.0205 s	**2.33/0.0280 s**

Table 2-20 Clamshell Grooved Top Plate Bolt Minimum Factors of Safety for 9m CG-Forward-of-Corner Drops			
ID (Figure 38)	**FS/Time**		
	11° Forward Rotation	**18° Forward Rotation**	**25° Forward Rotation**
B6168781	2.33/0.0182 s	2.29/0.0187 s	2.31/0.0197 s
B6168780	3.86/0.0397 s	5.32/0.0200 s	4.32/0.0200 s
B6168779	2.84/0.049 s	6.08/0.0510 s	12.06/0.0217 s
B6168778	2.31/0.039 s	2.34/0.0447 s	2.37/0.0470 s
B6168773	2.25/0.0367 s	2.26/0.0430 s	2.26/0.0410 s
B6168774	**2.23/0.0367 s**	**2.22/0.0427 s**	**2.22/0.0410 s**
B6168775	2.31/0.0387 s	2.30/0.0435 s	2.32/0.0467 s
B6168776	2.91/0.0485 s	5.39/0.0555 s	9.58/0.0465 s
B6168777	7.04/0.0495 s	6.20/0.0467 s	4.84/0.0205 s

Table 2-21 Clamshell Lipped Top Plate Bolt Minimum Factors of Safety for 9m CG-Forward-of-Corner Drops			
ID (Figure 38)	**FS/Time**		
	11° Forward Rotation	**18° Forward Rotation**	**25° Forward Rotation**
B6168770	1.76/0.0165 s	1.81/0.0180 s	1.77/0.0195 s
B6168771	1.79/0.0207 s	1.77/0.0177 s	1.75/0.0197 s
B6168772	1.78/0.0360 s	1.76/0.0477 s	1.80/0.0117 s
B6168765	1.76/0.0350 s	1.76/0.0170 s	1.73/0.0135 s
B6168766	1.77/0.0125 s	1.77/0.0150 s	**1.72/0.0125 s**
B6168767	1.78/0.0200 s	**1.75/0.0150** s	**1.72/0.0127 s**
B6168768	1.77/0.0362 s	1.76/0.0152 s	1.76/0.0277 s
B6168762	1.76/0.0362 s	1.77/0.0510 s	1.76/0.0187 s
B6168783	1.77/0.0192 s	1.77/0.0155 s	1.77/0.0202 s

Clamshell Top End Plate Joint – The analyses indicate the Clamshell top end plate joint (Figure 2-39) will separate slightly, but not come completely apart during CG-forward-of-corner impacts. In particular, the lip on the top plate is predicted to remain within the groove in the V-shaped top plate along both edges but slip completely out in the middle. This is shown in Figure 2-51 for the CG-forward-of-corner drop rotated 11°. It should be noted that this separation is predicted to be permanent, not transient. It should also be noted that predicted deformations were similar but lesser for CG-forward-of-corner drops rotated 18° and 25°. However, in these latter two orientations, the lip on the top plate is predicted to remain within the groove in the V-shaped top plate along its entire length. **This extent of deformation was not observed in full-scale testing of Traveller XL prototypes and is therefore conservative**.

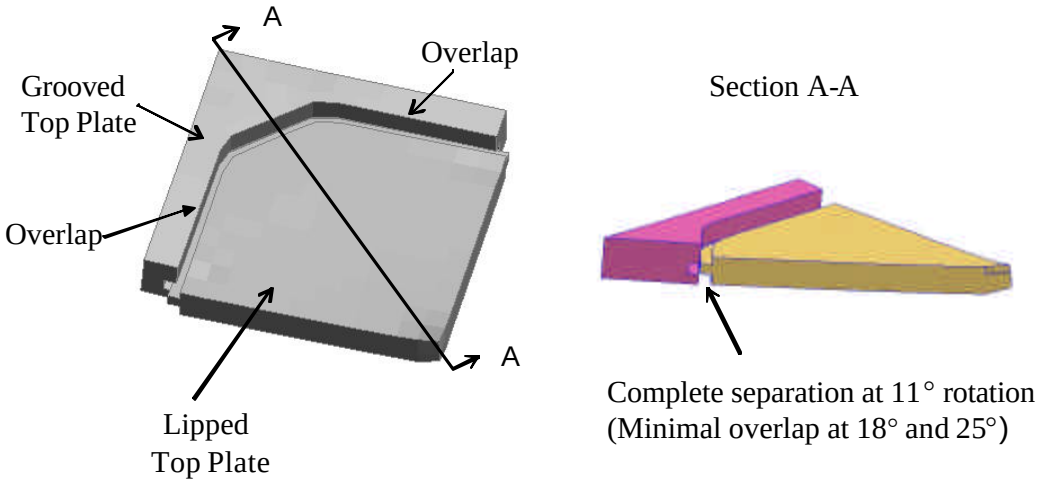

Figure 2-51 Clamshell Top Plate Geometry

Clamshell Bottom End Plate/Door Joints – The analyses indicated the Clamshell bottom end plate is minimally loaded during CG-forward-of-corner drops onto the top end of the shipping package. These trivial loads are not reported herein.

In summary, horizontal side drops onto the Outerpack hinges/latches result in the highest predicted Outerpack loads. Even so, a CG-forward-of-corner drop onto the top nozzle end of the package with 18° forward rotation, Figure 2-48 is predicted most damaging to the Outerpack. This is because the predicted opening of the seam between the upper and lower Outerpack assemblies may compromise the ability of the Traveller XL shipping package to withstand the 30 minute HAC burn test. Drop test are described in appendix 2.12.4 and the fire test are described in section 3 demonstrated that this was not a serious concern.

2.12.3.2.4 Orientation Predicted Most Damaging to the Fuel Assembly

Determining the drop orientation most damaging to a fuel assembly is greatly facilitated by the geometry of the assembly itself. In particular, the fuel rods within a fuel assembly are very long (4.4 m or more), slender (approx. 9 mm), and relatively flexible. Thus, they are quite susceptible to buckling. For this reason, our hypothesis is that drop orientations which impart the highest axial loads to the assembly are most damaging. Buckling of the fuel rods is also of paramount importance with respect to criticality safety. For criticality safety, fuel rods must not be allowed to buckle in a configuration which results in an unsafe nuclear condition. See Section 6 for a complete description of the criticality safety of the Traveller packages.

Obviously, highest axial loads are generated by vertical or nearly vertical loadings. Near-vertical orientations may impart higher loads to a portion of the fuel rods than the average load applied to a fuel rod in truly vertical drops. However, in these orientations, the adjacent rods or Clamshell structure will provide lateral support. Thus, our focus was entirely on (truly) vertical drops for fuel assembly damage, Figure 2-52. Vertical orientations result in higher impact loads because the larger footprint impacts the ground and therefore the system is stiffer than a high angle orientation where the initial contact is a point which "grows" a footprint.

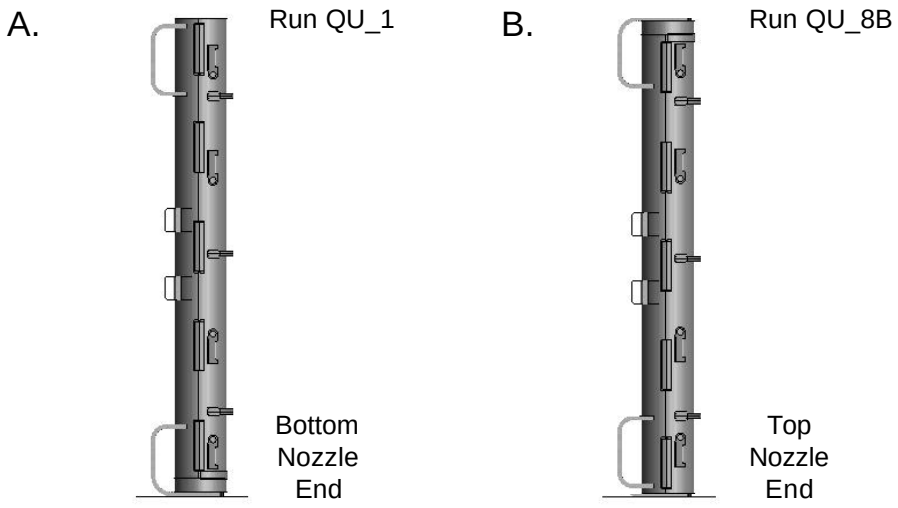

Figure 2-52 Traveller Drop Orientations Analyzed For Maximum Fuel Assembly Damage

The tendency of the fuel rods to buckle proved a severe modeling limitation because post-buckling behavior was simply beyond our current modeling capability. Post-buckling involves one or more buckled fuel rods impacting a nearby rod or Clamshell wall. These collisions involved a large momentum transfer because the fuel rods are so heavy. In our model, the mesh of the walls and nearby rods and was simply not capable of properly absorbing this energy. The result was the analysis aborted almost immediately once any fuel rods buckled. This was due to "negative volumes" (highly distorted solid elements) which resulted from the inability of the Clamshell walls, as meshed, to properly absorb the momentum transferred from the fuel rods. This occurred in all analyses we attempted and often with as much as 30 percent of the drop energy not yet absorbed. The mesh of the surrounding structure was simply not capable of properly absorbing this energy. Successful resolution of this problem would have required significantly finer meshes of both the fuel rods and surrounding structure and perhaps many other changes. From a practical standpoint, this level of analysis is beyond the capabilities of current computer systems. Rather, the fuel rods and associated fuel assembly structure (i.e., the grids), except for the top and bottom nozzles, were converted into a rigid part using the LS-DYNA® deformable-to-rigid option. This prevented the fuel rods from buckling and eliminated the associated problems with negative volumes allowing an analysis that absorbed all the available energy.

This approach prevented any associated loading of the structure surrounding the sides of the fuel assembly (the Clamshell walls), forfeiting the ability to predict the maximum loads and stresses on the Clamshell walls and latches in regions adjacent to the fuel rods. Since the fuel nozzles and other structures near the Clamshell top and bottom ends were kept deformable, Clamshell loads and stresses at the ends of the Clamshell were still fairly accurate. Further, the energy not transferred to the Clamshell walls was now forced into other structures – primarily the fuel assembly nozzles (which were kept deformable) and the end impact limiters in the case of axial drops. Thus, our analyses should be non-conservative for Clamshell regions adjacent to the fuel rods, accurate for the Clamshell top and bottom ends, and probably overly conservative for the displacements in the Outerpack impact limiters.

2.12.3.2.5 Vertical Drops

Our analysis determined that a vertical drop onto the bottom end of the package would be more damaging to the fuel assembly than a drop onto the top end. This is because the Clamshell is subjected to larger impact forces and the fuel assembly must withstand larger accelerations.

Energy and Work Histories – Global energy and work for vertical drops onto the top and bottom end of the package are shown in Figures 2-53 and 2-54, respectively. As before, both plots have an initial total energy (TE) of 204 kJ. The total energy rises slightly, reflecting the external work done by the package under gravity loading. Hourglass, sliding, and stonewall energies were small relative to the total energy. This indicates a good overall numerical analysis was obtained in both simulations.

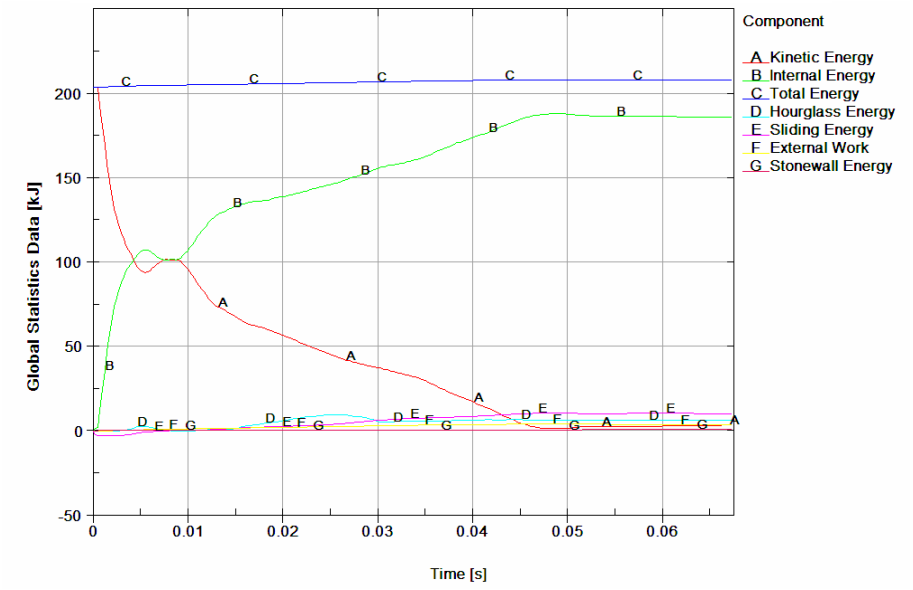

Figure 2-53 Predicted Energy and Work Histories for a 9m Vertical Drop Onto the Top Nozzle End of the Package

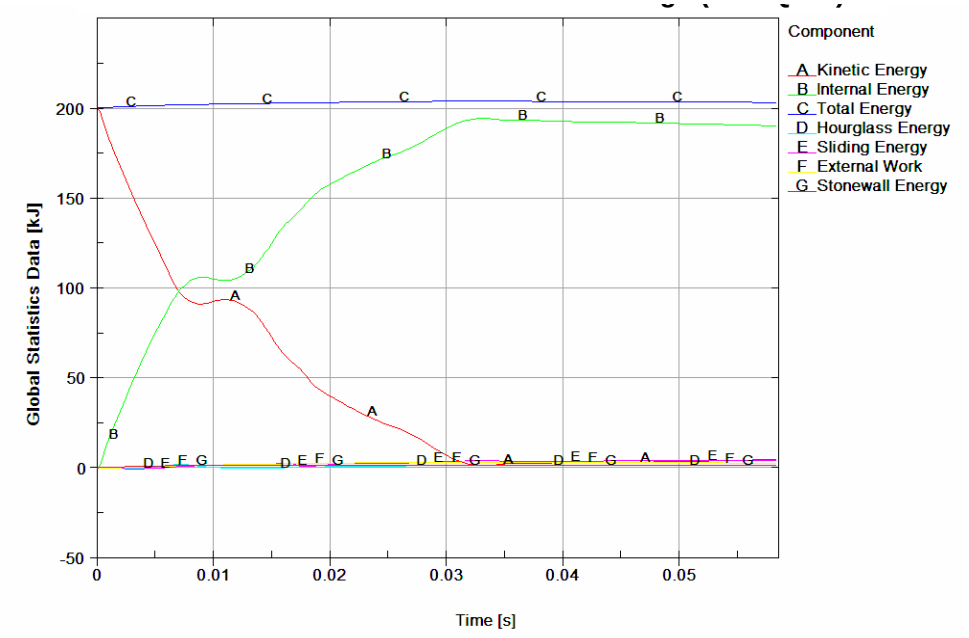

Figure 2-54 Predicted Energy and Work Histories for a 9m Vertical Drop Onto the Bottom Nozzle End of the Package

Rigid Wall Forces – Predicted force histories between Outerpack and drop pad are shown in Figure *2-49* for top and bottom end vertical drops. The near de-coupling of the Clamshell and Outerpack is clearly evident in both simulations. In the drop onto the bottom end of the package, the initial impact between

Outerpack and drop pad has a 12 milliseconds (approx.) duration. The Clamshell is not involved in this impact as it is still in free-fall (neglecting the small forces of the shock mounts.) At approximately 15 milliseconds into the simulation, the Clamshell contacts the inner surface of the bottom impact limiter and pushes it back into the drop pad. The Clamshell and Outerpack impact further into the drop pad while the fuel assembly is now essentially decoupled from the Clamshell and still in free-fall. As the Outerpack and Clamshell begin to re-bound (at ~25 milliseconds into the simulation) the fuel assembly impacts the Clamshell and all three components (Outerpack, Clamshell and fuel assembly) crash back into the drop pad. The shipping package begins to rebound at approximately 31 milliseconds into the simulation and has left the drop pad after 45 milliseconds. A similar scenario is evident for the vertical drop onto the top nozzle end of the package.

Referring to Figure 2-55, it is noted that the predicted maximum Outerpack load for the top end drop is more than 2X that for the bottom end drop (5.1 versus 2.5 MN, respectively). This shows the higher cushioning capability of the bottom impact limiter design. Further, this indicates that bolts in the Outerpack hinges and latches in the vicinity of impact will be loaded more significantly in a vertical drop onto the top end of the package. Finally, the predicted 5.1 MN load on the Outerpack for a vertical top end drop is still 2-3X less than that predicted for horizontal side drops, Figure 2-29.

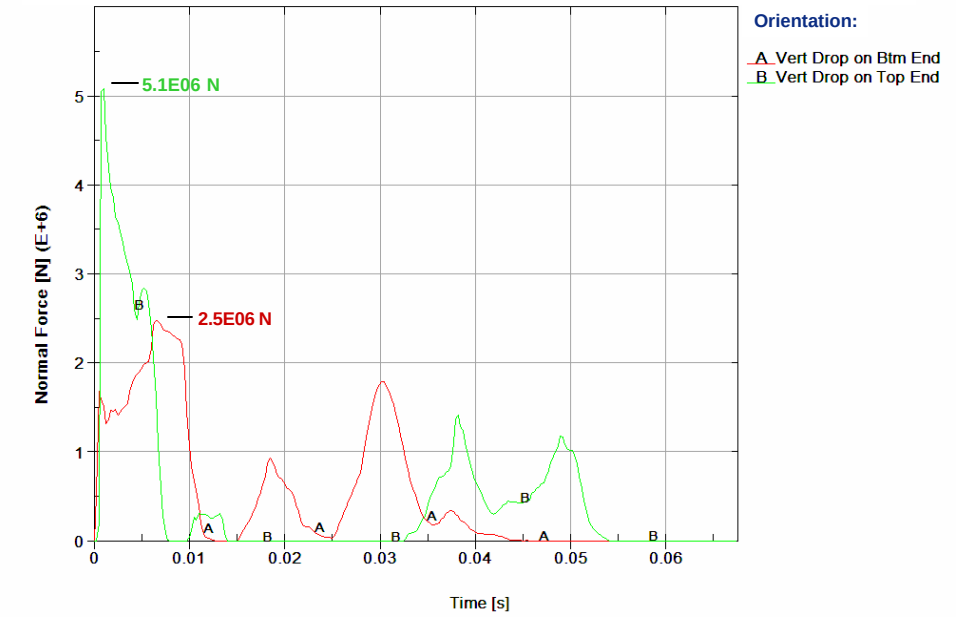

Figure 2-55 Predicted Rigid Wall Histories for 9m Vertical Drops onto the Bottom (QU-1) and Top (QU-8B) Ends of the Package

Clamshell Loads and Accelerations – The force between Clamshell and impact limiter was determined for vertical drops by specifying contacts between the CS top and bottom plates and the innermost impact limiter covers. For drops onto the top end of the package, this required defining contacts between the two CS top plates (the grooved and the lipped plate) and the innermost plate of the top impact limiter and summing the predicted forces. This technique was only used for vertical drops because these are the only

drop orientations in which the Clamshell impacts into only one surface.

Results are shown in Figure 2-56 (for the primary impact only as previously explained.) Note that the force is zero until almost 9 milliseconds into the drop simulation (which starts right before the Outerpack hits the drop pad. This is the time it takes the Clamshell to fall through the approximate 120 mm sway space separating the Clamshell and inner and the top and bottom impact limiters.

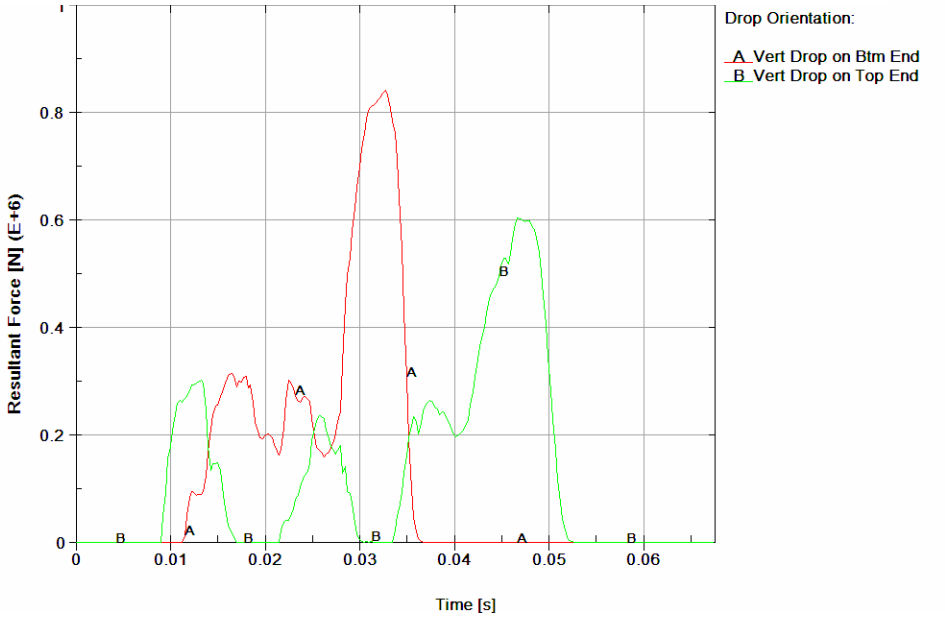

Figure 2-56 Predicted Force Between Clamshell and Impact Limiter for 9m Vertical Drops

Note also in Figure 2-56 that drops onto the bottom end of the package are more severe for the Clamshell than those onto the top end. Indeed, predicted CS loads for vertical drops onto the top and bottom end of the package are, respectively, 605 and 843 kN. These loads resulted in higher accelerations for the fuel assembly (FA) as well. As shown in Figure 2-57, predicted FA accelerations are 102 and 126 g's, respectively, for drops onto the bottom and top ends of the package.

The predicted sequence for a drop onto the bottom nozzle end of the package is shown in Figure 2-58. Impact between the Clamshell and inside covering of the bottom impact limiter occurs at approximately 13 milliseconds into the simulation; the maximum load between CS and bottom impact limiter is predicted to occur at approx. 33 milliseconds; and, the Clamshell is in full rebound by 40 milliseconds. Note the predicted crushing of the bottom nozzle legs shown in Figure 2-58.

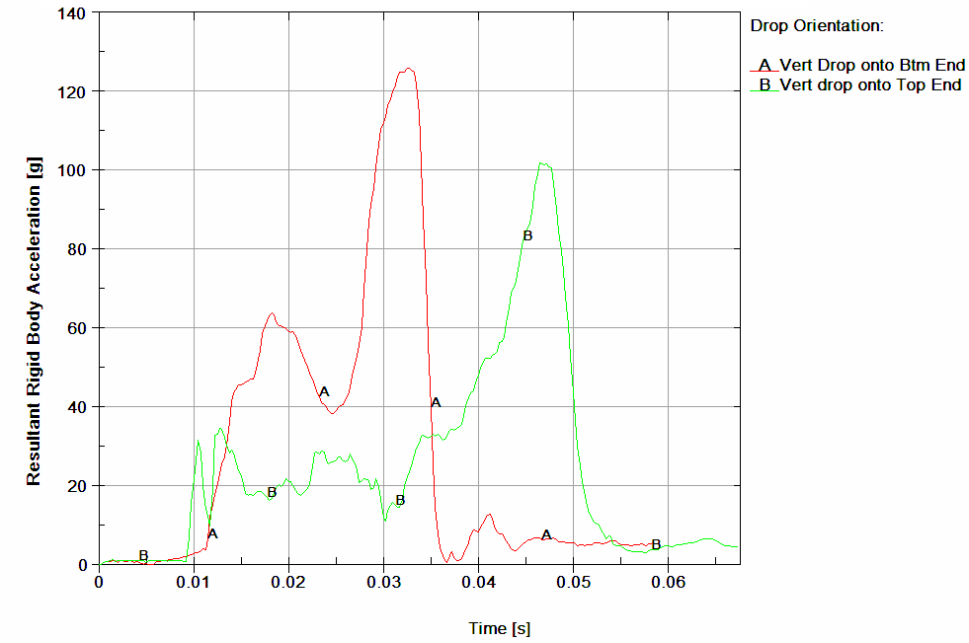

Figure 2-57 Predicted Fuel Assembly Accelerations for 9m Vertical Drops

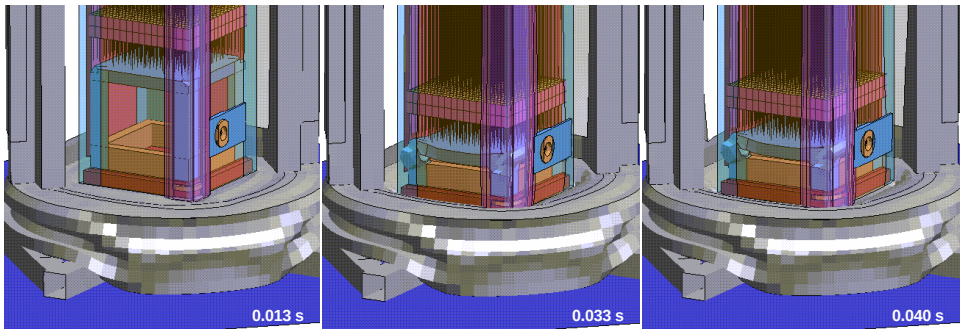

Figure 2-58 Impact Between Clamshell and Bottom Impact Limiter for Vertical Drop onto Bottom End of Package

It is interesting to note the Clamshell and top impact limiter are predicted to collide three times during the primary impact of top end drops. These impacts are depicted in Figures 2-59, 2-60 and 2-61. As shown in Figure 2-59, the first impact involves the Clamshell hitting the top impact limiter from free-fall (at ~9 milliseconds) and the XL pins and top nozzle hold-down posts buckling under the load of the fuel assembly until the top nozzle slides off the hold-down posts (at ~17 milliseconds.) The Clamshell now begins to rebound and leaves the top impact limiter. However, as shown in Figure 2-60, the fuel assembly continues its downward motion and the top nozzle contacts the midsection of the hold-down posts at about 21.5 milliseconds. At approximately 30.5 milliseconds, Figure 2-60, the hold-down posts are predicted to break near their connection to the cross member connecting them. Then, the fuel assembly

pushes the Clamshell back into the top impact limiter. This momentarily removes the fuel assembly loading from the Clamshell and it no longer is pushed into the Outerpack. However, the FA continues falling and the top nozzle begins pushing into the cross member at approximately 33.5 milliseconds. The FA continues its downward fall until motion is arrested at approximately 53 milliseconds, Figure *2-61*.

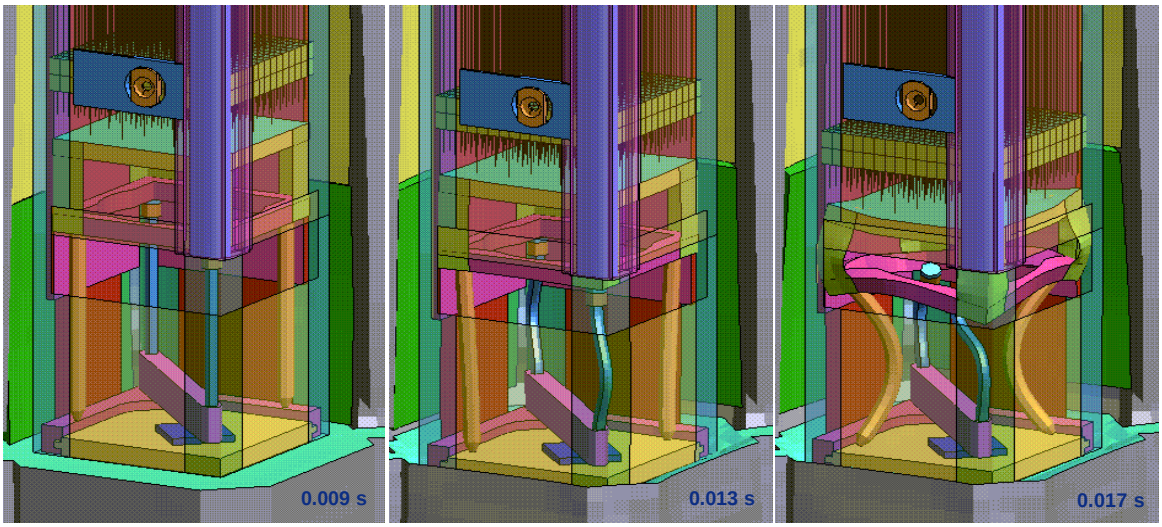

Figure 2-59 First Impact Between Clamshell and Top Impact Limiter for Vertical Drop onto Top End of Package

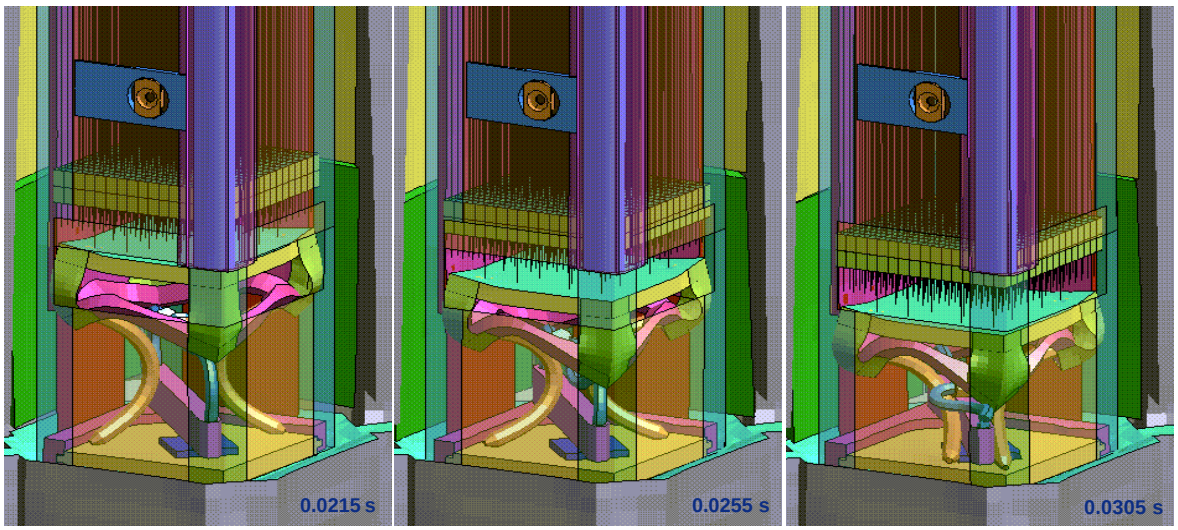

Figure 2-60 Second Impact Between Clamshell and Top Impact Limiter for Vertical Drop onto Top End of Package

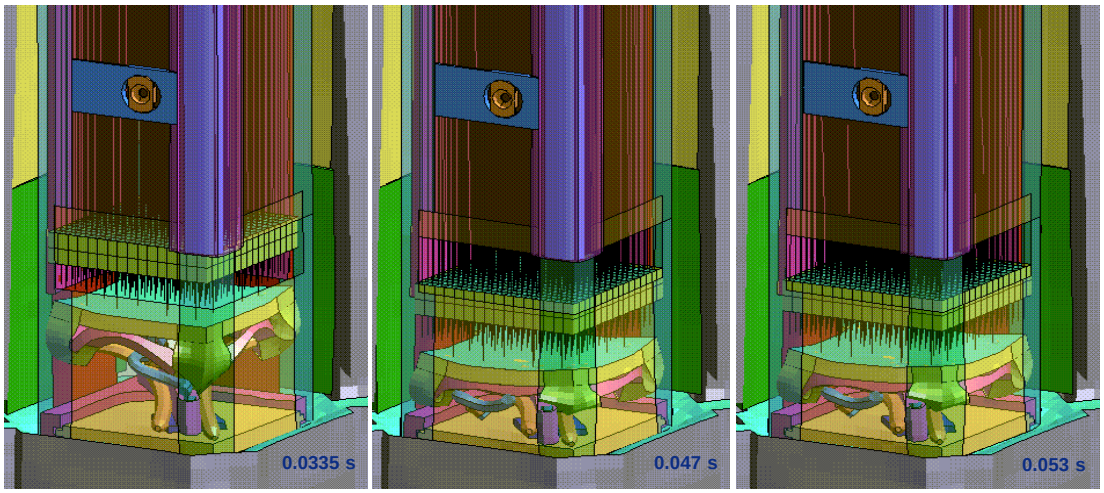

Figure 2-61 Third Impact Between Clamshell and Top Impact Limiter for Vertical Drop onto Top End of Package

From the results shown in this section, we conclude that a CG-forward-of-corner drop onto the top nozzle end of the package with an 18° forward rotation, Figures 2-44 and 2-45 is most damaging to the Outerpack. Further, as also shown, we conclude that the drop most damaging to a fuel assembly is a vertical one onto the bottom nozzle end of the package, Figure 2-52A. Thus, successful drop tests in these two orientations are an adequate demonstration that the Traveller XL design meets/exceeds the HAC drop test requirements.

2.12.3.2.6 Temperature and Foam Density Effects

The Traveller XL package must be capable of passing the HAC drop tests at any temperature within the range -40 to 160°F. Furthermore, foam crush strength is also directly related to foam density. The drop orientation previously determined most damaging to the Outerpack was selected to study the effect of temperature and density (the 9 meter CG-forward-of-corner drops onto the TN end of package with an 18° forward rotation, Figure *2-44*). Our finding is that a Traveller XL package with nominal foam density and at "normal temperature" (75°F) experiences slightly higher Outerpack loads when dropped in this orientation compared with packages containing low density foam and dropped at 160°F or containing high density foam and dropped at -40°F, see Figure *2-62*. In particular, the predicted maximum Outerpack load for the 75°F temperature/nominal density scenario is 1.69 MN. This is 8.5% more than the maximum load predicted for the -40°F/high density scenario and 13.7% more than that for the 160°F/low density scenario. Our analyses also indicates fuel assemblies in packages containing the highest allowable density foam and dropped at the lowest temperature extreme will experience accelerations that are very similar to those in packages with lowest allowable density foam and dropped at the highest temperature extreme, see Figure *2-63*. However, the accelerations at these extremes are only 5% greater than for a package dropped at 75°F containing nominal density foam. Thus, temperature and foam density have a minor effect on drop performance of the Traveller XL package.

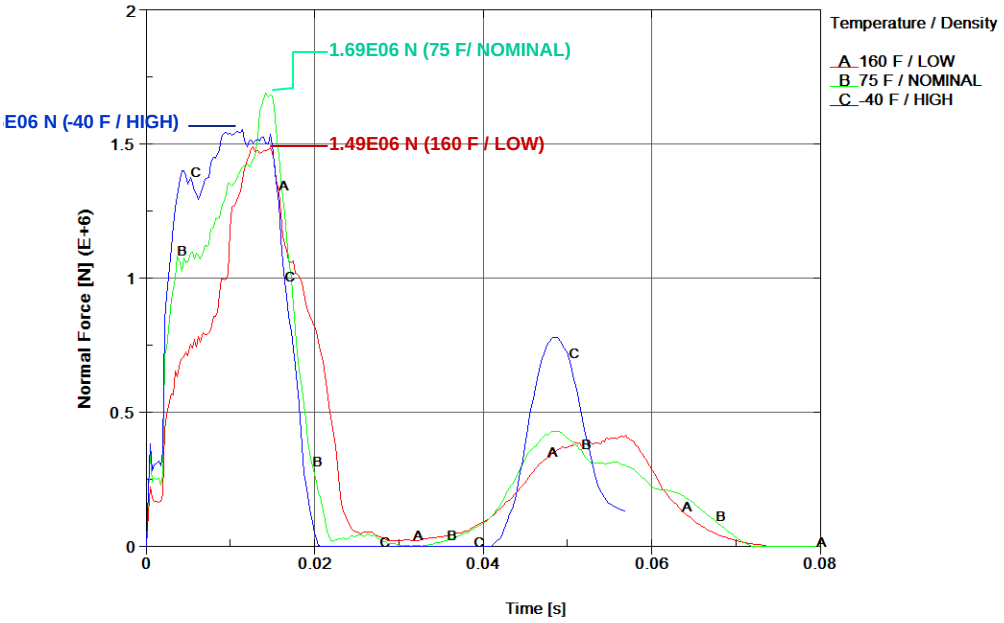

Figure 2-62 Predicted Temperature and Foam Density Effect on Outerpack/Drop Pad Interface Forces (9m CG-Forward-of-Corner with 18° Rotation Drop onto the Top End of the Package)

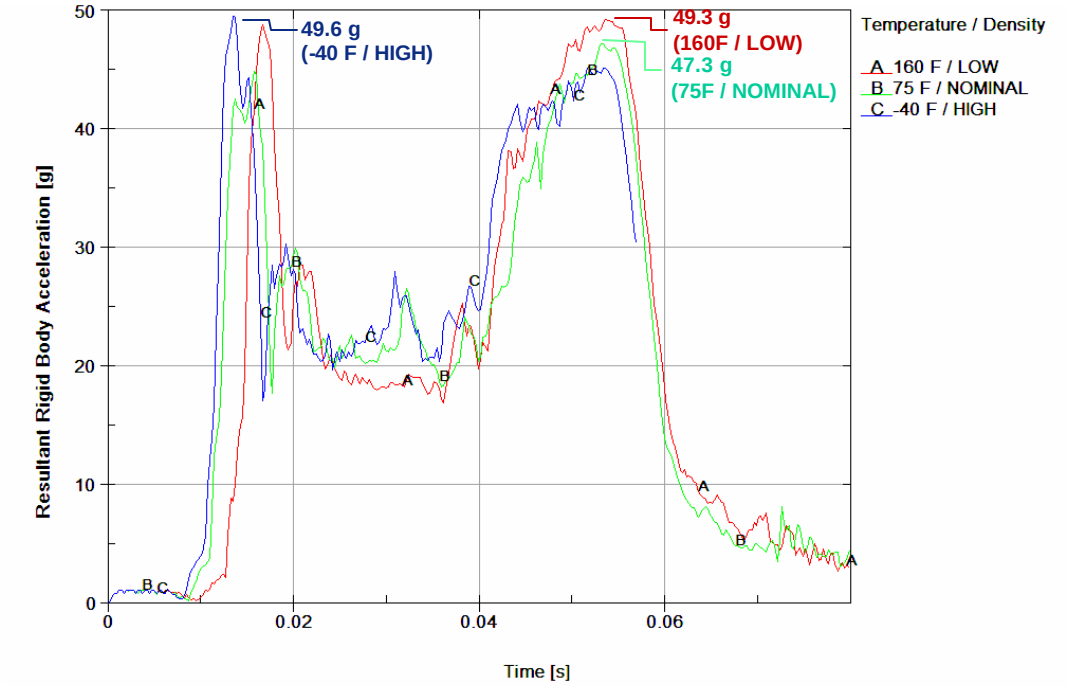

Figure 2-63 Predicted Temperature and Foam Density Effect on Outerpack/Drop Pad Interface Forces (9m CG-Forward-of-Corner with 18° Rotation Drop onto the Top End of the Package)

In addition, the 9 meter vertical bottom-end down drop was analyzed using material properties for -40°C (-40°F) with foam density at the upper end of the tolerance band and 71°C (160°F) with foam density at the lower end of the tolerance band. The predicted results were compared with each other and with those at 24°C (75°F) and nominal foam density previously reported in Section 2.12.3.2.5. The results support the conclusions obtained from analysis of the 9 meter CG-forward-of-corner drops: temperature and variation in foam density due to manufacturing tolerances have only a minor effect on the drop performance of the Traveller package.

Temperature/foam tolerance effects for the 9 meter vertical drop onto the bottom nozzle end of the package were evaluated for the three previously noted conditions. Both predicted outerpack/drop pad force histories and fuel assembly accelerations were compared as shown in Figures 2-63A and 2-63B.

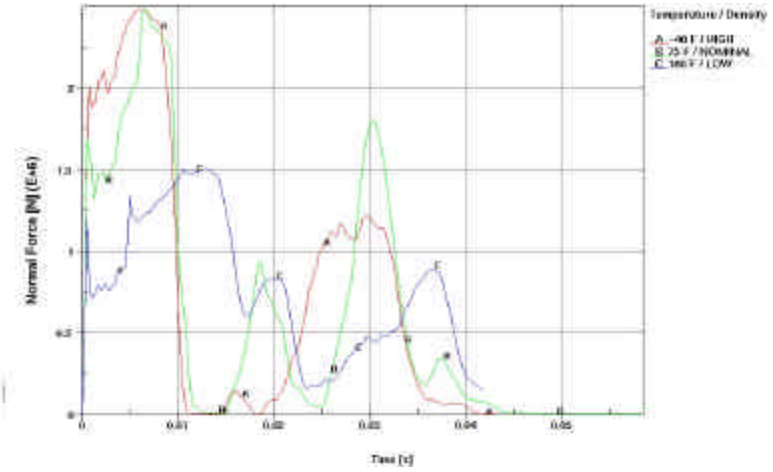

Figure 2-63A Predicted Temperature and Foam Density Effect on Outerpack/Drop Pad Interface Forces (9m Vertical Drop onto the Bottom End of the Package)

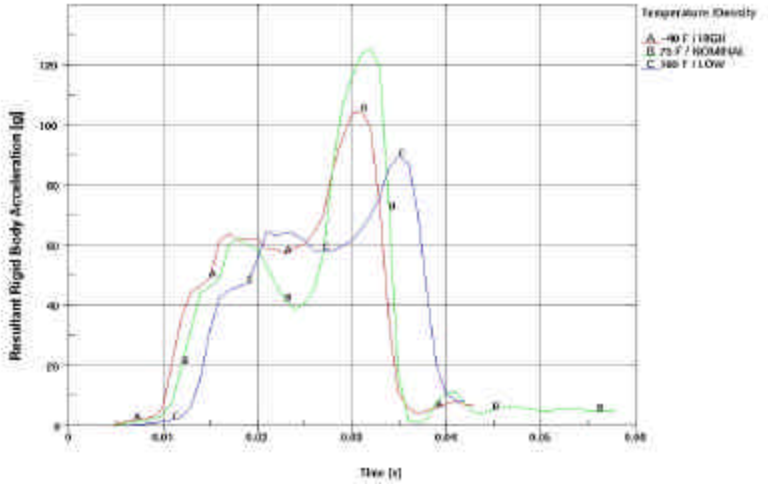

Figure 2-63B Predicted Temperature and Foam Density Effect on Fuel Assembly Acceleration (9m Vertical Drop onto the Bottom End of the Package)

Both of these figures predict that the highest forces occur when the package is 24°C (75°F) with the package having nominal foam density. (This does not necessarily mean that a package dropped at 24°C/75°F having foam densities at either the high or low end of the tolerance band would have had lower outerpack/drop pad forces and lower FA accelerations since that was not investigated.) In particular, the predicted maximum outerpack load for the 75°F (24°C)/nominal foam density scenario was 2.5E6 N. This was equal to that predicted for -40°C (-40°F) with foam density at the upper end of the tolerance band and about 67% greater than the 1.5E6 N load predicted for 71°C (160°F) with foam density at the lower end of the tolerance band. Moreover, a maximum FA acceleration of 126 g's was predicted for drops at 24°C (75°F) with the package having nominal foam density. This was approximately 20% higher than the 105 g's predicted for the -40°C (-40°F) with foam density at the upper end of the tolerance band scenario and approximately 40% higher than the 90.1 g's predicted for 71°C (160°F) with foam density at the lower end of the tolerance band case.

Energy and Work Histories – The predicted global energy and work histories for the package at 75°F containing nominal density foam was previously shown in Figure 2-29 (18° rotation.) This information is repeated in Figure *2-64* along with the corresponding results for a package dropped at 160°F with low density foam and at -40°F and high density foam. Although not discernable from these graphs, the initial total energies were slightly different for the three runs. In particular, the initial energy for the 160°F/low foam density run was 202 kJ, 204 kJ for the 75°F/nominal foam density run, and 205 kJ for the -40°F/high foam density run. These slight differences were obviously a result of the slight differences in predicted weight. Hourglass, sliding, and stonewall energies were small relative to the total energy. This indicates good overall numerical analyses.

2.12.3.2.7 Pin Puncture

In addition to the 9m drops, the package must survive a "pin puncture" test. The pin puncture test involves dropping the shipping package onto a flat-headed (15 cm diameter with 6 mm chamfer all around) steel pin from a 1 m height. The orientation of the package and location of pin impact must be chosen to achieve the greatest damage to the package.

The pin damage investigation consisted of two approaches. First, the pin drop was analyzed, based on maximum impact forces imparted to the Outerpack. Then, the cumulative damage that a pin drop could cause following a 9 m drop was studied. The latter study was naturally based on the 9 m drop predicted to cause the most Outerpack damage.

Maximum Loads – Our analysis indicates the shipping package will be subjected to the higher loads when dropped in a horizontal orientation, Figure 2-65A, compared to an inclined one Figure 2-65B. For example, when the package is tilted 20° (with the top nozzle end of the package towards the ground), our analysis predicts the maximum impact load is 561 kN. This is 10% less than the 624 kN load predicted for a fully horizontal drop Figure 2-66.

This page intentionally left blank.

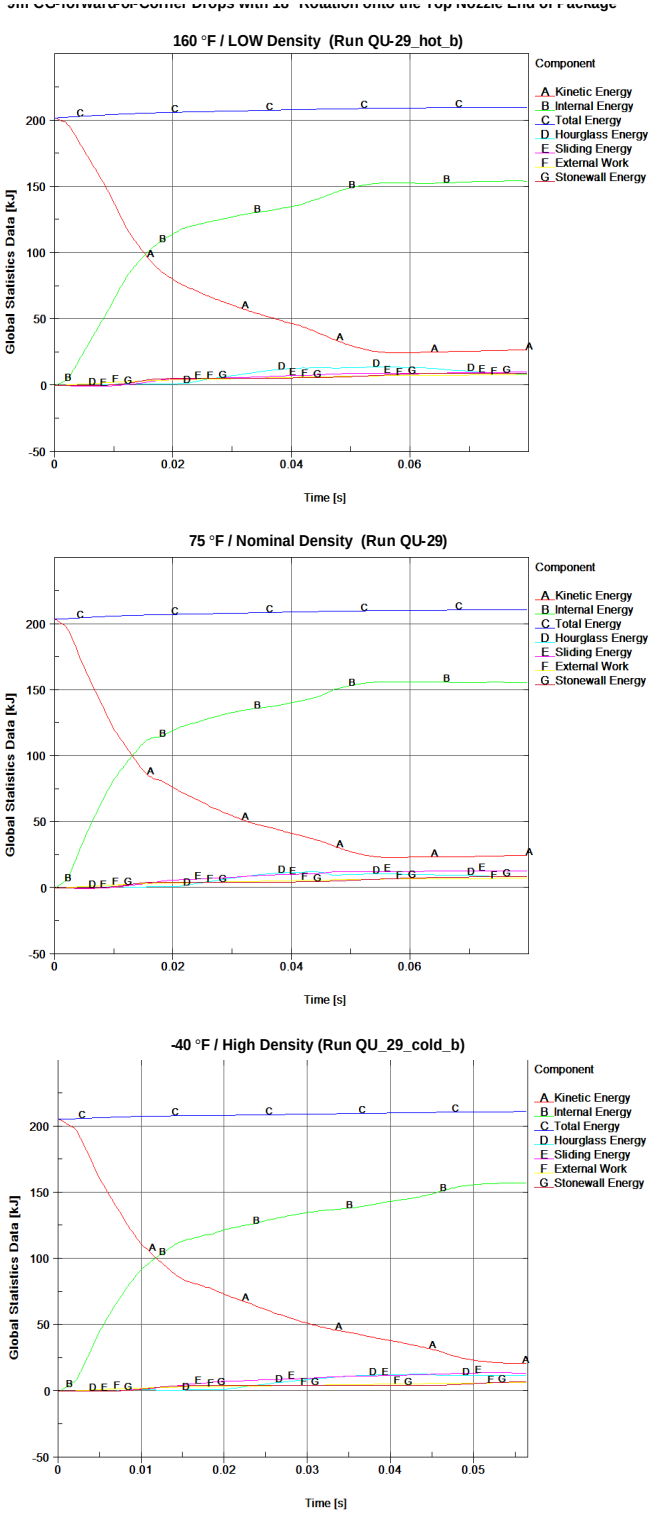

Figure 2-64 Predicted Energy and Work Histories at Various Temperatures

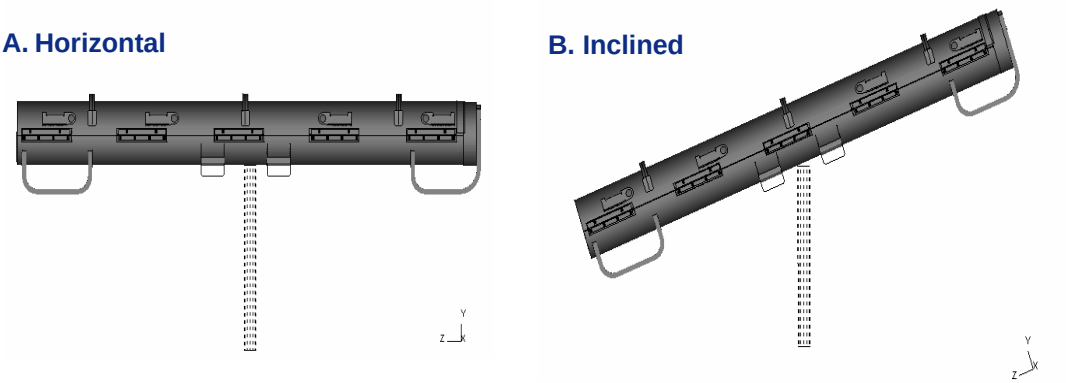

Figure 2-65 Pin Drop Orientations

A comparison of predicted fuel assembly accelerations is shown in Figure 2-67. Note the fuel assembly is predicted to experience approximately 9% higher accelerations in a fully horizontal pin drop than one inclined at 20 degrees.

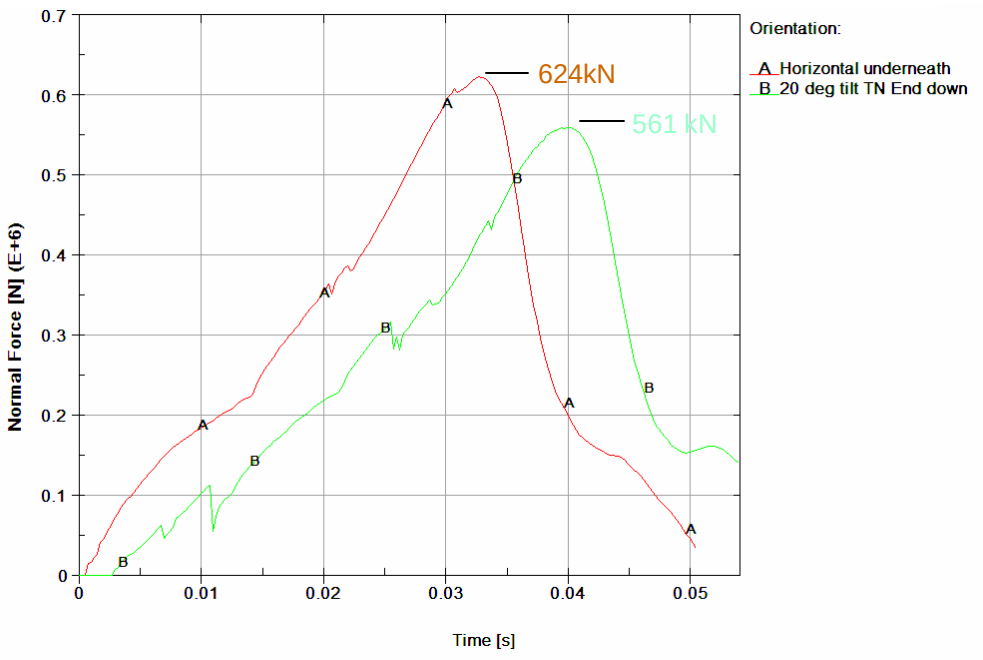

Figure 2-66 Predicted Outerpack/Pin Interference Forces (1m Drop onto 15mm Diameter Steel Pin)

Thus, a fully horizontal pin puncture drop produces higher Outerpack loads and fuel assembly accelerations than inclined pin puncture drops.

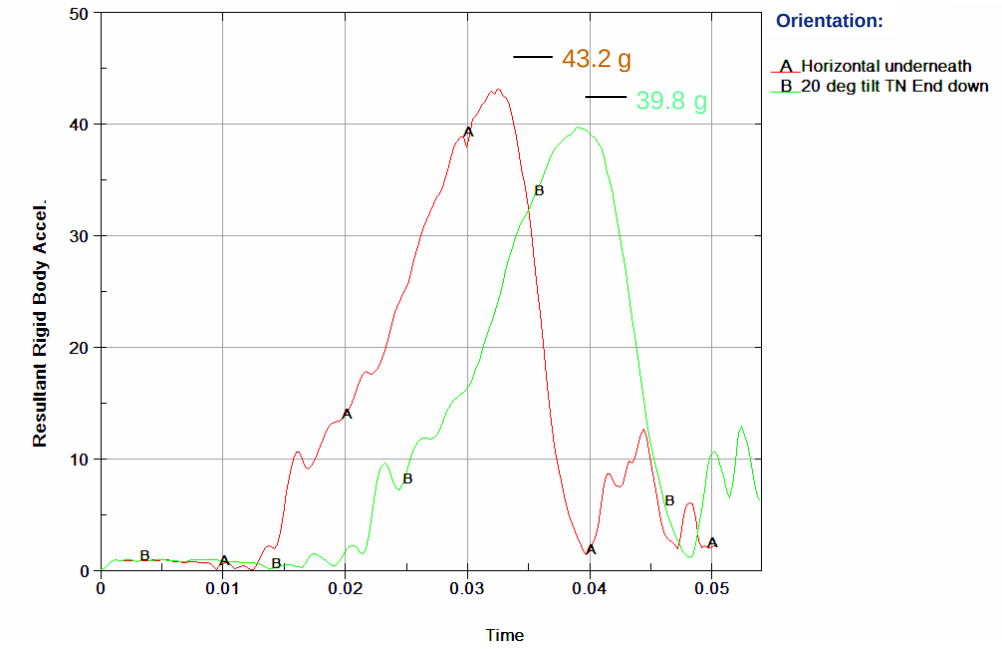

Figure 2-67 Predicted Fuel Assembly Accelerations (1m Drop onto 15mm Diameter Steel Pin)

Worst Horizontal Pin Drop – Two axial rotations were compared when studying the horizontal pin puncture drops. These were the previously described orientation in which the pin impacts the shipping package from underneath, Figure 2-65A, and one where the pin impacts the Outerpack hinges, Figure 2-68. In both cases, the pin was positioned directly under the package CG.

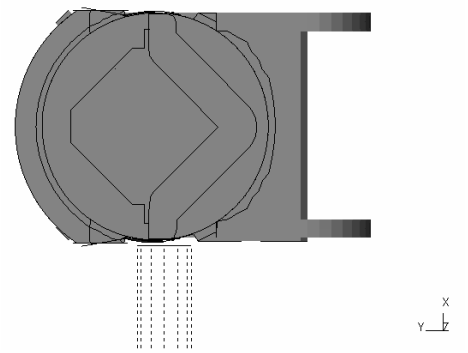

Figure 2-68 Pin Drop onto Outerpack Hinges

Interestingly, predicted Outerpack loads were practically the same for a horizontal pin puncture to the underneath side of the Outerpack and a pin impact directly to a hinge, Figure 2-69. However, there was less cushioning for the fuel assembly in the latter drop. This is evident from the predicted fuel assembly accelerations of 43.2 g's for the impact to the underneath region of the Outerpack and 82.1 g's for the hinge impact, Figure 2-70.

In fact, all of these pin puncture orientations were tested using full-scale Traveller XL units. In all cases, the pin puncture tests were passed without any puncturing of the outer skins of the units, nor any detrimental effects to the Clamshell/fuel assembly, or criticality safety aspects of the package.

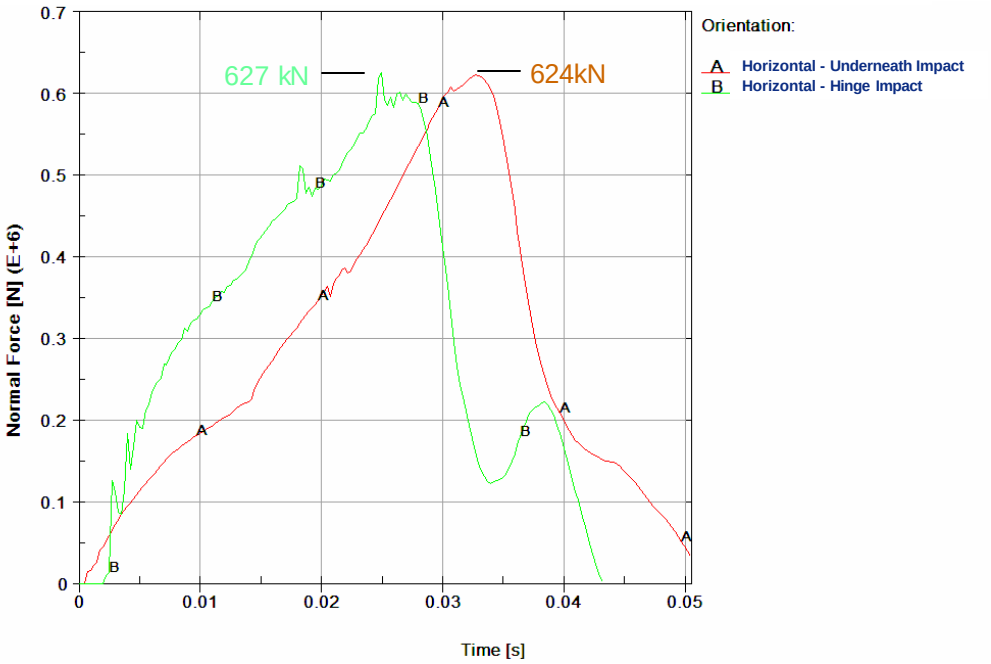

Figure 2-69 Predicted Outerpack/Pin Interface Forces (1m Drop onto 15mm Diameter Steel Pin)

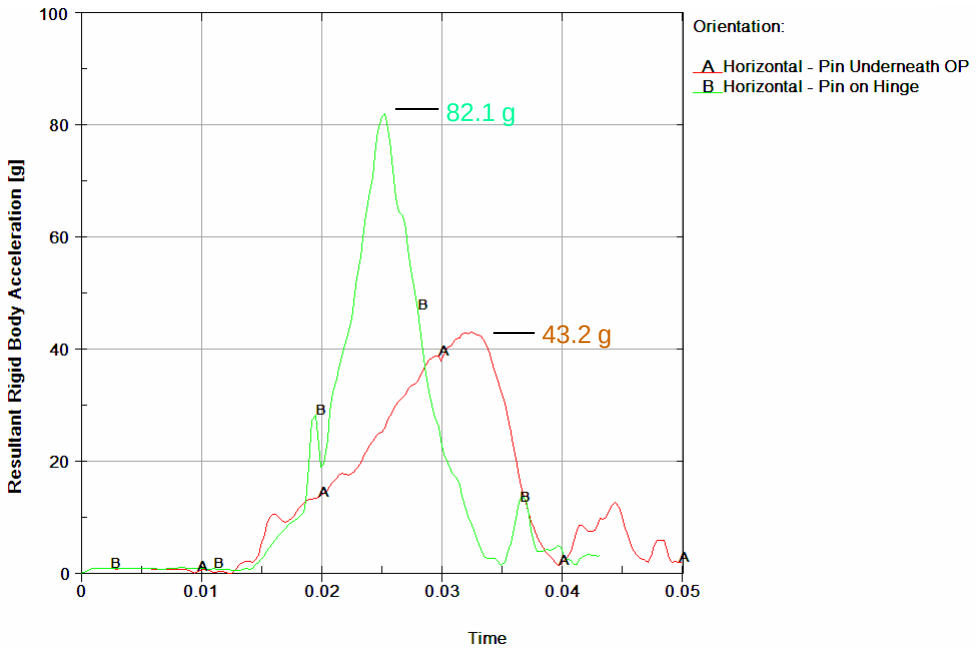

Figure 2-70 Predicted Fuel Assembly Accelerations (1m Drop onto 15mm Diameter Steel Pin)

Energy and Work Histories – Global energy and work for the 1 m pin puncture drops discussed above are shown in Figures 2-71, 2-72 and 2-73. These plots have an initial total energy (TE) of 22.3 kJ. This value correctly reflects the initial velocity (v) of 4.43 m/s applied to the 2,270 kg package mass (m) since our pin puncture simulations are initiated at the end of Outerpack free fall from 1 m; the total energy is comprised only of kinetic energy (KE), and $KE = \frac{1}{2}mv^2$. Total energy rises about 8% in these drop simulations. This reflects the work done by the package under gravity loading, i.e., the bending of the shipping package around the pin. Depending on drop orientation, the event was completed within 4 to 5 milliseconds as seen by the flattening of the kinetic energy and internal energies after that time. Moreover, acceptable levels of hourglass, sliding, and stonewall energies were obtained. This indicates a good overall numerical analysis was obtained in each simulation.

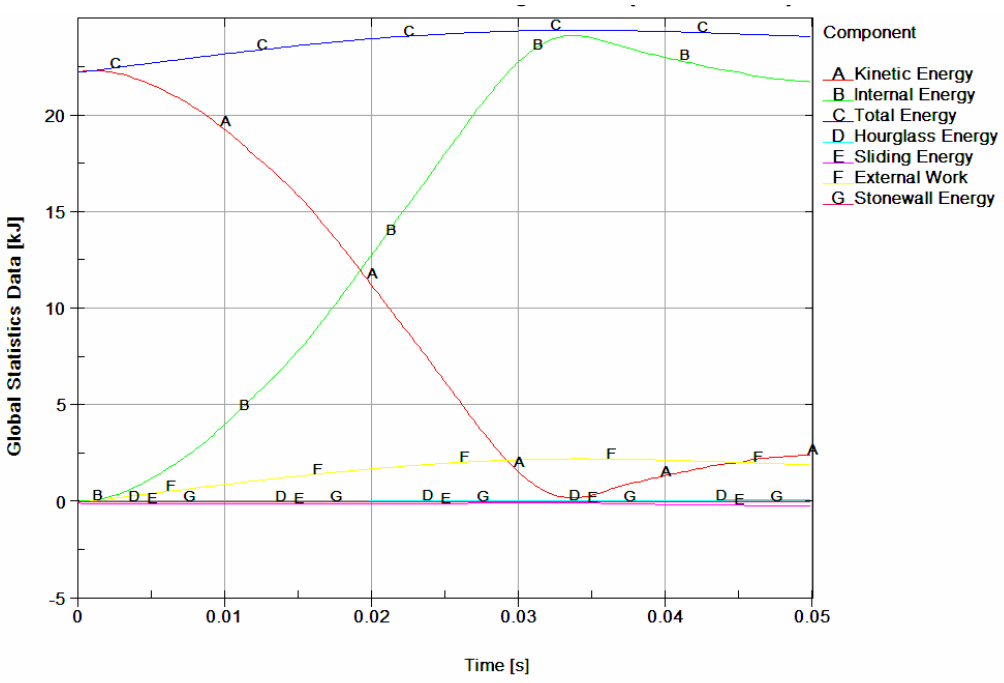

Figure 2-71 Predicted Energy and Work Histories for a 1 m Horizontal Pin Drop (Pin Underneath the Package CG)

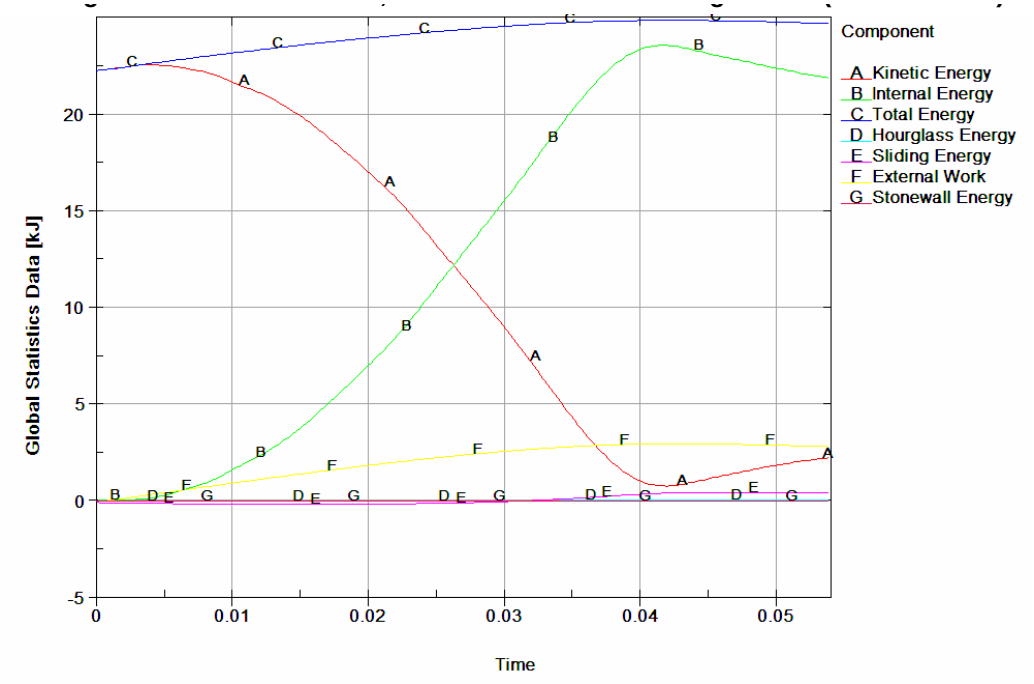

Figure 2-72 Predicted Energy and Work Histories for a 1 m Tilted Pin Drop (20° Tilt With TN End Down

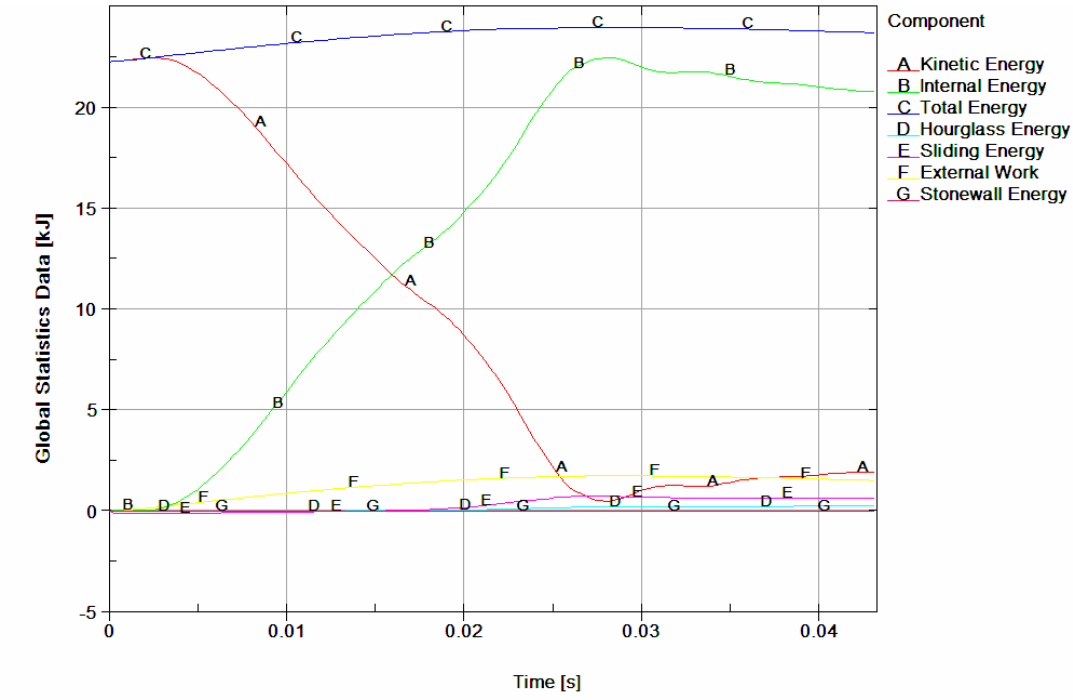

Figure 2-73 Predicted Energy and Work Histories for a 1 m Horizontal Pin Drop (Pin Hitting Hinge at Package CG)

Maximum Pin Indention – Predicted maximum pin indention for the horizontal underneath, inclined, Figure 2-65 and hinge pin puncture drops Figures 2-68 were, 67, 54 and 50 mm, respectively. This is shown in Figure 2-74.

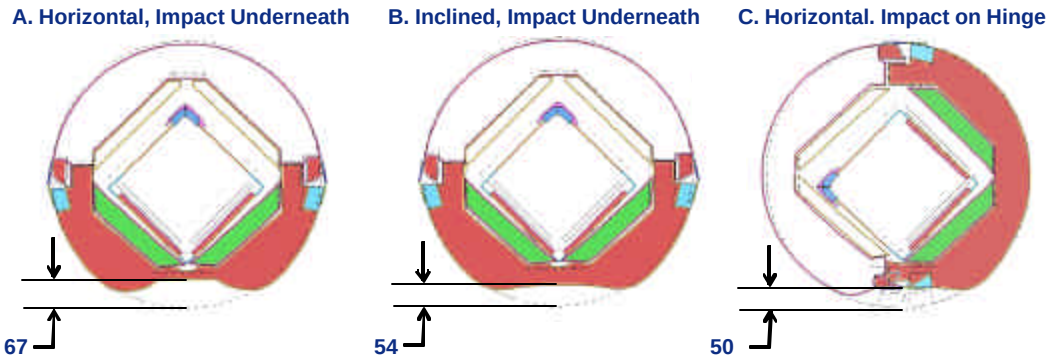

Figure 2-74 Comparison of Predicted Maximum Pin Indentions

Outer Steel Skin Damage – Predicted maximum plastic strains in the steel skin were only 12.6 and 15.7% for the horizontal and 20° tilted pin puncture simulations Figures 2-65A and 2-65B, respectively. These values are much less than the allowable 46.7% failure strain. Thus, it is unlikely the steel skin will be ruptured by the pin puncture test. Initial testing of the Traveller XL Prototype units were demonstrated that 11 gage (0.120" nominal thickness, 3.0 mm) 304 stainless steel had little difficulty passing the pin puncture tests. Those full-scale tests, in addition to the analytic work discussed previously, allowed designers the confidence to reduce the thickness of the Outerpack shells to 12 gage material (0.105" nominal thickness, 2.7 mm). Therefore, the QTU and CTU packages were all fabricated using 12 gage sheet material of the outer shells. Pin drop tests of QTU-1, QTU-2 and CTU packages confirmed that 12 gage material survived the pin puncture tests without failure.

Cumulative Damage – As previously stated, analysis of cumulative pin damage was based on the 9 m drop predicted to cause the most Outerpack damage. Indeed, this analysis placed the pin 1 m under, and normal to, the region of the top impact limiter which was (previously) predicted to flatten during the 9 meter CG-forward-of-corner drop onto the TN end of package with an 18° forward rotation Figures 2-64 and 2-25. The position of the pin was at the apex of the top impact limiter Figure 2-67. This location was chosen since it would most exacerbate the opening of the Outerpack seam predicted from the 9 m drop analysis.

Deformations, strains, and stresses from the previous 9 m analysis were used as the initial starting point for the cumulative pin puncture drop analysis. Inclusion of deformations was accomplished by use of the LSTC/LSPOST[1] capability to output deformations at the appropriate time (state) in LS-DYNA keyword format. The corresponding strains and stresses from the 9m analysis were written to a file (in LS-DYNA

[1] LSPOST is the pre- and postprocessor by LSTC provided with LS-DYNA.

keyword format) via the LS-DYNA *INTERFACE_SPRINGBACK_DYNA3D command. A new master 1 m pin puncture analysis keyword file was created that defined all parts, materials, nodes (with deformed positions), element connectivity, loading, etc. Stresses and strains were then brought into the analysis by use of the LS-DYNA *INCLUDE and *STRESS_INITIALIZATION commands.

Maximum Loads – The Westinghouse analysis indicates the shipping package is subjected to higher loads when dropped on a previously damaged end than in any other orientation analyzed, including a drop onto a hinge. Indeed the maximum predicted Outerpack load was 734 kN for the 2nd hit Figure 2-75. This is 17% higher than the 627 kN predicted for a drop onto the Outerpack hinge Figure 2-69. The greater load is attributed to the lower cushioning available due to the foam in being highly compressed during the 9m drop. Even so, the maximum predicted fuel assembly acceleration was just 38.2 g's Figure 2-76.

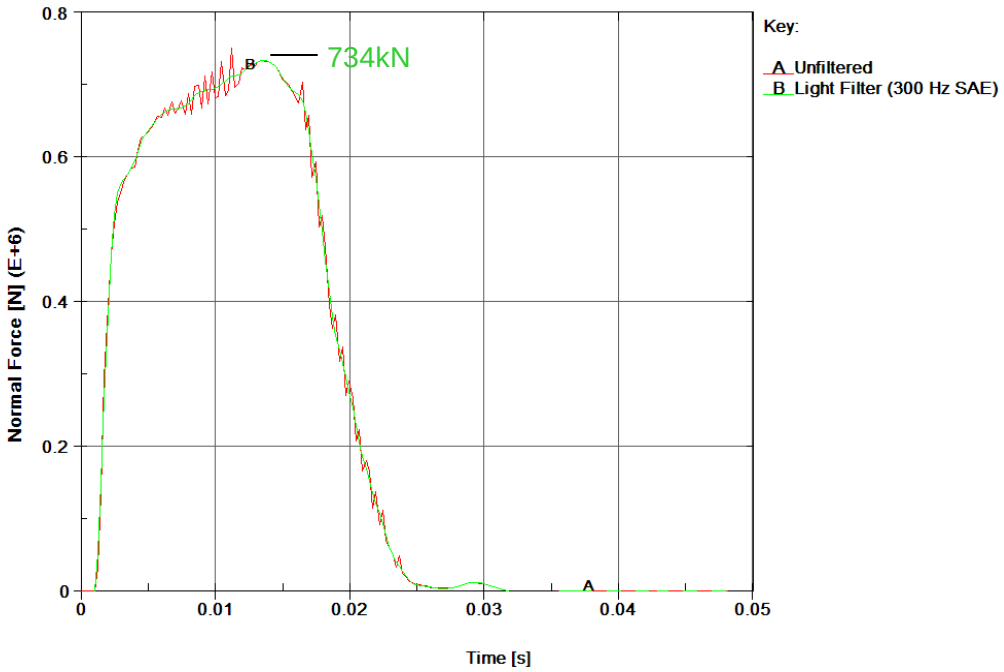

Figure 2-75 Predicted Outerpack/Pin Interface Forces (1 m Drop onto 15 mm Diameter Steel Pin After 9m Drop)

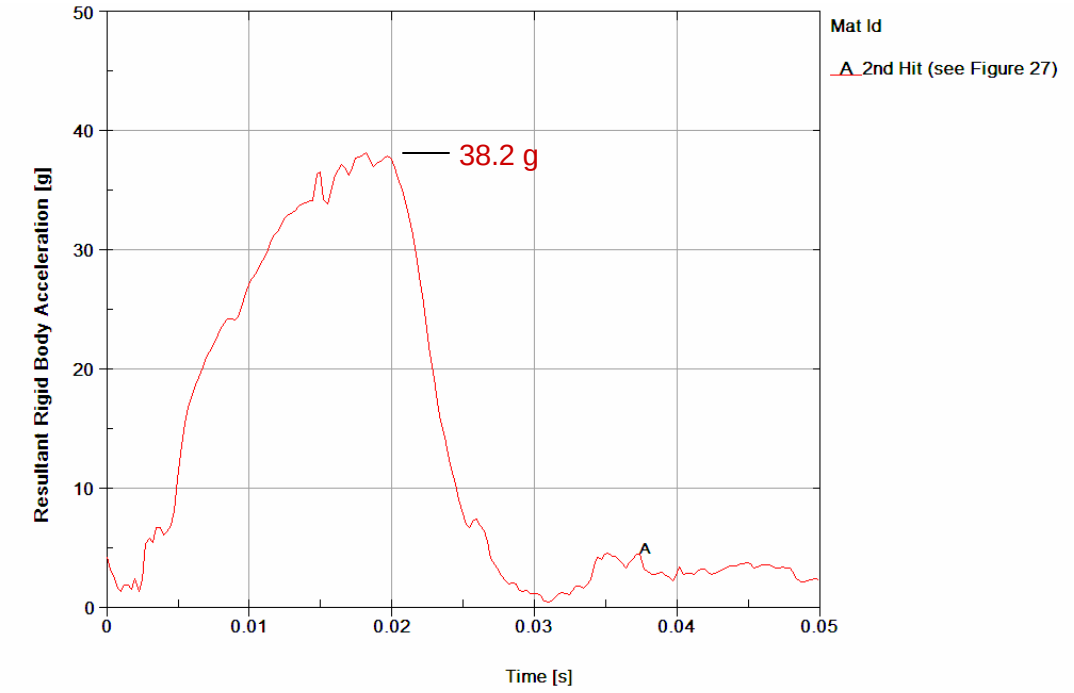

Figure 2-76 Predicted Fuel Assembly Accelerations (1 m Drop onto 15mm Diameter Steel Pin after 9 m Drop)

Additional Damage – As previously discussed, our primary concern for this sequence of drops (a 9 m CG-forward-of-corner drop onto the top nozzle end of the package followed by the 1 m pin puncture) was the extent of Outerpack seam opening Figure 2-28. Our measures of Outerpack seam opening, D1 and D2 (see Figure 2-48), would increase from 20 to 22.9 mm and from 20 to 22.2 mm, respectively.

Energy and Work Histories – Predicted global energy and work for the 1 m pin puncture drop following a 9 m CG-forward-of-corner drop onto the top nozzle end of the package is shown in Figure 2-77. The sliding energy in this plot is related to the initial penetration between the crushed impact limiter foam and outer steel skins. It is not necessarily an error. Moreover, the predicted increase in damage due to the pin puncture test simply does not warrant further investigation of this issue.

Pin Puncture Summary – Our analyses indicate the Traveller XL package is very capable of withstanding the 1 m pin puncture test. Indeed, it was determined that the likelihood of rupturing the outer steel skin is very low. Thus, the 1 m pin puncture test is a relatively benign test for the Traveller XL package. These conclusions were confirmed by the prototype test results as subsequently discussed.

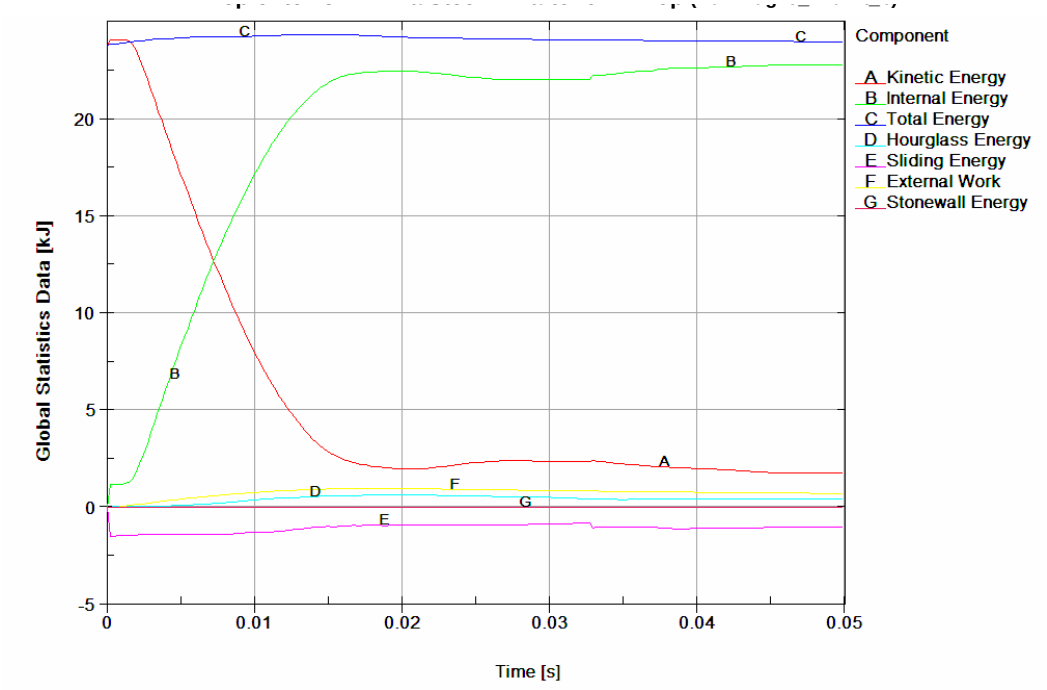

Figure 2-77 Predicted Energy and Work Histories (1 m Drop onto 15 mm Diameter Steel Pin after 9 m Drop)

2.12.3.3 Comparison of Test Results and Predictions

Two prototype Traveller XL packages were drop tested on January 28 and 29, 2003. Details of these tests are provided in Appendix 2.12.4, Traveller Drop Test Results.

Results from the extensive prototype tests in January, 2003 were reviewed to find the best ones for comparison with FEA predictions. Comparison cases were chosen to include tests with prototype units which did not have extensive previous test damage, those which represented a unique test configuration (i.e., the pin puncture) and those in which accelerometer data was obtained. The four selected cases are identified in Table 2-22 and Figure 2-78.

There was good overall agreement between predicted and actual drop performance of the prototype Traveller XL package. This is evident by comparisons of predicted and actual permanent deformations, failed parts and measured and predicted accelerations at specific positions on the Outerpack and Clamshell.

Table 2-22 Prototype Tests Used to Compare with Analysis					
Test ID (corresponds to [6])	**Analysis ID**	**Drop Height [m]**	**T_x**	**T_z**	**Comment**
1.1, 9 m Low Angle	C1-25	9.1	14.5°	180°	T/N primary impact on OP top
1.2, 9 m CG-over-corner	C1-31	9.1	-71°	90°	B/N primary impact on OP hinge
2.2, 1 m Pin-puncture	Punc2-2nh	1.04	20°	135°	CG (Axial) on OP topside, T/N end down
2.3, 9 m CG-over-corner	C1-29	9.1	108°	0°	T/N primary impact on OP top

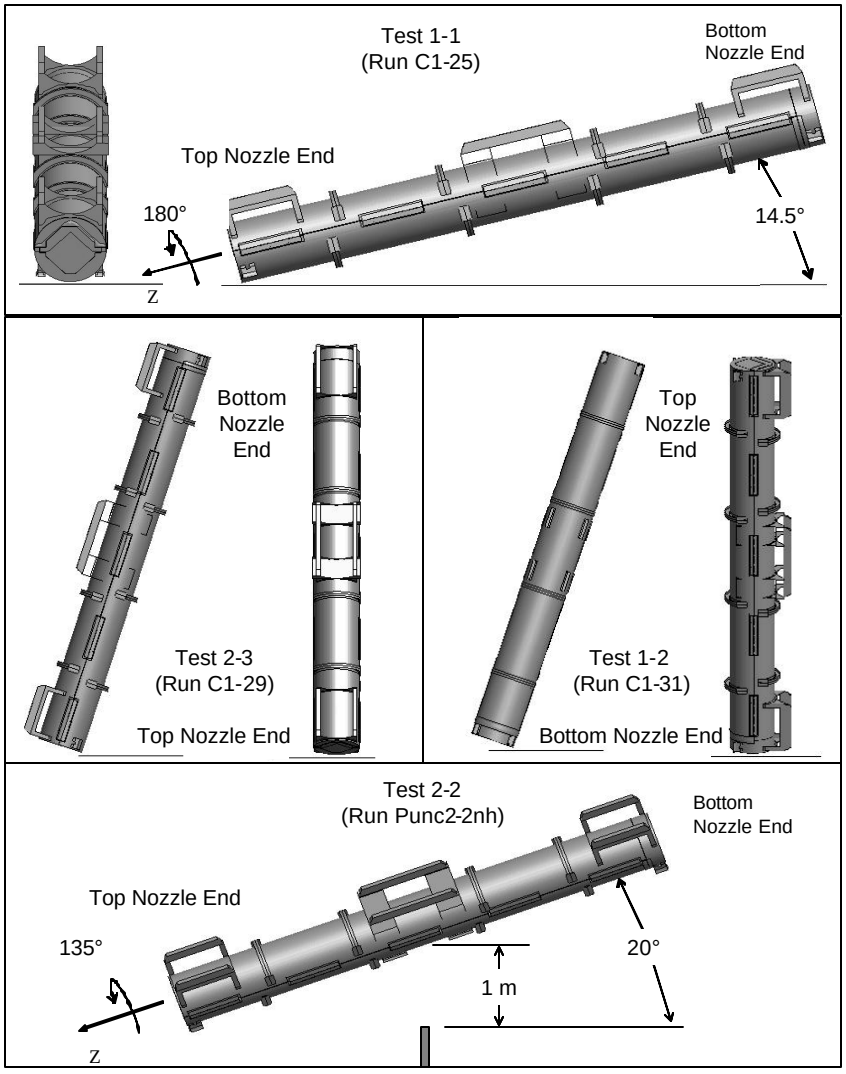

Figure 2-78 Prototype Drop Tests Used To Benchmark Analysis

2.12.3.3.1 Prototype Unit-1 Test 1.1

Prototype Unit-1, Test 1.1 was chosen for the first comparison. As indicated in Table 2-22 and Figure 2-78, this was an inclined drop from 9.1 meters onto the upper Outerpack (the unit was rotated 175° about its long axis and inclined 14.5° with the end of the package nearest the top of the fuel assembly hitting first.[1] Four frames taken from a video recording of test 1.1 are shown in Figure 2-79. These frames show the test sequence was comprised of the initial impact on the top nozzle end of the package (frame 1), rollover (frames 2 and 3), and a secondary impact to the bottom nozzle end of the package (frame 4).

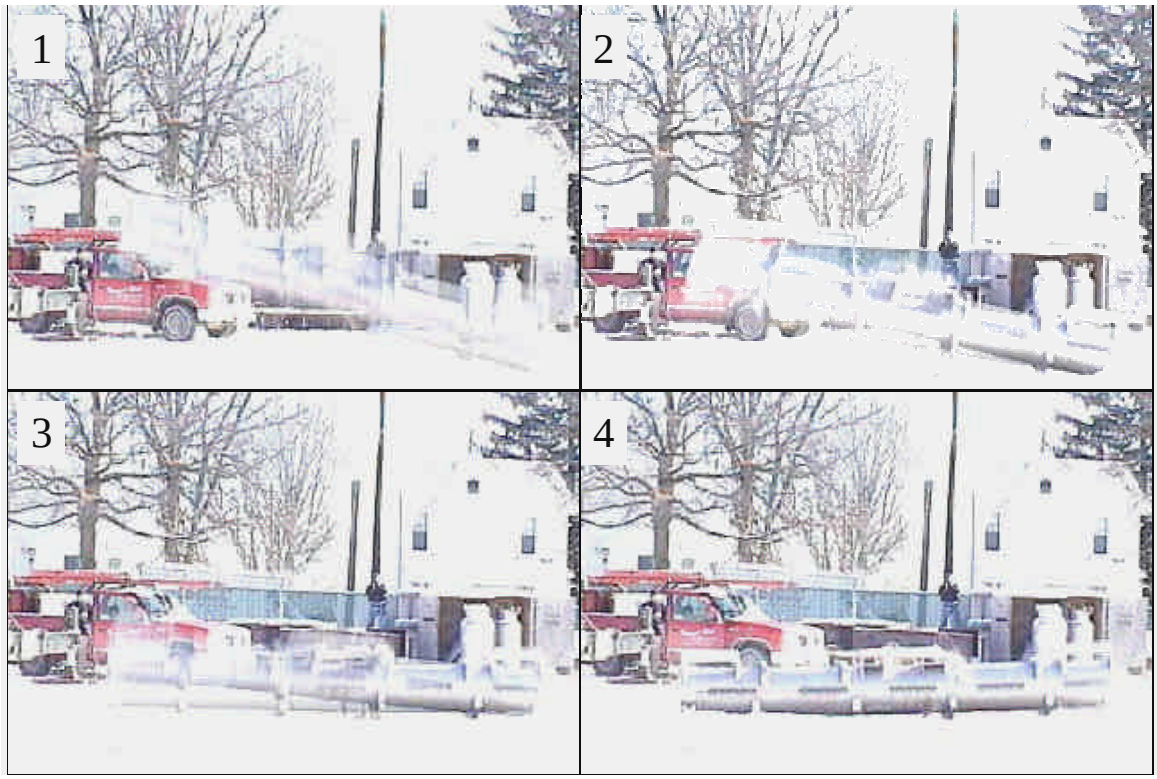

Figure 2-79 Prototype Unit 1 Drop Test

Deformations – As reported in, test 1.1 produced noticeable permanent deformations in several locations of the Outerpack and no significant permanent deformations in the Clamshell. Outerpack permanent deformations were primarily at the ends of the package.

[1] This will be referred to as the "top nozzle end" of the package. Likewise, the end of the package nearest the bottom of the fuel assembly will be called the "bottom nozzle end."

An overall sense of the correspondence between predicted and actual Outerpack permanent deformations may be obtained by reviewing Figures 2-80 through 2-87. Quantitative comparison between predicted and documented measurements is given in Table 2-23.

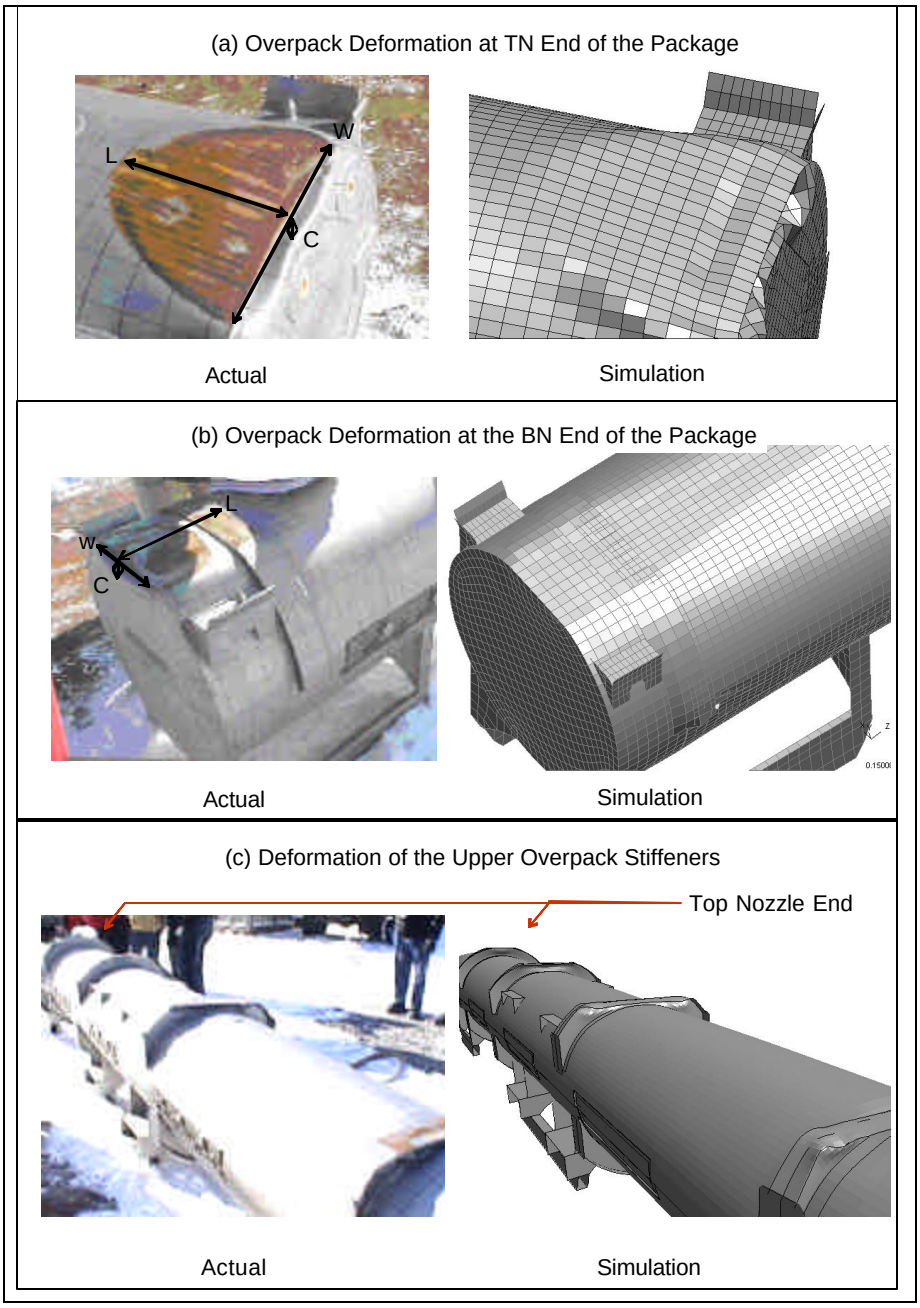

Figure 2-80 Comparison of Test 1.1 with Analytical Results

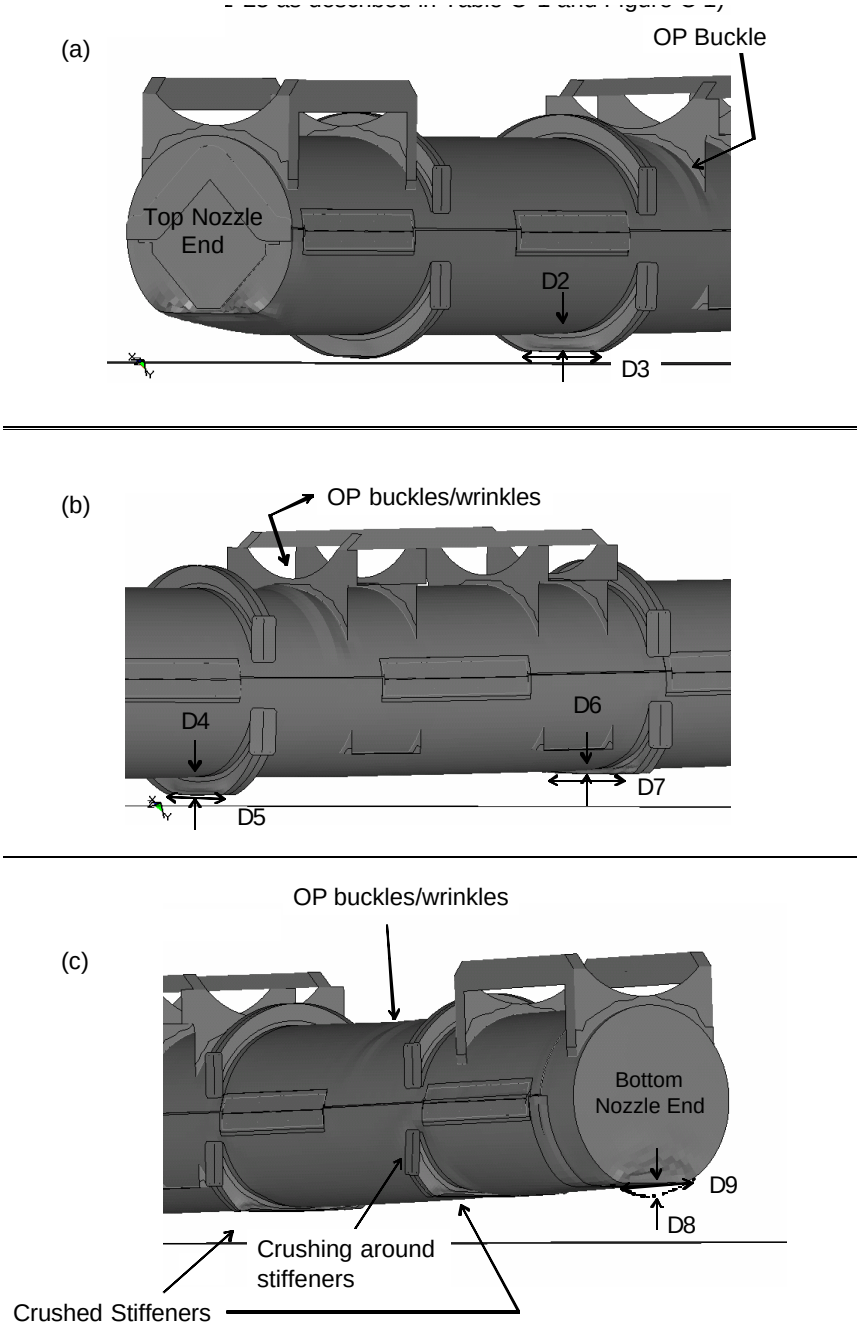

Figure 2-81 Comparison of Test 1.1 with Analytical Results

Table 2-23 Comparison of Predicted and Actual Deformations for Test 1-1

Item	Location	Measured (Reference 6)		Predicted		Nodes used to make Prediction		Difference	Conservative
		(in)	(mm)	(in)	(mm)				
1	Top nozzle end								
	Dim L in Figure 2-80	9.0	229	11.9	302	192658	134223	32.2%	Yes
	Dim W in Figure 2-80	12.0	305	14.6	371	134052	134170	21.7%	Yes
	Dim C in Figure 2-80	1.5	38	1.65	42	134062	223918	10.0%	Yes
2	Bottom nozzle end								
	Dim W in Figure 2-80	11.5	292	11.9	302	214342	190946	3.5%	Yes
	Dim L in Figure 2-80	10.57	268	13.0	330	94120	213639	23.0%	Yes
	Dim C in Figure 2-80	0.75	19	1.5	38	93833	214433	100.0%	No
3	Upper Overpack Stiffeners								
	Dim D2 in Figure 2-81	0.8	19	0.7	17	115715	115853	-10.7%	Yes
	Dim D3 in Figure 2-81	N/A		11.9	303	115702	116484	-	
	Dim D4 in Figure 2-81	2.4	60	2.2	56	112621	112759	-6.4%	No
	Dim D5 in Figure 2-81	N/A			-			-	
	Dim D6 in Figure 2-81	N/A		1.0	26	109526	110131	-	
	Dim D7 in Figure 2-81	16.0	406	18.4	468			15.1%	Yes
	Dim D8 in Figure 2-81	N/A			-			-	
	Dim D9 in Figure 2-81	23	584	22.6	574			-1.7%	No
							Average Difference:	22.4%	

(a) Overpack Deformation at Top Nozzle End of the Package

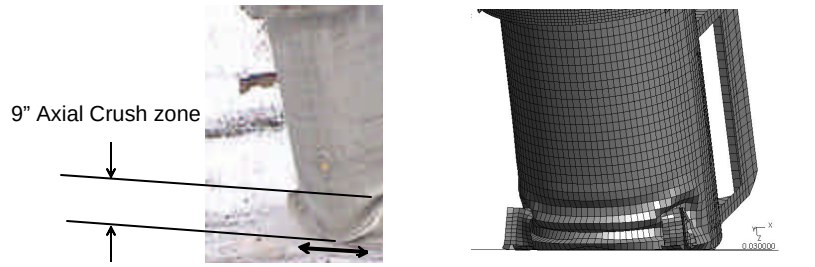

(b) Overpack Deformation at the Top Nozzle End of the Package

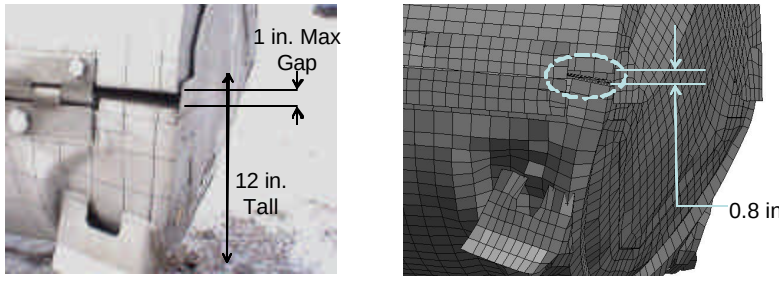

Figure 2-82 Deformations at End of Package

(a) FA Displacement at Bottom Nozzle End of the Package

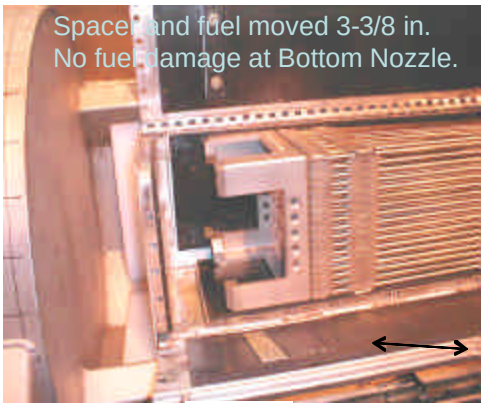

Actual

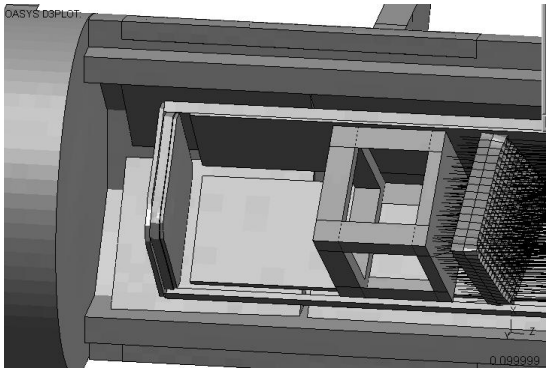

Simulation

(b) Deformation at the Top Nozzle End of the Package

Actual

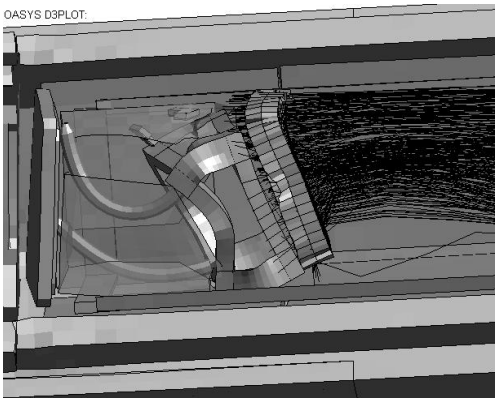

Simulation

Figure 2-83 Internal Deformations at Inside Outerpack

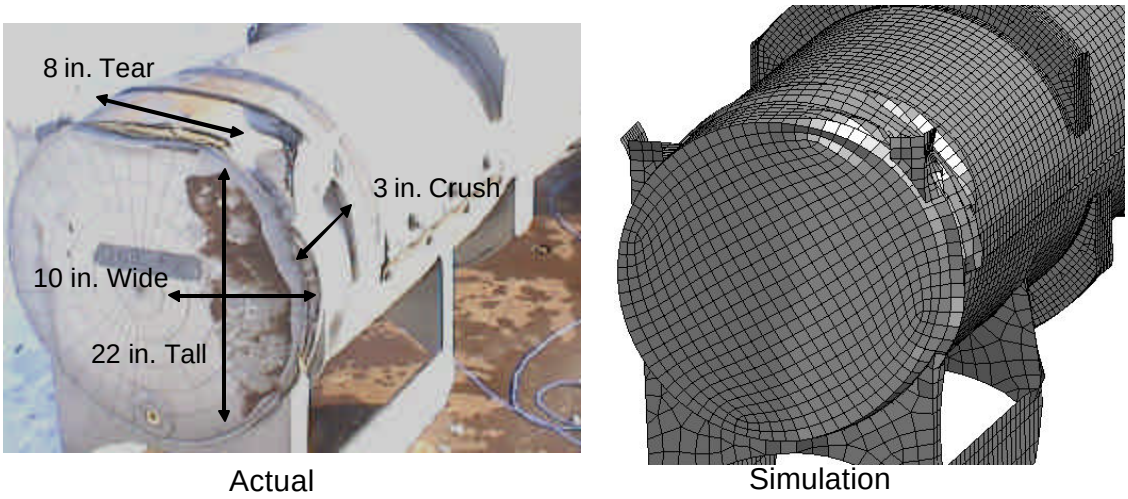

Figure 2-84 Outerpack Deformations at Bottom Nozzle End of Package

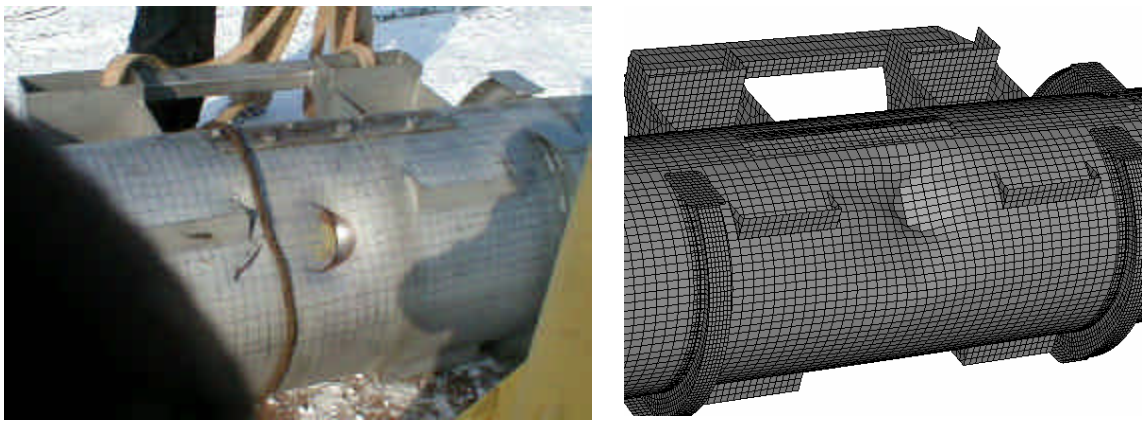

Figure 2-85 Pin Puncture Deformations

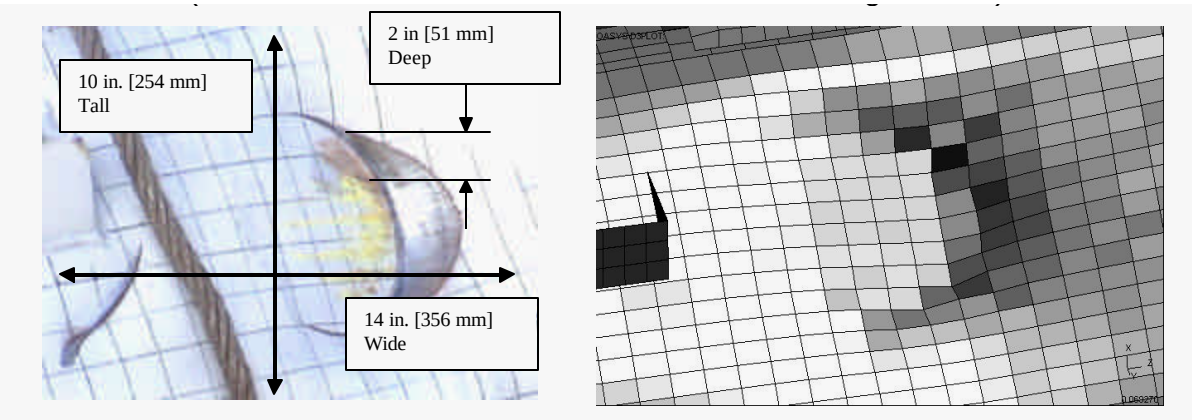

Figure 2-86 Dimensions of Pin Puncture Deformations

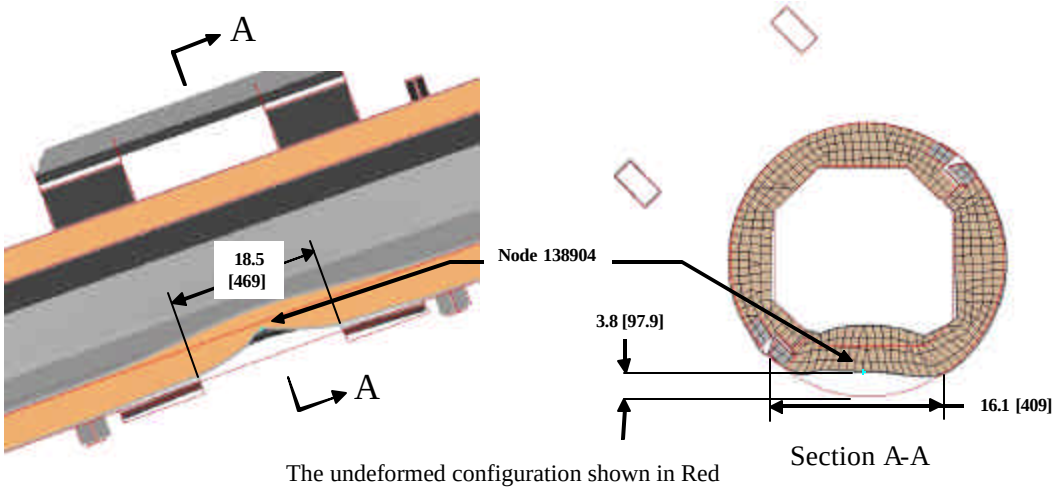

Figure 2-87 Outerpack Predicted Deformations of Pin Drop

2.12.3.3.2 Accelerations

Vertical accelerations (Y-direction) measured during test 1.1 are compared with the FE-based predictions in Figures 2-88 through 2-92. Agreement was good. Indeed, discrepancies between the two could easily be attributed to the inherent error associated with obtaining such data.

For the Outerpack, both measured and predicted traces contained two peaks, Figure 2-88. These corresponded to the two impacts associated with this test as illustrated in Figure 2-78. (Note: the larger acceleration with the secondary impact should not be interpreted as meaning larger forces were associated with the second impact. Rather, the larger magnitude simply reflects that the accelerometer was much nearer the secondary impact end.) While there were two visible peaks, the measured response was very small for the primary impact. For the secondary impact, the predicted acceleration was 1270 g's. This was in accordance with the measured peak acceleration which indicated accelerations were greater than 950 g's.

For unknown reasons, the accelerometers on both the Clamshell top and bottom plates gave erroneous readings late into the drop. This is clearly evident from accelerometer data in Appendix 2.12.4 that the accelerometers "saturate" for over 0.025 seconds and provide no meaningful response afterwards. Thus, only the first 0.05 seconds of the Clamshell data was compared in this report. For the accelerometer on the Clamshell top plate, measured and predicted accelerations corresponding to the first impact (at time 0.01 seconds in Figure 2-90) were 555 g's. This was also in accordance with measurements which indicated a peak acceleration greater than 525 g's was experienced. As shown in Figure 2-91, peak accelerations of 205 g's were measured on the Clamshell bottom plate. The corresponding predicted acceleration is also shown. Note the peak predicted acceleration was 155 g's.

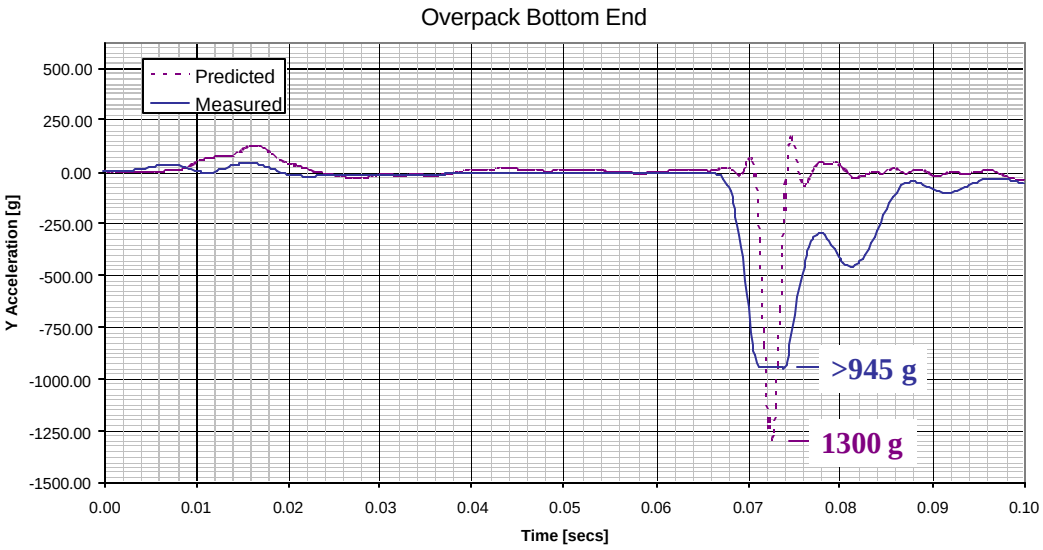

Figure 2-88 Predicted and Measured Y Accelerations

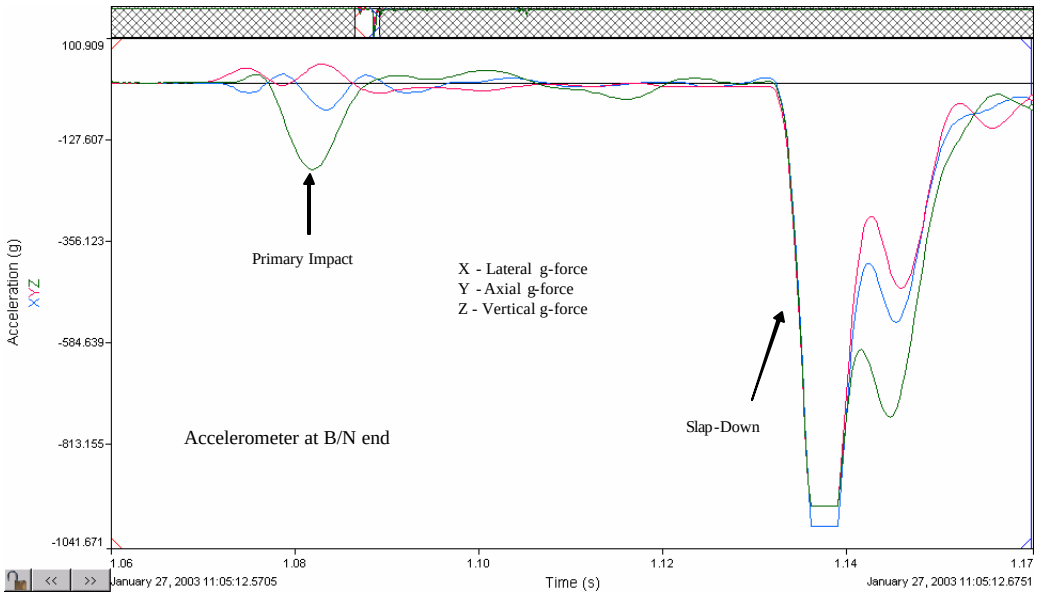

Figure 2-89 Three Axis Measured Accelerations

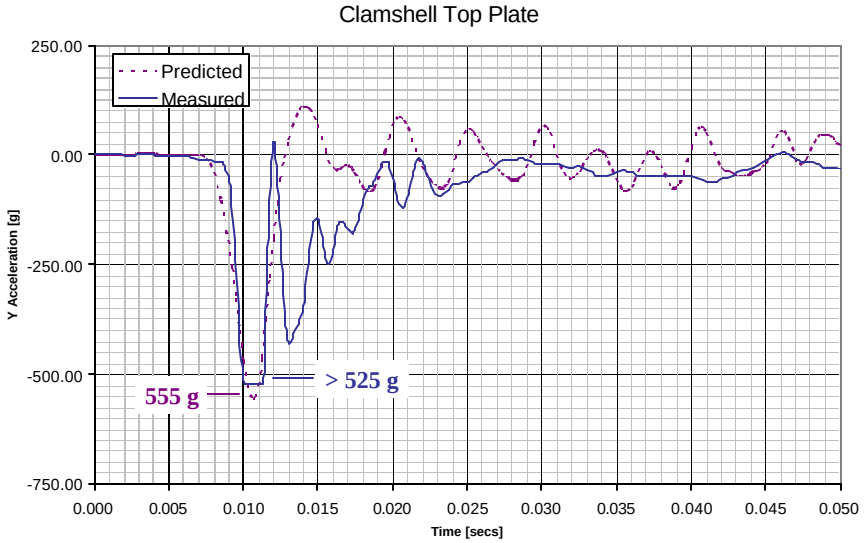

Figure 2-90 Predicted and Measured Y Accelerations

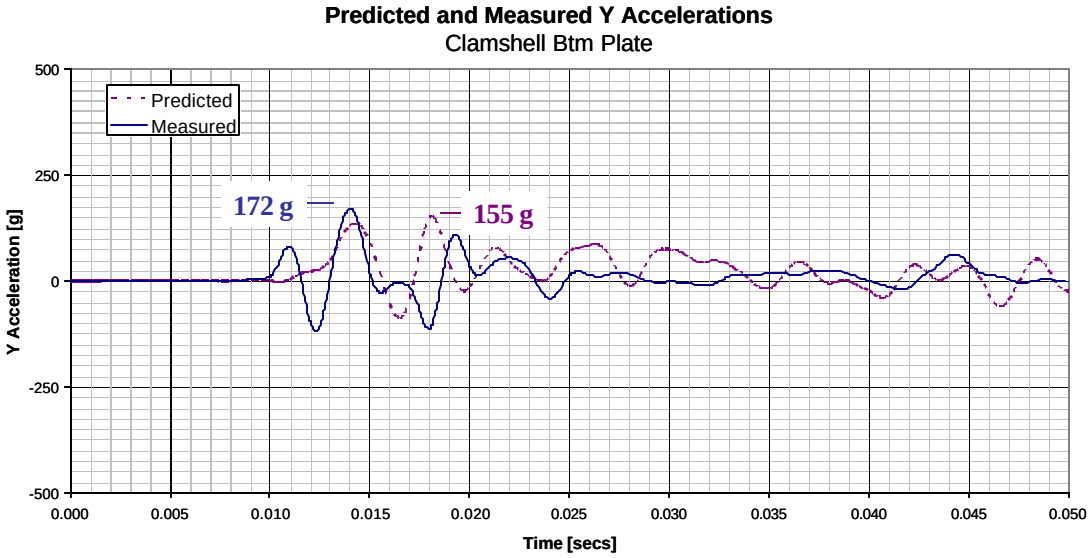

Figure 2-91 Predicted and Measured Y Accelerations

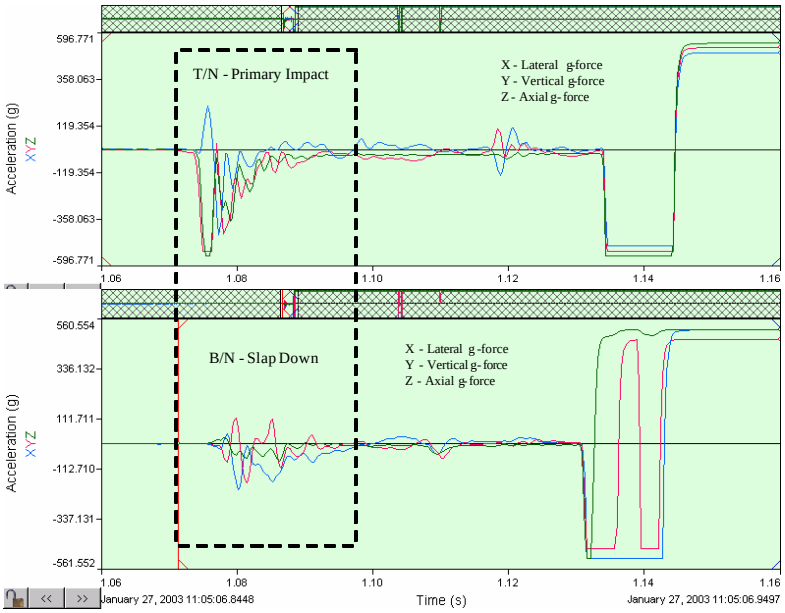

Figure 2-92 Measured Primary and Secondary Accelerations

2.12.3.4 Discussion of Major Assumptions

The many assumptions used to develop the LS-DYNA non-linear finite element stress code, including those needed to model the materials and impact, were found valid for simulating drop tests of the Traveller XL package. It is clearly evident from comparisons between prototype test results and predictions that the key physical phenomena governing shipping container impacts is captured within the LS-DYNA code.

The only major additional assumption was that bowing of the fuel assembly did not result in excessive additional loading of the Clamshell side walls, hinges and latches. Test results showed this was a valid assumption.

LS-DYNA 960 build no. 1647 (single precision, MPP) was used in these calculations because it has the very needed “no put-back” contact capability. However, the official quality tested and assured version is currently DYNA 960 build no. 1106 (single precision, MPP) which does not have the no put-back contact capability. ARUP is expecting to officially release LS-DYNA 970 (probably build no. 3858) in late October, 2004. This version, which does have the no put-back capability, must be installed and tested on the claxgen computers. Then a Traveller XL drop test case must be run to verify results in this calculation note correspond with results from the quality-assured version of LS-DYNA.

2.12.3.5 Calculations

2.12.3.5.1 Method Discussion

The finite element method was used to determine the loads, displacements, accelerations, strains, etc. of a Traveller XL shipping package containing an XL fuel assembly when dropped on a flat surface from 9 m and onto a 15 mm diameter pin from 1 m. The LS-DYNA explicit finite element code was used. This software was selected because it allowed the analysis to include the effects of large deformation, large strain, material non-linearity, contact, and failure of connections between parts and assemblies.

The goal of the analysis was to predict the deformation and damage that the Traveller XL shipping package and contained fuel will experience when subjected to the HAC impact tests. Although it would have been more conservative, it was not feasible to build a model which allowed failure of all joints and any deformation pattern. Such a model would have been unduly complex and calculation intensive and have required extraordinary development time. Rather, the Traveller XL prototype and qualification unit finite element models were constructed with consideration of all probable relative displacements, contact and failures. The premise in choosing this deliberately restrictive approach was that it would not affect accuracy because it would include provisions for the actual deformation and damage. Test results substantiated the accuracy of the prototype unit model, see Appendix 2.12.4.

The models described herein were primarily developed to aid in determining the drop orientations and number of drops needed to meet the HAC requirements. Thus, any point on the Outerpack outer periphery was a potential impact point and there was no one point in which a finer mesh could be afforded. Thus, the actual strains and stresses determined in the model can not be considered refined. Rather, the relative deformations, decelerations and energy absorption between drop orientations should be considered. This limitation applies to both models of the prototype unit and the qualification unit.

Model Descriptions – A basic description of the Traveller XL prototype and qualification units is discussed in section 1 above. All design details are available in and. Details of the finite element models are described in the following two sections.

In both models, units were tonnes (mass), millimeters (length), seconds (times) and Newtons (force).

2.12.3.5.2 Prototype Models

The Prototype models, Units 1 and 2, were constructed from many input files, Figure 2-94. These files defined various details of the model and were included with, or without, transformations of coordinates and renumbering of identities as the model was assembled.

The main file, Apr6.key, contains the control cards, specifies outputs, contact definitions, and many attributes common to more than one subassembly. The major subassemblies were the Outerpack, Clamshell, and fuel assembly. These were defined in the OP.key, CS.key, and XL_FAr.key files, respectively. These subassemblies are detailed in Figures 2-95 through 2-97. A total of 363,646 elements were used in the model (199128 shells, 150717 solids and 13801 beams).

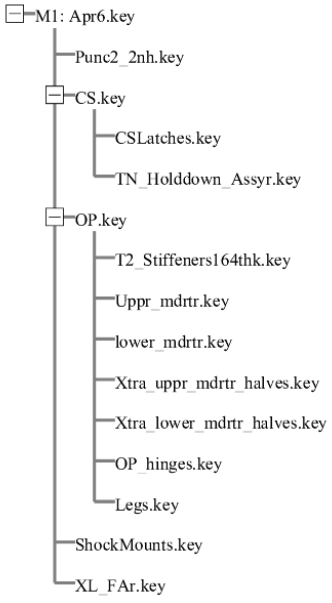

Figure 2-93 FEA Model Input Files

The orientation for each run was defined in individual load case files. Obviously, only one load case file and one material file was invoked per run.

The Clamshell Figure 2-96 is mounted to the Outerpack, Figure 2-94 with 22 rubber shock mounts. These shock mounts were modeled as discrete elements (springs). The stiffness of these elements was 92.7 N/mm in the global X direction, 135.4 N/mm in the global Y direction and 42.3 N/mm in the global Z direction. These values were obtained through tests. These details are included in the 'ShockMounts.key' file.

Predicted model weight for the Prototype units was 2.39 tonnes (5258 lbs). This matched the Prototype unit's 5065 lb. average weight within 3.8%.

Predicted model weight for the Qualification units was 2.27 tonnes (4994 lbs). This matched the Qualification unit's 4786 lb. average weight within 4.4%.

The Traveller program performed drop tests as input into the design process. As a result, there were changes in the design of the Traveller between the prototypes discussed on page 2-130 and the qualification test units described on page 2-133. The changes resulted in slightly different weights as noted in the descriptions.

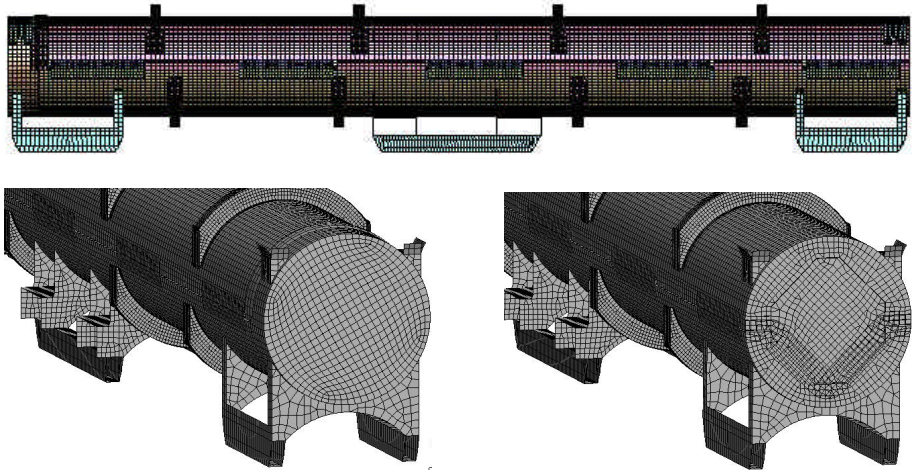

Figure 2-94 Outerpack Mesh in Prototype Model

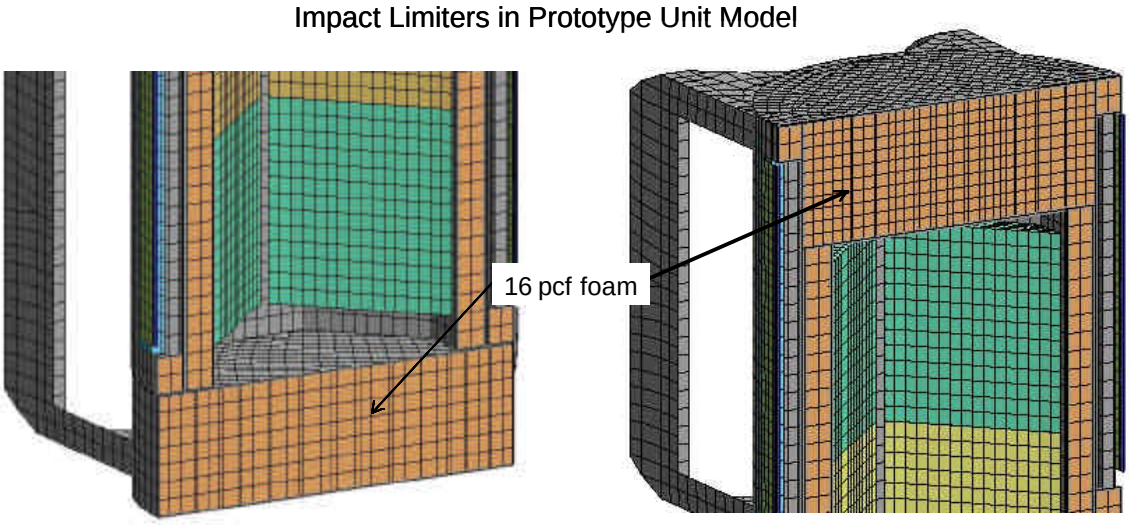

Figure 2-95 Impact Limiter in Prototype Unit Model

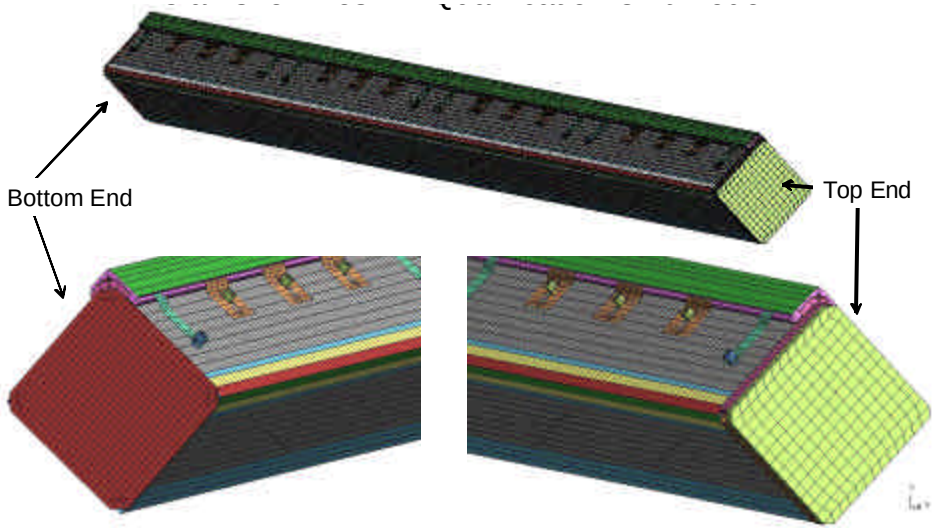

Figure 2-96 Clamshell Mesh in Qualification Unit Model

Figure 2-97 Fuel Assembly in Both Prototype and Qualification Unit Models

The Outerpack hinge details are shown in Figure 2-98. There were three bolts in the upper hinge plate in the Prototype models and only two for the Qualification unit models (shown). The bolts were modeled as spotweld beams. The spotweld beams and hinge plate shared nodes. The spotweld beam node at the hinge block was tied with LS-DYNA's NODAL_RIGID_BODIES. It should be noted that the manner of modeling the bolts allows for compression loading of the bolt, whereas in reality compression loads are not typically carried in bolted joints. However, in the horizontal side impact drops, the bolt heads themselves may impact the drop pad and compressive bolt loads are expected. Thus, our bolt model should be accurate in instances where compressive loads are developed and conservative elsewhere. The hinge pin was simulated using the LS-DYNA REVOLUTE_JOINT feature.

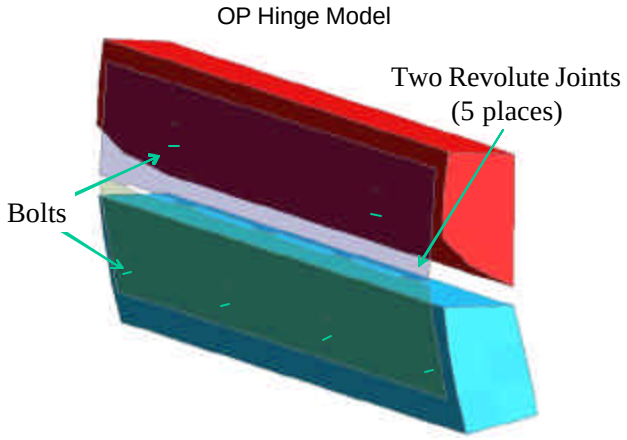

Qualification unit had two bolts in upper hinge block and the prototype unit had three. Both models had four bolts in bottom hinge block.

Figure 2-98 Outerpack Hinge Model

2.12.3.5.3 Qualification Unit Models (QTUs)

As with the Prototype units, the QTUs were constructed from many input files, see Figure 2-99. These files defined various details of the model and were included with, or without, transformations of coordinates and renumbering of identities as the model was assembled.

The main file, Aug19.key, contains the control cards, specifies outputs, contact definitions, and many attributes common to more than one subassembly. The major subassemblies were the Outerpack, Clamshell, and fuel assembly. These were defined in the OPs.key, CS_06_26sl6.key, and FA_remesh_FRslip.key files, respectively. The Outerpack and Clamshell subassemblies are detailed in Figures 2-101, 2-102 and 2-103 (The fuel assembly model was very similar to the one depicted previously in Figure 2-97. A total of 361,333 elements were used in the model (185985 shells, 157031 solids and 18317 beams).

The orientation for each run was defined in individual load case files. Likewise, the material property date was defined in three files which represented three different temperatures and foam densities. Obviously, only one load case file and one material file was invoked per run.

The Clamshell, Figure 2-102 is mounted to the Outerpack, Figure 2-100, with 14 rubber shock mounts. These shock mounts were modeled as discrete elements (springs). Outerpack hinge details were described in the previous section, see Figure 2-98.

Predicted model weight was 2.27 tonnes (4994 lbs). This matched the qualification unit's 4786 lb. average weight within 4.4%.

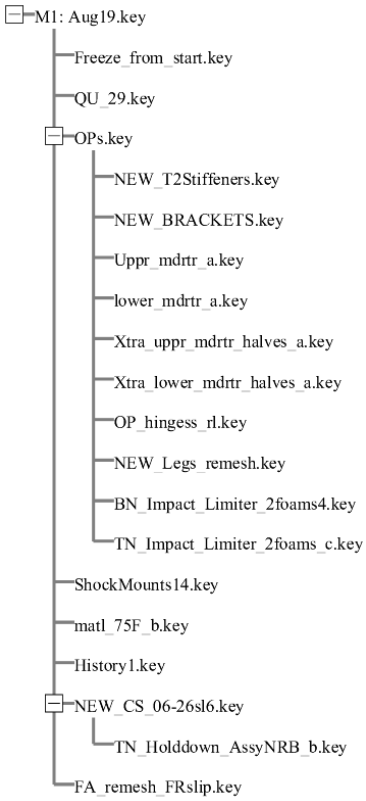

Figure 2-99 FEA Input Files

2.12.3.5.4 Qualification Unit – Outerpack Model Details

The FE model of the outerpack is shown in Figures 2-100 through 2-101A. Key features of the outerpack include the combination circumferential stiffeners/legs, the forklift pockets, the upper and lower outerpack halves, the hinges/latches on the sides, the stacking brackets, and the circumferential stiffeners on the upper outerpack. These features were included in the FE model as described below.

The circumferential stiffeners/legs and forklift pockets (Figure 2-100A) were modeled using 4-node Belytschko-Tsay shell elements (LS-DYNA elform = 2). These elements were integrated at three locations through the thickness using Gaussian quadrature. 1,008 of these elements were used to model the forklift pockets and 4,436 were used modeling the legs.

Both the circumferential stiffeners/legs and forklift pockets are welded to the lower overpack outer casing. In the model, these parts were attached to one another using a penalty based tied contact algorithm (LS-DYNA's TIED_NODES_TO_SURFACE_OFFSET contact algorithm).

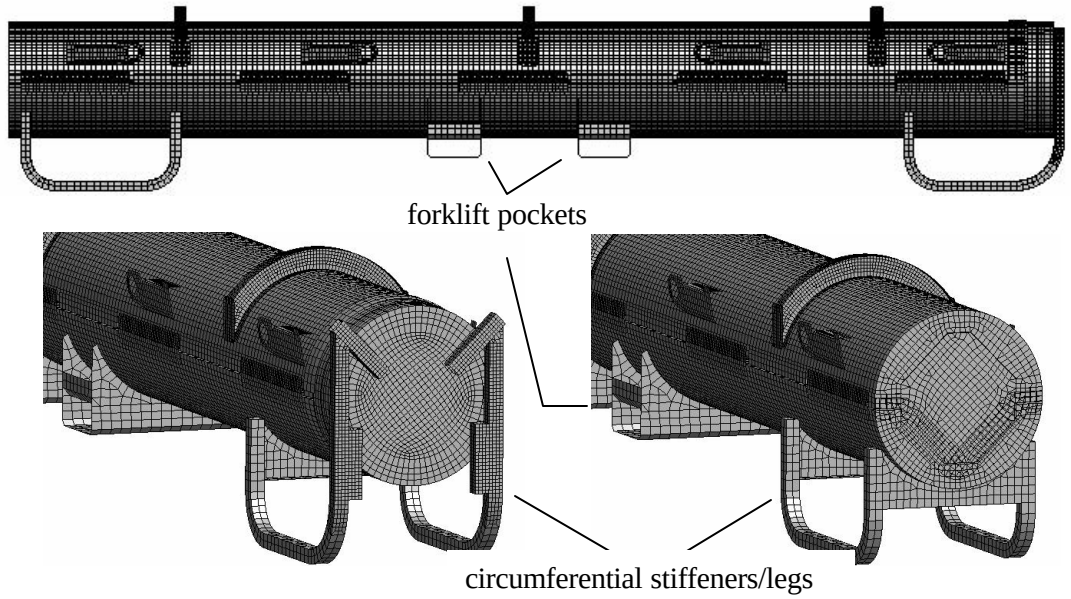

Figure 2-100 Outerpack Mesh in Qualification Unit Model

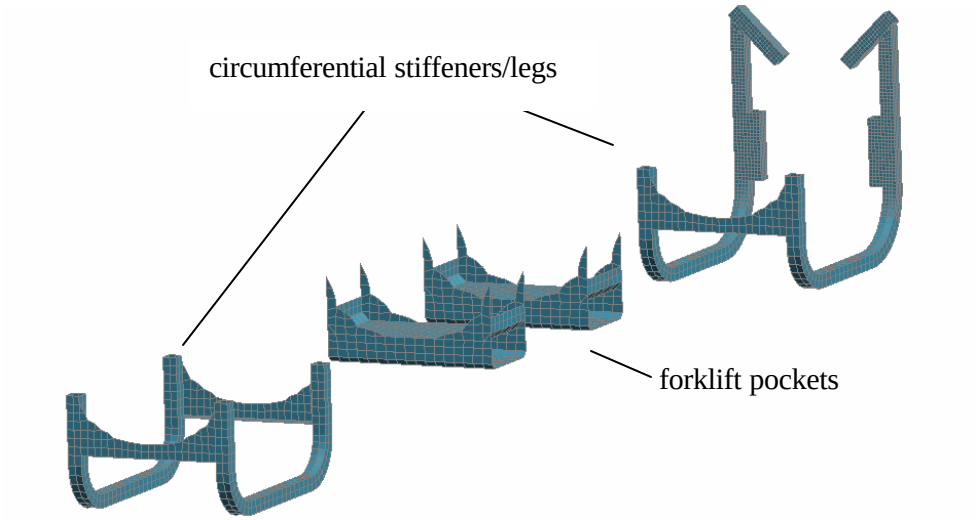

Figure 2-100A FE Meshes of Outerpack Legs and Forklift Pockets

The FE model of the QTU lower outerpack is depicted in Figures 2-100B and 2-100C. In addition to the previously mentioned circumferential stiffeners/legs, the lower outerpack is comprised of a long thick-walled "half-barrel" body and an impact limiter attached to one end (Figure 2-100A). The "half barrel" body is a sandwich construct of 10 pcf foam encased in 0.105 inch thick 304 stainless steel (Figure 2-100C). The outer steel casing was modeled using the same element formulation and integration scheme used for the circumferential stiffeners/legs. 19,516 elements were required. The 10 pcf foam was modeled using 8 node selectively reduced fully integrated solid elements (LS-DYNA elform = 2) in

conjunction with a material formulation developed especially for crushable foam (LS-DYNA material type = 63). Modeling the 10 pcf foam in the lower outerpack required 36,617 elements. Since this foam was poured-in-place, it is adhered to the stainless steel casing. This was modeled by enforcing tied contact between the outer nodes of the foam and the casing. The moderator blocks in the lower outerpack were modeled using 26,368 constant stress solid elements (LS-DYNA elform =1). Linear elastic material properties were used. The moderator blocks were attached to the lower outerpack using four bolts each for the full length moderator sections and two bolts each for the half-length moderator sections at the ends. These bolts were modeled using beam elements (LS-DYNA elform = 9) with a "spot weld" material formulation (LS-DYNA material type = 100.) Contacts between the moderator blocks, the lower outerpack, and the clamshell were defined using a penalty-based contact algorithm that accounts for shell thicknesses and for self contact as well as contact between different parts (LS-DYNA's AUTOMATIC_SINGLE_SURFACE contact algorithm). Contact stiffness was found by dividing the nodal mass by the square of the time step size with a scale factor to ensure stability (LS-DYNA's SOFT=1 contact option.) This approach was used because the foam has stiffness that is one or more orders of magnitude less than the metal parts. (Contact would possibly have broken down with other approaches that basically use the minimum stiffness of the two contact surfaces.)

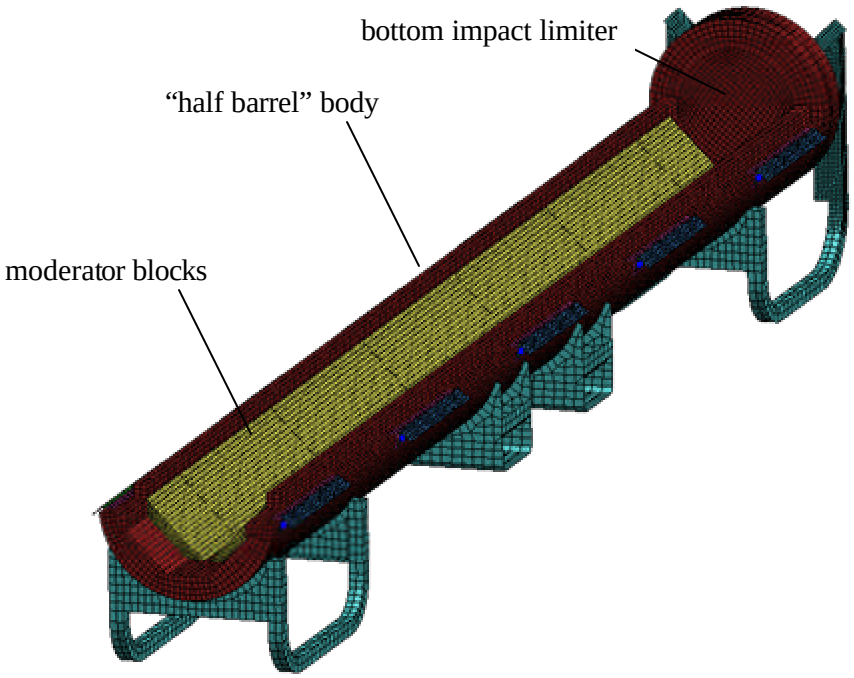

Figure 2-100B Lower Outerpack Mesh for Qualification Unit Model

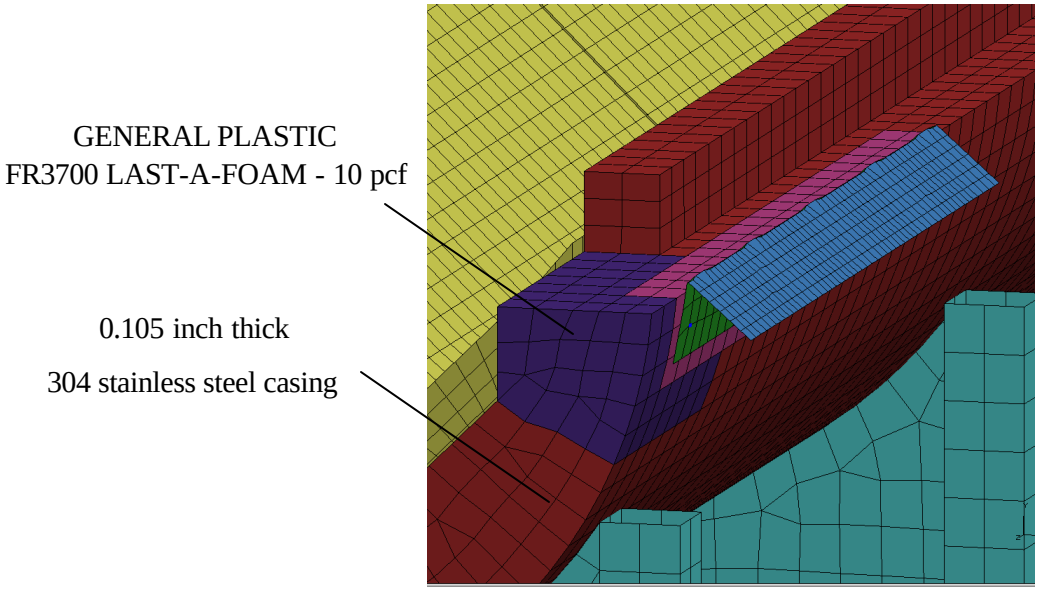

Figure 2-100C Qualification Unit Model Mesh Detail

The FE model of the QTU upper outerpack is depicted in Figure 2-100D. It primarily consists of a long thick-walled "half-barrel" body and an impact limiter attached to one end (Figure 2-100D). The "half barrel" body is a sandwich construct of 10 pcf foam encased in 0.105 inch thick 304 stainless steel. The outer steel casing was modeled using the same element formulation and integration scheme used for the circumferential stiffeners/legs and lower outerpack casing. 18,634 elements were required. The 10 pcf foam was modeled using 8 node selectively reduced fully integrated solid elements (LS-DYNA elform = 2) in conjunction with a material formulation developed especially for crushable foam (LS-DYNA material type = 63). Modeling the 10 pcf foam in the lower outerpack required 36,094 elements. Since this foam was poured-in-place, it is adhered to the stainless steel casing. This was modeled by enforcing tied contact between the outer nodes of the foam and the casing. The moderator blocks in the upper outerpack were modeled using 26,368 constant stress solid elements (LS-DYNA elform = 1). Linear elastic material properties were used. The moderator blocks were attached to the upper outerpack using four bolts each for the full length moderator sections and two bolts each for the half-length moderator sections at the ends. These bolts were modeled using beam elements (LS-DYNA elform = 9) with a "spot weld" material formulation (LS-DYNA material type = 100). Contacts between the moderator blocks, the upper outerpack, and the clamshell were defined using a penalty-based contact algorithm as described for the lower outerpack.

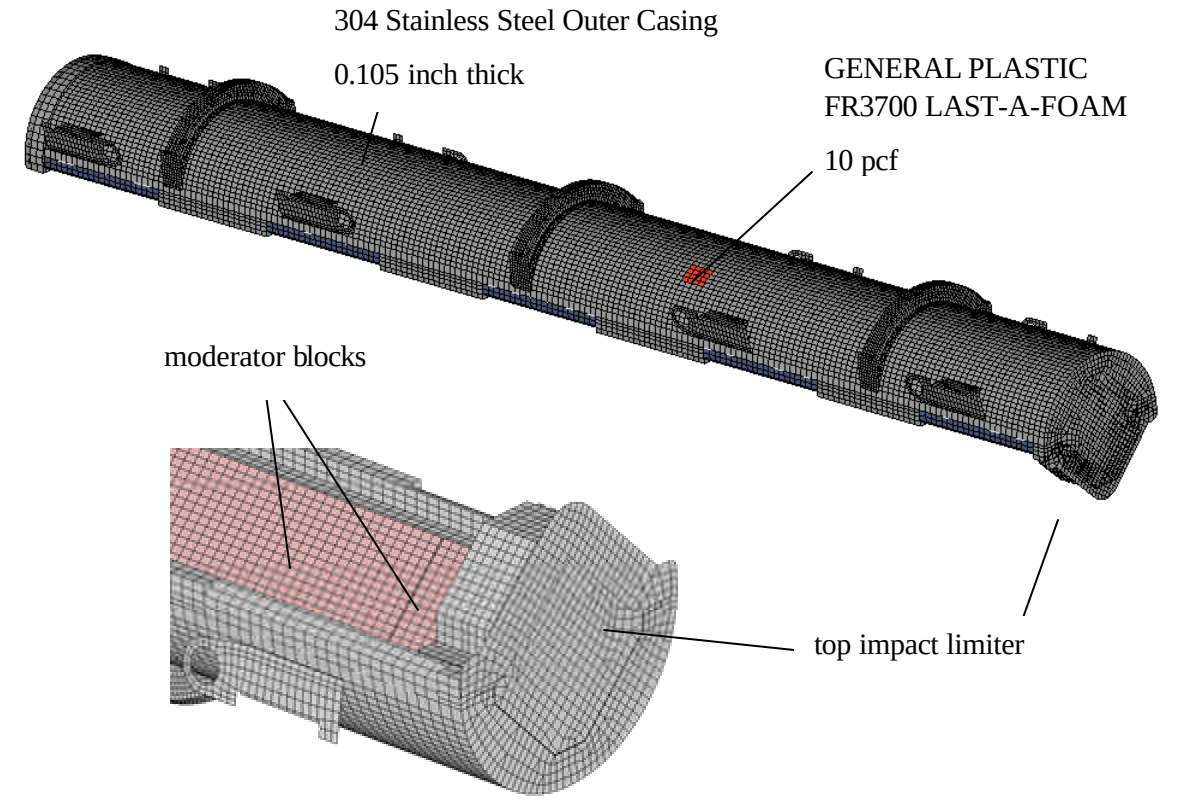

Figure 2-100D Upper Outerpack Mesh for Qualification Unit Model

Model details of the impact limiters are shown in Figure 2-101. Both consisted of two separate foam pieces: a 7 pcf foam block was placed inboard nearest the clamshell and 14 pcf foam covered both ends of the overpacks. These foam pieces were separated and covered by stainless steel. The foams were modeled using the same element formulation and material model as described for the 10 pcf foam in the overpack "barrels" except that each foam density had its own stress-strain curve. The 7 pcf foam in the bottom impact limiter was modeled with 2112 solid elements; the 14 pcf foam was modeled with 4480. The 7 pcf foam in the top impact limiter was modeled with 5248 elements; the 14 pcf foam was modeled with 1755 elements. Because these foams were "cut-to-fit," they were not bonded to the steel cases. Thus, contact between the steel casings and the foam was defined using LS-DYNA's AUTOMATIC_SINGLE_SURFACE contact algorithm as previously described (for contact between the lower outerpack, moderator blocks and clamshell).

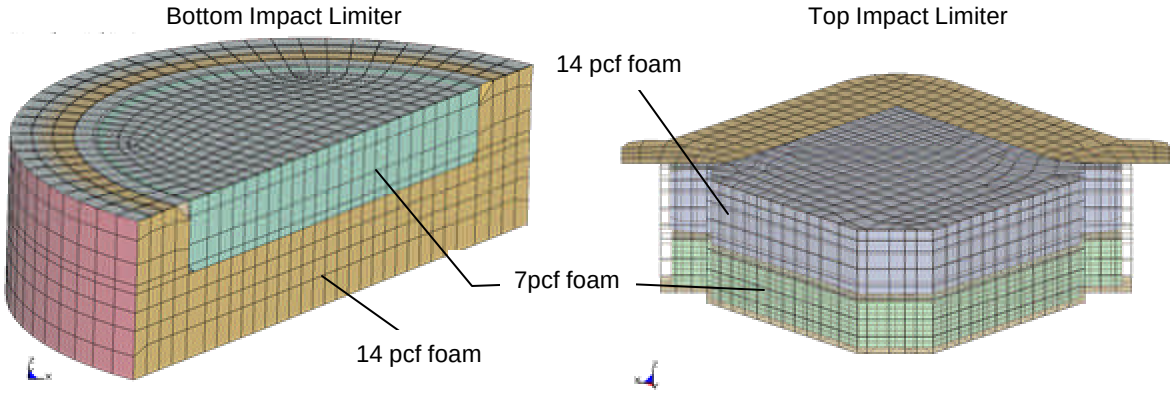

Figure 2-101 Impact Limiter Meshes in Qualification Unit Model

The stacking brackets and circumferential stiffeners on the upper overpack (Figure 2-100D) were modeled using the same element formulation and integration scheme used for the circumferential stiffeners/legs and outerpack casings. 4,404 of these elements were used to model the stiffeners and 1,376 were used modeling the stacking brackets. Both the stiffeners and brackets were secured to the upper outerpack casing using a tied contact algorithm as described for the circumferential stiffeners/forklift pockets and lower overpack casing.

The bolts which secure the outerpack hinges/latches are all that prevent the upper and lower outerpacks from separating upon impact. This was simulated in the model by replication of each physical part of the hinge/latch assemblies. In particular, hinge/latch assemblies including mounting blocks, hinge leaves, and the bolts were modeled (see Figure 2-98 and associated description in Section 2.12.3.5). These assemblies were attached to the upper and lower overpacks via tied (penalty-based) constraints. This methodology permitted relative rotations between the upper and lower outerpacks along the axes of the hinges/latches while resisting any relative translations. Thus, the model forced the overpack latch bolts to prevent the displacement shown in Figure 2-101A. This allowed predicted deformations at the outerpack seam to be realistic (e.g., Figures 2-30B and 2-74.)

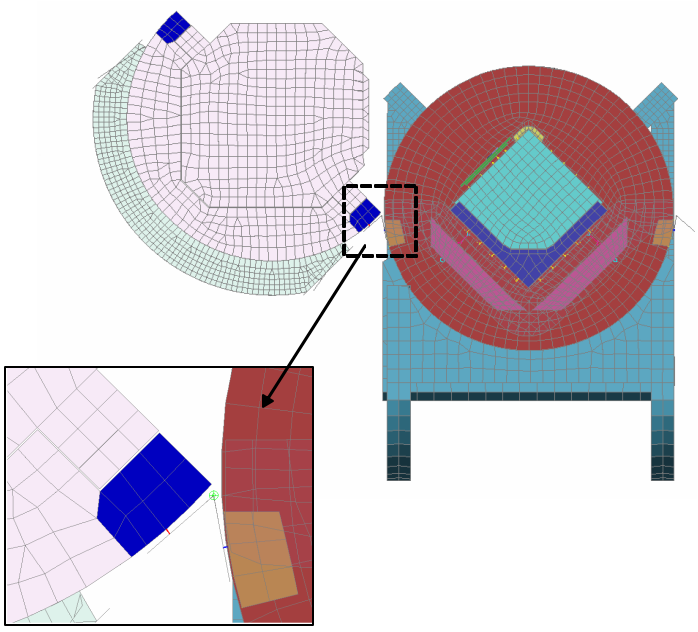

Figure 2-101A Hinge/Latch Feature in Qualification Unit Model

2.12.3.5.5 Qualification Unit – Clamshell Model Details

The FE model of the clamshell is shown in Figures 2-102 through 2-102C. Key features of the clamshell include: the clamshell top assembly, the V-shaped extrusion, the two doors including the hinges, middle latch and locks, and the bottom plate. These features were included in the FE model as described below.

The clamshell top assembly has two major features. First it can swivel from either side to allow access to the top portion of the fuel assembly. This is shown in Figure 2-102A where the CS head is swiveling about its right side. This feature was built into the FE model using the LS-DYNA revolute joint elements. (This is very similar to what was done for the overpack hinges/latches.)

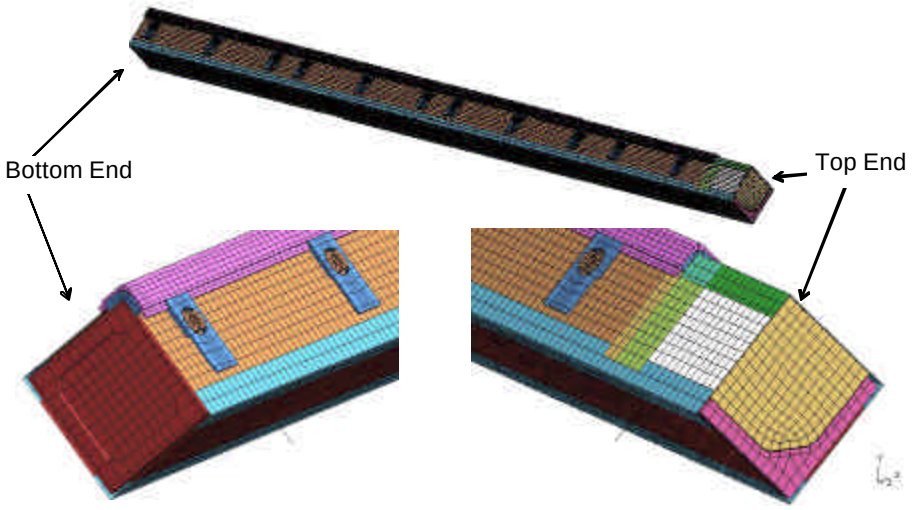

Figure 2-102 Clamshell Mesh in Qualification Unit Model

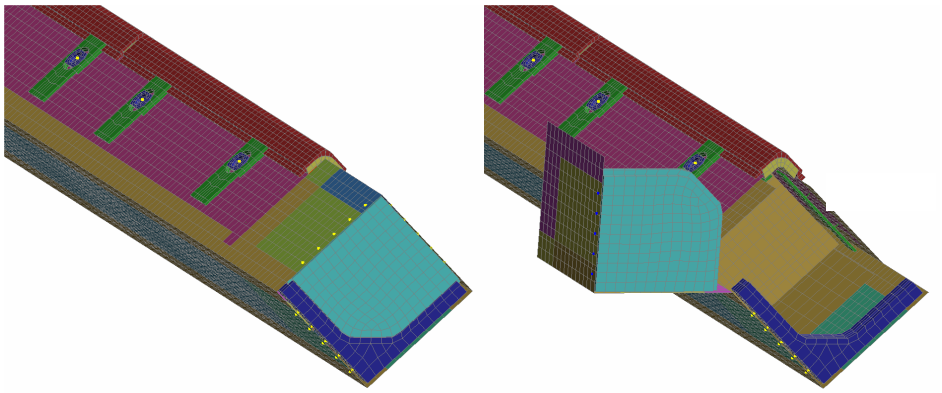

Figure 2-102A Clamshell Top Head in Qualification Unit Model

The second major feature was the top nozzle hold-down bars as shown in Figure 2-102B. Although this hardware has length adjustments to accommodate different fuel assembly heights, the hold-down bar was modeled for the height of an XL fuel assembly. If other fuels were to be modeled, the hold-down bars would need to be scaled in the z-direction. The hold-down bars were modeled with 8 node solid elements and contact between the top nozzle and other fuel and clamshell parts in the near vicinity was defined using LS-DYNA's AUTOMATIC_SINGLE_SURFACE contact algorithm.

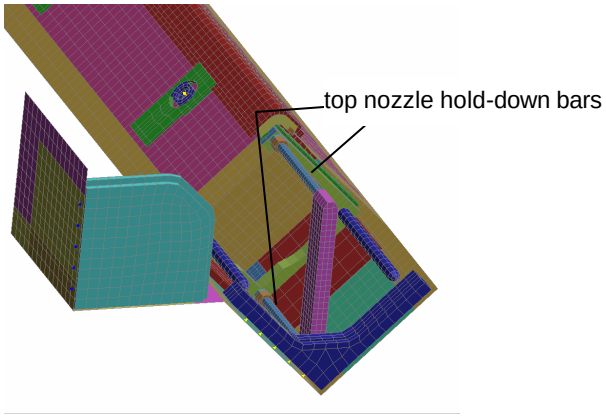

Figure 2-102B Clamshell Top Nozzle Hold-down Bars in Qualification Unit Model

The model of the clamshell latch and hinges allow the doors to rotate about the hinge centerlines as depicted in Figure 2-102C. These features were added using the LS-DYNA revolute joint element as already described.

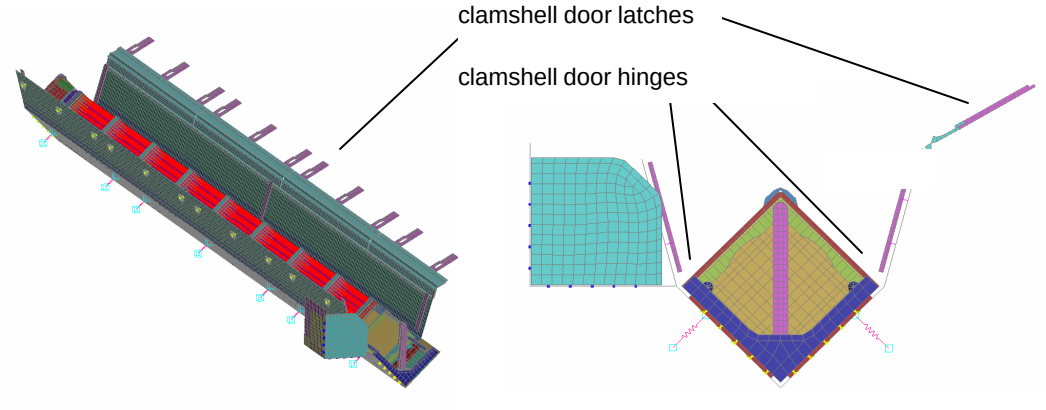

Figure 2-102C Clamshell Hinges and Latches in Qualification Unit Model

2.12.3.6 Model *Input*

Information needed to construct finite element models of the prototype and qualification units included load and boundary condition details, the stiffness and density of the comprising materials, the shipping package geometry, and the interconnections between the various shipping container subassemblies.

Drop Orientation and Initial Conditions – For modeling convenience, different drop orientations were modeled by changing the velocity and gravitational fields instead of rotating the model relative to the

This page intentionally left blank.

model global axes. Loadings were therefore specific to each drop orientation. Further, each analysis was initiated just prior to impact with the shipping package positioned just above the impact surface, having an initial velocity based on drop height (9.14 m for the free drops and 1 m for the pin puncture), and undergoing earth's gravitational pull. This analysis approach minimized computation effort since only minimal calculations of the shipping package during free-fall were needed. The required calculations were as follows.

2.12.3.6.1 Initial Velocity Magnitude (Speed)

The velocity, V, of any object having fallen for a drop height, h, in a constant gravitational field, g, is:

$$V = \sqrt{2gh}$$

Thus, using 9810 mm/s as the value of g, the calculated magnitude of the initial velocities (speed) for the 9 meter free drop and 1 meter pin puncture tests were as shown in Table 2-24.

Table 2-24 Initial Velocities 9 Meter Drop and 1 Meter Pin Puncture Analyses

Test	Drop Height [m]	Initial Velocity (Speed) [mm/s]
9 m drop		
Prototype model	9.0	13288
Qualification model	9.14 (30 ft)	13389
Pin Puncture		
Prototype & Qualification models	1.0	4429

Velocity and Gravitational Fields – In general, a complete description of the position and orientation of an object in 3-dimensional space requires three coordinates and three direction cosines. However, for these drop tests, specification of only two direction cosines is sufficient. This is because both the drop pad and impact pin may be modeled as two-dimensional rigid walls or surfaces. In other words, these items have no distinct feature with respect to the shipping package that requires specification of the angle θ_y in Figure 2-103. Thus, only the angles θ_x and θ_Z are needed to define the velocity and gravitational fields.

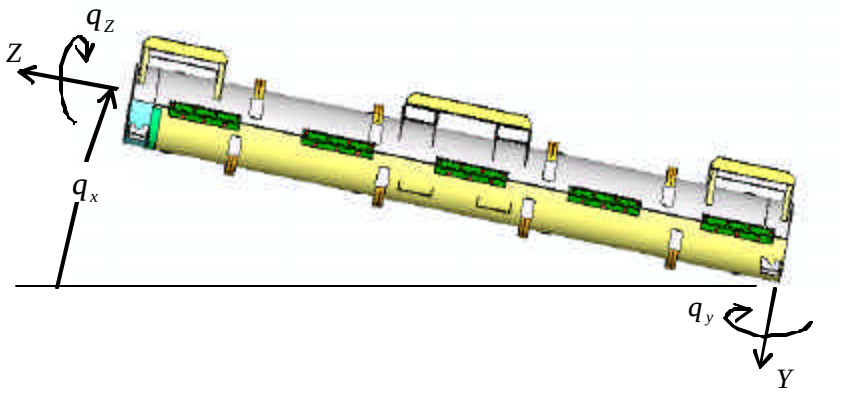

Figure 2-103 Package Drop Angle

Using the angles θ_x and θ_Z shown in Figure 2-69, the velocity and gravitational fields are, respectively,

$$v = A^T \begin{Bmatrix} 0 \\ -V \\ 0 \end{Bmatrix}$$

and

$$a = A^T \begin{Bmatrix} 0 \\ g \\ 0 \end{Bmatrix}$$

where

$$A = \begin{bmatrix} \cos q_z & \sin q_z & 0 \\ \cos q_x \cdot \sin q_z & \cos q_z \cdot \cos q_x & -\sin q_x \\ \sin q_x \cdot \sin q_z & \sin q_x \cdot \cos q_z & \cos q_x \end{bmatrix}$$

The normal to the plane of impact (drop pad surface or pin face) is given by

$$n = A^T \begin{Bmatrix} 0 \\ -1 \\ 0 \end{Bmatrix}$$

The initial velocity field was implemented into the finite element model with the *INITIAL_VELOCITY command in LS-DYNA. The gravity field was applied using the *LOAD_BODY_GENERALIZED

command. Finally, the impact plane was defined using the *RIGIDWALL_PLANAR or *RIGIDWALL_GEOMETRIC_CYLINDER commands. This approach allowed the drop orientation to be changed without altering the model coordinates. It should be noted that the gravity load was applied as a ramped load as shown in Figure 2-70. This was done as a precaution to minimize any numerical oscillations. However, this was probably unnecessary – applying the full gravity load at time zero would most likely produced equivalent results.

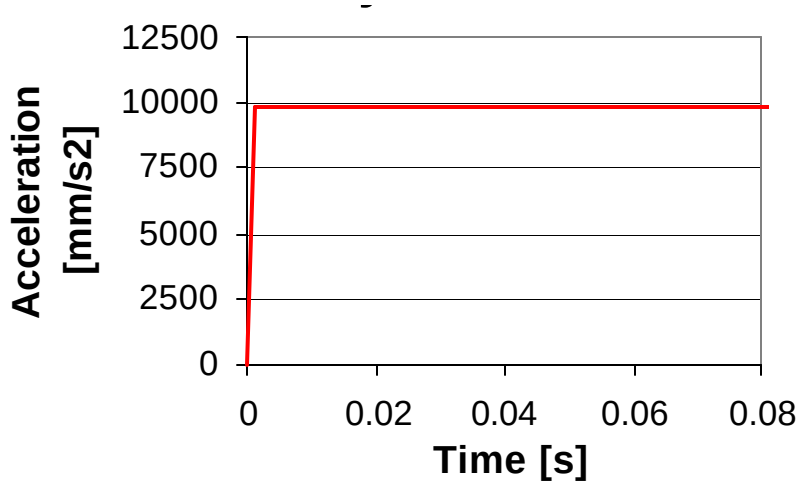

Figure 2-104 Gravity Load Profile

2.12.3.6.2 Material Properties

The crush strength of the polyurethane foam used in the Traveller XL package (LAST-A-FOAM® from General Plastics Manufacturing Company) is strongly influenced by temperature. For example, the perpendicular-to-rise dynamic crush strength of 10 pcf foam at 40% strain is approximately 940 psi at -40°F, 550 psi at 75°F, and just 338 psi at 160°F. Furthermore, foam crush strength is also directly related to foam density. Per the foam procurement specification, density is held within ±1 pcf for the 7 and 10 pcf foam and ±10% for the 14 pcf foam. Both effects were included in our analyses. This was accomplished by specifying the foam crush strength at highest temperature (160°F) and lowest density (nominal density minus 1 pcf or 10%) and at lowest temperature (-40°F) and highest density (nominal density plus 1 pcf or 10%). Foam stress-strain curves used in the qualification unit analysis are shown in Figure 2-105. These were obtained from General Plastics data except that; 1) the curves were extended past General Plastics' recommend maximum strain limit to fully compressed (100% strain) using linear regressions of the last three known points, and 2) the two most crushable foams (6 pcf @160°F and 7 pcf @75°F) were made to follow the 8 pcf @ -40°F curves at strains above 50%, Figure 2-105). The latter adjustment was needed to prevent the foam elements from inverting under the high strains (i.e., this prevented "negative volumes").

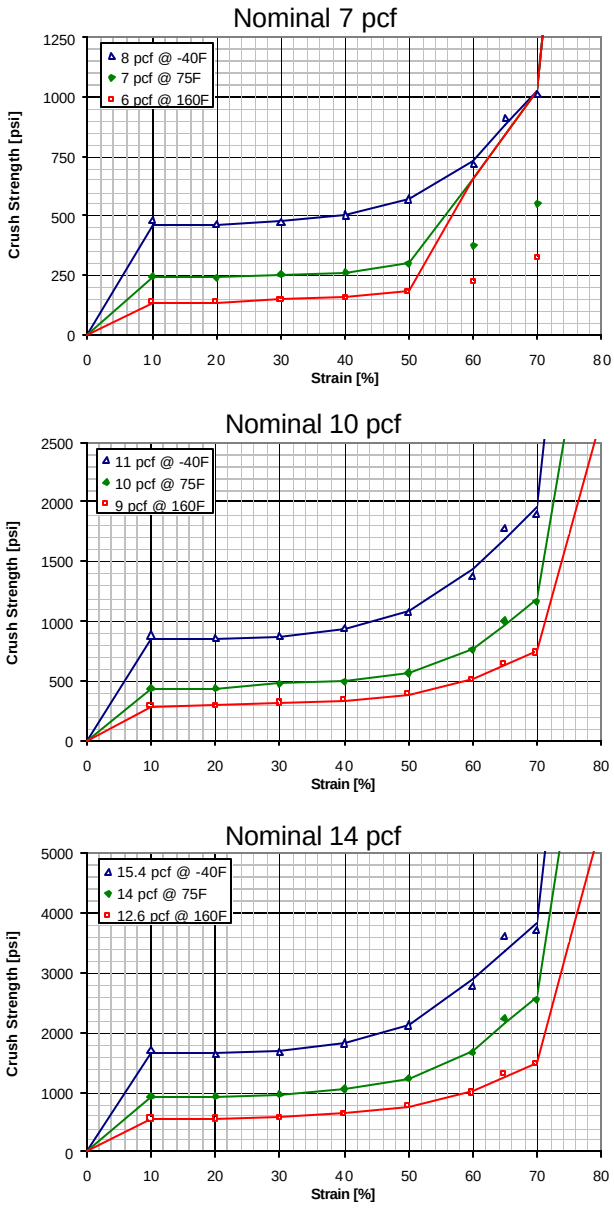

6 pcf @ 160F and 7 pcf @ 75F curves made to follow 8 pcf @ -40F curves for strains >50%.

Figure 2-105 Stress Strain Data for LAST-A_FOAM

The use of a linear elastic material model from 0-10% strain was selected to evaluate the effects of temperature and foam density on drop test reaction forces. From Section 2.12.3.2.6, foam linear data demonstrated that temperature and foam density have a minor effect on the drop test response of the Traveller. The use of true stress-strain data ranging from 0-10% would not impact the conclusions of the comparative analysis.

A typical comparison of foam stress-strain behavior demonstrates that the available strain energy of a linear model is less than that observed with true stress-strain data. The use of true stress-strain data is expected to result in greater foam deflection when compared to linear modeling. Since greater crushing would absorb more kinetic energy, the predicted reaction force of the outerpack using true stress-strain data is expected to be less compared to linear data. It is concluded that the use of linear stress-strain data in the 0-10% range adds additional conservatism to the model.

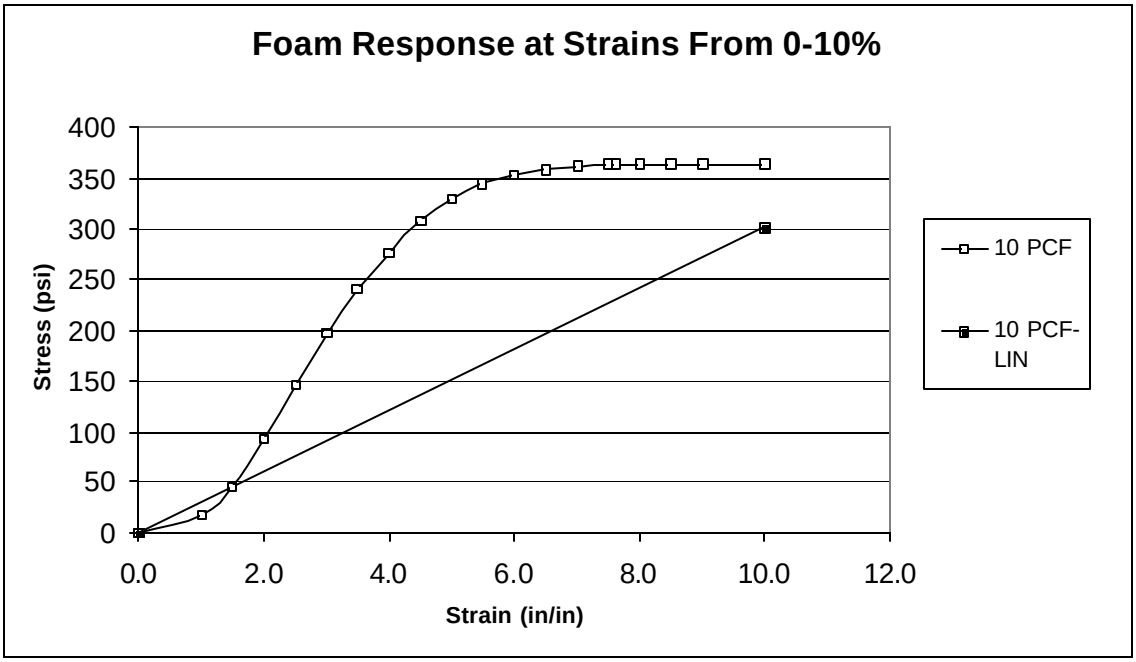

Figure 2-105A Foam Response at Strains from 0-10%

Stress strain characteristics for the 304 stainless steel used in these analyses are shown in Figure 2-106. The 75°F characteristics were obtained from pull tests of samples used in the prototype unit. Based on MIL_HDBK-5H "Metallic Materials and Elements for Aerospace Vehicle Structures," see Figure 2-107, performance at 160°F was estimated by lowering both yield and ultimate strengths to 90% of their values at 75°F. Similarly, the performance at minus 40°F was estimated by raising yield and ultimate strengths to, respectively, 112 and 132% of their values at 75°F, Figure 2-107.

This page intentionally left blank.

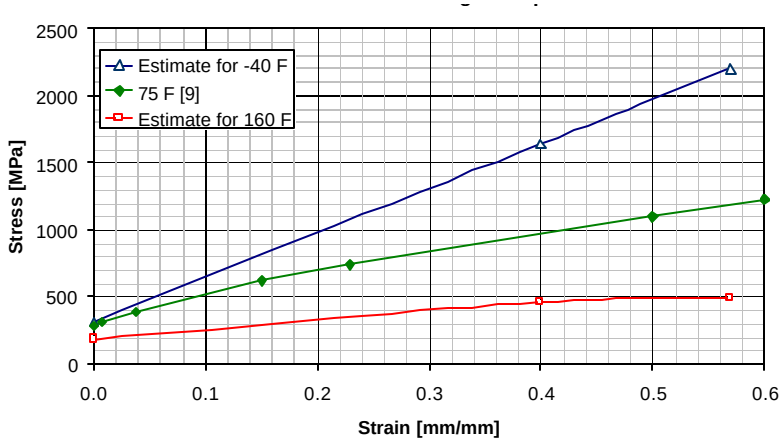

Figure 2-106 Stress- Strain Curves for 304 Stainless Steel

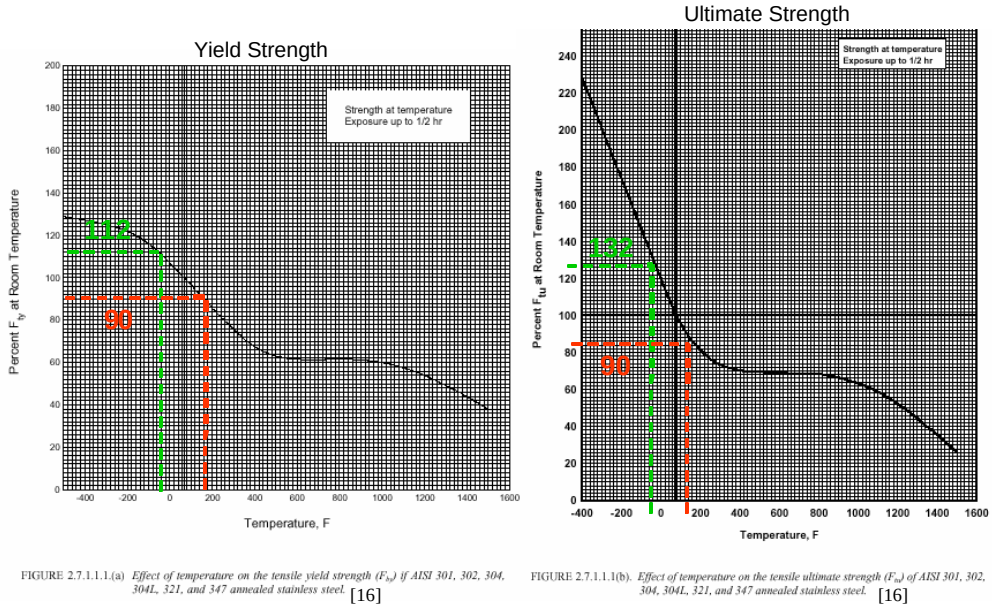

FIGURE 2.7.1.1.1(a) *Effect of temperature on the tensile yield strength (F_{ty}) if AISI 301, 302, 304, 304L, 321, and 347 annealed stainless steel.* [16]

FIGURE 2.7.1.1.1(b). *Effect of temperature on the tensile ultimate strength (F_{tu}) of AISI 301, 302, 304, 304L, 321, and 347 annealed stainless steel.* [16]

Figure 2-107 Temperature Effects on Tensile Properties of Annealed Stainless Steel

Estimated stress strain characteristics for the 6005-T5 aluminum used in these analyses are shown in Figure 2-108. The 75°F characteristics are typical of those for 6061-T6 used in the aerospace and automotive industries.[1] The 6005-T5 properties are similar based on their similar yield and ultimate strength and elongation. Because there was no available temperature dependent data, the curves for -40°F and 160°F were estimated based on the temperature dependence of aluminum alloy 6061T6. This was judged acceptable because alloy 6061-T6 is very similar to 6005-T5. However, for conservatism, we

[1] This data is not published. However, a similar curve is available from ALCAN.

doubled the impact that temperature had on 6061-T6 when estimating the temperature dependence of 6005-T5. For example, yield and ultimate strengths of 6061-T6 at 160°F is expected to be 6 and 4% less than at 75°F, Figure 2-109. However, we estimated these quantities for 6005-T5 by lowering the 75°F values by 12 and 8%. Likewise, when estimating the performance of 6006-T5 at -40°F, we increased the yield and ultimate strengths at 75°F by 8 and 12%, respectively. This is twice the reported impact this temperature reduction has on 6061-T6, Figures 2-109.

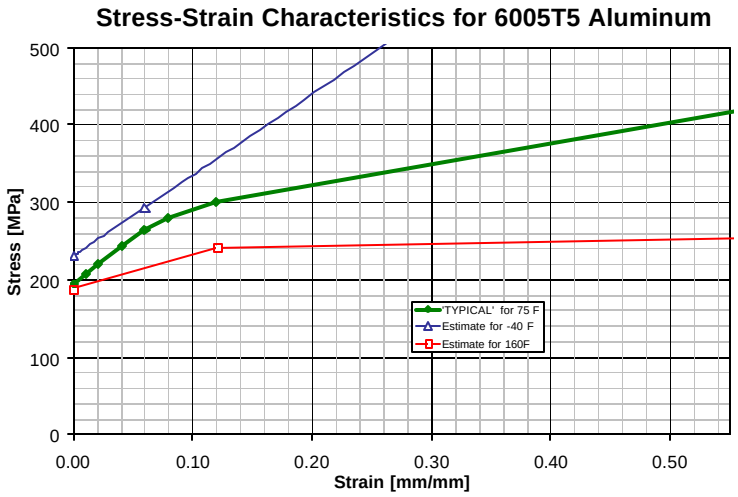

Figure 2-108 Stress-Strain Characteristics of Aluminum in Clamshell

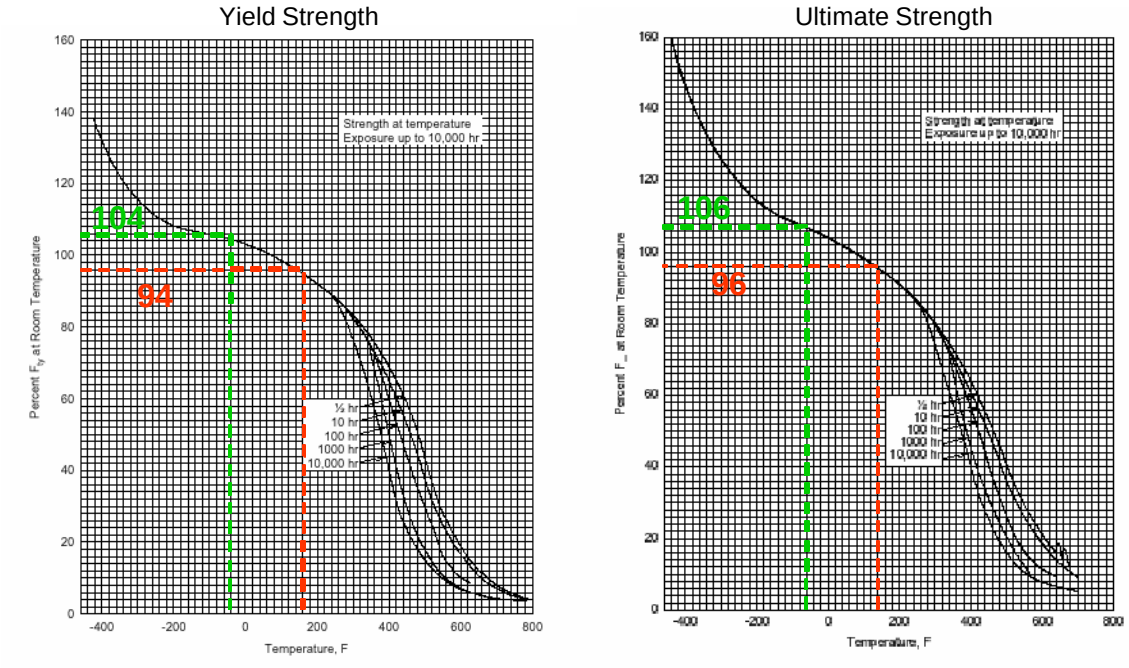

Figure 2-109 Temperature Effects on Tensile Properties of Aluminum in Clamshell

Finally, modulus of elasticity and Poisson's ratio are also influenced by temperature. However, this effect is minimal and was neglected in this highly inelastic analysis. Thus, elastic properties determined at 75°F were used in the model. These are shown in Table 2-25.

Table 2-25 Summary of Elastic Properties

Material	Modulus of Elasticity [GPa]	Poisson's Ratio
304 stainless steel	206.7[a]	0.32[a]
6005T5 aluminum	70 [10]	0.3 [10]
Foam	0.37[b]	N/A

Notes:

a. This value of modulus is approximately 8% higher than the 192.0 GPa recommended at Westinghouse. This Poisson's ratio is approximately 23% higher than the 0.26 recommendation. However, these elastic values were consistently used and these differences likely had little effect in this highly non-elastic analysis.

b. Determined by using stress value at 10% strain instead of offset yield point.

2.12.3.7 Evaluations, Analysis and Detailed Calculations

Many billions of calculations required in these analyses were performed on the HPJ6000 workstation cluster (claxgen1, 2, 3 and 4). However, three additional sets of calculations were required. These were; 1) the calculations of the gravity and velocity fields and the orientation for the rigid wall surface or pin, 2) calculations of bolt factors of safety, and 3) calculations of accelerations from differentiated velocities. Example Calculations of Impact Plane Normal, Gravity Field, and Velocity Field

Horizontal Drop onto Outerpack Latches – A horizontal drop onto the Outerpack latches is shown in Figure 2-26. Using the coordinate system shown in Figure 2-103, this orientation is obtained when $\theta_x = 0$ and $\theta_Z = 90°$. Further, V=13,389 mm/s for a 9.14 m drop, Table 2-24, and g=9810 mm/s^2. Thus,

$$A = \begin{bmatrix} 0.0 & 1.0 & 0.0 \\ 1.0 & 0.0 & 0.0 \\ 0.0 & 0.0 & 1.0 \end{bmatrix},$$

$$n = \begin{bmatrix} 0.0 & 1.0 & 0.0 \\ 1.0 & 0.0 & 0.0 \\ 0.0 & 0.0 & 1.0 \end{bmatrix}^T \cdot \begin{Bmatrix} 0 \\ -1 \\ 0 \end{Bmatrix} = \begin{Bmatrix} 1 \\ 0 \\ 0 \end{Bmatrix},$$

$$v = \begin{bmatrix} 0.0 & 1.0 & 0.0 \\ 1.0 & 0.0 & 0.0 \\ 0.0 & 0.0 & 1.0 \end{bmatrix}^T \cdot \begin{Bmatrix} 0 \\ -13{,}389 \\ 0 \end{Bmatrix} = \begin{Bmatrix} -13{,}389 \\ 0 \\ 0 \end{Bmatrix},$$

and

$$g = \begin{bmatrix} 0.0 & 1.0 & 0.0 \\ 1.0 & 0.0 & 0.0 \\ 0.0 & 0.0 & 1.0 \end{bmatrix}^T \cdot \begin{Bmatrix} 0 \\ 9{,}810 \\ 0 \end{Bmatrix} = \begin{Bmatrix} 9{,}810 \\ 0 \\ 0 \end{Bmatrix}.$$

Example Calculation of Bolt Factor of Safety – The equation below is utilized to calculate bolt factor of safety. For example, suppose a Clamshell bolt is subjected to an axial force of 5,134 lb_f and shear forces of 925 and 3380 lb_f. A factor of safety is calculated by first calculating the "Actual" (load) using these values of load, Table 2-26.

$$\begin{aligned} Actual &= \left(\frac{F_{axial}}{FN\_ult}\right)^2 + \left(\frac{F_{yshear}}{FS\_ult}\right)^2 + \left(\frac{F_{zshear}}{FS\_ult}\right)^2 \\ &= \left(\frac{5{,}134}{12{,}070}\right)^2 + \left(\frac{925}{6{,}040}\right)^2 + \left(\frac{3{,}380}{6{,}040}\right)^2 \\ &= 0.5175 \end{aligned}$$

.

This value must be divided into the "Allowable" which is 1.0. Thus, the factor of safety for the bolt in this example is 1.93. (These loads correspond to those predicted for the Clamshell keeper bolt which is third down from the top end of the Clamshell during a horizontal side drop onto the latches at time 0.0072s. The calculated value for factor of safety corresponds to that shown in Table 2-11.

Description of Acceleration Calculations – Predicted accelerations, as shown in Figures 2-88 through 2-92, were obtained by differentiating predicted nodal velocities sampled at a frequency of 4 KHz and applying a "light" (SAE 180 Hz) filter. This technique was used because the finite-difference technique used in LS-DYNA yields very noisy accelerations. These nodal accelerations are indeed accurate in an average sense, but not in an absolute value. The differentiated velocity technique allowed the true trend in accelerations to be discerned. The calculations were accomplished with the LS-POST program.

2.12.3.8 Accelerometer Test Setup

Prior to testing, piezoelectric accelerometers were mounted on the Outerpack and Clamshells of both test prototypes. The intent was to measure the accelerations at a few critical points so that the forces involved in the drops would be better known and so that the FEA results could be validated.

Three accelerometers were positioned on the Prototype Unit-1 Test series 1, Figure 2-110. One accelerometer was on the Clamshell top plate and thus was near the initial impact end. The other two were positioned on the secondary impact end at the Clamshell bottom plate and bottom impact limiter. Further details of this instrumentation are available in Appendix 2.12.4.

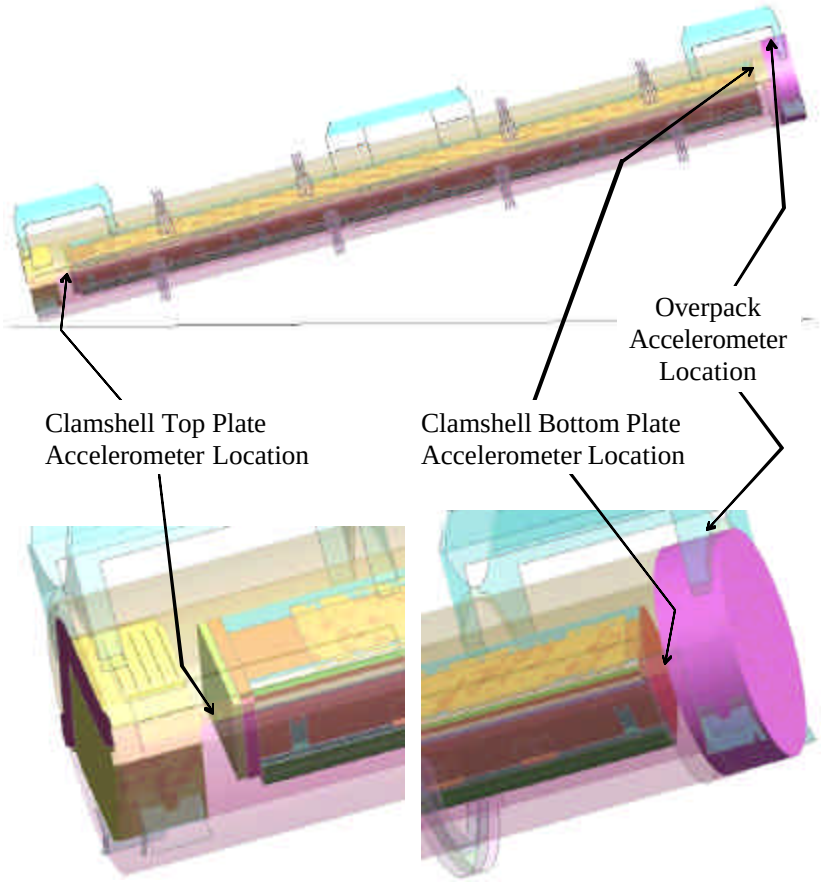

Figure 2-110 Accelerometer Locations on Prototype Unit 1

2.12.3.9 Bolt Factor of Safety Calculation

Bolt factors of safety (FS)

$$F.S. = \frac{\text{Allowable}}{\text{Actual}} \tag{H-1}$$

were based on the failure criteria

$$\left(\frac{F_{axial}}{FN\_ult}\right)^2 + \left(\frac{F_{yshear}}{FS\_ult}\right)^2 + \left(\frac{F_{zshear}}{FS\_ult}\right)^2 \geq 1. \tag{H-2}$$

This commonly-used criterion was chosen because it accounts for the effects of both axial and shear forces. (Note: the left side of equation H-2 is the "Actual" in equation H-1 and the "Allowable" is unity.)

The loads in equation H-2 were determined from the finite element analysis; the tensile and shear strengths are shown in Table 2-26. Initially, the tensile strengths were estimated from the tensile to proof strength ratios for Grade 2 bolts, Tables 2-27 and 2-28, obtained from. Use of the ratios obtained for Grade 2 bolts was justified because the proof strengths of these bolts should be just above Grade 2 levels based on their minimum strength of 70 ksi. However, bolt strengths estimated in this manner did not result in adequate factors of safety for each Outerpack bolt when the Traveller XL package was dropped horizontally, Figure 2-26. However, the specification for the Outerpack bolts was changed in the design of the CTU unit. The new bolt specification for CTU and production packages is ASTM A193 Class 1 B8 which has an ultimate tensile strength minimum of 75 ksi. Additionally, the number of Outerpack hinge bolts has increased to 12 bolts per side on the top leaf and bottom hinge leaf for both the XL and STD packages. This increase in the number of bolts, and the increase in strength results in a factor of safety of 1.12 for the bounding Traveller XL's worst bolt, in the worst case bolt failure orientation (the side drop).

Table 2-26 Bolt Strength Summary

Location	Size	Thread Area [in^2] [13]	Minimum Yield Strength [ksi]	Estimated Minimum Proof Strength [lbf](1)	Ratio of Tensile to Proof Strength(2)	FN_ult [lbf]	NS_ult [lbs](5)
CS bolts	1/2"-13	0.142	70 [14]	8,940	1.35	12,070(3)	6,040
Bottom OP hinge bolts	5/8"-11	0.226	70 [14]	14,240	1.35	19,200(3)	9,600
Top OP hinge bolts	3/4"-10	0.334	70 [14]	21,040	1.34	28,200(3)	14,100
			100 [18]	30,060	N/A	41,750(4)	20,900

Notes:

(1) 0.9 * thread area * min yield strength

(2) Based on estimated proof strength and Table *2-28*

(3) Estimated min proof strength * ratio of Tensile to proof strength

(4) Minimum Ultimate Tensile Strength of 125 ksi * thread area

(5) 0.5 *FN_ult

Table 2-27 Strengths of Various Classifications of Bolts [14]

Nominal Dia of Product and Threads per in	Stress Area, in^2	Grade 1		Grade 2		Grade 4		Grades 5 and 5.2		Grade 5.1		Grade 7		Grades 8, 8.1, and 8.2	
		Proof Load, lb	Tensile Strength min, lb	Proof Load, lb	Tensile Strength min, lb	Proof Load, lb	Tensile Strength min, lb	Proof Load, lb	Tensile Strength min, lb	Proof Load, lb	Tensile Strength min, lb	Proof Load, lb	Tensile Strength min, lb	Proof Load, lb	Tensile Strength min, lb
Coarse-Thread Series – UNC															
No. 6-32	0.00909	–	–	–	–	–	–	–	–	750	1,100	–	–	–	–
8-32	0.0140	–	–	–	–	–	–	–	–	1,200	1,700	–	–	–	–
10-24	0.0175	–	–	–	–	–	–	–	–	1,500	2,100	–	–	–	–
12-24	0.0242	–	–	–	–	–	–	–	–	2,050	2,900	–	–	–	–
1/4-20	0.0318	1,050	1,900	1.750	2,350	2,050	3,650	2,700	3,800	2,700	3,800	3,350	4,250	3,800	4,750
5/16-18	0.0524	1,750	3,150	2,900	3,900	3,400	6,000	4,450	6,300	4,450	6,300	5,500	6,950	6,300	7,850
3/8-16	0.0775	2,550	4,650	4,250	5,750	5,050	8,400	6,600	9,300	6,600	9,300	8,150	10,300	9,300	11,600
7/16-14	0.1063	3,500	6,400	5,850	7,850	6,900	12,200	9,050	12,800	9,050	12,800	11,200	14,100	12,800	15,900
1/2-13	0.1419	4,700	8,500	7,800	10,500	9,200	16,300	12,100	17,000	12,100	17,000	14,900	18,900	17,000	21,300
9/16-12	0.182	6,000	10,900	10,000	13,500	11,800	20,900	15,500	21,800	15,500	21,800	19,100	24,200	21,800	27,300
5/8-11	0.226	7,450	13,600	12,400	16,700	14,700	25,400	19,200	27,100	19,200	27,100	23,700	30,100	27,100	33,900
3/4-10	0.334	11,000	20,000	18,400	24,700	21,700	38,400	28,400	40,100	–	–	35,100	44,400	40,100	50,100
7/8-9	0.462	15,200	27,700	15,200	27,700	30,000	53,100	39,300	55,400	–	–	48,500	61,400	55,400	69,300
1-8	0.606	20,000	36,400	20,000	36,400	39,400	69,700	51,500	72,700	–	–	63,600	80,600	72,700	90,900
1-1/8 - 7	0.763	25,200	45,800	25,200	45,800	49,600	87,700	56,500	80,100	–	–	80,100	101,500	91,600	114,400
1-1/4 - 7	0.969	32,000	58,100	32,000	58,100	63,000	111,400	71,700	101,700	–	–	101,700	127,700	116,300	145,400
1-3/8 - 6	1.155	38,100	69,300	38,100	69,300	75,100	132,800	85,500	121,300	–	–	121,300	153,600	138,600	173,200
1-1/2 - 6	1.405	46,400	84,300	46,400	84,300	91,300	161,600	104,000	147,500	–	–	147,500	186,900	168,600	210,800

Table 2-28 Bolt Strength Ratio

Size	Tensile to Proof Strength Ratio					
	Grade 1	Grade 2	Grade 4	Grades 5, 5.1 and 5.2	Grade 7	Grades 8, 8.1 and 8.2
½-13	1.81	1.35	1.77	1.40	1.27	1.25
5/8-11	1.83	1.35	1.73	1.41	1.27	1.25
¾-10	1.82	1.34	1.77	1.41	1.26	1.25

2.12.4 TRAVELLER DROP TESTS RESULTS

Three series of full scale drop tests have been performed on the Traveller package to evaluate the performance of the design. This appendix will summarize structural performance of the Traveller during these tests. The objectives, test articles, results and lessons learned will be described. The three series were:

- Prototype Tests
- Qualification Tests
- Certification Tests

2.12.4.1 Prototype Test Unit Drop Tests

Testing was conducted at Columbiana High Tech Company (CHT) in Columbiana, Ohio during the week of January 27-30, 2003 (Ref. 3).

An as-built Traveller package prototype is shown in Figures 2-111 and 2-112. Figure 2-111 shows the internal packaging including the 17x71 XL fuel assembly, Clamshell, and moderator blocks. Figure 2-112 shows the closed Outerpack. The prototype packages employed 11 pcf foam along the axial section of the package and 16 pcf foam in the endcaps. Furthermore, the Outerpack consisted of 11 gage inner and outer skin. Each package also contained 22 shock mounts to connect the Clamshell to the Outerpack.

Test Series 1 – Test series 1 was conducted on January 27th through 28th and included two 9 meter drop tests plus a pin-puncture test. The package's test weight was 5072 pounds. Drop orientations are shown in Figure 2-113 and Table 2-29.

The Outerpack retained its basic circular pre-test shape except for localized plastic deformation from the 9 meter drop tests and the pin-puncture test. One bolt on the lower Outerpack hinge failed after completion of the last 9 meter drop test. The Outerpack did not separate after any impacts, and the pin did not perforate the inner or outer shell. The internal damage was minimal. The fuel assembly's envelope decreased from 8.418" nominal to 8.25" maximum after the first 9 meter drop test, and reduced further to 8.13" maximum after second 9 meter drop test. Fuel rod gaps globally decreased (the fuel envelope decreased), but local expansion was noted between a few rods with a maximum measured gap of .188" for the first 9 meter drop test and .625" maximum measured gap for second 9 meter drop test (compared to the nominal gap of .122"). The polyethylene moderator blocks and aluminum neutron "poison plates" maintained position. The Clamshell doors remained closed, but the top and bottom heads were separated from the Clamshell. The separation was caused by the fuel assembly deceleration forces reacting against the clamshell end plate. The bearing force of the bolts (a shear effect on the top head plate) from impact was sufficient to fail the material in the bolt slots for both head pieces. The fuel inspection indicated that no fuel rods had ruptured, and that the axial position of fuel rods maintained location between bottom and top nozzle. The failure the clamshell endplates was due to the bolt slots being modified as a result of warping of the clamshell during fabrication.

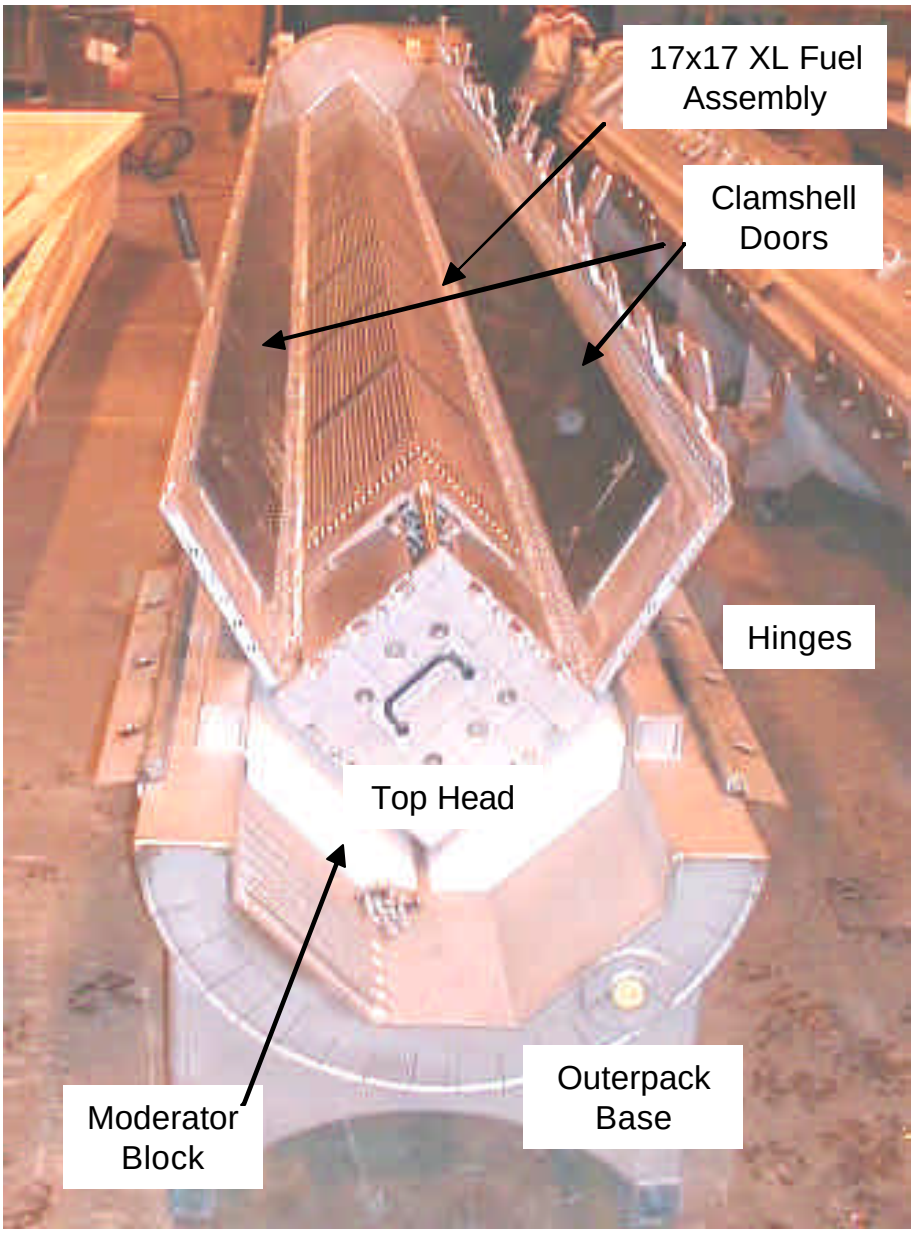

Figure 2-111 Traveller Prototype Internal View

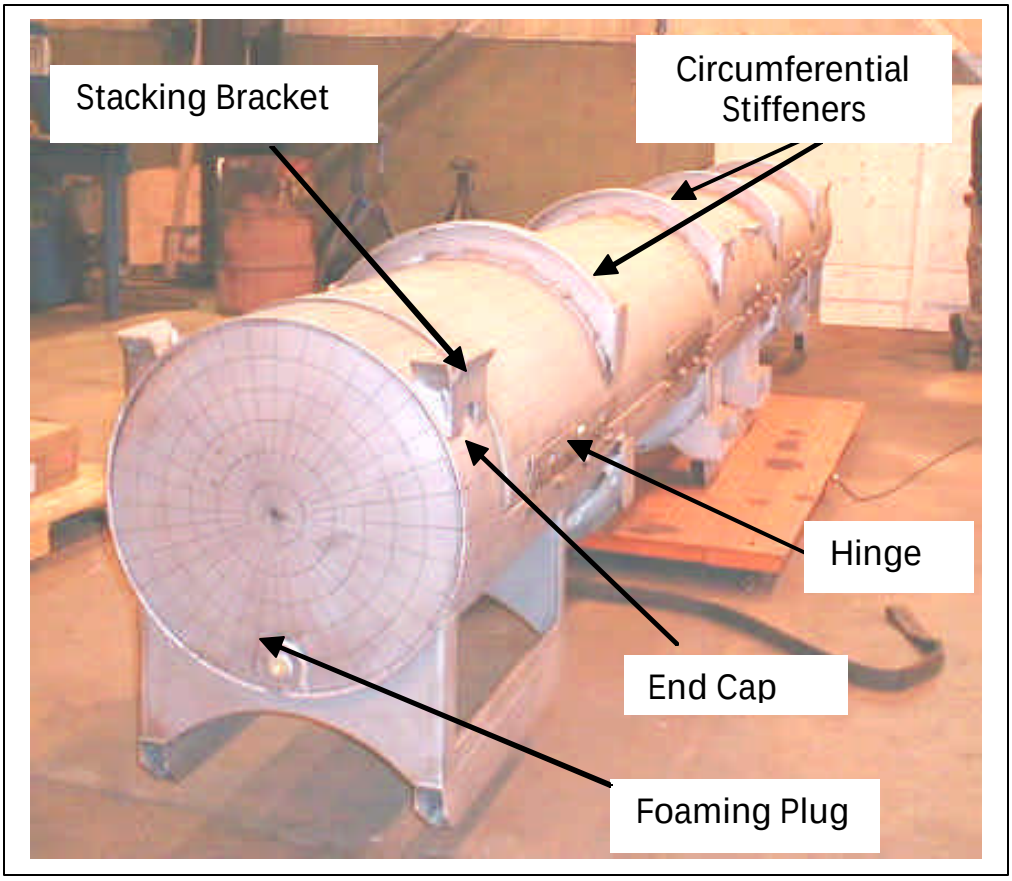

Figure 2-112 Traveller Prototype External View

Table 2-29 Series 1 As-Tested Drop Conditions

Test Sequence	Test Pitch Attitude	Test Roll Attitude	Impact Location
1.1) 9 m Low Angle	14.5°	180°	T/N primary impact on OP top
1.2) 9 m CG-over-corner	71°	90°	B/N primary impact on OP hinge
1.3) 1 m Pin-puncture	20°	180°	Center of Gravity (Axial) on OP top, T/N end down

Test 1.1 – The Outerpack retained its basic circular pre-test shape except for localized plastic deformation from the 9 meter drop test. Impact zones from the drop test were localized at the nozzle impact locations on the package ends. The Outerpack did not separate after the impact, and no bolt failures on the Outerpack hinge were noted. The top nozzle damage zone consisted of local crush approximately 12" wide, 9" axially and a maximum crush of approximately 1.5". The circumferential stiffeners were crushed (Figure 2-114) and inhibited global crushing on the Outerpack. The bottom nozzle damage zone consisted of local crush approximately 11.5" wide, a maximum crush of approximately 3/4", and axially from the package end to the edge of the stiffening ring. The internal damage was minimal as shown in Figures 2-113 and 2-114. The polyethylene moderator blocks and aluminum neutron "poison plates"

maintained position. The Clamshell doors remained closed, but the Clamshell bulged outwardly approximately 0.25" locally at the grid locations in a section 54" long at the bottom nozzle end. The fuel inspection indicated that no fuel rods had ruptured, and that the axial position of fuel rods maintained location between bottom and top nozzle. The average measured fuel envelope decreased from 8.418" nominally to 8.25" maximum, and the maximum measured fuel rod gap was found to be 0.188" locally (observed at one or two rods along the envelope) compared to the nominal gap of 0.122". Figures 2-114 and 2-115 summarize the results of this drop test.

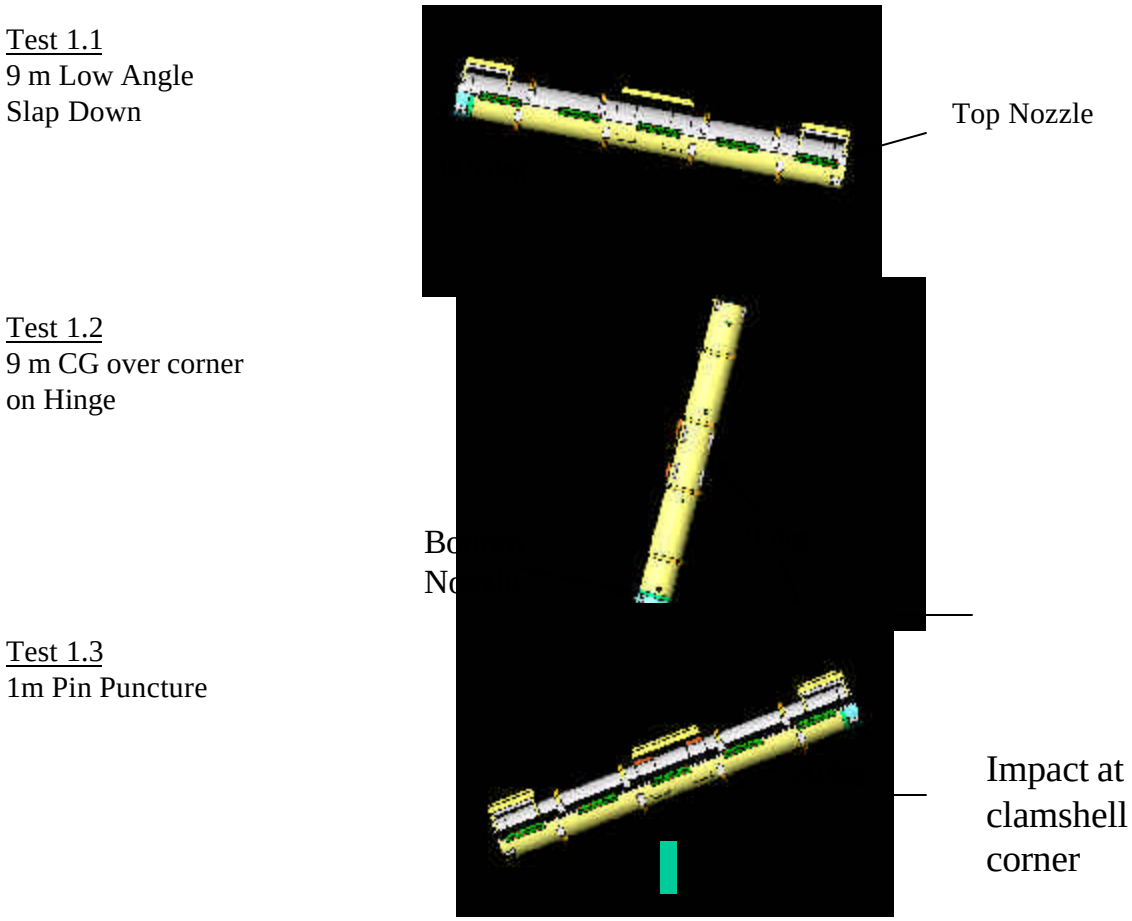

Figure 2-113 Drop Orientations for Prototype Test Series 1

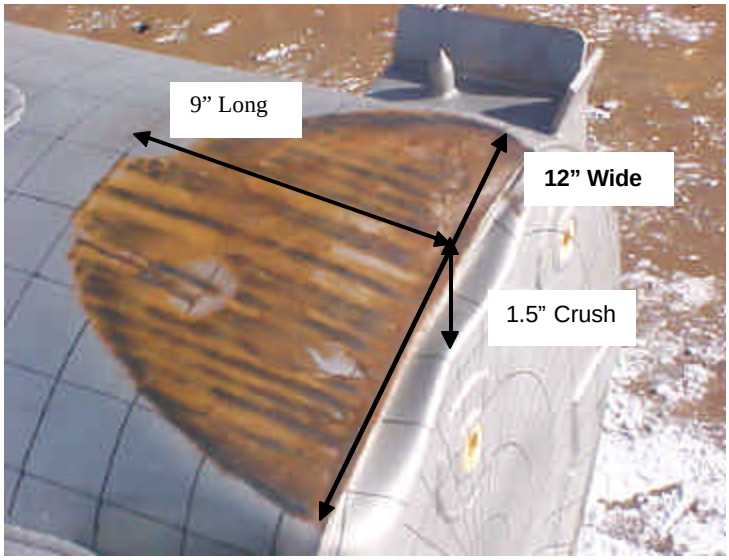

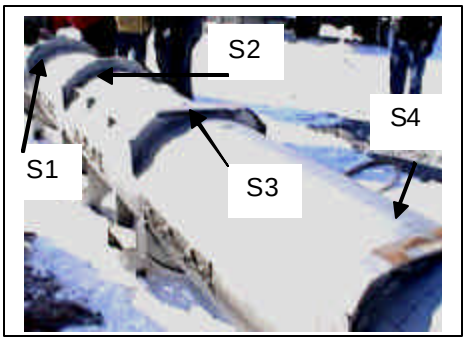

Stiffening rings show progressive damage from T/N

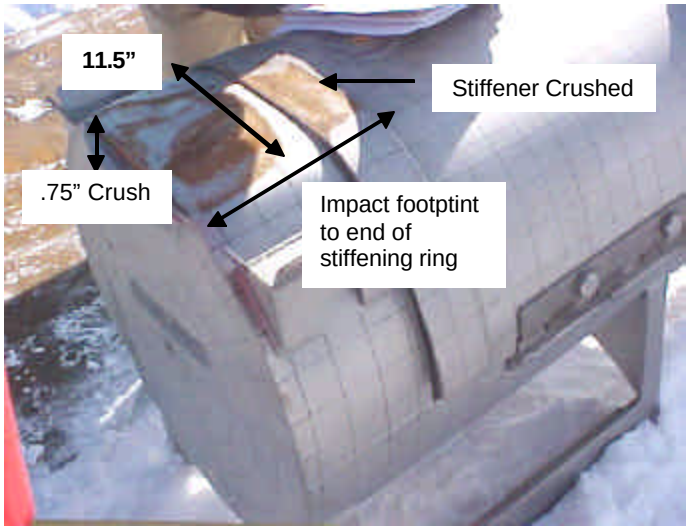

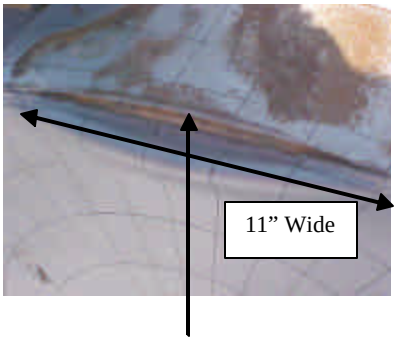

Small tear at Bottom End cap/Plate Seam

Figure 2-114 Traveller Prototype Exterior After Test 1.1

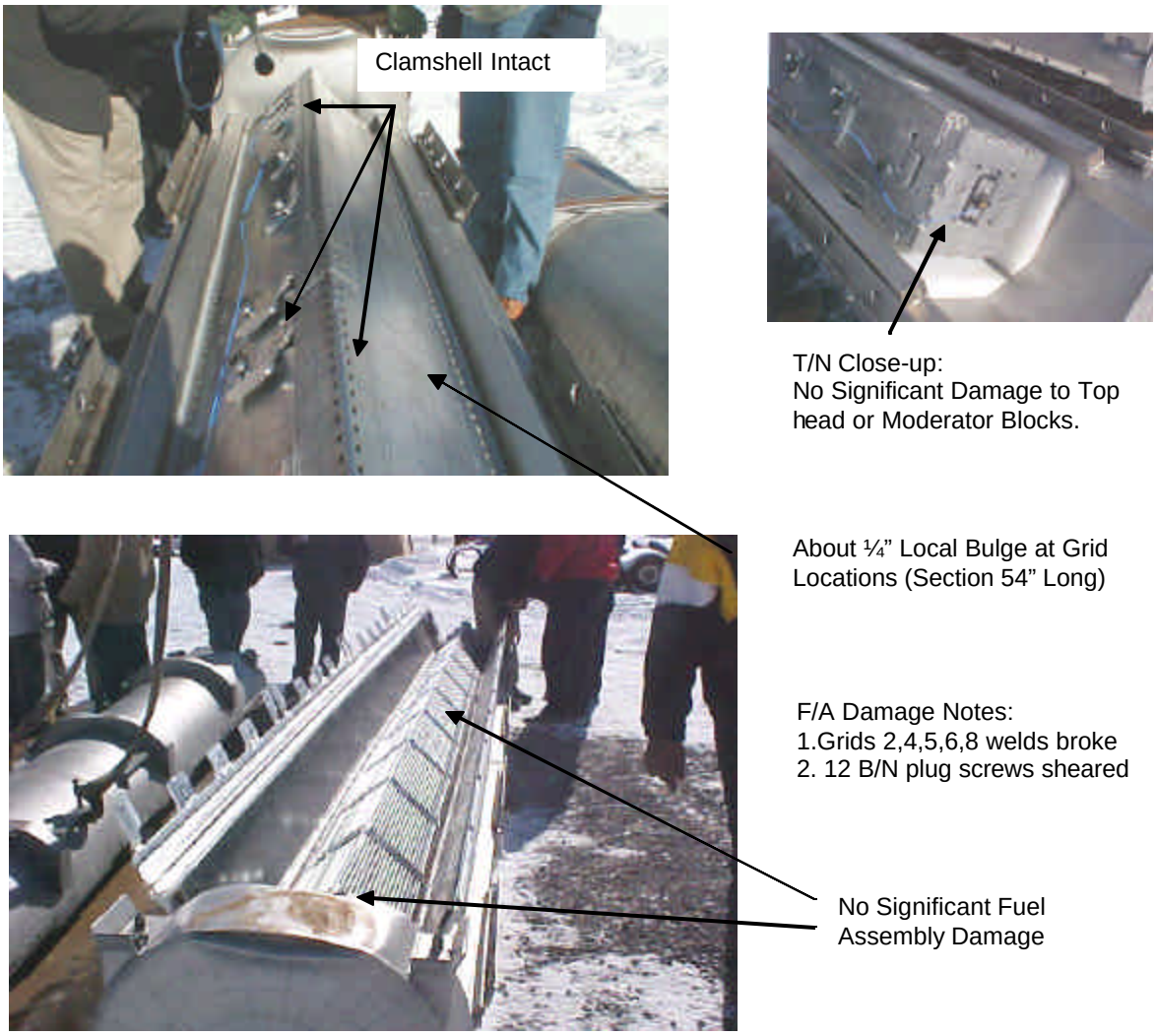

Figure 2-115 Traveller Prototype Interior After Test 1.1

Test 1.2 – The Outerpack retained its basic circular pre-test shape except for localized plastic deformation from the 9 meter drop test. Impact zones from the drop test were localized at the nozzle impact locations on the package ends. The Outerpack did not separate after the impact. One bolt failure on the Outerpack lower hinge, top nozzle end was noted. The bottom nozzle damage zone consisted of local crush approximately 10" wide, 22" tall and a maximum crush of approximately 3". The impact encompassed the stacking bracket which caused local buckling at the top/bottom Outerpack joint. A small ripple occurred in the Outerpack at this location. In addition, a tear in the Outerpack end cap measuring 8" wide resulted from the impact The top nozzle damage zone consisted of local crush approximately 6" wide, 13" long and a maximum crush of approximately 1/4". The relatively small amount of crushing is attributed the stacking bracket impacting the Outerpack in a normal direction and spreading the load more uniformly along the Outerpack length. The internal damage was more substantial than the previous drop test. The polyethylene moderator blocks and aluminum neutron"poison plates" maintained position. The Clamshell doors remained closed, but the top and bottom head pieces separated from the Clamshell. The separation

was caused by material shear-out as the top head connector bolts beared against the bolt slots. The bearing force of the bolts (a shear effect on the top head plate) from impact was of sufficient load to fail the material in the bolt slots for both head pieces. The fuel inspection indicated that no fuel rods had ruptured, and that the position of fuel rods maintained axial location between bottom and top nozzle. The maximum measured fuel envelope compressed from 8.25" after test 1.1 to 8.13", and the maximum measured fuel rod gap increased from 0.188" to 0.625" locally (observed at one or two rods along the envelope). The fuel rod gap expansion was also localized to Grids P, 1, 2, 3, and 4. In addition, Grid 2 failed by means of the weld joint tearing on the grid corner. External and internal results are summarized in Figures 2-116 and 2-117.

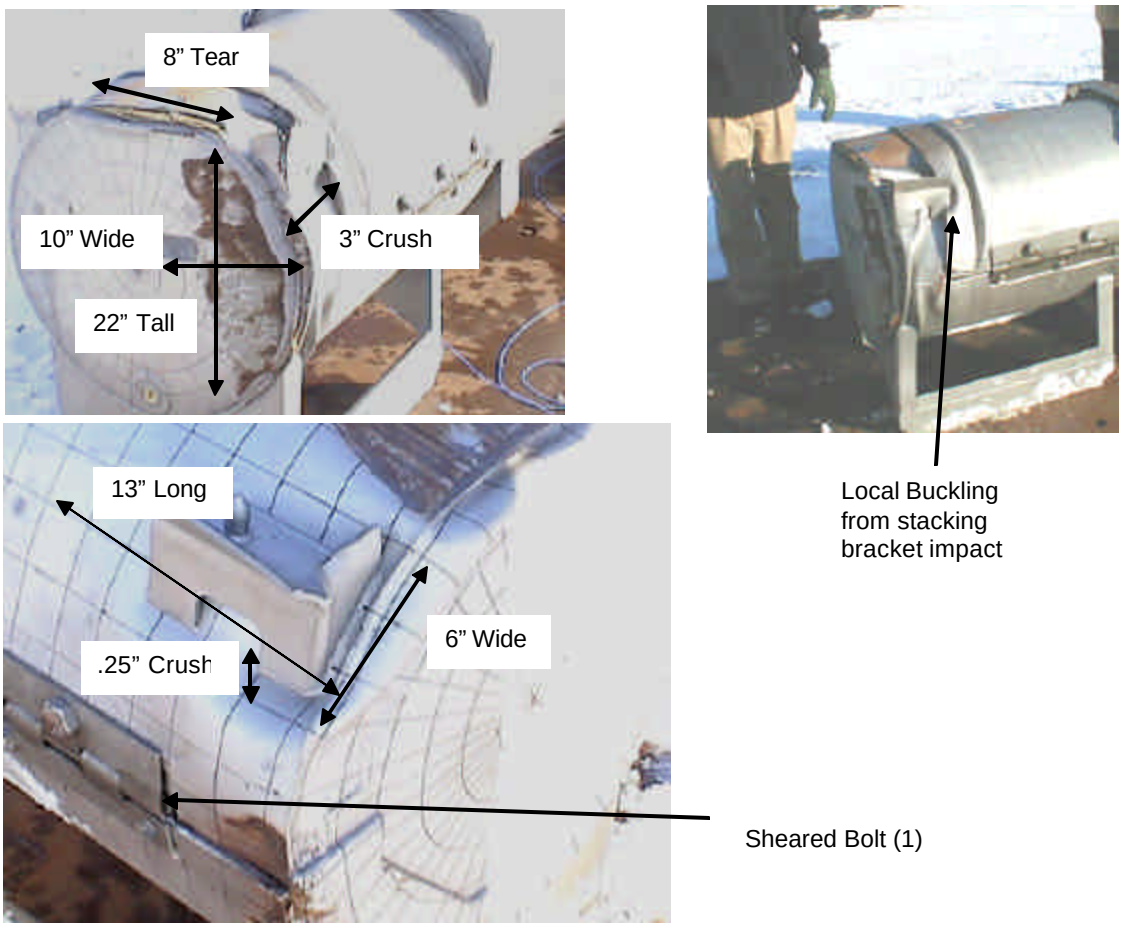

Figure 2-116 Traveller Prototype Exterior After Test 1.2

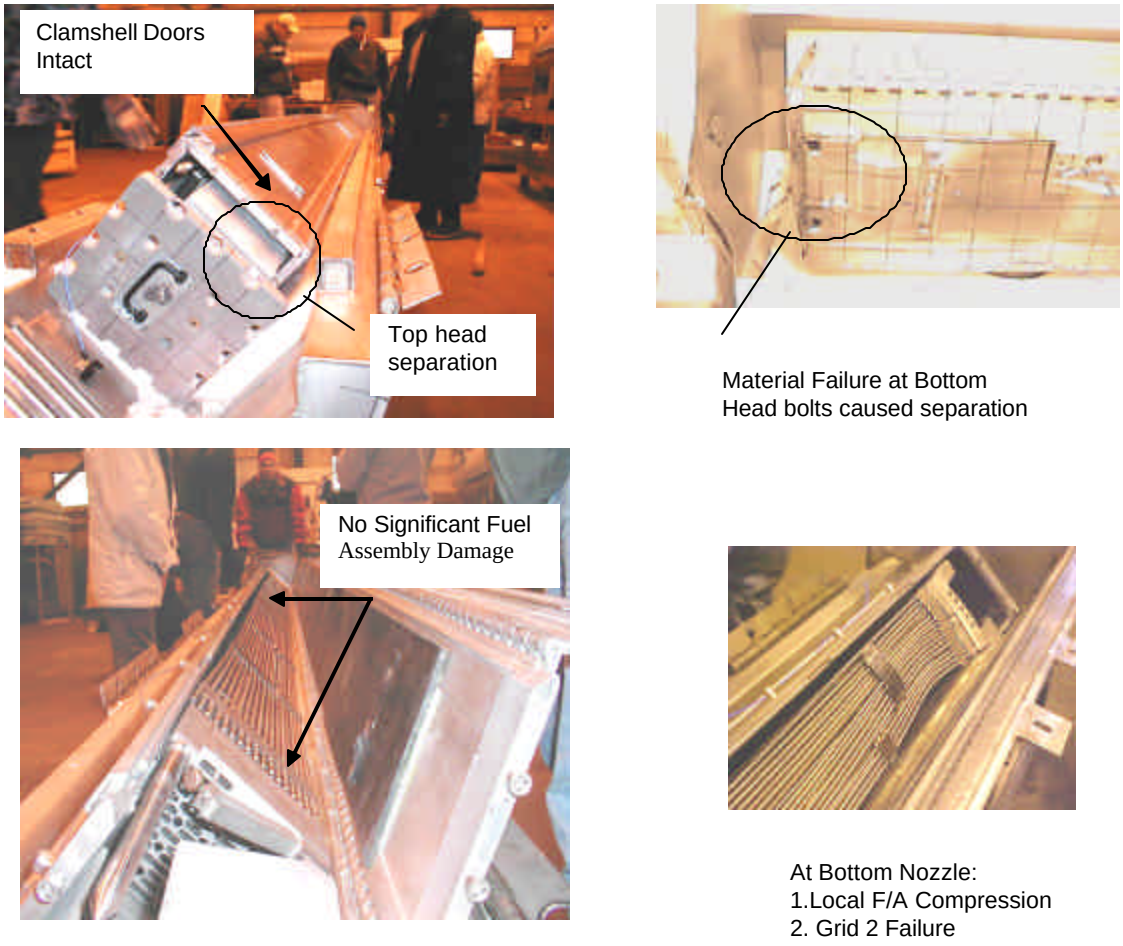

Figure 2-117 Traveller Prototype Interior After Test 1.2

Piezoelectric accelerometers were mounted on the Clamshell and Outerpack for drop tests 1.1 and 1.2. On the Clamshell, one 0-500 g accelerometer was mounted on the top head, and the other 0-500 g accelerometer on the bottom head. On the Outerpack, one 0-1000 g accelerometer was mounted on the underside of the bottom nozzle end (secondary impact location for test 1.1). After test 1.1, the accelerometer on the top head was replaced. *The locations of these accelerometers are shown in Figure 2-117A.* Figure 2-118 shows the accelerometer traces for the Clamshell from test 1.1. On the primary impact end (top nozzle), the accelerometer saturated in the vertical and axial directions, and the peak lateral deceleration was 453 g. The peak deceleration was 203 g and the resultant vector deceleration sum was 247 g at the secondary impact end (bottom nozzle).

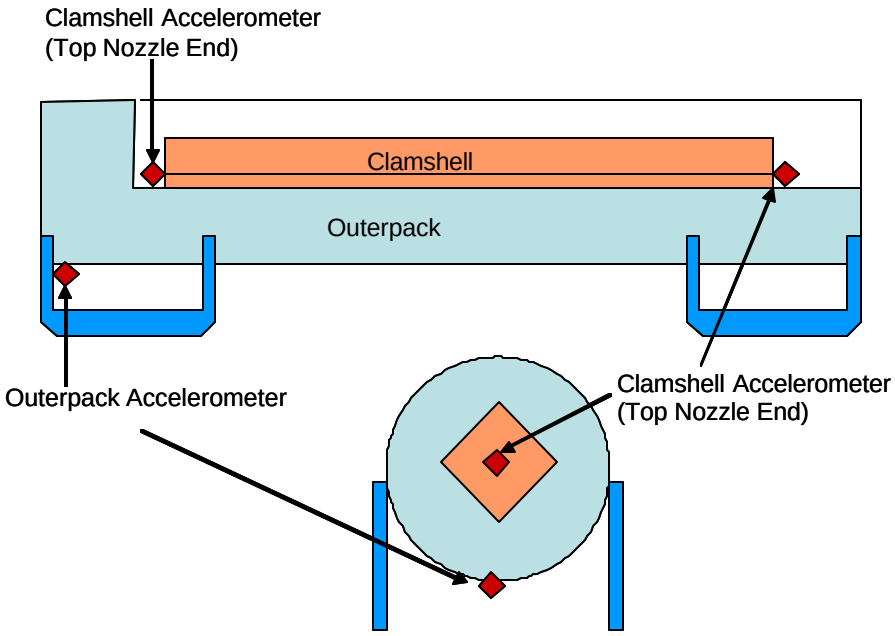

Figure 2-117A Accelerometer Locations on Prototype Drop Test

The 0-1000 g accelerometer trace is for the Outerpack is shown in Figure 2-119. The Outerpack vector deceleration sum for the primary impact measured 204 g, and the peak deceleration force measured 191 g in the vertical direction. The slap-down (secondary impact) resulted in decelerations which saturated each directional accelerometer.

The deceleration data for test 1.1 is summarized in Table 2-30.

This page intentionally left blank.

Table 2-30 Measured Decelerations in Prototype Test 1.1				
Accelerometer Position	Measured Deceleration Force, g			
	Vertical	Lateral	Axial	Vector Sum
Clamshell T/N end	>500	435	>500	N/A
Clamshell B/N end	118	203	78	247
Outerpack – Primary Impact	191	59	42	204
Outerpack – Slap Down	>1000	>1000	>1000	N/A

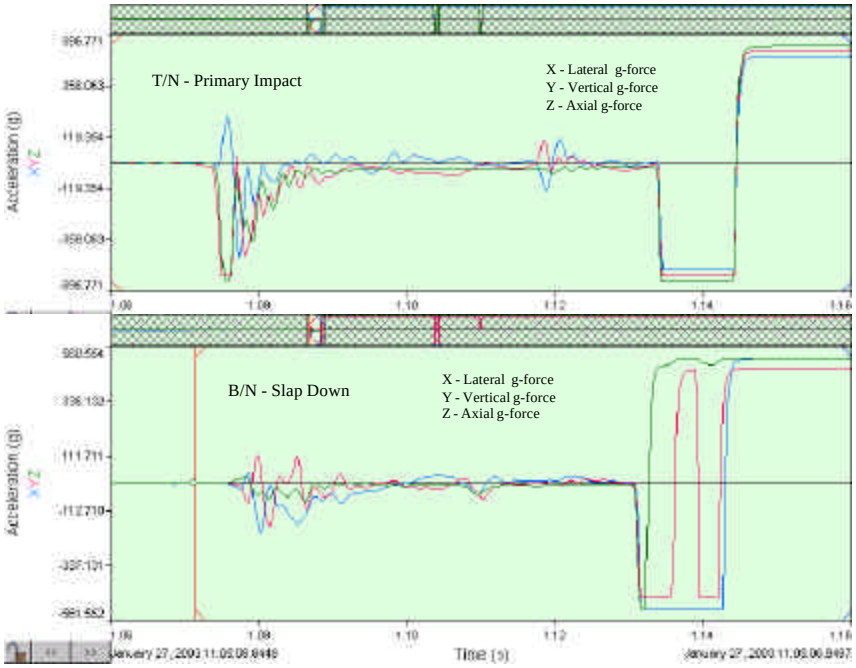

Figure 2-118 Clamshell Accelerometer Trace for Prototype Test 1.1

The top head accelerometer was replaced prior to test 1.2. Due to damaged instrumentation, no data was recorded for the bottom head or the Outerpack. The primary impact occurred on the bottom nozzle end. The top head accelerometer measured the deceleration trace of the primary impact as shown in Figure 2-119. The vector deceleration sum of the primary impact measured 417 g, and the peak deceleration force measured 260 g in the axial direction. The deceleration data for test 1.2 is summarized in Table 2-31.

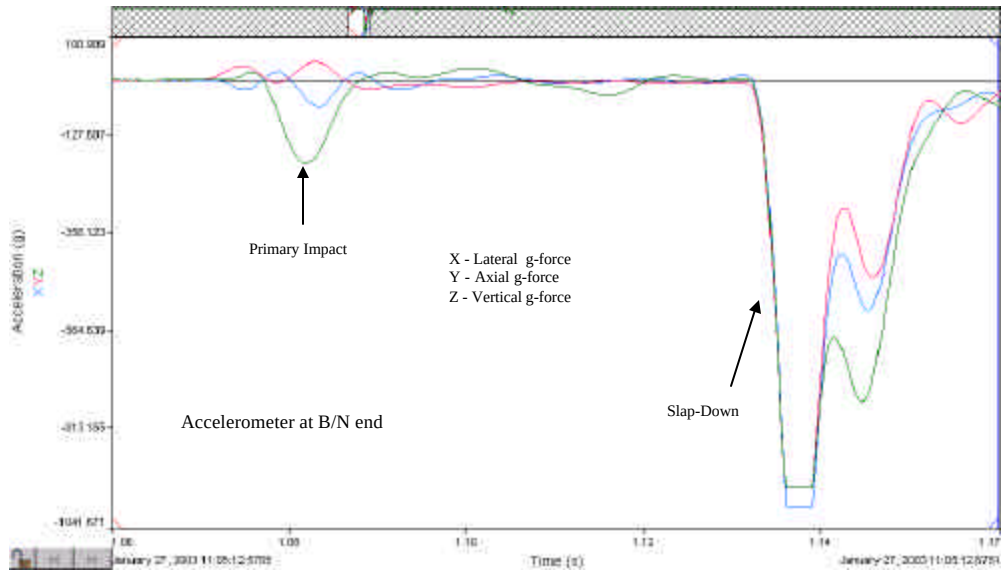

Figure 2-119 Outerpack Accelerometer Trace for Prototype Test 1.1

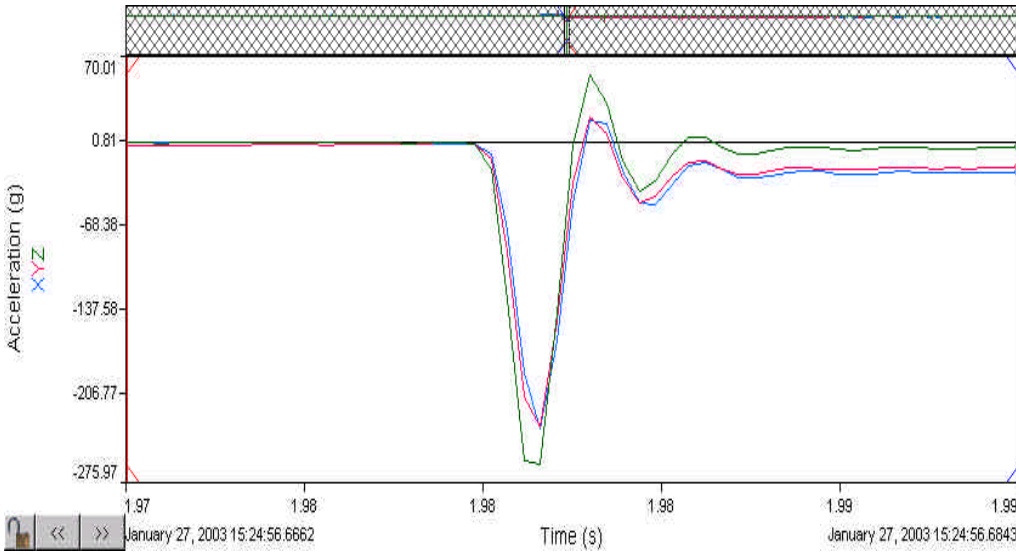

Figure 2-120 Clamshell Accelerometer Trace for Prototype Test 1.2

Table 2-31 Measured Accelerations in Test 1.2				
Accelerometer Position	Measured Deceleration Force, g			
	Vertical	Lateral	Axial	Vector Sum
Clamshell T/N end	230	232	260	417
Clamshell B/N end	No data	No data	No data	N/A
Outerpack – Primary Impact	No data	No data	No data	N/A
Outerpack – Slap Down	No data	No data	No data	N/A

Test 1.3 – The 1-meter pin puncture test resulted in little damage to the package. The outer skin of the Outerpack was locally punched approximately 1.63" and the width of the impact was approximately 10.5" as shown in Figure 2-121. The impact did not perforate the outer skin. The subsequent inspection of the inner side of the Outerpack top indicated that a small dent approximately 7/16" to 1/2" and 15" wide resulted from the pin puncture test. The moderator blocks were not impacted by the pin test.

Test Series 2 – Test series 2 was conducted on January 30th *(Table 2-32)* and included a 1.2-meter Normal accident condition free drop, a 1-meter pin-puncture test, and a 9-meter free drop test. The package's test weight was 5057 pounds.

The cumulative external damage from the regulatory drop test sequence was localized to plastic deformation at the impact zones. There was no significant changes in the Outerpack geometry, and no bolt failures were noted. Upon an internal inspection, the pin did not perforate the inner or outer shell. The internal damage was minimal. The fuel assembly's envelope decreased from 8.418" nominal to 8.25" maximum. Fuel rod gaps globally decreased (the fuel envelope decreased), but local expansion was noted between a few rods with a maximum measured gap of .188" compared to the nominal gap of .122". The polyethylene moderator blocks and aluminum neutron "poison plates" maintained position. The Clamshell doors remained closed, and the modified top head and bottom heads maintained position. A subsequent fuel inspection indicated that no fuel rods had ruptured, and that the axial position of fuel rods maintained location between bottom and top nozzle.

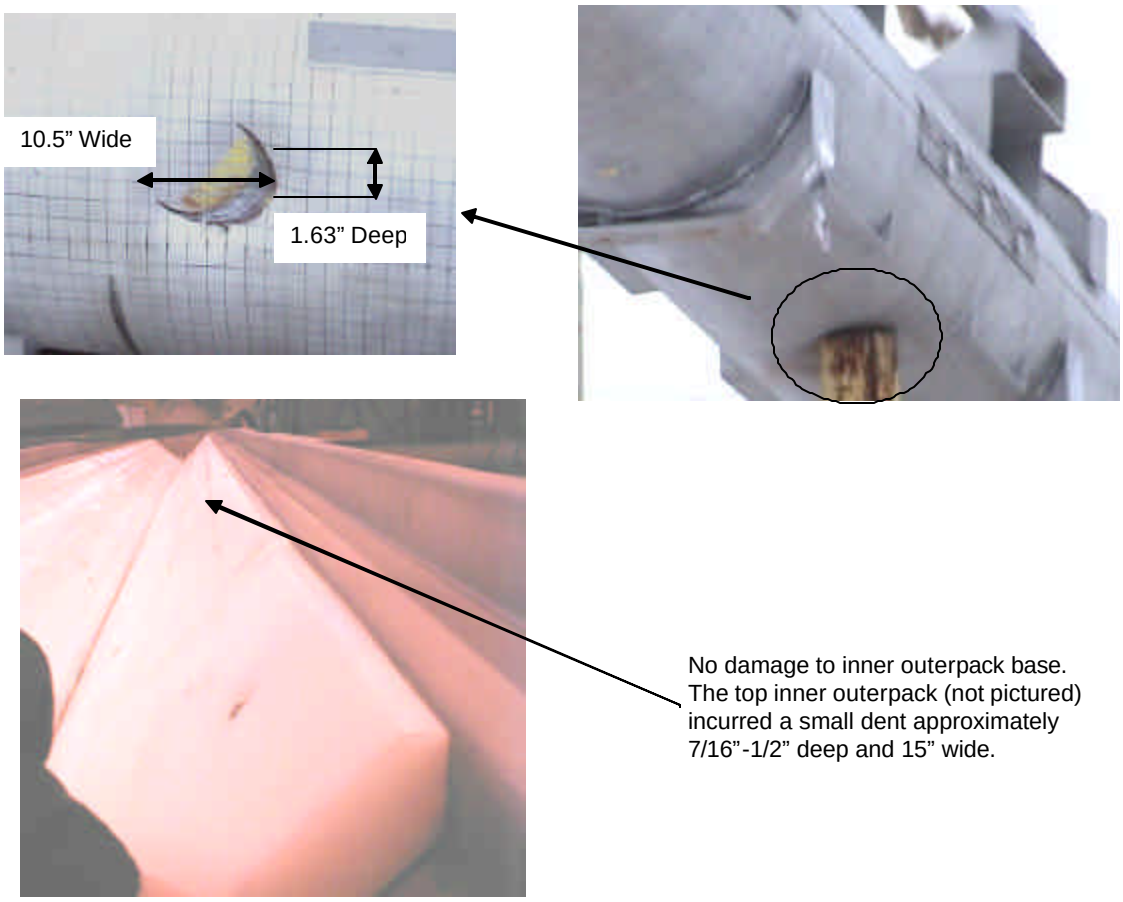

Figure 2-121 Traveller Prototype After Test 1.3

Table 2-32 Prototype Test Series 2

Test Sequence	Test Pitch Attitude	Test Roll Attitude	Impact Location
2.1) 1.2-m NAC drop	20°	180°	B/N primary impact on OP top
2.2) 1-m Pin-puncture	20°	135°	CG (Axial) on OP topside, T/N end down
2.3) 9-m CG-over-corner	72°	180°	T/N primary impact on OP top

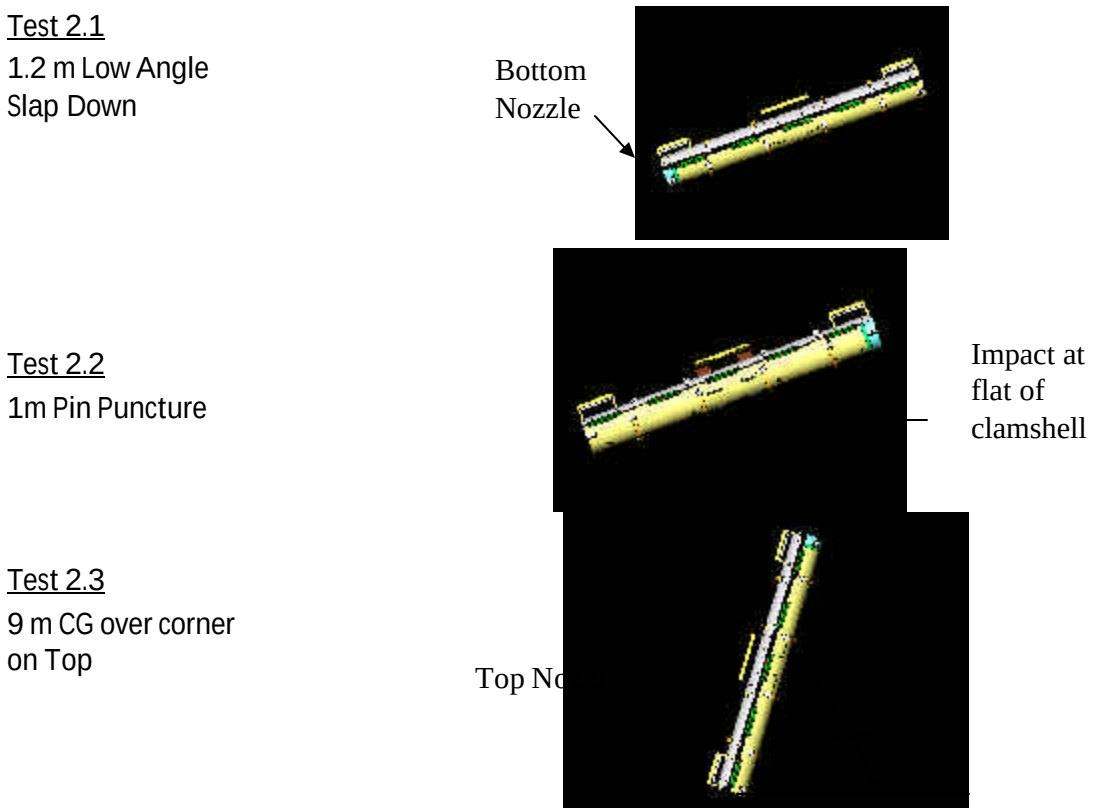

Figure 2-122 Drop Orientations for Traveller Prototype Test Series 2

Test 2.1 – The 1.2 meter normal condition drop test resulted in minimal damage to the Outerpack. The impact created an impact zone at the bottom end 9" wide, 2.5" in axial length, and crushed the Outerpack .75" as shown in Figure 2-123. Two stiffeners near the Outerpack center crushed approximately .75" over a width of 6". The energy absorption of the circumferential stiffeners precluded damage to the secondary impact end (top nozzle).

Test 2.2 – The second test of this drop sequence was a 1-meter pin drop on the package side, Figure 2-122. The 1-meter pin puncture test resulted in little damage to the package. The outer skin of the Outerpack was locally punched in approximately 2"as shown in Figure 2-124. The impact punch zone was 10" tall and the width of the impact was approximately 14". The impact did not perforate the outer skin.

Test 2.3 – The 9-meter drop test resulted in local damage to the primary impact region (top nozzle end). The secondary impact region was in the vicinity of the impact region of the 1.2-meter free drop and did not result in additional damage. From Figure 2-125, the damage zone was approximately 25" wide, 12" tall, and produced a crush zone approximately 9" axially. Due to the impact attitude, the Outerpack top tended to shear relative to the Outerpack bottom. A gap approximately 1" resulted from the impact, but did not comprise the Outerpack closure. No bolt failures were noted.

In general, the test sequence resulted in minimal Clamshell and fuel damage. The top nozzle end of the Clamshell was slightly bowed in a localized region at the top nozzle end (Figure 2-126), but did not result in fuel expansion. The modified top and bottom head pieces remained intact, and no shock mount failures were noted. The fuel inspection indicated that the assembly had moved axially toward the top nozzle 3-3/8" as a result of the spacer movement. There was no significant fuel damage at the bottom nozzle. Also the top nozzle region of the fuel assembly incurred some local damage. The guide pins buckled. Four (4) fuel rods moved axially (maximum of 1"), but did not extend beyond the neutron poison plates. The fuel inspection also indicated that no fuel rods had ruptured. The fuel rod gap measurements indicated the maximum measured fuel rod gap increased from 0.122" nominally to 0.188" locally (observed at one or two rods along the envelope). The measured fuel envelope compressed from 8.418" nominally to 8.25" maximum. The moderator blocks did not move from their original position even though two studs were sheared off. The pin-puncture test produced a 24" long by 5/8" deep dent on the inner Outerpack surface.

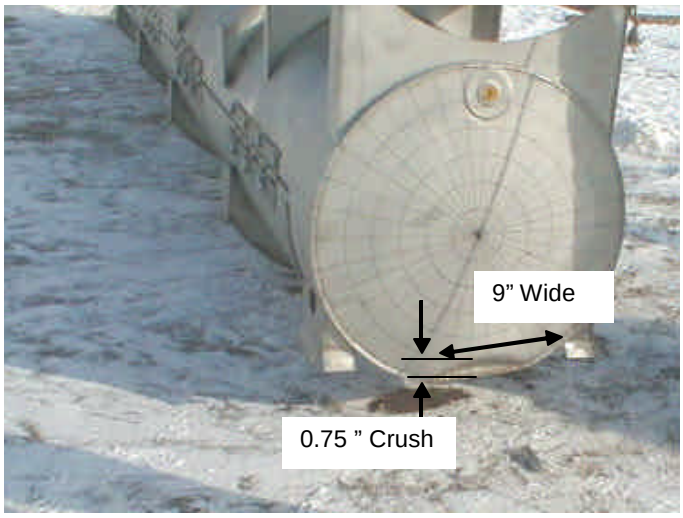

The axial damage zone is approximately 2.5”.

No damage at T/N end.

Stiffeners crushed about .75” and also dented OP about .75”. Crush width 6”.

Figure 2-123 Traveller Prototype After Test 2.1

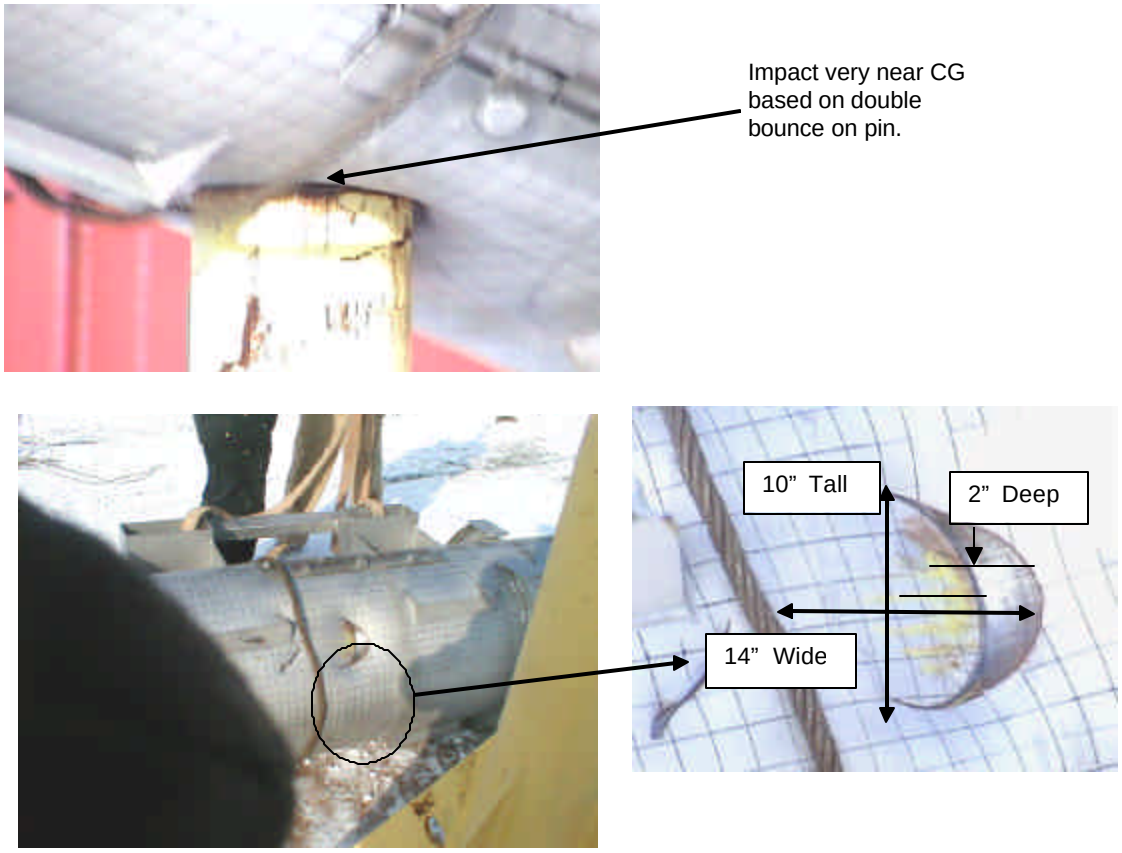

Figure 2-124 Traveller Prototype After Test 2.2

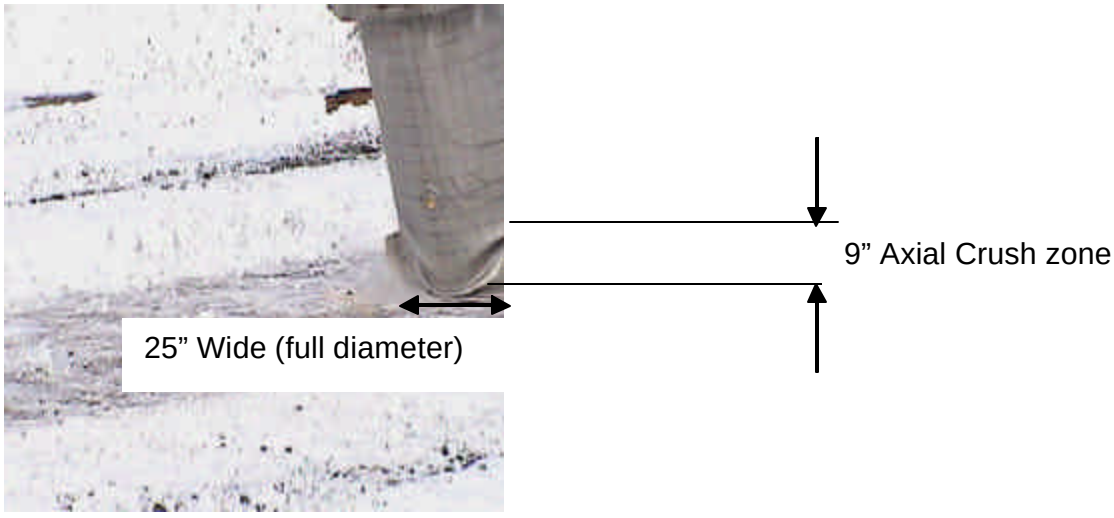

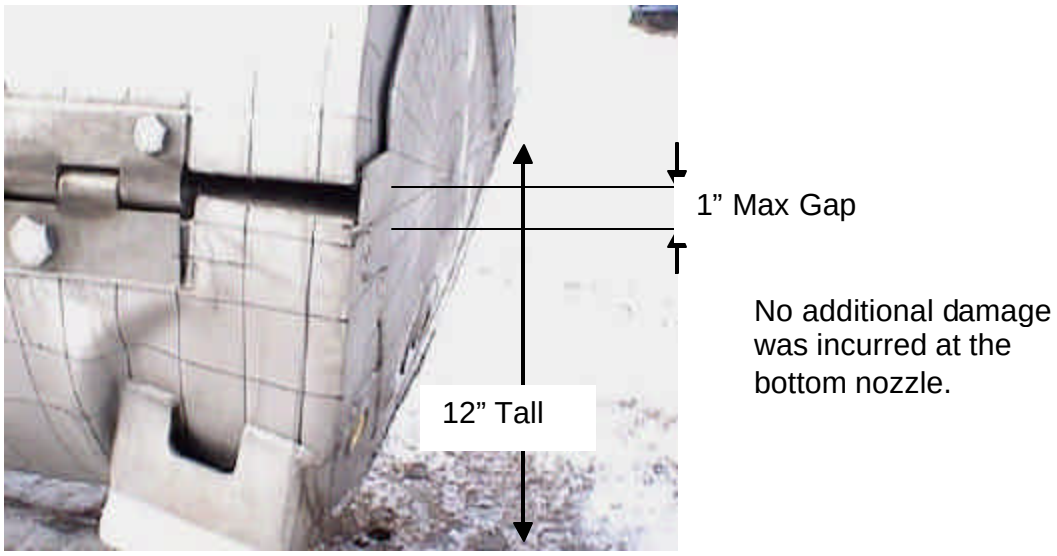

Figure 2-125 Traveller Prototype After Test 2.3

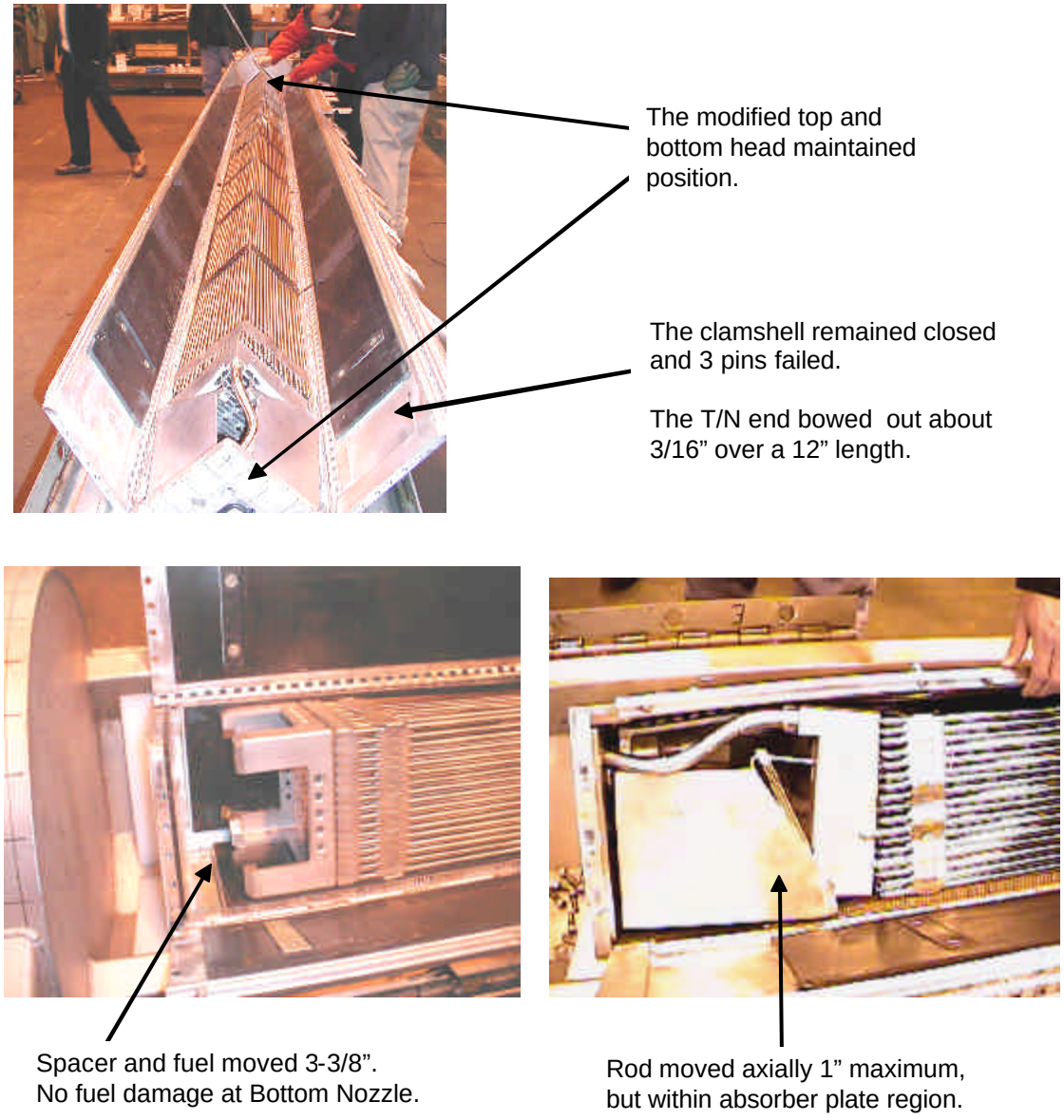

Figure 2-126 Traveller Prototype Interior After Test Series 2

Test Series 3 – Test Series 3 consisted of three 9-meter drop tests conducted to evaluate design features of the Outerpack after modifications to the Clamshell and Outerpack. The test sequence and measured drop attitudes are summarized in Table 2-33. The test series employed was Prototype 2 that had been used for test Series 2. The purpose of this test series was to evaluate design features and evaluate design margin. External damage assessments were performed following each supplementary drop test, and a general internal assessment was conducted after the completion of test 3.3. However, the inspections for this test series were not intended for use in nuclear criticality safety analysis. Prior to test 3.1, the following modifications were made to the package:

- Removed 1 bolt from each of the 5 top Outerpack hinges (reduced bolt count by 33%).
- Removed sheet metal from endcap inner surface
- Removed 2 of the 5 pins that secure each Clamshell clip

Table 2-33 Traveller Prototype Drop Tests Performed in Test Series 3

Test Sequence	Test Pitch Attitude	Test Roll Attitude	Impact Location
3.1) 9-m Axial End drop	90°	0°	B/N impact
3.2) 9-m Flat drop	0.5°	0°	Impact on OP feet
3.3) 9-m Side drop	0°	270°(90°CCW)	Impact on OP hinges

Figure 2-127 shows that the Outerpack sustained minimal damage. The Outerpack remained closed and no bolts failed after the completion of drop test series 3. The first drop test of this series resulted in slight crushing (approximately 1-5/8" deep) at the bottom nozzle end. The crushed circumferential stiffeners precluded excessive Outerpack damage as the package slapped down after the axial drop. Drop test 3.2 crushed the feet and forklift supports completely, but otherwise did not comprise the Outerpack structural integrity. The direct hinge impact (test 3.3) did not fail any hinges or result in any substantial damage to the Outerpack.

The cumulative overall damage to the Clamshell was also minimal as shown in Figure 2-127. The Clamshell retained its geometry, no Clamshell clip pins failed, and no shock mount failures were noted. The notable Clamshell damage was located at the bottom head, which was separated from the Clamshell by the impacting fuel, Figure 2-128. It is presumed that the 3-3/8" gap from the Clamshell bottom plate to the base of the fuel assembly bottom nozzle provided sufficient distance for the fuel assembly to attain enough kinetic energy to separate the Clamshell bottom head upon impact.

The fuel was in good condition. No measurements were taken since this test series was qualitative in nature.

Figure 2-127 Traveller Prototype After Test Series 3

Figure 2-128 Traveller Prototype Clamshell and Bottom Impact Limiter After Test Series 3

Minor design modifications were recommended for the Traveller package based on this testing. The top and bottom heads required additional bolting to preclude Clamshell separation. The number of Clamshell clip retaining pins (and clips) could be reduced. It was found that sufficient design margin against material failure existed allowing the Outerpack gage metal can be reduced slightly in thickness. In addition, the number of Outerpack bolts can be reduced on the top hinge by at least 1/3.

2.12.4.2 Qualification Test Unit Drop Tests

The following section delineates the second of three (3) full-scale testing campaigns of the Traveller development program. This campaign utilized two units called Quality Test Units, or QTU-1 and 2. A total of two (2) QTUs were built and tested, with minor changes to improve burn performance incorporated into the second QTU article.

2.12.4.2.1 QTU Test Series 1

Test series 1 was conducted on the afternoon of September 11 and included a 50 inch (1.27 m) slap down, a 33.3 feet (10.15 m) center of gravity-over-corner free drop test, and a 42 inch (1.07 m) pin-puncture test. The package's test weight was 4793 pounds (Table 2-34). The internal inspection of the fuel assembly was conducted after completion of the fire test on September 16, 2003.

Table 2-34 QTU-1 Measured Weight

Test Weights	Nominal	Actual
Weight of Outerpack (Empty):	3033 lb	**3032** lb
Weight of Clamshell (Empty):	425 lb	**400** lb
Weight of package (Empty) :	3477 lb	**3432** lb
Total package test weight:	5422 lb	**4793** lb

Test series 1 was conducted on the afternoon of September 11 and included a 50.75 inch (1.29 m) slap down, a 33.3 feet (10.15 m) free drop test, and a 42 inch (1.07 m) pin-puncture test. QTU1 pre-test data and observations are shown in Form 1A. The test sequence and measured drop attitudes are summarized in Table 2-35 and shown in Figure 2-129. *A pitch angle of 72 degrees was measured along the outerpack surface for Test 1.2. The angle of 108 degrees should be located as shown in Figure 2-129. The reference to "hinge side" in Test 1.3 indicates the package side that pivots, rather than the actual hinge. The impact point of Test 1.3 (Figure 2-132) was on the top nozzle end and on the pivot (left) side of the package.* A fuel damage assessment was conducted after the completion of the hypothetical fire condition test conducted on September 16, 2003 at the South Carolina Fire Academy near Columbia, SC.

The Outerpack retained its basic circular pre-test shape except for localized plastic deformation at the top nozzle end accumulated from the drop test series. No bolts failed on the Outerpack after completion of the drop test series. The Outerpack did not separate after any impacts, and the pin did not perforate the inner or outer shell. The most notable Outerpack damage was the resulting joint tear of approximately 1-1/8" at the Outerpack corner located at the top, left hinge side. The fuel assembly damage was minimal. At the top nozzle portion, the fuel assembly locally expanded from 8.375" nominal to 8.625" maximum over a length of approximately 2-3". The fuel rod gaps were globally unchanged but local expansion was noted between one rod near Grid 10 with a maximum measured gap of 0.250". The resulting measured maximum local pitch was 0.625 inches. Three rods were found to be in contact with each other while the remaining rods were nominally positioned. Intermediate grids 2-7 were buckled locally, but the fuel rod envelope was unchanged. The bottom nozzle portion of the fuel assembly was slightly compressed from 8.375" nominally to 8.250" measured. Based on the condition of the fuel assembly, the Clamshell was

concluded to have performed successfully. The fuel inspection also indicated that no fuel rods had visibly ruptured, and that the axial position of fuel rods maintained location between bottom and top nozzle.

Table 2-35 QTU-1 Drop Test Orientations

Test Article ID	F/A Type	Test Sequence	Test Pitch Attitude	Test Roll Attitude	Design Feature Tested
QTU1	17x17 XL	P1.1) 1.2 m, NAC, Low angle[1]	10°	180°	Operations of hinges/doors
		P1.2) 9 m CG-over-Corner[1]	108°	90°	OP hinge shear, CS latches
		P1.3) 1 m Pin-puncture[1]	83°	90°	Joint Integrity – Fire test

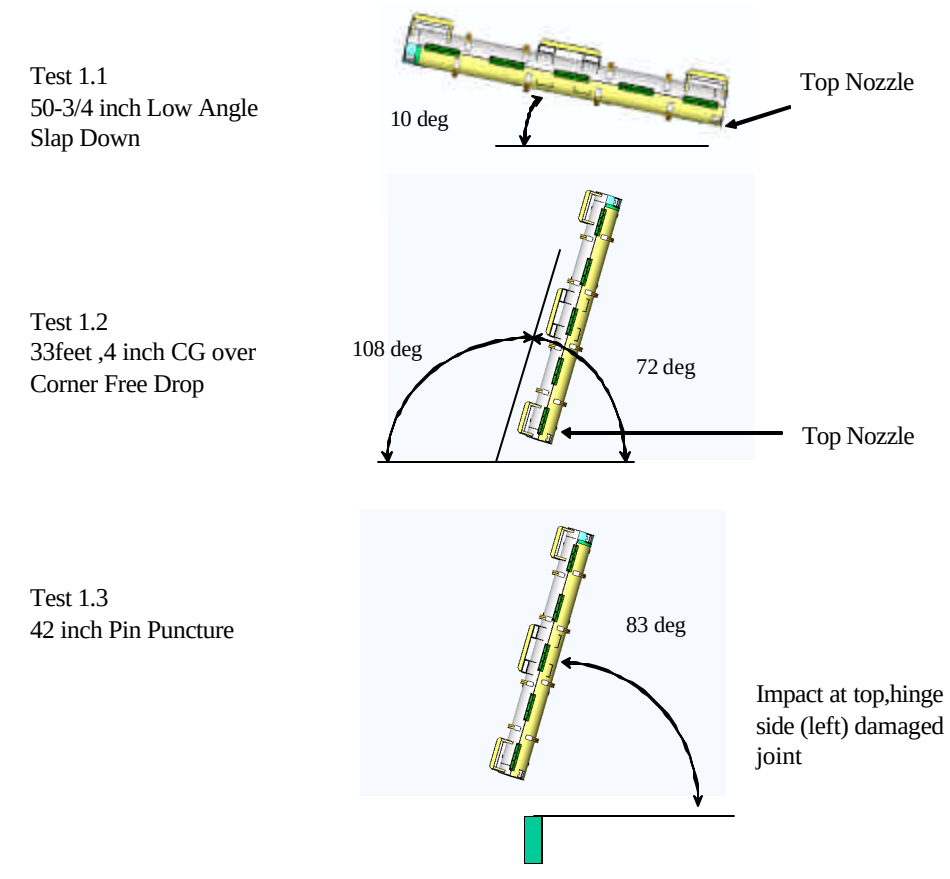

Figure 2-129 Drop Orientation for QTU Test Series 1

Test 1.1 – The 50.75 inches (1.29 m) drop onto the Outerpack lid was performed first. As shown in Figure 2-130, this drop resulted in a small indention in the outer skin of the Outerpack.

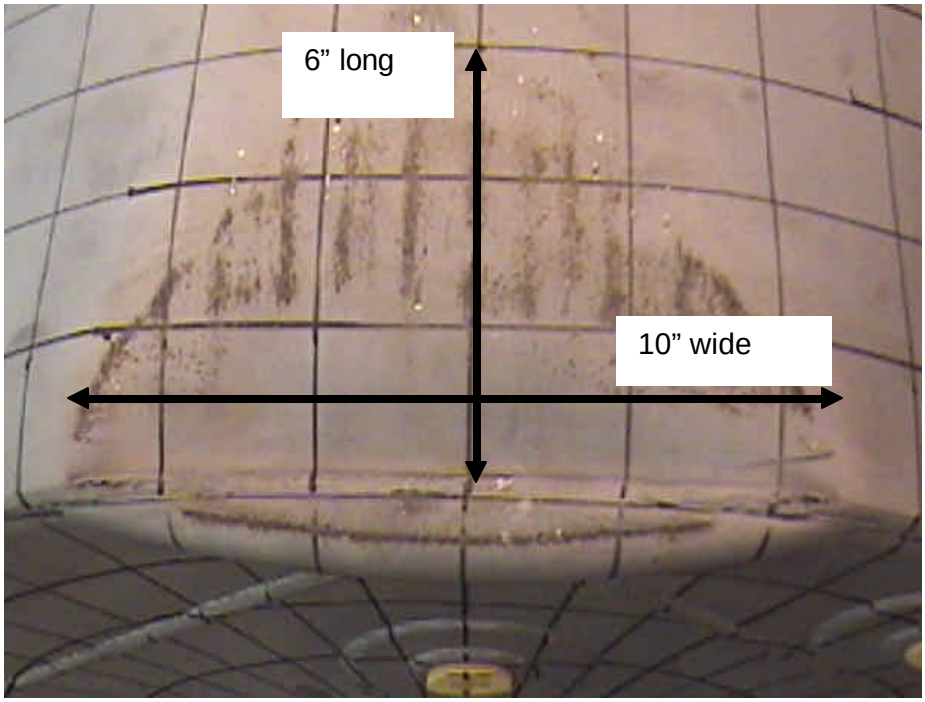

Figure 2-130 QTU-1 Outerpack After Test 1.1

Test 1.2 – The 33.3-foot free drop resulted in localized damage to the top nozzle end region. One of the hoist rings was sheared off as a result of the impact, Figure 2-131. The impact opened a small tear at the top and bottom Outerpack seam (also in circled region). The entire 25" diameter face of the top nozzle end was dented approximately 3-1/2". The stiffeners were also dented across their tops, but were intact. Two welds located at the bottom nozzle end stiffener were broken, but this did not compromise the stiffener position.

Test 1.3 – The pin puncture test was located in the top left (hinge) side of the Outerpack top nozzle end. The objective of the test was attempt to increase the Outerpack separation incurred by the previous 33.3-ft drop. Additional tearing of the joint was noted which resulted in measured tear of approximately 1-1/8". The indention resulting from the pin puncture was approximately 1-1/2" deep (Figure 2-132).

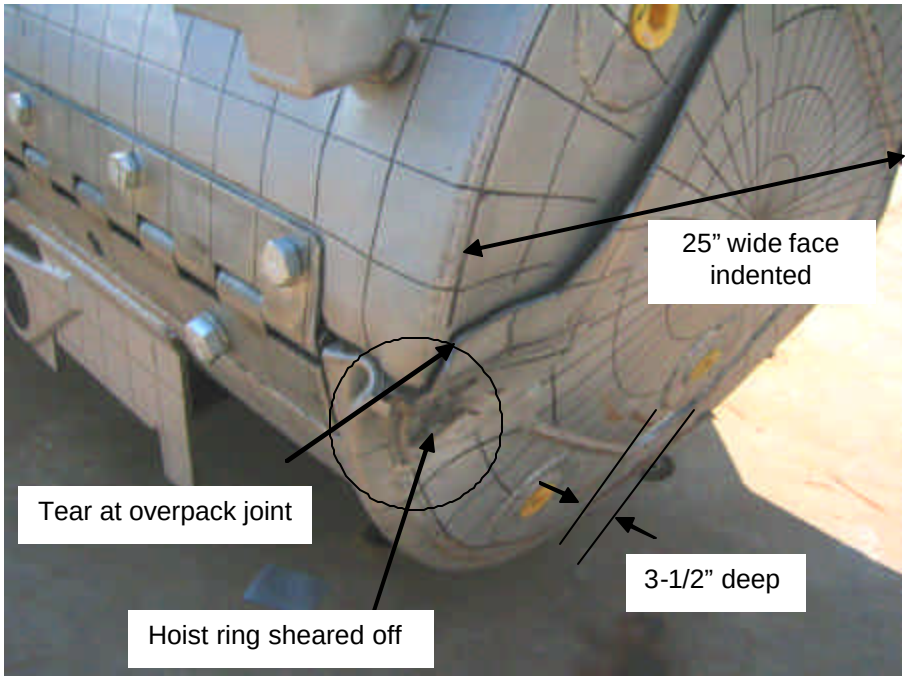

Figure 2-131 QTU-1 Outerpack After Test 1.2

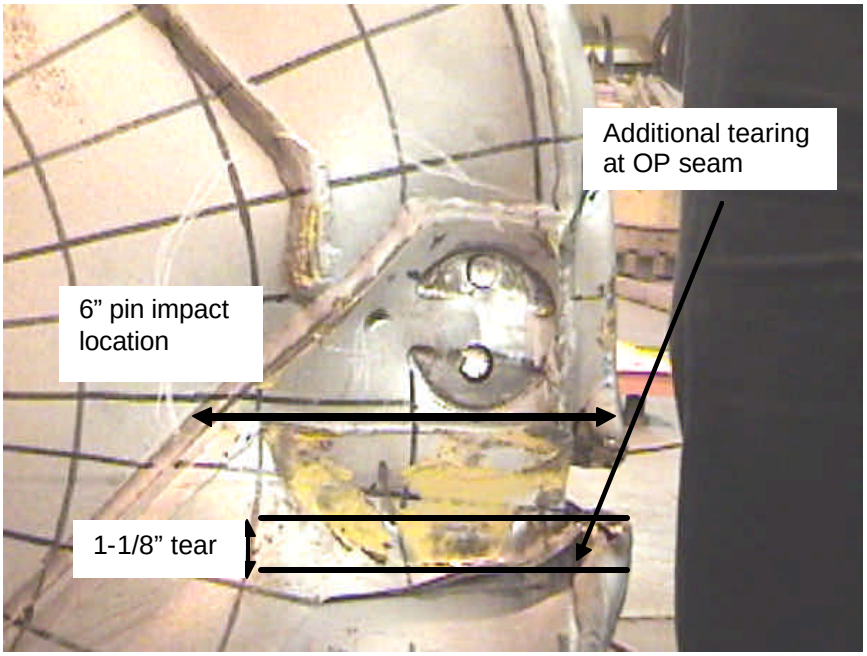

Figure 2-132 QTU-1 Outerpack After Test 1.3

QTU-1 was not opened until after the fire test. The Clamshell and fuel assembly were examined for damage at that time. The fuel assembly of QTU-1 was essentially undamaged, Figure 2-133. The most damage occurred at the top nozzle section where an area of approximately 2-3" in length increased from 8.375" nominal to 8.625". Grid 10 was torn, and all other grids were buckled but intact. The nozzles were essentially undamaged. The impact resulted in buckling of the core line-up pins attached to the top nozzle. The fuel rods appeared visibly undamaged.

The fuel assembly in QTU-1 was measured before the test and after the burn test at locations shown in Figure 2-134. Table 2-36 provides the pretest dimensions. Tables 2-37 and 2-38 provide the post test dimensions.

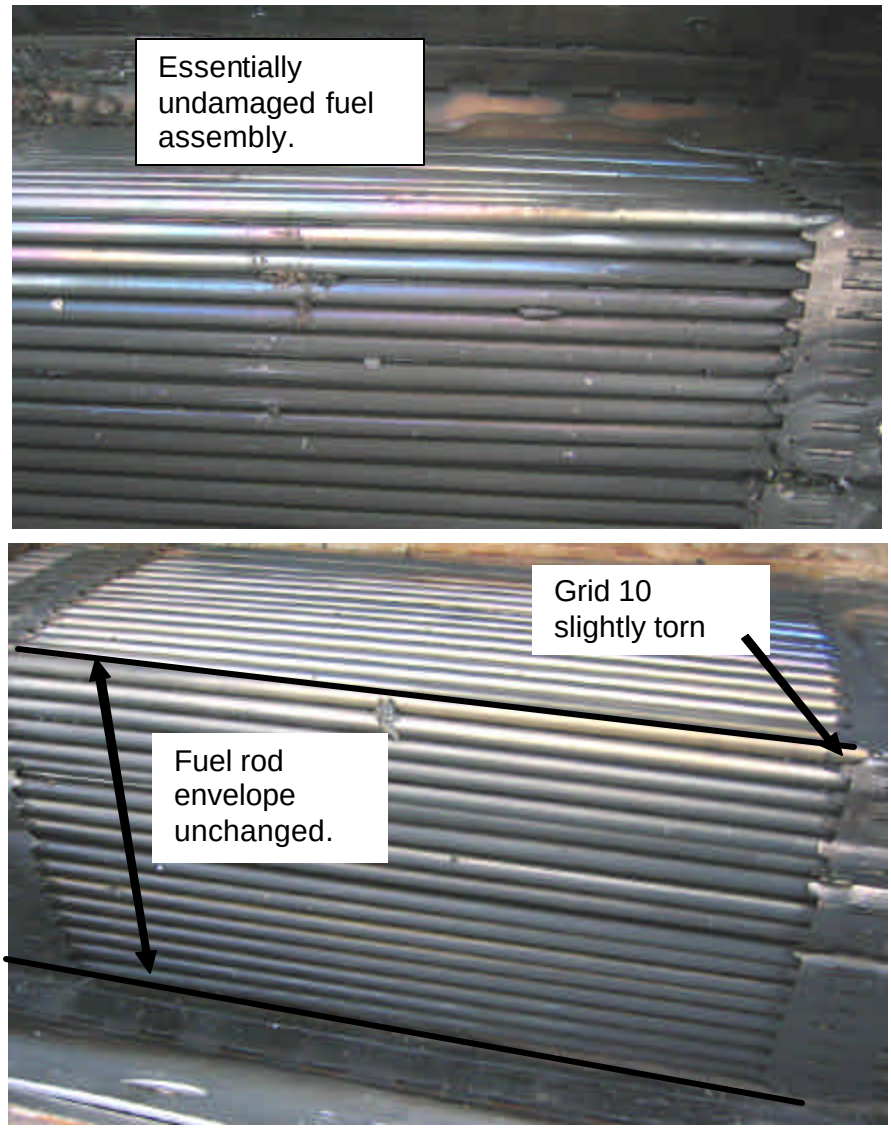

Figure 2-133 QTU-1 Fuel Assembly After Drop and Burn Tests

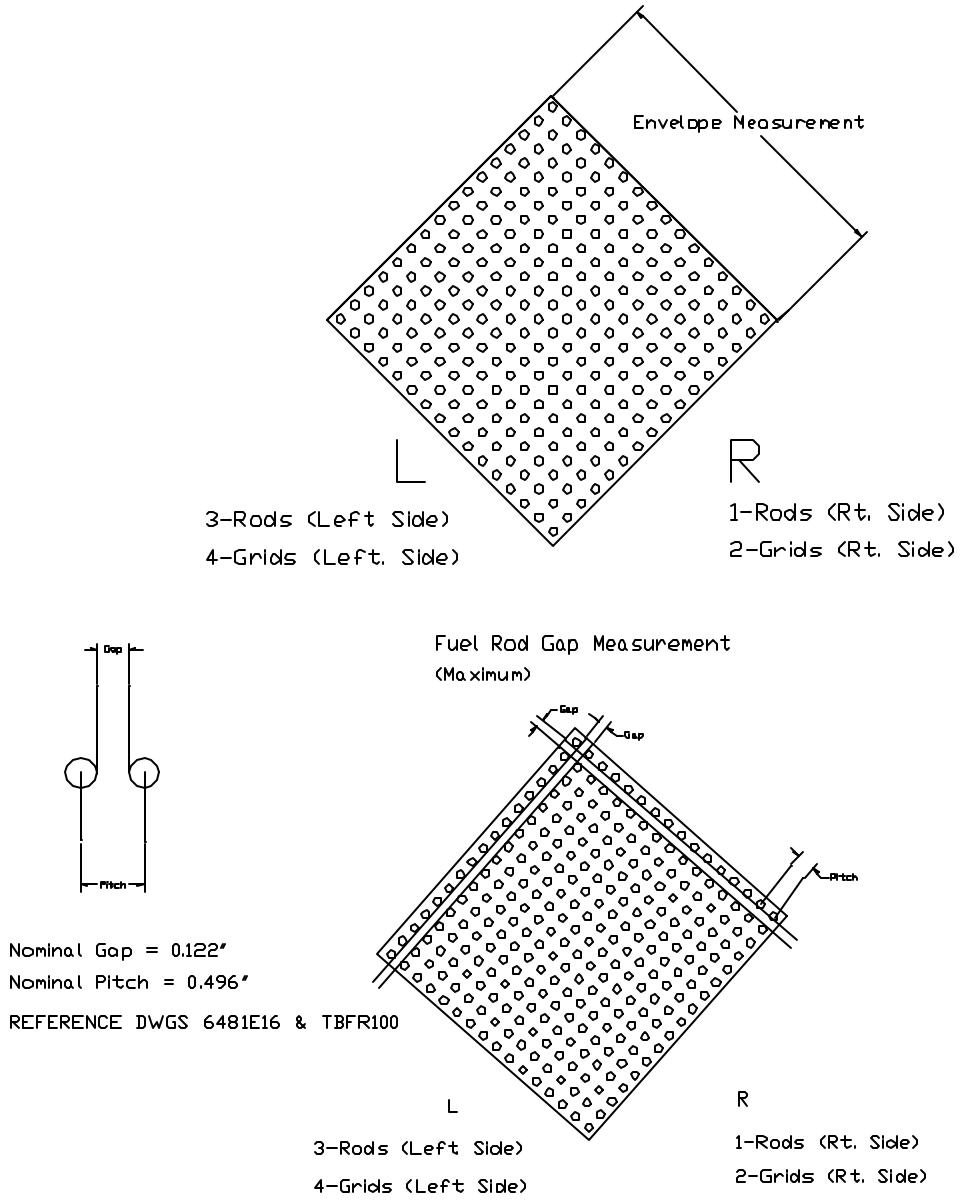

Figure 2-134 Measurements Made on QTU Fuel Assemblies Before and After Drop Tests

Table 2-36 Key Dimensions of QTU-1 Fuel Assembly Before Testing			
Fuel Assembly ID: 503007, B/N # 02-6703			
F/A Location	**Fuel Envelope (inches)**	**Gap (inches)**	**Pitch (inches)**
B/N – Grid 1	1 – 8.330 2 – 8.455 3 – 8.250 4 – 8.446 8.375 Meas. Nominal*	L – 0.122 R – 0.123 0.125 Meas. Nominal*	L – 0.497 R – 0.498 0.500 Meas. Nominal*
Grid 1 – Grid 2	1 – 8.338 2 – 8.418 3 – 8.326 4 – 8.415 8.375 Meas. Nominal*	L – 0.124 R – 0.124 0.125 Meas. Nominal*	L – 0.499 R – 0.499 0.500 Meas. Nominal*
Grid 2 – Grid 3	8.375 Meas. Nominal*	L – 0.123 R – 0.120 0.125 Meas. Nominal*	L – 0.498 R – 0.495 0.500 Meas. Nominal*
Grid 3 – Grid 4	8.375 Meas. Nominal*	0.125 Meas. Nominal*	0.500 Meas. Nominal*
Grid 4 – Grid 5	8.375 Meas. Nominal*	0.125 Meas. Nominal*	0.500 Meas. Nominal*
Grid 5 – Grid 6	8.375 Meas. Nominal*	0.125 Meas. Nominal*	0.500 Meas. Nominal*
Grid 6 – Grid 7	8.375 Meas. Nominal*	0.125 Meas. Nominal*	0.500 Meas. Nominal*
Grid 8 –- Grid 9	8.375 Meas. Nominal*	0.125 Meas. Nominal*	0.500 Meas. Nominal*
Grid 9 – Grid 10	8.375 Meas. Nominal*	0.125 Meas. Nominal*	0.500 Meas. Nominal*
Grid 10 – T/N	8.375 Meas.Nominal*	0.125 Meas. Nominal*	0.500 Meas. Nominal*
Note: * Measured nominal values were measured to nearest 1/8".			

Table 2-37 QTU-1 Fuel Assembly Grid Envelope After Testing			
Fuel Assembly Envelope Inspection Table			
Location	**Envelope Dimension, Inches**		**Maximum Fuel Rod Gap from Form 1F (Nominal Gap = 0.122")**
	Left Side, LS	**Right Side, RS**	
Between B/N and Grid 1	8.125	8.250	0.250
Between Grids 1 and 2	8.125	8.000	0.250
Between Grids 2 and 3	8.000	8.250	0.188
Between Grids 3 and 4	8.375	8.375	0.125
Between Grids 4 and 5	8.375	8.375	0.125
Between Grids 5 and 6	8.375	8.375	0.188
Between Grids 6 and 7	8.375	8.375	0.188
Between Grids 7 and 8	8.375	8.375	0.188
Between Grids 8 and 9	8.375	8.375	0.188
Between Grids 9 and 10	8.375	8.500	0.250
Between Grid 10 and T/N	8.500	8.625	0.250
MAXIMUM VALUE	8.500	8.625	0.250

Table 2-38 QTU-1 Fuel Rod Pitch Data After Testing			
Fuel Rod Pitch Inspection Table			
Location	Maximum Gap, inches		Maximum Pitch
	Left Side, LS	Right Side, RS	
Between B/N Grid 1	0.250	0.188	0.625
Between Grids 1 and 2	0.250	0.250	0.625
Between Grids 2 and 3	0.188	0.188	0.563
Between Grids 3 and 4	0.125	0.125	0.500
Between Grids 4 and 5	0.125	0.125	0.500
Between Grids 5 and 6	0.125	0.188	0.563
Between Grids 6 and 7	0.125	0.188	0.563
Between Grids 7 and 8	0.188	0.188	0.563
Between Grids 8 and 9	0.188	0.188	0.563
Between Grids 9 and 10	0.125	0.250	0.625
Between Grid 10 and T/N	0.125	0.250	0.625
MAXIMUM VALUE	0.250	0.250	0.625

2.12.4.2.2 QTU Test Series 2

Test series 2 was conducted on the afternoon of September 11 and included a 50 inch (1.27 m) slap down, a 33.4 feet (10.18 m) free drop test, and a 42 inch (1.07 m) pin-puncture test. The test sequence and measured drop attitudes are summarized in Table 2-39 and shown in Figure 2-135. Weights for QTU-2 are recorded on Table 2-40.

Table 2-39 QTU Series 2 As-Tested Drop Conditions					
Test Article ID	F/A Type	Test Sequence	Test Pitch Attitude	Test Roll Attitude	Design Feature Tested
QTU2	17x17 XL	P2.1) 1.2-m, NAC, Low angle(1)	10°	180°	Operations of hinges/doors
		P2.2) 9-m End (B/N)(1)	90°	0°	Lattice exp., FR axial position
		P2.3) 1-m Pin-puncture(1)	22°	0°	OP stiffness
Note: (1) Actual test heights are reported in Figure 163 and post-test forms.					

Table 2-40 QTU-2 Weights		
Test Weights	**Nominal**	**Actual**
Weight of Outerpack (Empty):	3033 lb	**2611** lb
Weight of Clamshell (Empty):	425 lb	**400** lb
Weight of package (Empty) :	3477 lb	**3011** lb
Total package test weight:	5422 lb	**4778** lb

The Outerpack retained its basic circular pre-test shape except for localized plastic deformation accumulated from the 1.2 meter and 33.4 foot (10.18m) drop test. Damage zones from the drop test were localized to impact locations on the package end. The Outerpack did not separate after the impact, and no bolt failures on the Outerpack hinges were noted. From Figure 2-136, the 1.2 meter free drop resulted in a local crush zone at the top nozzle end measuring approximately 9-1/2" wide, 6" long axially and 7/8" deep. The Outerpack damage from the 33.4 foot drop, Figure 2-136 consisted of local crumple zone approximately 7" long maximum as demonstrated by the buckled Outerpack at the bottom nozzle end. A small weld tear was noted on each side of the Outerpack where the leg stand is connected to the end cap. The pin puncture damage was isolated to the impact point located at the package center-of-gravity. From As shown in Figure 2-138, pin puncture damage zone was an indented oval of measured dimensions 9" long by 6" wide and 2-7/8" deep.

The Clamshell was essentially undamaged from the drop test series, Figure 2-138. No change in the Clamshell grid markings were noted indicating that the Clamshell had not bulged outward (nor compressed). The polyethylene moderator blocks and aluminum neutron “poison plates” maintained position. The fuel assembly was found to be within the confines of the Clamshell and intact. The impact resulted in a slight ovalizing of the fuel assembly at the bottom nozzle region. Figure 2-139 shows the approximate angle of ovality is 118° at Grid 1 location. Localized expansion from 8.375" nominal to 8.625" was measured over a length of approximately 12" (30.48cm). The maximum fuel rod gap measured was 0.722 inches resulting in a maximum measured fuel rod pitch of 1.097 inches. The top nozzle portion of the tested fuel assembly was essentially undamaged. The axial position of fuel rods maintained location between bottom and top nozzles.

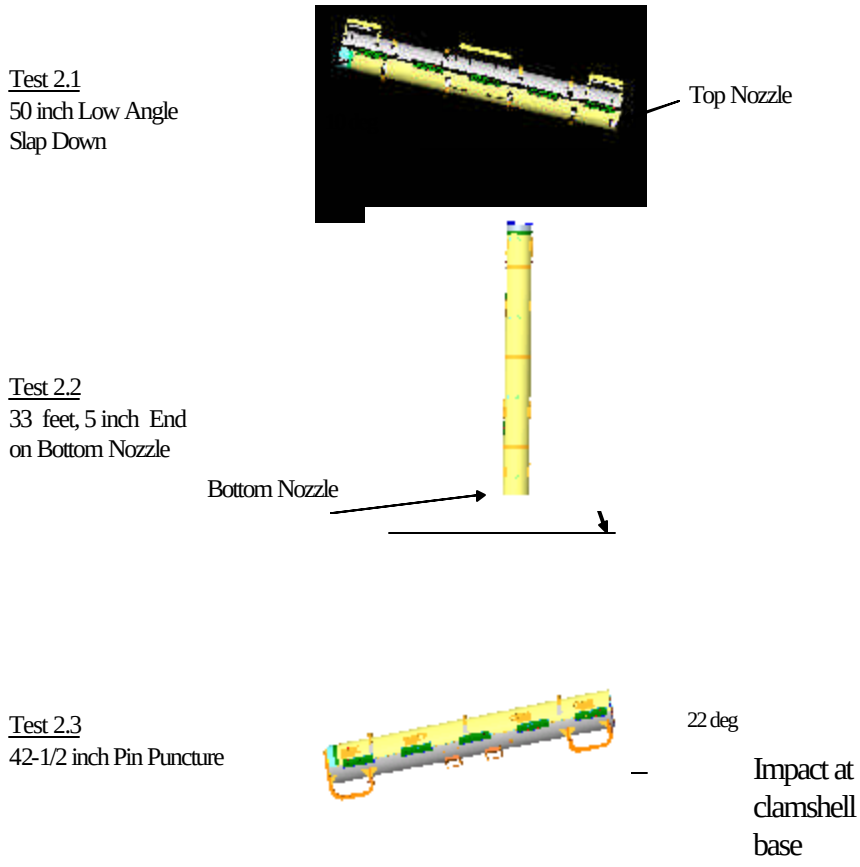

Figure 2-135 QTU Test Series 2 Drop Orientations

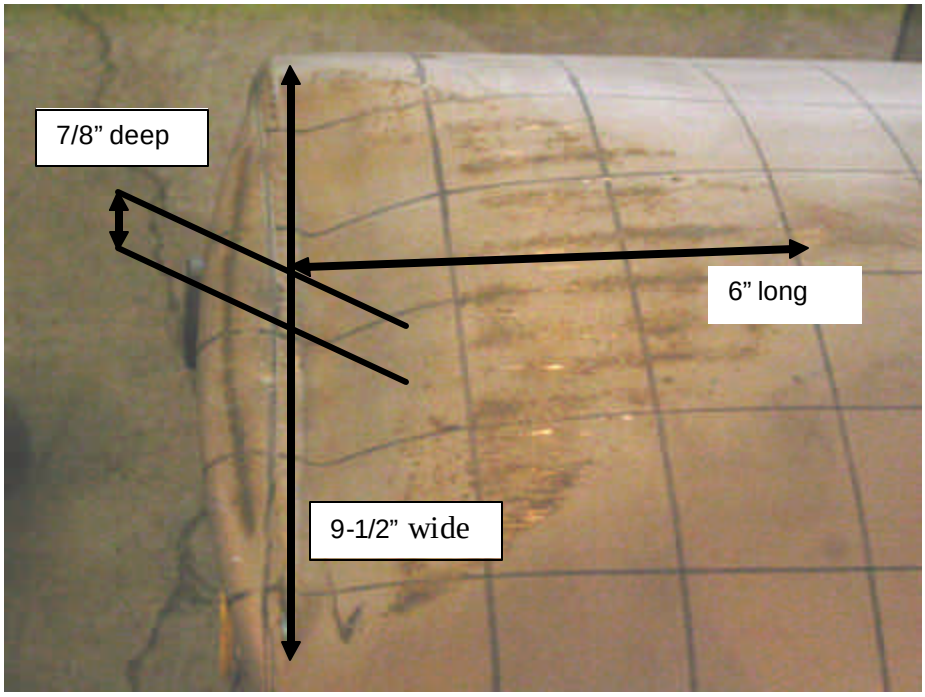

Figure 2-136 QTU Outerpack After Test 2.1

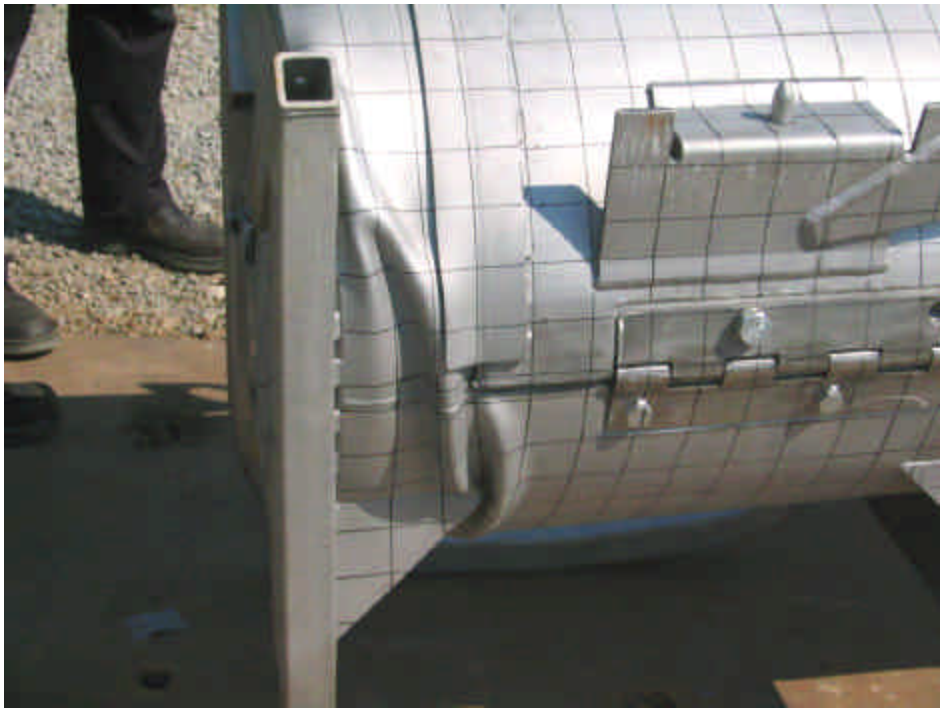

Figure 2-137 QTU Outerpack After Test 2.2

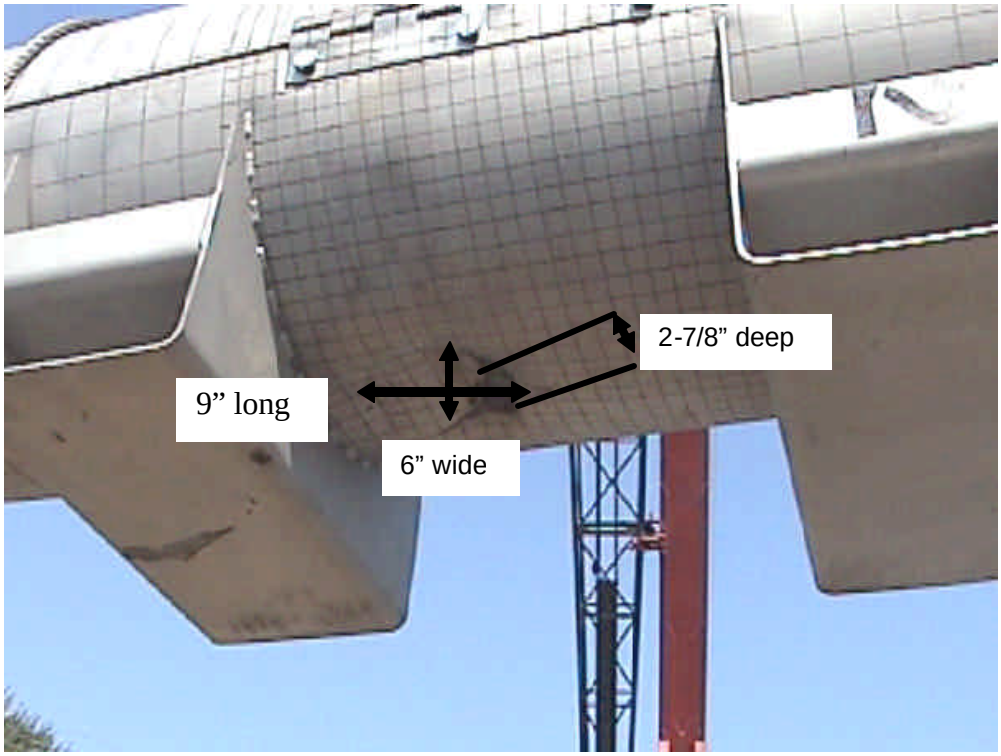

Figure 2-138 QTU Outerpack After Test 2.3

The fuel assembly in QTU-1 was measured before the test and after the burn test at locations shown in Figure 2-134 above. Table 2-41 provides the pretest dimensions. Tables 2-42 and 2-43 provide the post test dimensions.

The post-test inspections concluded that the tested configuration of the Traveller Outerpacks and Clamshells were acceptable. Furthermore, the tests concluded that Test Series 1 imparted the most damage to the Outerpack, and Test Series 2 imparted the most damage to the fuel assembly. Also, testing demonstrated that the Traveller Outerpack is suitable for transport with two top Outerpack bolts per hinge. The post-test geometry of the fuel assemblies for both test series was also acceptable.

In summary, testing demonstrated the Traveller package is suitable for compliance to normal and hypothetical mechanical drop test conditions described in 10 CFR 71 and TS-R-1.

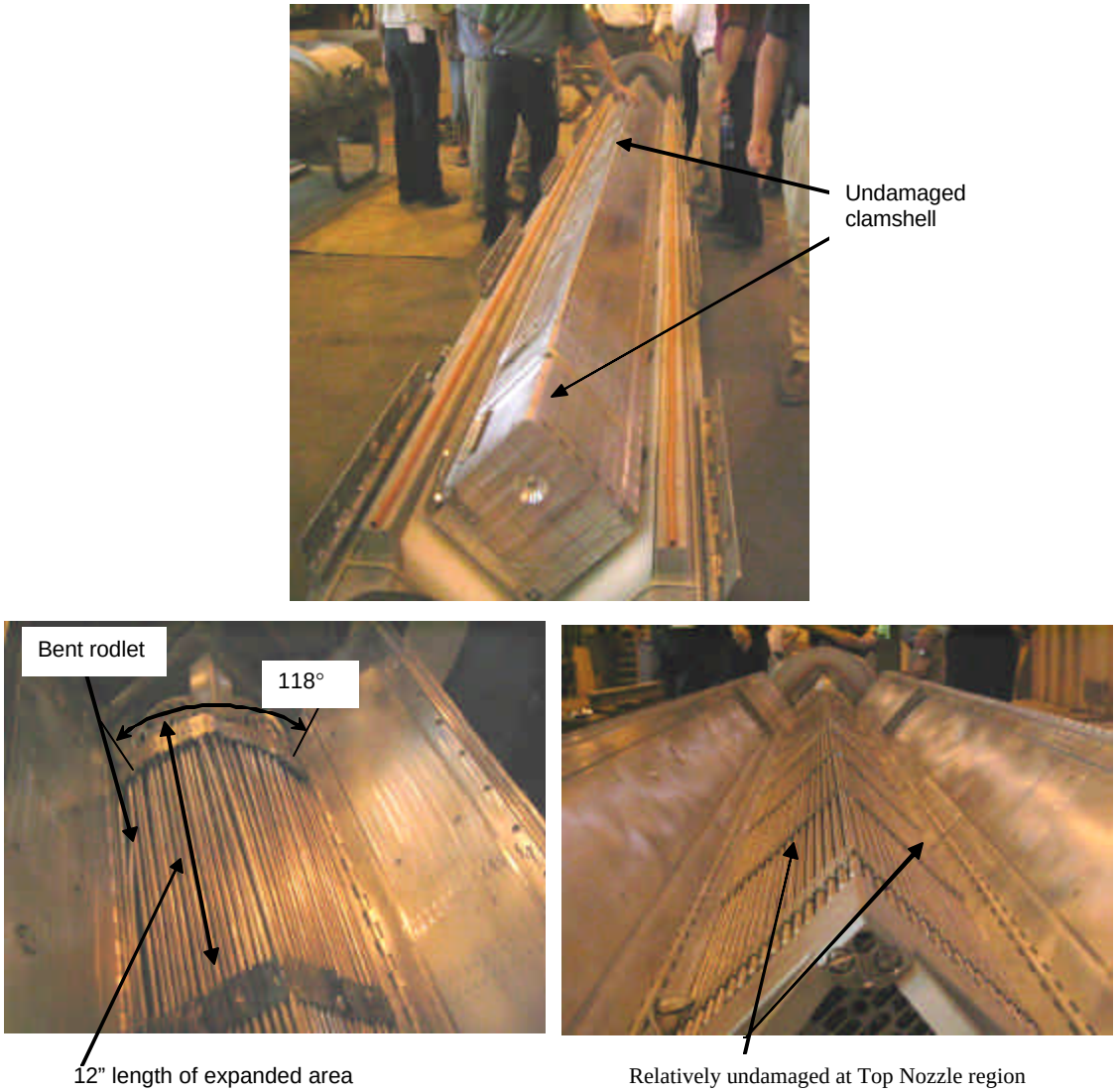

Figure 2-139 QTU-2 Clamshell and Fuel Assembly After Drop Tests

Table 2-41 Key Dimensions of QTU-2 Fuel Assembly Before Testing			
Fuel Assembly ID: 503005, B/N # 97-2480Y			
F/A Location	**Fuel Envelope (inches)**	**Gap (inches)**	**Pitch (inches)**
B/N – Grid 1	1 – 8.356 2 – 8.463 3 – 8.329 4 – 8.430 8.375 Meas. Nominal*	L – 0.124 R – 0.123 0.125 Meas. Nominal*	L – 0.499 R – 0.498 0.500 Meas. Nominal*
Grid 1 – Grid 2	1 – 8.325 2 – 8.415 3 – 8.319 4 – 8.420 8.375 Meas. Nominal*	L – 0.121 R – 0.123 0.125 Meas. Nominal*	L – 0.496 R – 0.498 0.500 Meas. Nominal*
Grid 2 – Grid 3	1 – 8.333 2 – 8.410 3 – 8.329 4 – 8.411 8.375 Meas. Nominal*	L – 0.121 R – 0.123 0.125 Meas. Nominal*	L – 0.496 R – 0.498 0.500 Meas. Nominal*
Grid 3 – Grid 4	1 – 8.311 2 – 8.435 3 – 8.310 4 – 8.24 8.375 Meas. Nominal*	L – 0.124 R – 0.123 0.125 Meas. Nominal*	L – 0.499 R – 0.498 0.500 Meas. Nominal*
Grid 4 – Grid 5	8.375 Meas. Nominal*	0.125 Meas. Nominal*	0.500 Meas. Nominal*
Grid 5 – Grid 6	8.375 Meas. Nominal*	0.125 Meas. Nominal*	0.500 Meas. Nominal*
Grid 6 – Grid 7	8.375 Meas. Nominal*	0.125 Meas. Nominal*	0.500 Meas. Nominal*
Grid 8 – Grid 9	8.375 Meas. Nominal*	0.125 Meas. Nominal*	0.500 Meas. Nominal*
Grid 9 – Grid 10	8.375 Meas. Nominal*	0.125 Meas. Nominal*	0.500 Meas. Nominal*
Grid 10 – T/N	8.375 Meas. Nominal*	0.125 Meas. Nominal*	0.500 Meas. Nominal*
Note: * Measured nominal values were measured to nearest 1/8".			

Table 2-42 QTU-2 Fuel Assembly Grid Envelope After Testing			
Fuel Assembly Envelope Inspection Table			
Location	Envelope Dimension, Inches		Maximum Fuel Rod Gap from Form 2F (Nominal Gap = 0.122")
	Left Side, LS	Right Side, RS	
Between B/N and Grid 1	8.625	8.500	0.722
Between Grids 1 and 2	8.000	7.938	0.539
Between Grids 2 and 3	7.938	7.688	0.316
Between Grids 3 and 4	7.813	7.625	0.137
Between Grids 4 and 5	8.063	7.875	0.153
Between Grids 5 and 6	8.250	8.250	0.143
Between Grids 6 and 7	8.375	8.375	0.146
Between Grids 7 and 8	8.375	8.375	0.141
Between Grids 8 and 9	8.375	8.375	0.162
Between Grids 9 and 10	8.375	8.375	0.141
Between Grid 10 and T/N	8.438	8.438	0.127
MAXIMUM VALUE	8.625	8.500	0.722

Table 2-43 QTU-2 Fuel Rod Pitch Data After Testing			
Fuel Rod Pitch Inspection Table			
Location	Maximum Gap, inches		Maximum Pitch, inches
	Left Side, LS	Right Side, RS	
Between B/N and Grid 1	0.722	0.501	1.097
Between Grids 1 and 2	0.539	0.501	0.914
Between Grids 2 and 3	0.250	0.316	0.691
Between Grids 3 and 4	0.137	0.125	0.512
Between Grids 4 and 5	0.153	0.132	0.528
Between Grids 5 and 6	0.142	0.143	0.518
Between Grids 6 and 7	0.145	0.146	0.521
Between Grids 7 and 8	0.141	0.138	0.516
Between Grids 8 and 9	0.162	0.122	0.537
Between Grids 9 and 10	0.139	0.141	0.516
Between Grid 10 and T/N	0.127	0.123	0.502
MAXIMUM VALUE	0.722	0.501	1.097

2.12.4.2.3 Certification Test Unit Drop Tests

A Traveller XL package was fabricated by Columbiana High Tech to serve as the certification test unit (CTU), Figures 2-140 and 2-141 and Table 2-44. This unit was subjected to a regulatory drop test performed February 5, 2004 in Columbiana, Ohio. The test included a 50 inch (1.27 m) slap down, a 32.8 feet (10.0 m) free drop test impacting the bottom nozzle, and a 42 inch (1.07 m) pin-puncture test, Figure 2-142 and Table 2-45. The CTU package was thermally saturated for approximately 15 hours prior to testing at a temperature of about 17ºF (-8.3ºC). At the time of testing the temperature was approximately 24ºF (-4.4ºC). The package's test weight was 4863 pounds.

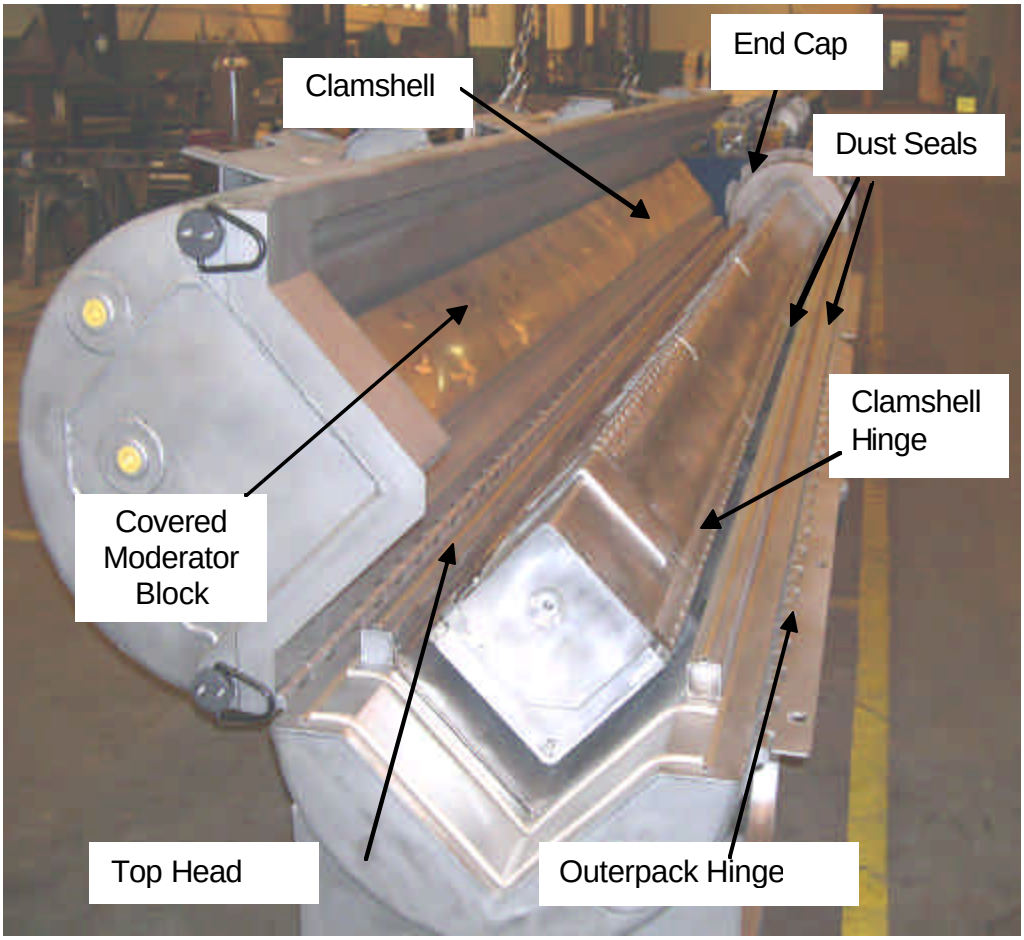

Figure 2-140 Traveller CTU Test Article Internal View

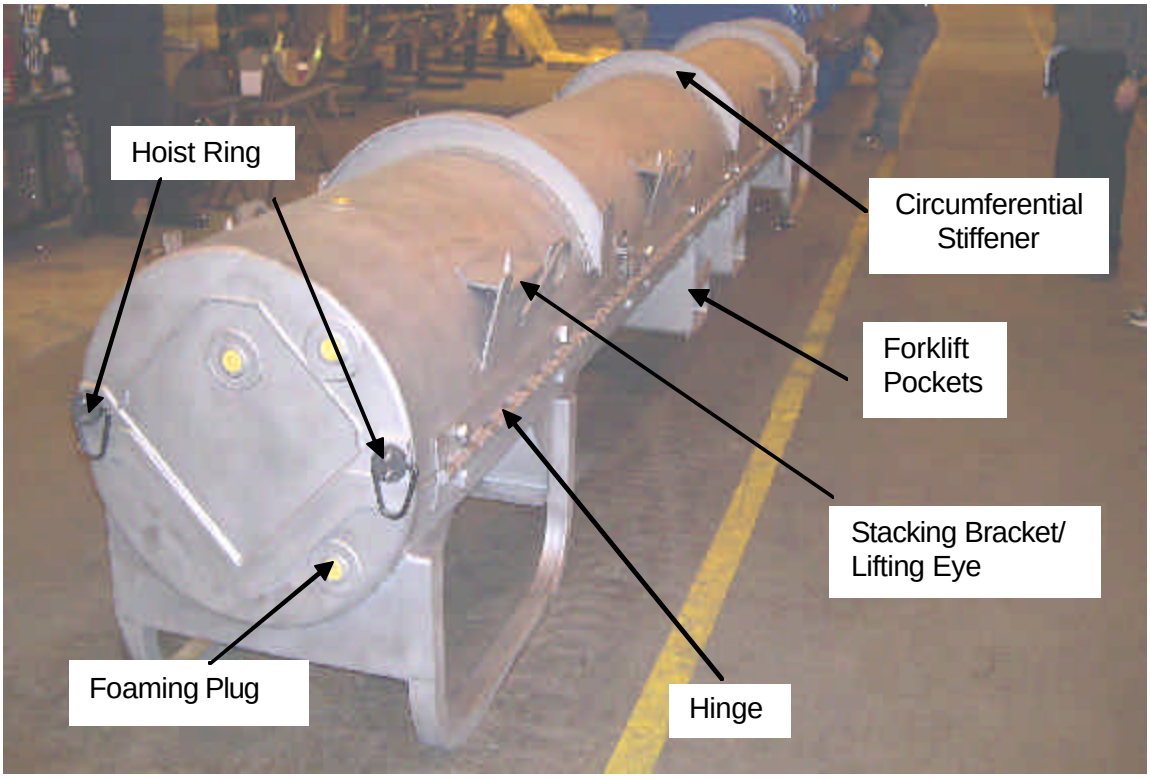

Figure 2-141 Traveller CTU External View

Table 2-44 Test Weights

	Nominal* Wt	Actual Wt
Weight of Outerpack (Empty):	2633 lb	2671 lb
Weight of Clamshell (Empty):	425 lb	440 lb
Weight of package (Empty) :	3058 lb	3111 lb
Total package test weight:	4810 lb	4863 lb

Note:

* Nominal total weight includes only Fuel Assembly since drop test was conducted without RCCA. Maximum expected design weight is estimated to be 5071 pounds (Ref. 3). The top Outerpack section weight is 1063 pounds empty and the bottom Outerpack section weight is 1608 pounds empty.

Exterior Inspections After Drop Tests – The exterior of the package was examined after each drop. The inspections found that the Outerpack retained its circular pre-test shape except for localized plastic deformation at the ends. No hinge bolts failed on the Outerpack, the Outerpack did not separate, and neither the inner nor outer shell were perforated in the pin drop test.

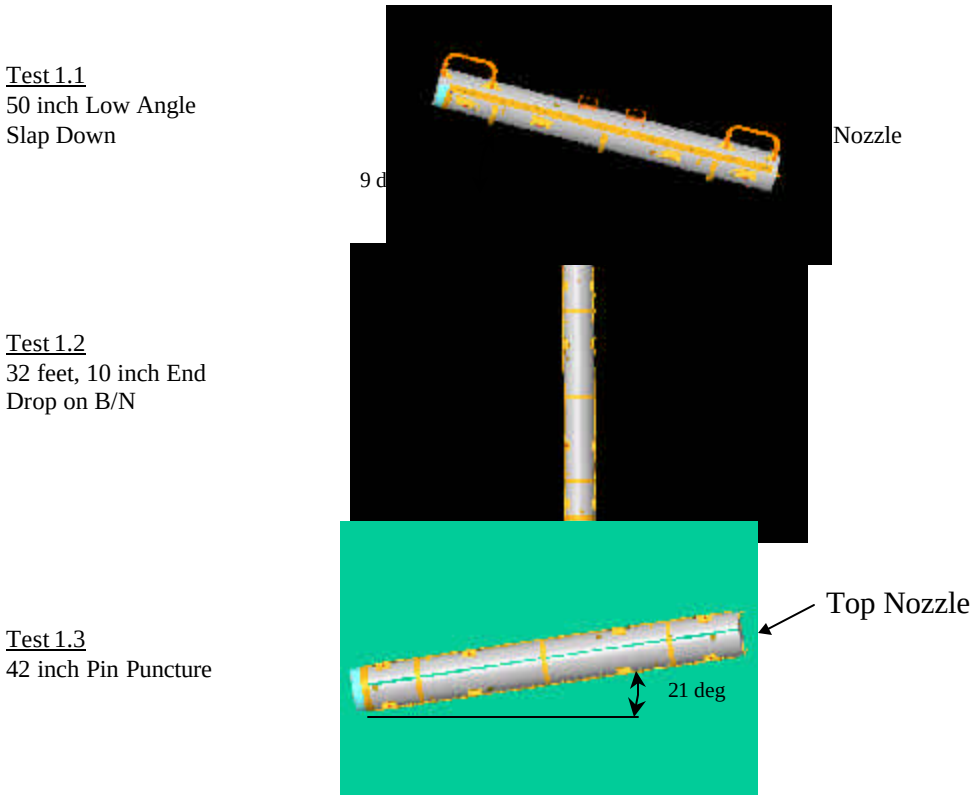

Figure 2-142 CTU Drop Test Orientations

Table 2-45 CTU Drop Test Orientations

Test ArticleID	F/A Type	Test Sequence	Test Pitch Attitude	Test Roll Attitude	Design Feature Tested
CTU	17x17 XL	P1.1) 1.2-m, NCT, Low angle[1]	9°	180°	Operations of hinges/doors
		P1.2) 9-m End Drop[1]	90°	0°	Lattice exp., FR axial position
		P1.3) 1-m Pin-puncture[1]	21°	90°	Hinge structural integrity

Test 1 – The 1.2 meter drop test resulted in a localized dent at the top nozzle end, and near the bottom nozzle end, the stiffener was dented over a length of about 8". Figures 2-143 and 2-144 shows the damage observed. The normal condition drop produced only local damage to the impact area. The depth of the crush was minimal.

Test 2 – The 9m (32.8-foot) free drop resulted in localized damage to the bottom nozzle end region. The two bottom nozzle stiffener keeper pins were detached as a result of the impact. The impact created a circumferential ripple located at 9" (bottom Outerpack) and 12" (top Outerpack) from the package bottom end. The ripple resulted in a 1/2" crumple impact, which effectively shortened that section of the package slightly. Two stitch welds located inside the bottom nozzle end stiffener were broken, but this did not

compromise the stiffener position. The bottom nozzle end cap stiffener separated to form a 1-3/16" gap, and the gap between the hinge and the cover lip was measured to be approximately 7/16". The hinge at the bottom nozzle end was separated about 1/16" from the Outerpack skin surface after the drop test. Figures 2-145 – 2-147 shows the damage observed.

Test 3 – The pin puncture test was located on the hinge of the Outerpack at approximately the axial center of gravity. The impact zone locally dented 6" of hinge length to a maximum measured depth of approximately 1-3/8", Figure 2-148. The hinge knuckles were not compromised as a result of the test. Hinge separation of 1/2" was noted about 7-1/2" from the impact point towards the top nozzle end.

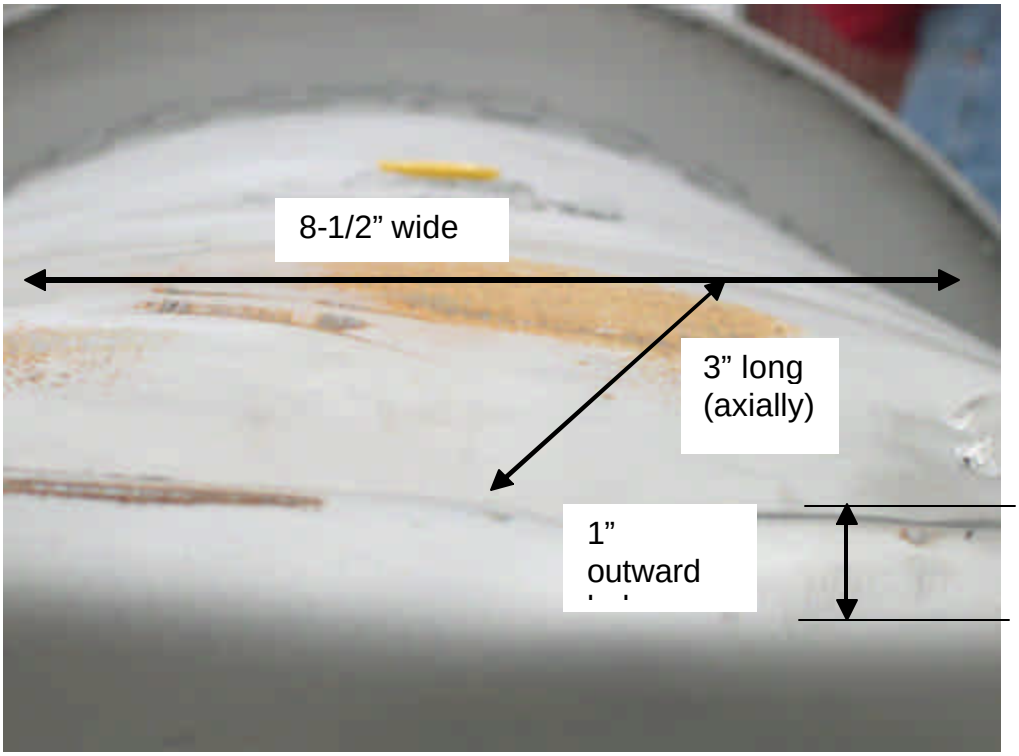

Figure 2-143 Top Nozzle End Outerpack Impact Damage

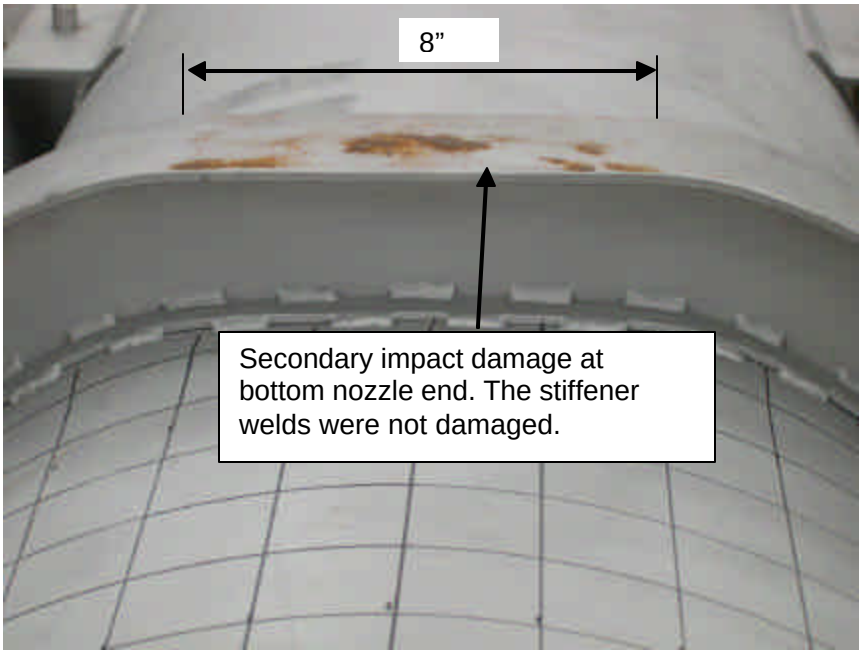

Figure 2-144 CTU Outerpack Stiffener After Test 1

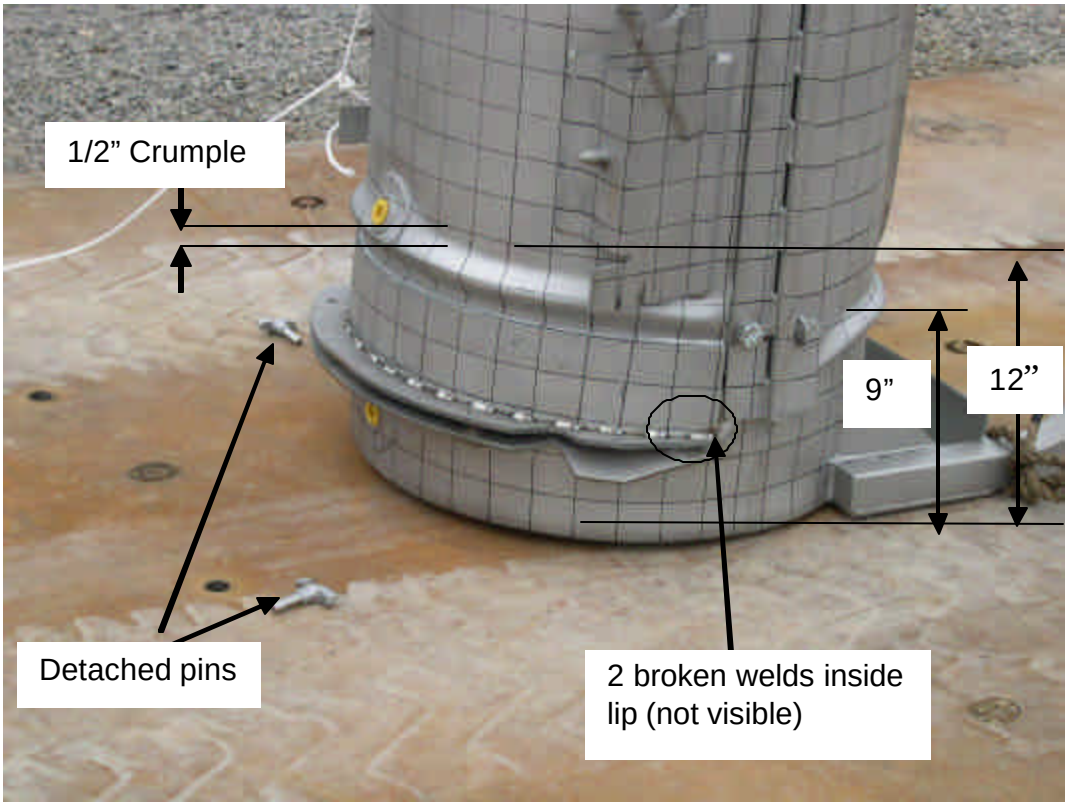

Figure 2-145 CTU Outerpack After Test 2

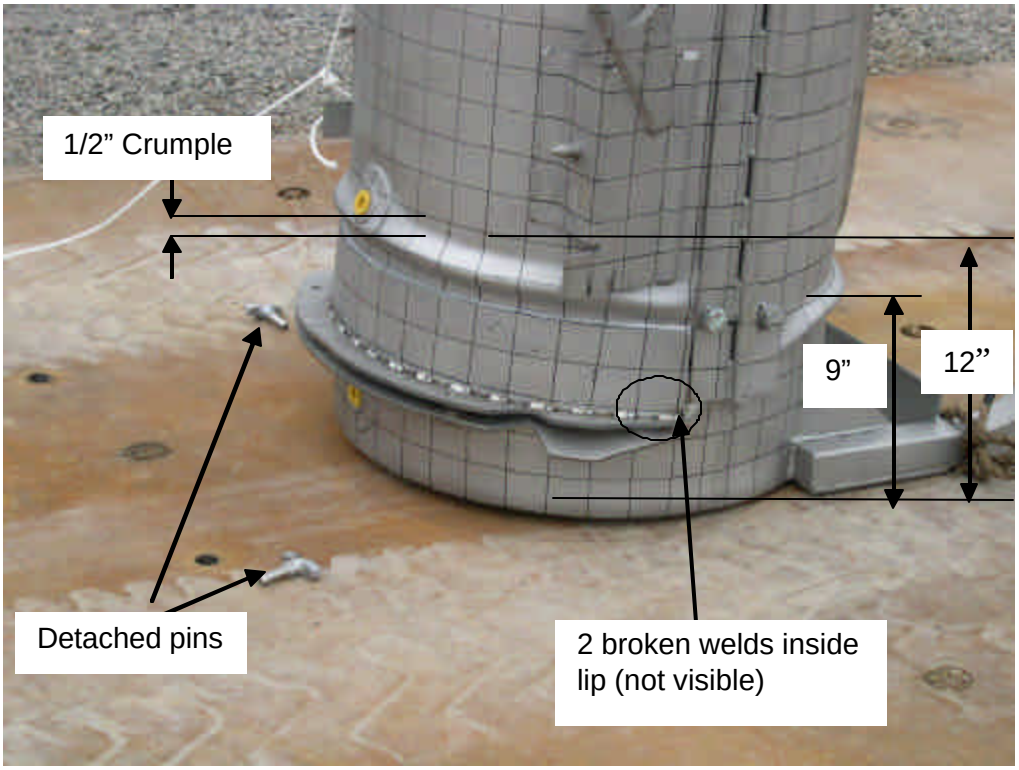

Figure 2-146 Bottom Nozzle End Cap Stiffener Damage From Test 2

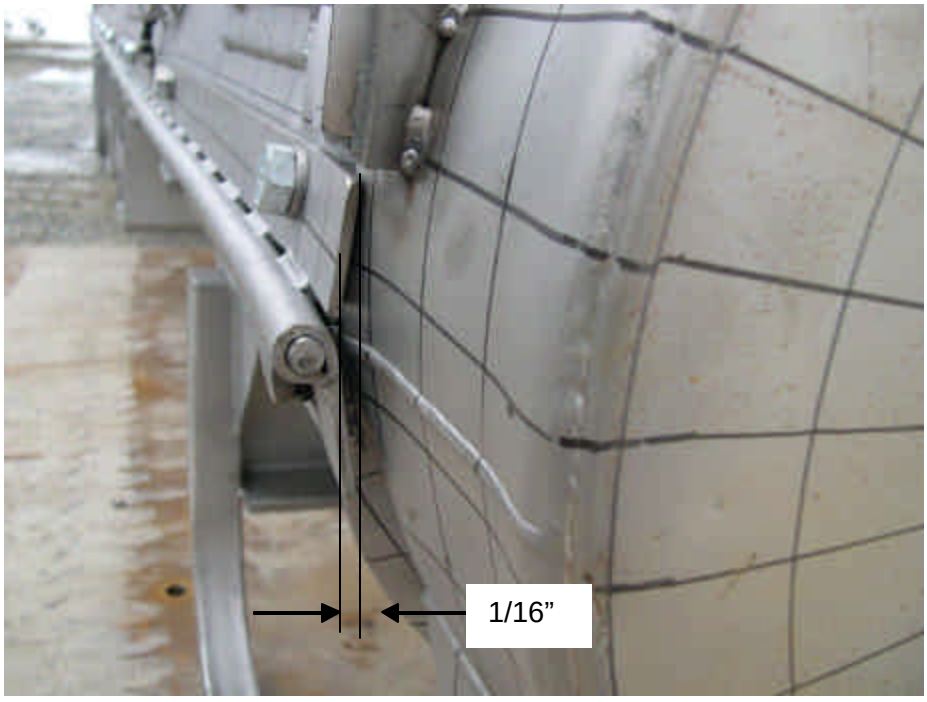

Figure 2-147 Hinge Separation at Bottom Nozzle End From Test 2

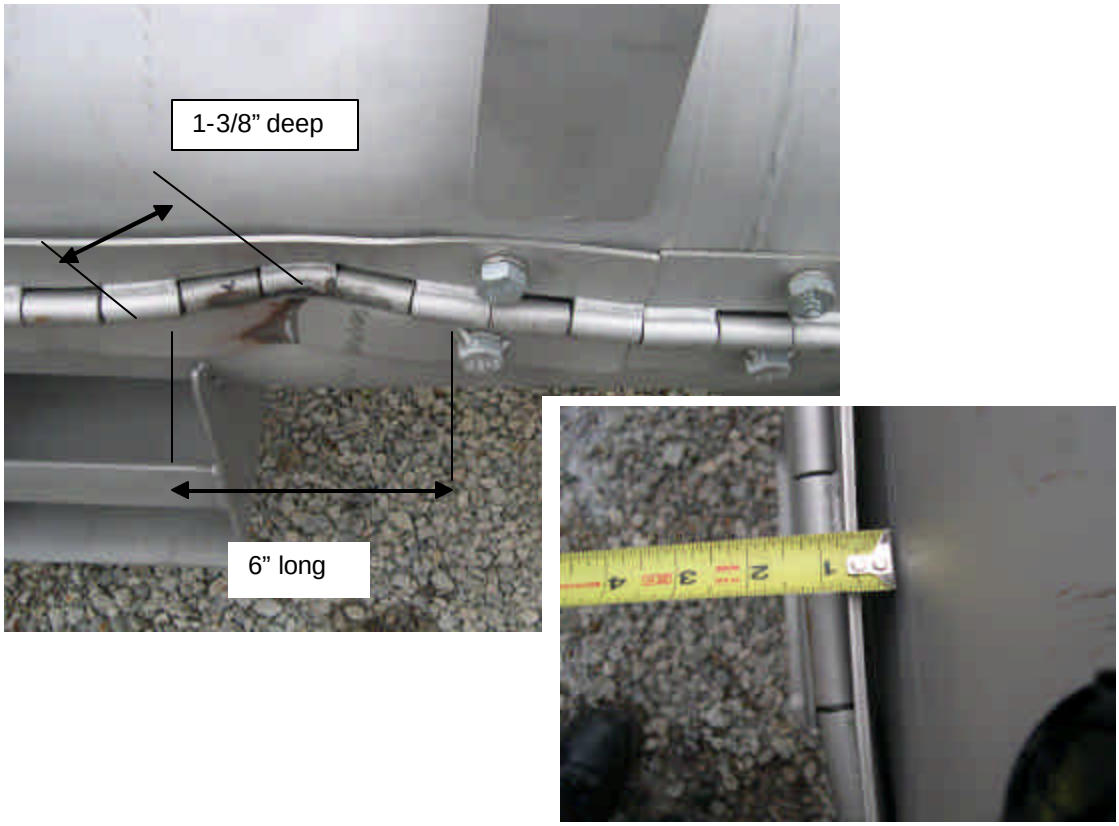

Figure 2-148 CTU Outerpack After Test 3

Interior Inspection Results – The CTU was sent to the South Carolina Fire Academy for the burn test immediately after the drop tests were completed. The package was not opened until the following week, approximately five hours after the fire test was completed. In general, the drop test and fire test resulted in minor damage to the Traveller internal structural components. The Clamshell was found intact and closed, Figure 2-149, and the simulated poison plates maintained position. At the bottom Clamshell plate, a 2-1/2" and a 2-3/4" piece of end lip sheared off. The measured gap was less than 1/16" and in the axial direction. The axial location of the fuel rods maintained position between the bottom and top nozzle. Finally, the moderator blocks were found to be intact and essentially undamaged after the completion of the drop and fire test. The moderator stud bolts on the top Outerpack were found sheared off, but the moderator cover maintained the moderator position. The stainless steel moderator cover was removed and the polyethylene moderator was examined. As shown in Figure 2-150, the moderator was intact and essentially undamaged.

Figure 2-151 provides the damage sketch overlaying the pre-tested fuel assembly for comparative purposes. For the 20" span from the bottom nozzle to Grid 2 of the fuel assembly, the fuel rod envelope expanded from 8-3/8" average nominal to 9-3/16". The grid envelope expanded from 8-7/16" nominal to 8-5/8" over the same 20" axial distance. The maximum measured fuel rod pitch in this region increased from 0.496" nominal to 0.990". This was caused by a single bent rod which was bent outward

approximately 1/2". Otherwise, the typical pitch pattern consisted of 2 rod rows touching and the remaining 14 rows at nominal pitch, Figure 2-152.

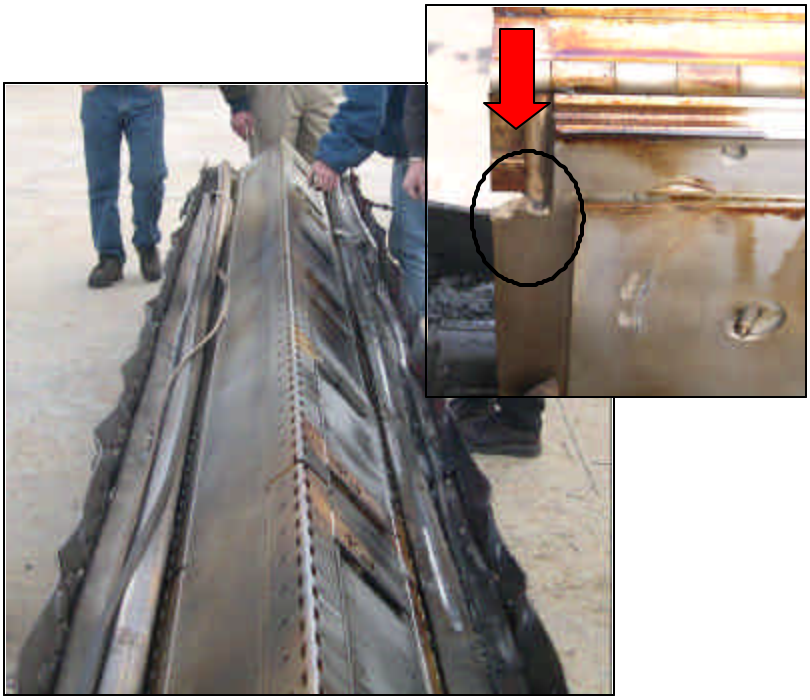

Figure 2-149 CTU Clamshell After Drop and Fire Tests

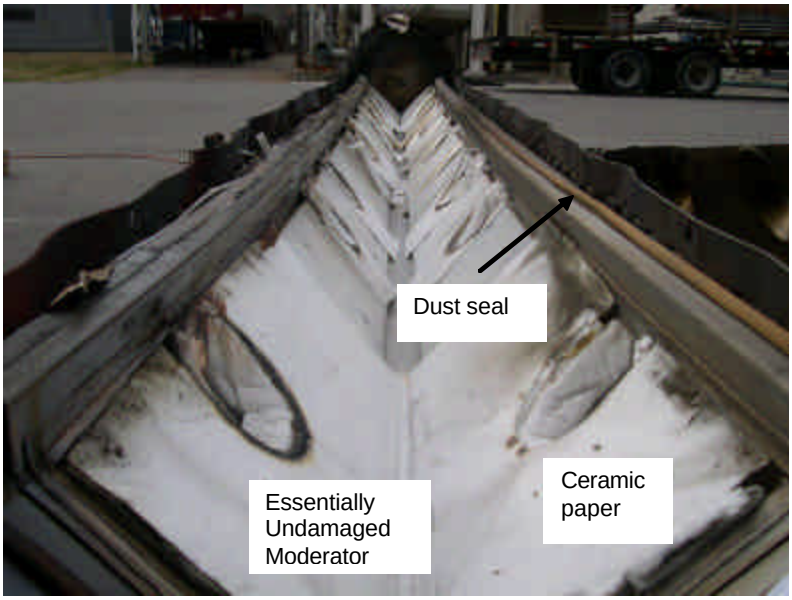

Figure 2-150 Outerpack Lid Moderator After Testing

For a length of 10" above Grid 2, the fuel rod envelope compressed from 8-3/8" nominal to 8-1/4". This slight compression is due to the single top rod slightly compressed inward. Above this 10" region, the single rod bent outward about 1/2" for a length of approximately 25".

For the 25" length from between Grids 2 and 3 and up to Grid 4, the single rod resulted in a measured envelope of 8-7/8", but the remaining envelope of 16 rows was slightly compressed (about 1/16"). The maximum pitch caused by the single rod was 0.740" compared to 0.496" nominal. Otherwise, the average pitch was nominal.

For the remainder of the fuel assembly from Grid 4 to the top nozzle, the fuel rod envelope compressed about 0.15" and the grid envelope compressed about 1/4". The average pitch decreased from 0.496" to 0.459" in this region.

Grid 1 was severely buckled, and the ovality was measured to be 120º for a length of about 20", Figure 2-153. Grids 2 and 3 were broken at the top corner, but otherwise intact. Grids 4-10 were relatively undamaged. The fuel inspection also indicated that 7.5% (20 of 265 rods) were cracked at the end plug locations (Figure 2-154). The average crack width measured was approximately 0.030" (30 mils) and the average length was 50% of the rod diameter. The cracked rods were located at the four corners, indicating the vertical impact created symmetrical impact forces to be transmitted through the bottom nozzle and fuel rods (Figure 2-155).

The fuel assembly in QTU-1 was measured before the test and after the burn test at locations shown in Figure 2-134 above. Table 2-46 provides the pretest dimensions. Tables 2-47 through 2-50 provide the post test dimensions.

2.12.4.3 Conclusions

Three series of drop tests were performed during the development and certification of the Traveller shipping package. This included two prototype units, two qualification test units and one certification test unit. Design improvements were made at each step based on the results of the drop tests and subsequent fire tests. The drop test series included a regulatory normal free drop of 1.2 meters, a 9-meter end drop onto the bottom nozzle, and a 1-meter pin-puncture test on the hinge. Minor structural Outerpack damage indicated that the Traveller Outerpack design satisfied the hypothetical accident condition defined in 10 CFR 71 and TS-R-1. Furthermore, the Clamshell was found to meet the acceptance criteria of the test by maintaining closure and its pre-test shape. The post-test geometry of the fuel assembly was determined to meet the acceptance criteria since only local expansion was noted in the lower 20" of the bottom nozzle region and the cracked rod gaps were all measured less than a pellet diameter.

In summary, testing demonstrated the Traveller package is suitable for compliance to normal and hypothetical mechanical drop test conditions described in 10 CFR 71 and TS-R-1.

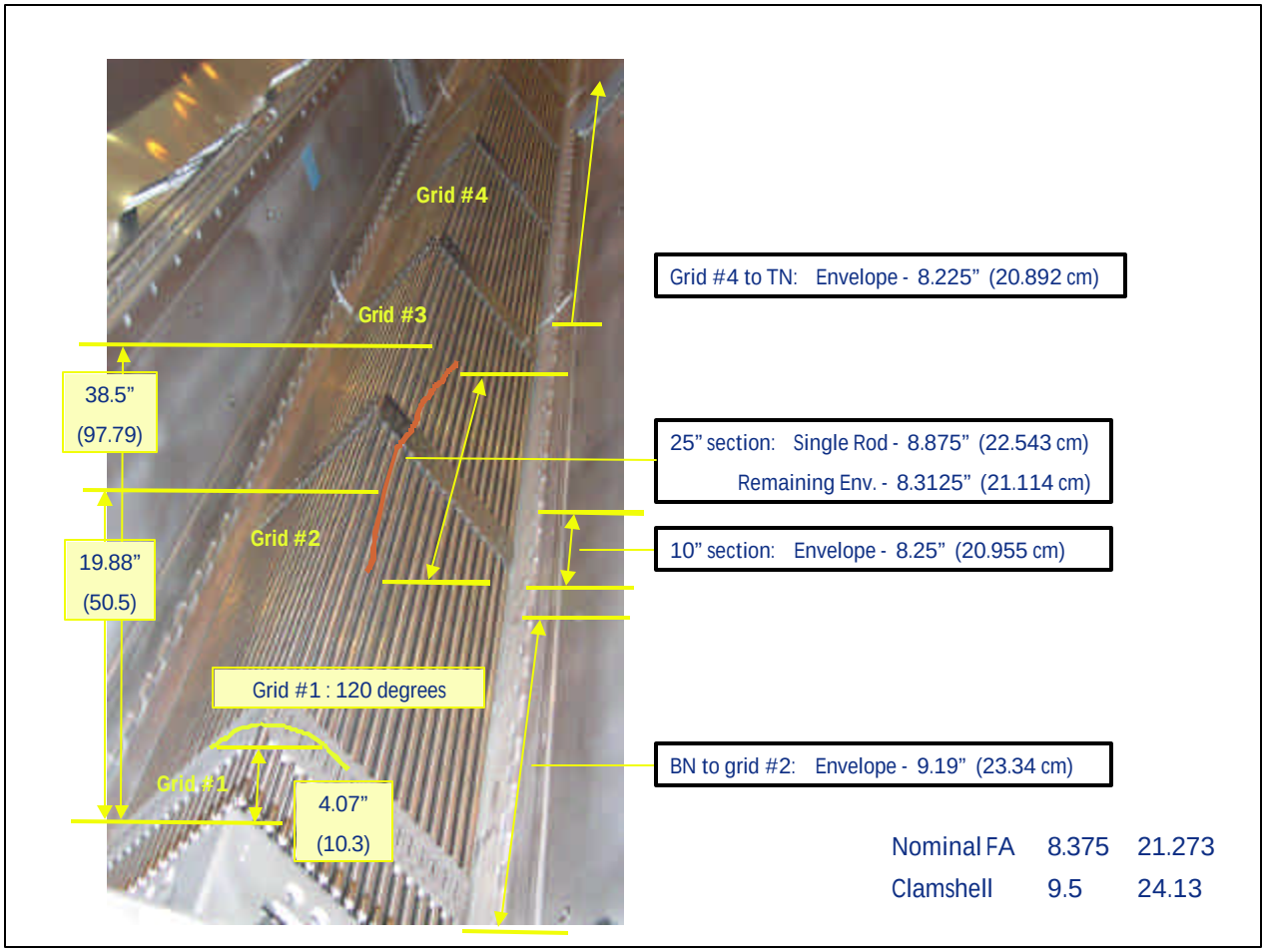

Figure 2-151 Fuel assembly Damage Sketch and Pre -test Assembly

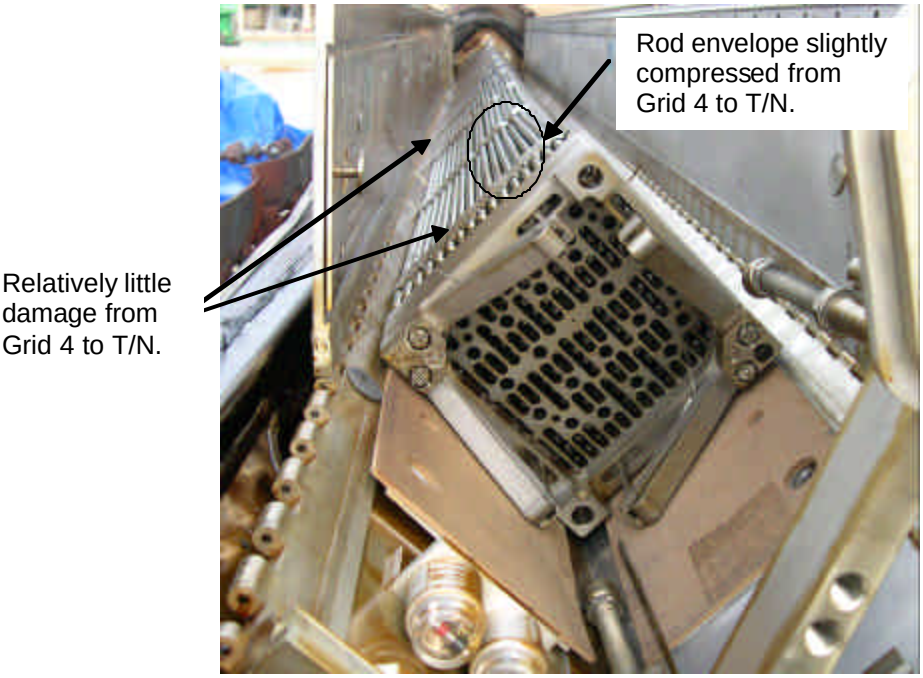

Figure 2-152 CTU Fuel Assembly After Testing

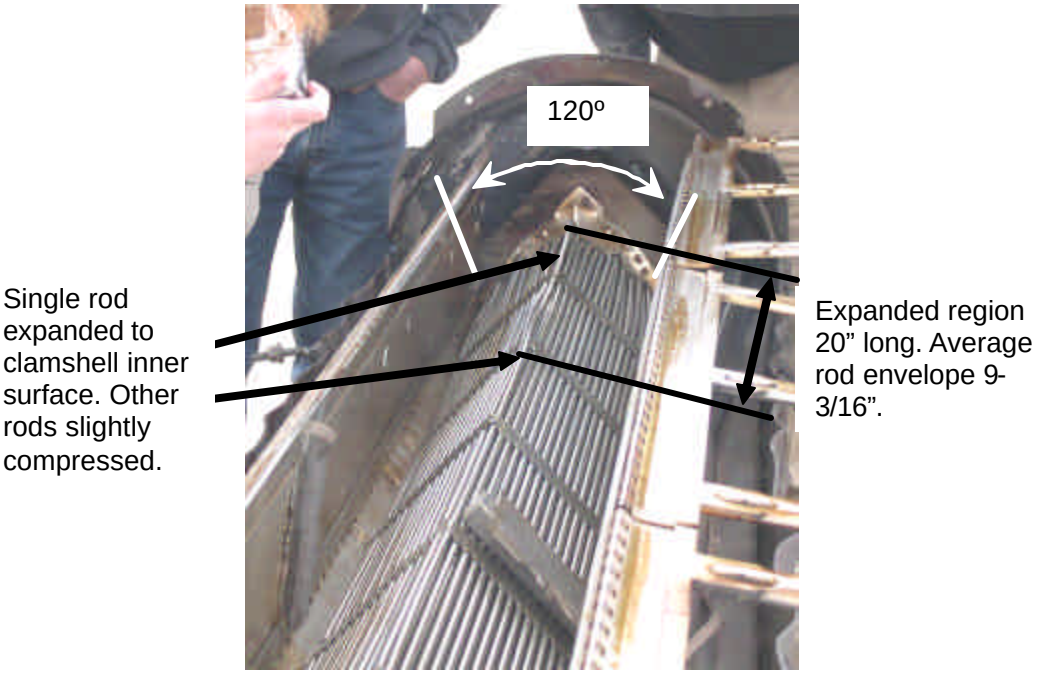

Figure 2-153 CTU Fuel Assembly Top End After Testing

Figure 2-154 Cracked Rod From CTU Fuel Assembly

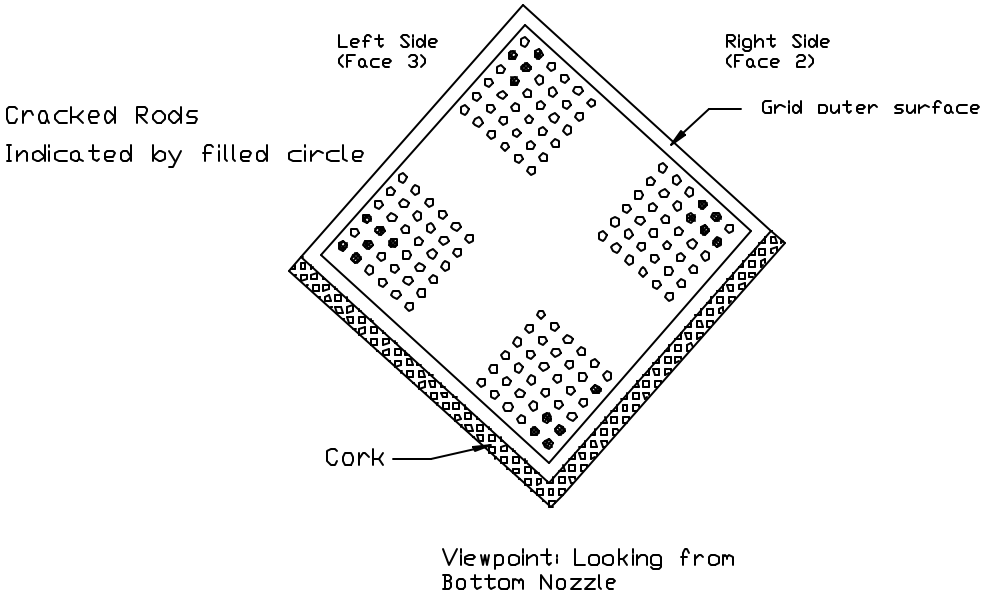

Figure 2-155 Cracked Rod Locations on CTU Fuel Assembly

Table 2-46 Fuel Assembly Key Dimension Before Drop Test

Fuel Assembly ID: T/N # LM1F2N

F/A Location	Fuel Envelope (inches)	Gap (inches)	Pitch (inches)
B/N – Grid 1	1: 8-3/8 2: 8-7/16 3: 8-3/8 4: 8-7/16	L – 0.123 R – 0.121	L – 0.498 R – 0.495
Grid 1- Grid 2	1: 8-3/8 2: 8-7/16 3: 8-3/8 4: 8-7/16	L – 0.123 R – 0.124	L – 0.497 R – 0.499
Grid 2- Grid 3	1: 8-3/8 2: 8-7/16 3: 8-3/8 4: 8-7/16	L – 0.121 R – 0.121	L – 0.495 R – 0.495
Grid 3- Grid 4	1: 8-3/8 2: 8-7/16 3: 8-3/8 4: 8-7/16	L – 0.123 R – 0.123	L – 0.497 R – 0.498
Grid 4- Grid 5	Rods: 8-3/8 Grids: 8-7/16	0.121	0.495
Grid 5- Grid 6	Rods: 8-3/8 Grids: 8-7/16	0.123	0.498
Grid 6- Grid 7	Rods: 8-3/8 Grids: 8-7/16	0.122	0.497
Grid 7- Grid 8	Rods: 8-3/8 Grids: 8-7/16	0.123	0.497
Grid 8- Grid 9	Rods: 8-3/8 Grids: 8-7/16	0.123	0.498
Grid 9- Grid 10	Rods: 8-3/8 Grids: 8-7/16	0.121	0.495
Grid 10 – T/N	Rods: 8-3/8 Grids: 8-7/16	0.122	0.497
AVERAGE	Rods: 8-3/8 Grids: 8-7/16:	0.122	0.497

Note:

* Measured fractional values were measured to nearest 1/16". Measured decimal values were measured to the nearest 0.001".

Table 2-47 CTU Fuel Assembly Grid Envelop Dimensions After Testing		
Location	Measured Grid Envelope Dimension, Inches	
	Left Side, LS	Right Side, RS
Grid 1	9-0	8-3/4
Grid 2	8-7/16	8-3/8
Grid 3	9-1/2	9-1/2
Grid 4	8-1/8	8-1/4
Grid 5	8-1/8	8-1/4
Grid 6	8-1/4	8-1/4
Grid 7	8-1/8	8-3/16
Grid 8	8-5/16	8-3/16
Grid 9	8-5/16	7-7/8
Grid 10	8-3/8	8-1/2
MAXIMUM VALUE	9-1/2	9-1/2

Table 2-48 CTU Fuel Assembly Rod Envelope Data After Testing

Fuel Assembly Rod Envelope Inspection Table

Location	Measured Envelope Dimension, In.		Calculated Maximum Fuel Rod Pitch from Form 1G (Nominal Pitch = 0.496")
	Left Side, LS	Right Side, RS	
Between B/N and Grid 1	9-0	8-3/4	0.566
Between Grids 1 and 2	8-5/16 (1)	8-5/16 (1)	0.990
Between Grids 2 and 3	8-1/2	8.-0	0.740
Between Grids 3 and 4	8-7/16	8-1/2	0.715
Between Grids 4 and 5	8-3/16	8-3/16	0.472
Between Grids 5 and 6	8-3/16	8-3/8	0.578
Between Grids 6 and 7	8-1/16	8-1/16	0.550
Between Grids 7 and 8	8-3/8	8-3/16	0.541
Between Grids 8 and 9	8-0	7-13/16	0.483
Between Grids 9 and 10	8-3/8	8-1/2	0.498
Between Grid 10 and T/N	8-3/8	8-0	0.497
MAXIMUM VALUE	9-0	8-3/4	0.990

Note:
(1) A single rod was measured to the inner Clamshell surface (9-1/2"). See Figure 2-153.

Table 2-49 CTU Fuel Assembly Rod Envelope After Testing

Fuel Assembly Rod Envelope Inspection Table

Location	Measured Envelope Dimension, In.		Calculated Maximum Fuel Rod Pitch from Form 1G (Nominal Pitch = 0.496")
	Left Side, LS	Right Side, RS	
Between B/N and Grid 1	9-0	8-3/4	0.566
Between Grids 1 and 2	8-5/16 (1)	8-5/16 (1)	0.990
Between Grids 2 and 3	8-1/2	8.-0	0.740
Between Grids 3 and 4	8-7/16	8-1/2	0.715
Between Grids 4 and 5	8-3/16	8-3/16	0.472
Between Grids 5 and 6	8-3/16	8-3/8	0.578
Between Grids 6 and 7	8-1/16	8-1/16	0.550
Between Grids 7 and 8	8-3/8	8-3/16	0.541
Between Grids 8 and 9	8-0	7-13/16	0.483
Between Grids 9 and 10	8-3/8	8-1/2	0.498
Between Grid 10 and T/N	8-3/8	8-0	0.497
MAXIMUM VALUE	9-0	8-3/4	0.990

Note:
(1) A single rod was measured to the inner Clamshell surface (9-1/2"). See Figure 2-153.

Table 2-50 CTU Fuel Rod Gap and Pitch Inspection After Testing

Fuel Rod Gap and Pitch Inspection Table

Location	Measured Maximum Gap, Inches		Calculated Maximum Pitch, Inches
	Left Side, LS	Right Side, RS	
Between B/N Grid 1	0.093 (between rows 9 & 10)	0.193 (between rows 6 & 7)	0.566
Between Grids 1 and 2	0.616 (out-lying rod only)	0.563 (out-lying rod only)	0.990
Between Grids 2 and 3	0.207 (one rod) Others touching	0.366 (one rod) Others touching	0.740
Between Grids 3 and 4	0.336	0.340	0.715
Between Grids 4 and 5	0.099	0.050	0.472
Between Grids 5 and 6	0.204	0.084	0.578
Between Grids 6 and 7	0.173 (between rows 2 & 3) Others Nominal	0.176 (between rows 6 & 7) Others Nominal	0.550
Between Grids 7 and 8	0.166	0.064	0.541
Between Grids 8 and 9	0.109	0.060	0.483
Between Grids 9 and 10	0.124	0.090	0.498
Between Grid 10 and T/N	0.123	0.074	0.497
MAXIMUM VALUE	0.616	0.563	0.990

Note:
The pitch is calculated by adding the measured gap to the fuel rod diameter.